Nuclear effective field theory: Status and perspectives

H.-W. Hammer[*]

*Technische Universität Darmstadt, Department of Physics, 64289 Darmstadt, Germany
and ExtreMe Matter Institute EMMI, GSI Helmholtzzentrum für Schwerionenforschung GmbH,
64291 Darmstadt, Germany*

Sebastian König[†]

*Technische Universität Darmstadt, Department of Physics, 64289 Darmstadt, Germany,
ExtreMe Matter Institute EMMI, GSI Helmholtzzentrum für Schwerionenforschung GmbH,
64291 Darmstadt, Germany, Department of Physics,
The Ohio State University, Columbus, Ohio 43210, USA,
and Department of Physics, North Carolina State University, Raleigh, North Carolina 27695, USA*

U. van Kolck[‡]

*Université Paris–Saclay, CNRS/IN2P3, IJCLab, 91405 Orsay, France
and Department of Physics, University of Arizona, Tucson, Arizona 85721, USA*

(published 23 June 2020)

The nuclear-physics landscape has been redesigned as a sequence of effective field theories (EFTs) connected to the standard model through symmetries and lattice simulations of quantum chromodynamics (QCD). EFTs in this sequence are expansions around different low-energy limits of QCD, each with its own characteristics, scales, and ranges of applicability regarding energy and number of nucleons. The three main nuclear EFTs—chiral, pionless, and halo/cluster—are reviewed, highlighting their similarities, differences, and connections. The structural properties and reactions of nuclei that have been derived from the *ab initio* solution of the few- and many-body problem built upon EFT input are surveyed.

CONTENTS

[*]Hans-Werner.Hammer@physik.tu-darmstadt.de
[†]sekoenig@theorie.ikp.physik.tu-darmstadt.de
[‡]vankolck@ipno.in2p3.fr

I. INTRODUCTION

The challenge of obtaining the properties of atomic nuclei from the interactions among the constituent nucleons has been central to nuclear physics since its inception. Attempts to derive nuclear forces and currents from the exchange of mesons—in particular the lightest meson, the pion—were derailed in the 1950s by a lack of renormalizability, that is, by an uncontrolled sensitivity to physics at short distances.[1] The

---

[1]Not long after the successful renormalization of QED, it was understood that the only relativistic pion-nucleon coupling that is renormalizable in the same sense is pseudoscalar (Matthews and Salam, 1951). However, pseudoscalar coupling differs from pseudo-vector coupling by a large nucleon-pair term, which was found to be in conflict with pion phenomenology (Marshak, 1952). The favored pseudovector coupling required the introduction of short-distance cutoffs, on which the description of two-nucleon data depended sensitively; see, for example, Gartenhaus (1955). Subsequent work increasingly emphasized the phenomenology of short-range interactions. A brief history of nuclear potential models was given by Machleidt and Entem (2011) and Machleidt (2017).

rise in the 1970s of a renormalizable theory of strong interactions, quantum chromodynamics (QCD), did not immediately offer a path forward: because QCD, formulated in terms of quarks and gluons, is nonperturbative for processes characterized by external momenta $Q \lesssim M_{QCD} \sim 1$ GeV, it is difficult to calculate the properties of hadrons and nuclei, a problem that becomes more severe as the number A of nucleons increases. Yet a precise and accurate description of nuclei is crucial for the transition from the perturbative regime of the standard model to the atomic domain and beyond, governed by QED and its small fine-structure constant. Examples relying on input from nuclear physics include tests of fundamental symmetries (such as neutrinoless double-beta decay to probe lepton-number violation) and reactions in astrophysical environments.

About a quarter of a century ago, effective field theories (EFTs) entered nuclear physics (Weinberg, 1990, 1991, 1992; Rho, 1991; Ordóñez and van Kolck, 1992; van Kolck, 1993). EFTs had been developed in particle and condensed-matter physics to deal with systems containing multiple momentum scales. An EFT captures the most general dynamics among low-energy degrees of freedom that is consistent with some assumed symmetries. In nuclear physics, where the symmetries of QCD are known, an EFT provides a realization of QCD in terms of hadrons instead of quarks and gluons. All details of the QCD dynamics at short distances are encoded in the EFT interaction strengths (*Wilson coefficients* or *low-energy constants*). Scattering amplitudes and their poles representing bound states and resonances are calculated as expansions in Q/M_{hi} and M_{lo}/M_{hi}, with M_{hi} the momentum scale where the EFT breaks down and M_{lo} the low-energy scales of physics we want to capture. An EFT is renormalizable in the sense that at each order in the expansion the sensitivity to unaccounted short-distance physics is small, that is, of relative $\mathcal{O}(Q/M_{hi}, M_{lo}/M_{hi})$. EFTs opened the door to a description of nuclear phenomena with systematic error estimates.

EFTs have, in fact, revolutionized nuclear physics. Most of the *ab initio* studies of nuclear structure, based on the explicit solution of the Schrödinger equation or its equivalents, are now carried out with potentials inspired by EFT. A host of nuclear properties have been predicted or postdicted from two- and three-nucleon forces and one- and two-body currents, with low-energy constants determined from $A \leq 3$ experimental data. In parallel, starting with Beane *et al.* (2006), fully dynamical simulations of QCD on a discretized and boxed spacetime have been able to access some $A \leq 4$ properties. Matching an EFT to results from lattice QCD (LQCD) allows for a determination of the low-energy constants without direct input from experiment. EFTs thus build a bridge between QCD and nuclear structure and reactions.

Historically, the first nuclear EFT was *chiral* (or *pionful*) EFT (Weinberg, 1990, 1991, 1992; Rho, 1991; Ordóñez and van Kolck, 1992; van Kolck, 1993), which is designed for momenta of the order of the pion mass. In addition to nucleons, it includes explicit pions, whose interactions are constrained by an approximate global symmetry of QCD, the chiral symmetry of independent flavor rotations of left- and right-handed quarks. Chiral EFT generalizes a popular

hadronic EFT, chiral perturbation theory (ChPT) (Weinberg, 1979; Gasser and Leutwyler, 1984, 1985), to $A \geq 2$. Despite its phenomenological successes, chiral EFT has proven to be extremely challenging to renormalize due to the singularity of the dominant interactions, which have to be treated non-perturbatively to produce bound states and resonances, i.e., nuclei. Originally conceived as a renormalization playground, a simpler EFT, *pionless* (or *contact*) EFT, focuses on momenta below the pion mass (van Kolck, 1997, 1999b; Bedaque, Hammer, and van Kolck, 1998, 1998; Kaplan, Savage, and Wise, 1998a, 1998b; Birse, McGovern, and Richardson, 1999). This EFT, whose renormalization is relatively well understood, is constrained only by QCD spacetime symmetries. It exhibits a high degree of universality, and except for the degrees of freedom it is formally identical to other EFTs where all interactions are of short range. Light nuclei are well described within the same framework that has been successful for atomic systems with large scattering lengths (for example, near a Feshbach resonance) (Braaten and Hammer, 2006). A variant of this EFT (*halo/cluster EFT*) has been applied (Bertulani, Hammer, and van Kolck, 2002, 2003) to bound states and reactions involving halo and cluster nuclei, characterized by such low energies that one or more tight clusters of nucleons can be treated as elementary degrees of freedom.

No doubt there are "more effective" EFTs to be discovered for larger nuclei. In fact, a description of rotational and vibrational bands in heavy nuclei was initiated by Papenbrock (2011), with successful applications to different nuclei and processes (Papenbrock and Weidenmueller, 2014; Coello Pérez and Papenbrock, 2015, 2016; Chen *et al.*, 2018; Coello Pérez, Menéndez, and Schwenk, 2018a, 2018b; Chen *et al.*, 2019). These recent developments extend the EFT paradigm to generalized degrees of freedom that capture the low-energy physics of deformed nuclei.

Here we present a summary of the main ideas, achievements, and prospects for nuclear EFTs formulated in terms of nucleons and clusters thereof. These theories can be thought of as a tower of EFTs at successively lower M_{hi}, starting at M_{QCD}. Our emphasis is not on phenomenology, but on the conceptual similarities and differences among chiral, pionless, and halo/cluster EFTs. Our hope is that a focused approach will stimulate a reformulation of our understanding of heavy nuclei, just as these EFTs have shed new light on the structure and reactions of light nuclei.

In the remainder of this section, some common aspects of nuclear EFTs are presented. Sections II–IV deal with one nuclear EFT each. In Sec. V, we address the connection between these EFTs and QCD, as well as broader applications. We conclude in Sec. VI. We use throughout units such that $\hbar = 1$ and $c = 1$.

A. Nuclei from the perspective of QCD

As an $\mathrm{SU}(3)_c$ gauge theory of colored quarks and gluons, QCD is characterized by a coupling constant g_s that becomes strong at low momenta. The fact that most hadron masses are about 1 GeV or higher, for example, the nucleon mass $m_N \simeq 940$ MeV, reveals that nonperturbative QCD phenomena are associated with a mass scale $M_{\mathrm{QCD}} \sim 1$ GeV. The

EFT at the scale of a few GeV includes not only strong interactions but also electroweak and even weaker interactions. In contrast to most textbooks, for convenience we refer to this EFT, which is our starting point, simply as QCD. Focusing on the two lightest (up and down) quarks most relevant to nuclear physics, the QCD Lagrangian is written in terms of quark $q = (u\,d)^T$, gluon G_μ, and photon A_μ fields as

$$\mathcal{L}_{\mathrm{QCD}} = \bar{q}[i\gamma^\mu(\partial_\mu + ig_s G_\mu + ieQA_\mu) + \bar{m}(1 - \varepsilon\tau_3)]q - \tfrac{1}{2}\mathrm{Tr}G_{\mu\nu}G^{\mu\nu} - \tfrac{1}{4}F_{\mu\nu}F^{\mu\nu} + \cdots, \tag{1}$$

where γ_μ and τ_i are the Dirac and Pauli matrices and $G_{\mu\nu}$ and $F_{\mu\nu}$ are the gauge and photon field strengths. Neglecting the ellipsis, which includes, for example, weak interactions, the only parameters in QCD are the quark masses and electromagnetic charges. We can express quark masses in terms of the common mass $\bar{m} = (m_u + m_d)/2 \sim 5$ MeV and of the relative mass splitting $\varepsilon = (m_d - m_u)/(m_u + m_d) \sim 1/3$. The quark charges are fractions $Q = \mathrm{diag}(2/3, -1/3)$ of the proton charge $e = \sqrt{4\pi\alpha} \sim 1/3$.

Below M_{QCD}, QCD is best represented as a theory of colorless hadrons, where $\mathrm{SU}(3)_c$ is realized trivially. An important role is played by pions, which arise as pseudo Goldstone bosons from the spontaneous breaking of approximate $\mathrm{SU}(2)_L \times \mathrm{SU}(2)_R$ chiral symmetry down to its vector subgroup $\mathrm{SU}(2)_V$ of isospin. In the chiral limit $\bar{m} = 0$, $\varepsilon = 0$, and $e = 0$, chiral symmetry is exact. Pions in this limit are massless and interact purely derivatively. Away from the chiral limit, the common quark mass breaks chiral symmetry explicitly and leads to a nonzero common pion mass $m_\pi \simeq 140$ MeV and nonderivative pion interactions. The QCD interactions associated with ε and e further break isospin and appear in relatively small quantities such as the pion mass splitting $\delta m_\pi^2 = m_{\pi^\pm}^2 - m_{\pi^0}^2 \simeq (36\text{ MeV})^2$ and the neutron-proton mass difference $\delta m_N = m_n - m_p \simeq 1.3$ MeV.

A more complete understanding of the low-energy consequences of QCD can be achieved if we consider alternative realities where $\bar{m}$, ε, and e are varied from their real-world values. To date, LQCD simulations of nuclear quantities have been carried out in the isospin-symmetry limit, where $\varepsilon = 0$ and $e = 0$. The only remaining QCD parameter $\bar{m}$ can be traded for the pion mass m_π. Because the signal-to-noise ratio for A-nucleon correlation functions at large time t scales as $\exp[-A(m_N - 3m_\pi/2)t]$ (Lepage, 1989a; Beane *et al.*, 2011), current simulations are limited to unphysically large m_π and to small A. Although one can expect future simulations at smaller pion masses and more nucleons, it is more efficient to switch to an EFT description suited to the large distances involved in nuclear physics.

Years of experience suggest that nuclei can be seen as bound states or resonances made out of nucleons, or perhaps clusters of nucleons. The choice of degrees of freedom determines the range of validity M_{hi} of the respective EFT. Because isospin violation is a relatively small effect for most nuclear dynamics (more so for light nuclei), we can classify nuclear EFTs by their regions of applicability according to typical momentum and pion mass; see Fig. 1. A possible
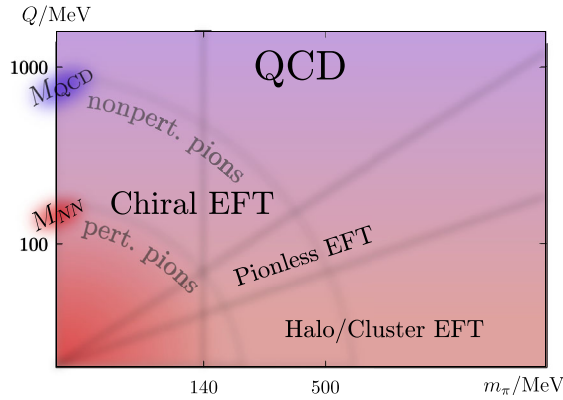
FIG. 1. Landscape of nuclear EFTs in the plane of typical momentum Q and pion mass m_π.

estimate of the typical binding momentum, where each nucleon contributes equally to the binding energy B_A, is $Q_A \sim \sqrt{2m_N B_A/A}$. Nuclear saturation for large A leads, at physical pion mass, to a constant $B_A/A \sim 10$ MeV and nuclear radii $R_A \sim R_0 A^{1/3}$, where $R_0 \sim 1.2$ fm. Numerically, $Q_A \sim R_0^{-1}$ is not that different from m_π, and it has been assumed that chiral EFT is best suited to typical nuclei. (In fact, we see in Sec. IV how $B_A/A \sim 10$ MeV arises naturally within chiral EFT.) At sufficiently small Q and m_π [i.e., below a scale $M_{NN} \sim 270$ MeV at the physical pion mass; see Eq. (76) for a precise definition], one expects pions to be perturbative. As Q increases at fixed m_π, chiral-symmetric pion interactions become nonperturbative for $A \geq 2$, and as Q increases further the EFT eventually ceases to converge. As m_π increases at fixed Q, chiral-symmetry breaking becomes more important and the chiral EFT expansion eventually fails again. We expect that $M_{hi} \sim M_{QCD}$, but the exact breakdown values of Q and m_π are not well known. It seems that for $A = 0$, for example, chiral EFT (in the form of ChPT) has $M_{hi} \leq 500$ MeV (Dürr, 2015).

Light nuclei are weakly bound, and radii scale differently than in the saturation regime. Pions can be treated as short-range interactions, and in pionless EFT we expect $M_{hi} \sim m_\pi$ at all m_π, including values beyond the breakdown of chiral EFT such as in LQCD simulations to date. For Q smaller than the inverse radius of a nucleus, the nucleus itself can be treated as an elementary particle in more complex systems where it appears as a subunit. In the halo/cluster EFT relevant for clusterized nuclei, $M_{hi} \sim R_c^{-1}$, the inverse cluster radius. Pionless and halo/cluster EFTs carry the information of QCD to the large distances of nuclear dynamics near the driplines.

B. The way of EFT

How does one ensure that a nuclear EFT reproduces QCD in the appropriate energy domain? Once degrees of freedom have been selected according to the energies of interest, one constructs the most general Lagrangian $\mathcal{L}$ involving the corresponding set of fields $\{\psi\}$, which is constrained only by the QCD symmetries,

$$\mathcal{L} = \sum_i c_i(M_{lo}, M_{hi}, \Lambda) O_i(\{\psi\}), \qquad (2)$$

where the $O_i(\{\psi\})$ are operators that involve fields at the same spacetime point but contain an arbitrary number of derivatives and $c_i(M_{lo}, M_{hi}, \Lambda)$ are the low-energy constants (LECs). Here Λ denotes an arbitrary regulator parameter with dimension of mass. With $\mathcal{L}$ or the corresponding Hamiltonian, the propagation and interaction of the low-energy degrees of freedom can be calculated. The procedure might be entirely perturbative, as represented by Feynman diagrams with a finite number of loops, or partially nonperturbative, as obtained by an infinite sum of Feynman diagrams or the solution of an equivalent integral or differential equation such as, respectively, the Lippmann-Schwinger or the Schrödinger equation. In either case, the interactions are singular, which requires regularization. When the calculation can be reduced to a finite number of loops, dimensional regularization can be employed, which introduces a renormalization scale μ. However, in nuclear physics we are most often faced with summing an infinite number of loops with overlapping momenta that, with present techniques, can be made finite only by the introduction, at either interaction vertices or propagators, of a momentum-regulator function $f(p/\Lambda)$ such that $f(0) = 1$ and $f(x \to \infty) = 0$. Here p refers to the momentum of a nucleon, in which case the regulator is separable, or the transferred momentum, when the regulator is nonseparable. We can alternatively look at position space, where the nonseparable regulator is local (i.e., a function of position only) and the separable regulator is nonlocal.

The goal is to construct the T matrix for a low-energy process as an expansion in $Q/M_{hi} < 1$. Schematically,

$$T(Q) = \mathcal{N} \sum_{\nu=0}^{\infty} \left(\frac{Q}{M_{hi}}\right)^\nu F^{(\nu)}\left(\frac{Q}{M_{lo}}, \frac{Q}{\Lambda}; \gamma^{(\nu)}\left(\frac{M_{lo}}{M_{hi}}, \frac{\Lambda}{M_{hi}}\right)\right), \quad (3)$$

where $\mathcal{N}$ is a normalization factor, $F^{(\nu)}$ is a function generated by the dynamics of the $\{\psi\}$, $\gamma^{(\nu)} = \mathcal{O}(1)$ is a dimensionless combination of the c_i, and ν is a counting index. "Power counting" is the relation between ν and the interaction label i in Eq. (2). While the form of the O_i in the Lagrangian (2) depends on the choice of fields, the expansion (3) must not (Chisholm, 1961; Kamefuchi, O'Raifeartaigh, and Salam, 1961). Likewise, observables obtained from Eq. (3) must not depend on the arbitrary regularization procedure— *renormalization-group (RG) invariance*.

Once the expansion (3) has been achieved, one can truncate the sum at a given $\nu = \mathcal{V}$ with a small error,

$$T(Q \sim M_{lo}) = T^{(\mathcal{V})}(Q, \Lambda)\left[1 + \mathcal{O}\left(\frac{Q^{\mathcal{V}+1}}{M_{hi}^{\mathcal{V}+1}}\right)\right]. \qquad (4)$$

Before renormalization, non-negative powers of Λ can appear that originate in the short-distance part of the loops. The uncertainty principle ensures that such contributions cannot be separated from that of LECs. Renormalization is the procedure that fixes the cutoff dependence of the LECs so that the

truncated amplitude $T^{(\mathcal{V})}(Q, \Lambda)$ satisfies approximate RG invariance,

$$\frac{\Lambda}{T^{(\mathcal{V})}(Q, \Lambda)} \frac{dT^{(\mathcal{V})}(Q, \Lambda)}{d\Lambda} = \mathcal{O}\left(\frac{Q^{\mathcal{V}+1}}{M_{\mathrm{hi}}^{\mathcal{V}} \Lambda}\right). \quad (5)$$

This condition ensures the error introduced by the arbitrary regularization procedure is no larger than the Q/M_{hi} error stemming from the neglect of higher-order terms in Eq. (4), as long as $\Lambda \gtrsim M_{\mathrm{hi}}$. In this "modern view" of renormalization, there is no need to take the $\Lambda \to \infty$ limit (Lepage, 1989b). However, while in analytical calculations Eq. (5) can be verified explicitly, in numerical calculations varying the regulator parameter widely above the breakdown scale is usually the only tool available to check RG invariance. In contrast, $\Lambda < M_{\mathrm{hi}}$ generates relatively large errors from the regularization procedure. Failure to satisfy Eq. (5) altogether means uncontrolled sensitivity to short-distance physics: results depend on the value of Λ and on the choice of the regulator function $f(x)$, which acquires the status of a physical, model-dependent *form factor*.

After renormalization, when the contribution from momenta of the order of the large cutoff have been removed, the dominant terms in loop integrals come from momenta of $\mathcal{O}(Q)$. Counting powers of Q in individual contributions to Eq. (3) is similar to determining the superficial degree of divergence of diagrams. There is, in general, also residual Λ dependence [Eq. (5)] that can be absorbed in the LECs of higher-derivative interactions. Since shuffling short-range physics between loops and LECs does not change the observables, the finite part of an LEC is expected to be set by the replacement $\Lambda \to M_{\mathrm{hi}}$ [see, for example, Veltman (1981)],[2] which then places an upper bound on the order at which these interactions appear. The exception is when a symmetry suppresses the corresponding interaction ('t Hooft, 1980). "Naturalness" assumes that all terms in the effective Lagrangian (respecting the relevant symmetries) have dimensionless coefficients of $\mathcal{O}(1)$ when the appropriate powers of M_{lo} and M_{hi} are factored out. Renormalization is thus a powerful tool to estimate the sizes of the LECs.

This framework is a generalization of the ancient requirement of renormalizability by a finite set of parameters. If all interactions needed for Eq. (5) are present at each order, the resulting S matrix incorporates the relations among QCD S-matrix elements demanded by symmetries, with no other assumption than an expansion in $Q/M_{\mathrm{hi}} < 1$. Every low-energy observable depends on a finite number of LECs at leading order (LO), where $\mathcal{V} = 0$, a few more at next-to-leading order (NLO), where $\mathcal{V} = 1$, etc. Once the LECs are determined from a finite number of data, all other observables can be predicted or postdicted with a controlled error. Traditionally, the input data have been experimental, but LQCD results can now be used instead (Barnea *et al.*, 2015; Beane *et al.*, 2015; Kirscher *et al.*, 2015).

One of the virtues of the model independence encoded in Eq. (5) is that it provides an *a priori* estimate of theoretical errors. At the simplest level, errors can be estimated from the higher-order terms in Eq. (4) with a guess for M_{hi}. A lower bound on the theoretical error is provided by cutoff variation from M_{hi} to much higher values. The breakdown scale M_{hi} itself can be inferred by comparing the energy dependence at various orders with the data (Lepage, 1997). Reliance on data can be minimized by using instead EFT results at different cutoffs (Grießhammer, 2016). Up to now both data fitting and propagation of errors have employed standard statistical analyses previously used for models. However, these methods can lead to biases because they are not particularly well suited to the *a priori* EFT error estimates, which typically increase with Q, while experimental data are sometimes more precise at higher Q. A comprehensive theory of EFT error analysis based on Bayesian methods is currently being developed (Schindler and Phillips, 2009; Furnstahl, Klco *et al.*, 2015; Furnstahl, Phillips, and Wesolowski, 2015; Wesolowski *et al.*, 2016), with the promise of becoming the standard in the field.

C. Nuclear EFTs

The implementation of these ideas in nuclear physics has posed some unexpected challenges. They can be traced to the fact that at LO some interactions need to be fully iterated, or, equivalently, a dynamical equation should be solved exactly, to produce the bound states and resonances that we refer to as nuclei.

Nuclear EFTs typically include fields for the nucleon or clusters of nucleons. These particles have masses of $\mathcal{O}(M_{\mathrm{QCD}})$, and the expansion (3) includes a Q/m_N expansion around the nonrelativistic limit. Creation of virtual heavy particle-antiparticle pairs takes place at small distances $r \lesssim 1/(2m_N)$, and its effects can be absorbed in the LECs. As a consequence, a process involving A heavy particles is not affected by interactions in Eq. (2) involving more than $2A$ fields associated with these heavy particles. The simplest way to incorporate the fact that the large particle rest energy does not play a role is to employ a *heavy field* from which the trivial evolution factor due to the rest energy is removed (Jenkins and Manohar, 1991a). Lorentz invariance for these fields is encoded in *reparametrization invariance* (Luke and Manohar, 1992). Kinetic terms reduce to the standard nonrelativistic form that respects Galilean invariance, with relativistic corrections suppressed by inverse powers of m_N appearing at higher orders.

There is a crucial difference between $A = 1$ and $A \geq 2$ processes. The former also involve light particles (e.g., photons) in initial and final states with momenta $Q \sim M_{\mathrm{lo}}$. They deposit on the nucleon an energy of $\mathcal{O}(Q)$ that is larger than the recoil of $\mathcal{O}(Q^2/(2m_N))$, so the nucleon is essentially static and the deviation from the static limit can be treated as a perturbation. Intermediate states differ in energy from the initial state by an amount of $\mathcal{O}(Q)$. In contrast, there are Feynman diagrams for the T matrix of an $A \geq 2$ process, whether it involves external probes or not, that include intermediate states that differ in energy from the initial state by only a small difference in nucleon kinetic energies of $\mathcal{O}(Q^2/(2m_N))$. In these *reducible* diagrams nucleons are not static, and there is an infrared (IR) enhancement relative to intermediate states for $A = 1$ processes (Weinberg, 1991).

---

[2]Burgess (2015) offers a clear discussion in the specific context of the cosmological constant.

Nucleon recoil cannot be treated perturbatively, although relativistic corrections remain small.

The "full" nuclear potential V is defined as the sum of irreducible diagrams for a process involving A nucleons in initial and final states. The T matrix (3) is obtained by sewing potential subdiagrams with nucleon lines representing the free A-body Green's function G. This gives rise to the Lippmann-Schwinger equation, schematically

$$T = V + \int VGT = V + \int VGV + \cdots, \quad (6)$$

or alternatively to the Schrödinger equation and its many-body relatives. The full potential so defined involves all A bodies but includes components with $1 \le C \le A - 1$ separately connected pieces. Frequently, the potential is thought of as one of these connected pieces. One thus defines the A-nucleon (AN) potential as the sum of diagrams with $C = 1$ in the A-nucleon system. For $A = 2$, all diagrams in the nuclear potential are connected ($C = 1$), but starting at $A = 3$ multiply connected diagrams appear, i.e., the full potential is made up of a sum of fewer-body potentials. Diagrams with $C = A - 1$ are made out of the $2N$ potential and $A - 2$ disconnected nucleon lines. Diagrams in the full potential that have $1 < C < A - 1$ are made of combinations of lower-A potentials and disconnected nucleon lines.

In contrast to phenomenological models, all mesons with masses $\gtrsim M_{\rm QCD}$ and nucleon excitations heavier than the nucleon by the same amount can be integrated out because their effects can be captured by the LECs. As we see in Sec. II, in pionless EFT the potential consists purely of contact interactions, while in chiral EFT pion exchanges are present as well; see Sec. IV. In either case, the potential involves small transfers of energy $\mathcal{O}(Q^2/(2m_N))$, and the total exchanged four-momentum is close to the total transferred three-momentum. Dependence on the latter translates into a function of the position in coordinate space: the potential is local. Meanwhile, dependence on other nucleon momenta leads to derivatives with respect to position, i.e., the momentum operator in quantum mechanics, and the potential becomes nonlocal. We expect to be able to expand the potential in momentum space analogously to Eq. (3),

$$V(Q, \Lambda) = \sum_{\mu=0}^{\infty} V^{(\mu)}(Q, \Lambda) = \tilde{\mathcal{N}} \sum_{\mu=0}^{\infty} \left(\frac{Q}{M_{\rm hi}}\right)^{\mu} \tilde{F}^{(\mu)} \left(\frac{Q}{M_{\rm lo}}; \frac{Q}{\Lambda}; \tilde{\gamma}^{(\mu)}\left(\frac{M_{\rm lo}}{M_{\rm hi}}, \frac{\Lambda}{M_{\rm hi}}\right)\right), \quad (7)$$

where $\tilde{\mathcal{N}}$ is a normalization factor,[3] $\tilde{F}^{(\mu)}$ are functions obtained from irreducible diagrams, $\tilde{\gamma}^{(\mu)} = \mathcal{O}(1)$ are dimensionless combinations of c_i, and μ is a counting index for the potential.

When the nucleus is struck by low-momentum external probes (photons, leptons, and perhaps pions), similar considerations apply. One can define nuclear currents, or reaction kernels, as the sum of irreducible diagrams to which the probes are attached. Currents again involve all A nucleons but include disconnected diagrams. A subtlety is that a probe can deposit an energy $\mathcal{O}(Q)$ on a nucleon line, and thus there can be purely nucleonic intermediate states in irreducible diagrams. Observables come from the sandwich of currents between wave functions of the initial and final states. Currents have an expansion similar to Eq. (7).

The nuclear potential and associated currents can always be defined as such intermediate quantities between $\mathcal{L}$ and T. We have reduced the EFT to a quantum-mechanical problem, but one in which the form of the potential and currents is determined. This is a distinct improvement over a purely phenomenological approach, particularly in what concerns the bewildering variety of many-body potentials and currents one can construct. This feature is one of the major reasons for the dominant role nuclear EFTs now play in the nuclear theory community.

However, one should keep in mind that the potential and currents are not directly observable. There are important differences between Eqs. (7) and (3):

- The potential does not need to obey an equation such as Eq. (5). EFT potentials involve terms that are singular and often attractive, in the sense that they diverge faster than $-1/(4m_N r^2)$ as the relative position $r \to 0$. The potential would generate strong regulator dependence in Eq. (6) integrals if it did not itself depend strongly on Λ; see, e.g., the pedagogical discussion by Lepage (1997).
- Since after renormalization Λ disappears from T (apart from arbitrarily small terms),

$$\int VGV \sim \frac{Q^3}{4\pi} \frac{m_N}{Q^2} V^2 \sim \frac{m_N Q V}{4\pi} V, \quad (8)$$

and the expansion (6) is in the dimensionless ratio $m_N QV/(4\pi)$ (Bedaque and van Kolck, 2002). For $Q \gtrsim 4\pi/m_N V^{(0)}$, $F^{(0)}$ in Eq. (3) stems from an infinite iteration of the LO potential $V^{(0)}$. This is good because nuclear bound states and resonances, as poles of T matrices, can be obtained only from a nonperturbative LO.

- Equations (7) and (6) do not imply that all terms in V should be treated on the same footing. One cannot immediately identify μ with ν because a term in V contributes to various orders in the T matrix. Higher-order

---

[3]Note that in the units we use the momentum-space potential, like the T matrix, has mass dimension -2. Its Fourier transform, which involves three powers of momentum, has mass dimension $+1$, as it should.

$F^{(\nu>0)}$ can be obtained from $V^{(\mu>0)}$ in a distorted-wave Born expansion: $F^{(1)}$ from a single insertion of $V^{(1)}$, $F^{(2)}$ from a single insertion of $V^{(2)}$ or two insertions of $V^{(1)}$, etc. Treating the potential truncated at a subleading order exactly, i.e., treating it as a phenomenological potential, is in general not correct from a renormalization point of view. In an expansion in Q, the potential gets more and more singular with increasing order. Resumming a partial subset of higher-order terms will in general not include all LECs needed for proper renormalization.[4]

The agelong challenge in nuclear physics has been to achieve RG invariance when some interactions are nonperturbative and some others can be treated as small. In an EFT that translates into the nontrivial task of developing a power counting that guarantees Eqs. (4) and (5). In a purely perturbative context the cutoff dependence of loops can be obtained analytically. Assuming naturalness and looking at individual loop diagrams, a simple rule has been devised for the size of the LECs needed for perturbative renormalization (Manohar and Georgi, 1984; Georgi and Randall, 1986). This *naive dimensional analysis* (NDA) states that, for an operator O_i in Eq. (2) with canonical dimension D_i involving N_i fields ψ,

$$c_i = \mathcal{O}\left(\frac{(4\pi)^{N_i-2}}{M_{\mathrm{QCD}}^{D_i-4}} c_{i\,\mathrm{red}}\right), \qquad (9)$$

where the dimensionless *reduced* LEC $c_{i\,\mathrm{red}}$ is of the order of the combination of reduced QCD parameters that give rise to it. Examples for chiral perturbation theory are given in Sec. IV. It is, however, not immediately obvious that NDA applies to LECs of operators involving four or more nucleon fields subject to nonperturbative renormalization, i.e., which are renormalized once LO interactions are resummed. In fact, as we see later, cutoff variations in the Lippmann-Schwinger equation (6) require significant departures from NDA for contact interactions among nucleons. These departures were first understood within pionless EFT. Its simplicity makes pionless EFT the poster child for nuclear EFT, and we therefore make it the start of this review.

II. PIONLESS EFT

A. Motivation

At very low energies, i.e., for momenta $Q \ll m_\pi$, few-nucleon systems are not sensitive to the details associated with

pion or other meson exchange. This fact makes it possible to describe such systems with short-range interactions alone (i.e., interactions of finite range or falling off at least as an exponential in the interparticle distance), an approach dating back to Bethe and his effective-range expansion (ERE) for nucleon-nucleon (NN) scattering (Bethe, 1949); see also related work by Bethe and Peierls (1935a, 1935b), Fermi (1936), Schwinger (1947), and Jackson and Blatt (1950). Casting this basic idea into a modern systematic framework leads directly to what has become known as pionless EFT.

Historically, pionless EFT emerged out of an effort to understand the renormalization of EFTs where a certain class of interactions need to be treated nonperturbatively. It had been shown by Kaplan, Savage, and Wise (1996), Phillips, Beane, and Cohen (1998), and Beane, Cohen, and Phillips (1998) that the original prescription (Weinberg, 1990, 1991) to extend chiral perturbation theory to few-nucleon systems (discussed in Sec. IV) could not be implemented while satisfying RG invariance. It turned out that there is a surprisingly rich structure of phenomena in the low-energy regime where explicit pion exchange cannot be resolved.

Formally, the pion can be regarded as "integrated out" if all other dynamical scales are much smaller than the pion mass. Consider, for example, the Yukawa potential corresponding to the one-pion exchange:

$$\langle \mathbf{k}'|V_{2N,\pi}|\mathbf{k}\rangle \propto \frac{1}{\mathbf{q}^2 + m_\pi^2}, \qquad \mathbf{q} = \mathbf{k}' - \mathbf{k}, \qquad (10)$$

where $\mathbf{k}$ and $\mathbf{k}'$ are incoming and outgoing momenta of two scattered nucleons (in their center-of-mass frame). If these are both small compared to m_π, Eq. (10) can be expanded in $\mathbf{q}^2$, with the leading term being just a constant and the following terms involving ever higher powers of $\mathbf{q}^2$. This shrinking of the original interaction to a point is illustrated in Fig. 2. Fourier transforming into configuration space one obtains a series of delta functions with a growing number of derivatives. In chiral EFT, which includes pions, analogous contact interactions represent the exchange of heavier mesons. Integrating out pions to arrive at pionless EFT means merging unresolved pion exchange with these operators. It should be noted, however, that chiral EFT is based on an expansion around a vanishing pion mass, whereas pionless EFT treats m_π as a large scale. As such, these two EFTs are significantly different—in particular, the respective LECs cannot in general be related by perturbative matching—but they are both well-defined low-energy limits of QCD.

In practice, one does not have to derive pionless EFT from a more fundamental EFT by integrating out explicit pions. Instead, one can just follow the EFT paradigm and write down

---

[4]An example of resummation of higher-order interactions is found in lattice implementations of nonrelativistic QCD (NRQCD) (Thacker and Lepage, 1991). In heavy quark effective theory, all Q/m_Q corrections in the heavy quark mass m_Q are treated perturbatively, and lattice simulations have a continuum limit (Sommer, 2010). For NRQCD, lattice practice is to treat exactly not only heavy quark recoil but also the associated, subleading gluon interactions. Thus, only for relatively large values of the lattice spacing a do observables look like they might converge, before $1/a$-type effects take over. There are also situations where one can resum higher-order interactions without introducing essential regulator dependence. An example is given by Lepage (1997).
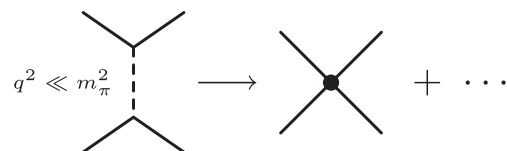

FIG. 2. Reduction of pion exchange (dashed line) to a series of contact interactions between nucleons (solid lines) for $q^2 \ll m_\pi^2$.

an effective Lagrangian, Eq. (2), with all contact interactions between nucleons that are allowed by symmetry. This restriction means that one requires invariance under "small" Lorentz boosts (Galilean boosts plus systematic relativistic corrections), rotations, isospin, and discrete symmetries like parity and time reversal, the systematic breaking of which can also be accounted for. The same EFT with other particles substituted for nucleons can describe different systems where the important dynamics takes place at distances beyond the range of the force. Some of these systems are discussed in Secs. III and V. In particular, pionless EFT captures the universal aspects of Efimov physics (Braaten and Hammer, 2006).

In this section, we discuss the basic features and formalism of pionless EFT, first in the context of two-body systems (Sec. II.B) and later for a larger number of particles (Sec. II.C). Some of the outstanding issues are raised in Sec. II.D.

B. Weakly bound S-wave systems

Two very-low-energy particles, represented by a field ψ, can be described by an effective Lagrangian

$$
\mathcal{L} = \psi^\dagger \left(i\partial_0 + \frac{\nabla^2}{2m_N} \right) \psi - \frac{C_0}{2} (\psi^\dagger \psi)^2
$$
$$
+ \frac{C_2}{16} [(\psi\psi)^\dagger (\psi \overset{\leftrightarrow}{\nabla}^2 \psi) + \text{H.c.}] + \cdots, \quad (11)
$$

where $\overset{\leftrightarrow}{\nabla} = \overset{\leftarrow}{\nabla} - \overset{\rightarrow}{\nabla}$ is the Galilei-invariant derivative and H.c. denotes the Hermitian conjugate. The ellipsis represents local operators with other combinations of derivatives, including relativistic corrections. Here we adopt the notation of Hammer and Furnstahl (2000), but various forms for the Lagrangian—differing by prefactors absorbed in the low-energy constants (C_0, C_2, etc.) or choice of equivalent operators—exist in the literature. One can treat the two NN S-wave channels ($^3S_1$ or $^1S_0$, in the spectroscopic notation $^{2s+1}l_j$, where l, s, and j denote, respectively, orbital angular momentum, spin, and total angular momentum) simultaneously using a nucleon field N that is a doublet in spin and isospin space. We come back to this after discussing the general features of the two-body sector on the basis of Eq. (11).

1. Two-body scattering amplitude

To fill the theory described by the effective Lagrangian (11) with physical meaning, we need to equip it with a power counting. We seek an expansion taking the form of Eq. (3) where M_{hi} is expected to be set by the pion mass m_π since pion exchange has been integrated out. In particular, we want to reproduce the ERE (Bethe, 1949) for the on-shell NN scattering amplitude:

$$
T(k, \cos\theta) = -\frac{4\pi}{m_N} \sum_l \frac{(2l+1)P_l(\cos\theta)}{k \cot\delta_l(k) - ik}, \quad (12a)
$$

$$
k^{2l+1} \cot\delta_l(k) = -\frac{1}{a_l} + \frac{r_l}{2} k^2 + \mathcal{O}(k^4), \quad (12b)
$$

with a Legendre polynomial P_l, the scattering angle θ, and energy $E = k^2/m_N$ in the center-of-mass frame, and where $\delta_l(k)$ is the scattering phase shift in the lth partial wave, while

a_l and r_l denote the corresponding scattering length and effective range, respectively. Here we focus on S waves with $l = 0$. Higher partial waves are discussed later.

In a "natural" scenario, the LECs C_{2n} in Eq. (11) scale with inverse powers of their mass dimension, e.g., $C_0 \propto M_{\text{hi}}^{-1}$. (Note that an overall scaling with $1/m_N$ from the non-relativistic framework is shared by all terms in the effective Lagrangian.) In this case, to lowest order T is simply given by the tree-level C_0 vertex, and we can identify $C_0 = 4\pi a_0/m_N$. However, the low-energy NN system is not natural. From the relation for C_0, it is immediately clear what this means here: the actual NN scattering lengths $a_{1S_0} \simeq -23.7$ fm and $a_{3S_1} \simeq 5.4$ fm are large compared to the pion Compton wavelength $m_\pi^{-1} \simeq 1.4$ fm, so $C_0 = 4\pi a_0/m_N$ is incompatible with $C_0 \propto M_{\text{hi}}^{-1}$ if one assumes $M_{\text{hi}} \sim m_\pi$. Turning the argument around, the perturbative expansion in C_0 has a breakdown scale set by $1/a_0 \ll m_\pi$, rendering it useful only for the description of extremely low-energy NN scattering.

The physical reason for the rapid breakdown of the perturbative expansion is that the large NN S-wave scattering lengths correspond to low-energy ("shallow") bound states (virtual, in the case of the $^1S_0$ channel). For example, it is well known that the deuteron binding momentum $\gamma_d = \sqrt{m_N B_d} \simeq 45.7$ MeV is given at about 30% accuracy by $1/a_{3S_1}$. These states directly correspond to poles of the amplitude T (located on the imaginary axis of the complex k plane, or on the negative energy axis in the first or second Riemann sheet). It is clear that a Taylor expansion of T in k^2 converges only up to the nearest pole in any direction in the complex plane. Thus, the presence of the shallow NN bound states limits the range for a perturbative description of NN scattering.

A nonperturbative treatment is necessary to generate poles in T since a finite sum of polynomials can never have a pole. As pointed out by Weinberg (1991), this can be achieved by "resumming" the C_0 interaction, i.e., by writing the LO amplitude as the tree-level C_0 diagram plus any number of C_0 vertices with intermediate propagation, as shown in Fig. 3; see also the related analysis by Luke and Manohar (1997). The result for a single generic NN channel is

$$
T^{(0)} = C_0 + C_0 I_0(k)C_0 + C_0 I_0(k)C_0 I_0(k)C_0 + \cdots
$$
$$
= [C_0^{-1} - I_0(k)]^{-1}, \quad (13)
$$

where I_0 is the two-body "bubble integral," discussed in more detail later. Having C_0 now in the denominator means that it can be adjusted to give a pole at the desired position.

2. Power counting

The power counting of the theory should be such that it actually *mandates* this procedure. The small inverse NN scattering lengths introduce a genuine new low-momentum
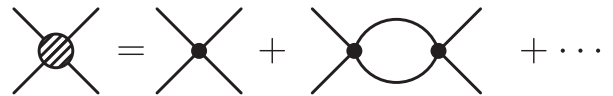

FIG. 3. Bubble chain for a generic S-wave NN scattering amplitude at LO from the C_0 interaction (solid circle).

scale M_{lo} or large length M_{lo}^{-1}. Typically, this is referred to as *fine-tuning* because the existence of this scale, at odds with the perfectly natural assumption that pion exchange should set the lowest energy scale, implies that different contributions from quarks and gluons have to combine in just the right way to produce this scenario; see Sec. V.A.

Equation (13) is simply Eq. (6) for a two-body potential C_0, which from the previous discussion is enhanced by a factor M_{lo}^{-1}. The loops connecting two insertions of the potential contain nucleon propagators, which from Eq. (11) we read off to be

$$iD_N(p_0, \mathbf{p}) = i\left(p_0 - \frac{\mathbf{p}^2}{2m_N} + \cdots + i\varepsilon\right)^{-1}. \qquad (14)$$

Here p_0 and $\mathbf{p}$ are the energy and momentum associated with a nucleon line in Fig. 3. If a total momentum $k \sim Q$ runs through the diagram, we see that after regularization effects are removed by renormalization the dominant contribution in a loop integral $dq_0 d^3q$ comes from the region where $q \sim Q$. Hence, keeping in mind that q_0 is a nonrelativistic kinetic energy $\sim q^2/m_N$, we count

$$\text{nucleon propagator} \sim m_N Q^{-2}, \qquad (15a)$$

$$\text{(reducible) loop integral} \sim (4\pi m_N)^{-1} Q^5. \qquad (15b)$$

Equations (15a) and (15b) lead directly to the estimate (8) and imply that the one-loop contribution in Fig. 3 scales like the tree-level one times a factor Q/M_{lo}. In fact, each additional dressing by one loop with a C_0 vertex contributes such a factor. Hence, in the regime where $Q \sim M_{\text{lo}} \ll M_{\text{hi}}$ each such diagram is equally important, and they all have to be summed up to get the LO amplitude nonperturbatively. On the other hand, for $Q \ll M_{\text{lo}}$ one can still use a perturbative approach, so the counting here is able to capture both scenarios.

Operators with derivatives in the effective Lagrangian must contain inverse powers of M_{hi} in order not to introduce additional low-energy poles in the LO T matrix. They provide corrections to the $2N$ potential,

$$V_{2N}(\mathbf{p}', \mathbf{p}) = C_0 + C_2(\mathbf{p}'^2 + \mathbf{p}^2) + \cdots. \qquad (16)$$

Being suppressed, higher orders can be calculated in perturbation theory and matched to an expansion of Eq. (12a),

$$T = \frac{4\pi}{m_N} \frac{1}{1/a_0 + ik}\left(1 + \frac{r_0 k^2/2}{1/a_0 + ik} + \cdots\right). \qquad (17)$$

The specific scaling with M_{hi} can be inferred from this and from regulator effects considered later.

For example, the NLO amplitude $T^{(1)}$ is the result of inserting a single C_2 vertex into each combination that can be formed with the LO amplitude (van Kolck, 1997, 1999b; Bedaque, Hammer, and van Kolck, 1998; Bedaque and van Kolck, 1998; Kaplan, Savage, and Wise, 1998a, 1998b), as shown in Fig. 4. Matching to the k^2 coefficient in Eq. (17) shows that the C_2 contributions are related to the effective ranges. Since the values of the NN S waves are $r_{^3S_1} \simeq 1.75$ fm
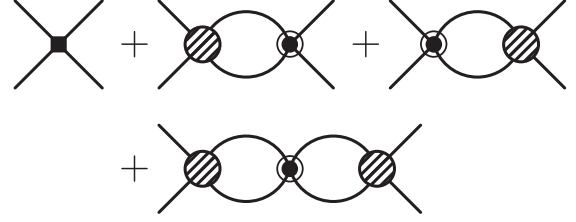

FIG. 4. NLO correction to the NN scattering amplitude from the C_2 interaction (circled circle).

and $r_{^1S_0} \simeq 2.7$ fm, and thus of the order $m_\pi^{-1} \sim M_{\text{hi}}^{-1}$, we conclude that C_2 is indeed an NLO effect,

$$\frac{C_2 Q^2}{C_0} \sim \frac{Q^2}{M_{\text{lo}} M_{\text{hi}}}. \qquad (18)$$

For comparison, given that the C_0 term is a dimension-6 operator, whereas the one with C_2 is dimension 8, the naive natural scaling is $C_2 Q^2/C_0 \sim (Q/M_{\text{hi}})^2$. The additional low-energy enhancement M_{lo} also occurs in the scaling of the C_2 parameters.

This procedure can be generalized to higher orders and other operators. At N^2LO we must consider two insertions of C_2 and one insertion of C_4; the latter is determined entirely in terms of r_0^2, the shape parameter emerging at N^3LO (Kaplan, Savage, and Wise, 1998a, 1998b; van Kolck, 1999b). Generally, enhancements depend on the partial waves involved. The interactions contributing to such waves are operators in the ellipsis of Eq. (11) that make T dependent on the scattering angle. There is no enhancement for operators that contribute only to higher waves as long as there are no other low-energy poles, as is the case in NN scattering. Thus, for example, a P-wave operator leading to a term $\propto \mathbf{k}' \cdot \mathbf{k}$ appears first at N^3LO. The enhancement is partial only for operators that connect an S wave to other waves. The short-range tensor force that connects S and D waves is present at N^2LO because it is enhanced by one power of M_{lo}^{-1} (Chen, Rupak, and Savage, 1999a). The lowest orders in the potential are shown schematically in Fig. 5.

Summarizing, the $2N$ potential (16) is a particularly simple form of Eq. (7) where there are no nonanalytic functions and

$$\mu = d/2 \quad (s_2 = 2), \qquad \mu = d + 1 - s_2 \quad (s_2 = 0, 1), \qquad (19)$$

$$\tilde{\mathcal{N}} = \mathcal{O}((4\pi)^{A-1} m_N^{-1} M_{\text{lo}}^{5-3A}), \qquad (20)$$

with $A = 2$, d the number of derivatives, and $s_2 = 0, 1, 2$ the number of S waves connected by the operator (van Kolck, 1997, 1999b; Bedaque, Hammer, and van Kolck, 1998; Bedaque and van Kolck, 1998; Kaplan, Savage, and Wise, 1998a, 1998b). Using the standard graph equalities to eliminate the number of internal lines I and loops L, $I = \sum_i V_i + L - 1$ and $I = -A + \sum_i f_i V_i/2$, where V_i is the number of vertices with f_i nucleon lines, we obtain Eq. (3) for the amplitude with
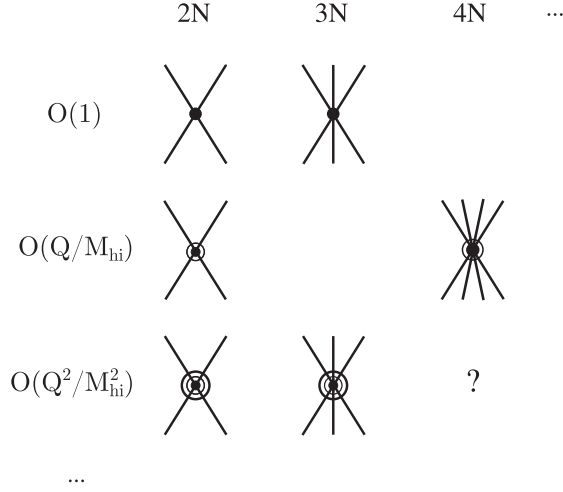
FIG. 5. Diagrams representing the AN nuclear potential in pionless EFT. The order of the contributions is indicated as $\mathcal{O}(Q^\mu/M_{\mathrm{hi}}^\mu)$, $\mu \geq 0$, where $Q \sim M_{\mathrm{lo}}$ and $M_{\mathrm{hi}} \sim m_\pi$, so that the circles around the central solid circle denote inverse powers of M_{hi}.

$$\nu = \sum_i V_i \mu_i, \qquad \mathcal{N} = \mathcal{O}((4\pi)^{A-1} m_N^{-1} M_{\mathrm{lo}}^{5-3A}). \quad (21)$$

Assuming $M_{\mathrm{lo}} \sim \gamma_d$, a rough estimate of the expansion parameter is $M_{\mathrm{lo}}/M_{\mathrm{hi}} \sim \gamma_d/m_\pi \sim 1/3$.

3. Regularization and renormalization

Loops in quantum field theory often do not converge, and the same is true in pionless EFT. Observables are rendered finite by renormalization. For example, if we introduce a separable regulator function $f(x)$ at the vertices, the nucleon bubble integral becomes

$$I_0(k) = m_N \int \frac{d^3q}{(2\pi)^3} \frac{[f(\mathbf{q}^2/\Lambda^2)]^2}{k^2 - \mathbf{q}^2 + i\varepsilon}$$
$$= -\frac{m_N}{4\pi}[\theta_1\Lambda - \sqrt{-k^2 - i\varepsilon} + \mathcal{O}(k^2/\Lambda)], \quad (22)$$

where θ_1 is a dimensionless number that depends on the form of $f(x)$ (for example, $\theta_1 = 2/\pi$ for a step function). With Eq. (12b) truncated at the scattering length as a renormalization condition, the choice

$$C_0(\Lambda) = \frac{4\pi}{m_N} \frac{1}{1/a_0 - \theta_1\Lambda} \quad (23)$$

ensures to this order that the physical amplitude is independent of Λ up to corrections that vanish as $\Lambda \to \infty$. The latter can be removed by higher-order LECs such as $C_2(\Lambda)$. It is the nonanalytic dependence on the energy, which is regulator independent, that characterizes a loop. The corresponding term in Eq. (22) is an explicit example of the estimates (15a) and (15b).

a. Schemes and power counting

In the early stages there was much confusion about whether or not the choice of regularization should be understood as

affecting the power-counting scheme. The difference between the *artificial* regulator parameter Λ and the breakdown scale M_{hi} of the theory has not always been appreciated. For example, Kaplan, Savage, and Wise (1998a) argued that $C_0 \propto \Lambda^{-1}$ would again give a theory with a very limited range of applicability. The need to choose $\Lambda \gtrsim M_{\mathrm{hi}}$ to suppress regulator artifacts of $\mathcal{O}(1/\Lambda)$ does seem to invalidate the scaling $C_0 \propto M_{\mathrm{lo}}^{-1}$, but there are correlations among the diagrams that are captured by determining $C_0(\Lambda)$ *after* resummation, reflecting the original M_{lo} counting.

If one uses dimensional regularization to render integrals finite, the I_0 bubble does not have a pole in four spacetime dimensions, so in the minimal subtraction scheme there is no divergence at all. Instead, Kaplan, Savage, and Wise (1998a) advocated explicitly subtracting the pole in three dimensions (corresponding to the linear divergence in the cutoff scheme), thereby introducing a renormalization scale μ that can be chosen freely and giving Eq. (23) with $\theta_1\Lambda \to \mu$. This procedure, called *power-divergence subtraction* (PDS), makes the need for resummation of the bubble diagrams more transparent. Picking $\mu \sim Q$, the *running* coupling C_0 scales like Q^{-1}, implying again that each diagram in Fig. 3 is of the same order. With this scheme, power counting is "manifest" in the sense that it is reflected by the scaling of coupling constants even after renormalization has been carried out. Phillips, Beane, and Birse (1999) showed that if *all* poles of a divergent loop integral are subtracted—like the original PDS, one particular choice of infinitely many possibly schemes—one recovers exactly the same result as with a simple momentum cutoff.

Under an appropriate power counting, changing the low-energy points used as renormalization conditions affects the running of the LECs by $1/\Lambda$ terms and leads to the same T matrix up to higher-order terms. Taking, for example, the pole position $i\gamma$ instead of zero energy generates the LO amplitude with $1/a_0 \to \gamma$; the relative difference is an NLO correction $\sim r_0/a_0 = \mathcal{O}(M_{\mathrm{lo}}/M_{\mathrm{hi}})$. While the *a priori* EFT error estimate is always determined by neglected higher orders, the freedom to choose what input parameters are used at a given order can improve agreement of the *central values* with experimental data. Gegelia (1999a) discussed the relation of subtractive renormalization to the previously mentioned approaches.

It was eventually realized (Lepage, 1997) that cutoff variation can be used (and is particularly useful in numerical calculations) as a diagnostic for missing interactions at a given order, an example of which is given in Sec. II.C.2. Long and Yang (2012b) pointed out that the leading *residual* cutoff dependence can be used to infer the existence of next-order operators. Equation (22), for example, indicates that $C_2 \propto M_{\mathrm{hi}}^{-1}$ for the residual dependence on $\Lambda \gtrsim M_{\mathrm{hi}}$ to be no larger than NLO. Thus, renormalization provides guidance for the power counting.

b. Subleading resummation

Experience with nonsingular potentials makes it almost automatic to solve the Schrödinger equation exactly with a truncation of the potential (16). At LO this is equivalent to the resummation (13). Renormalization of the truncation at the

level of C_2, however, leads to $r_0 \lesssim \Lambda^{-1}$ (Cohen, 1997; Phillips and Cohen, 1997; Scaldeferri *et al.*, 1997), a version of the so-called Wigner bound (Wigner, 1955). This is problematic for *NN* scattering where $r_0 > 0$. At first interpreted as a failure of EFT, this observation instead reveals the danger of resumming subleading singular potentials (van Kolck, 1999b). Such a resummation includes a subset of arbitrarily high-order contributions without all of the LECs needed for perturbative renormalization, such as C_4 when C_2 is inserted twice at N²LO. It is still possible to work with a fixed cutoff that reproduces r_0, at the cost of losing the ability to use cutoff variation $\Lambda \gtrsim M_{\mathrm{hi}}$ as a diagnostic for missing interactions. Moreover, there is no guarantee that results for other observables would be any better than those obtained from a perturbative treatment of subleading corrections. An example was given by Stetcu *et al.* (2010a).

4. Renormalization group

a. Running coupling

Imposing renormalizability of physical amplitudes leads to solutions of RG equations. Their detailed form depends on the regularization scheme. For example, for the dimensionless coupling constant $\hat{C}_0 \equiv m_N \mu C_0/(4\pi)$ one finds in PDS (Kaplan, Savage, and Wise, 1998a)

$$\mu \frac{d}{d\mu} \hat{C}_0 = \hat{C}_0(1 + \hat{C}_0), \qquad (24)$$

where the right-hand side is given by the beta function. It is convenient to consider the flow of $\hat{C}_0$ instead of C_0 to separate the behavior of the operator from the behavior of the coupling constant. The RG equation (24) has two fixed points: the free fixed point $\hat{C}_0 = 0$ and a nontrivial fixed point $\hat{C}_0 = -1$ (Weinberg, 1991), which correspond to $a_0 = 0$ and to the unitary limit $1/a_0 = 0$, respectively. Similar equations can be derived for all coupling constants in the effective Lagrangian, and the beta function, in general, changes as one goes to higher orders. Thus, the expansion in pionless EFT can be thought of as an expansion around the unitary limit of infinite scattering length, similar to the expansion in chiral EFT around the chiral limit of vanishing quark masses. An equation similar to Eq. (24) holds for a simple momentum cutoff Λ, leading then to Eq. (23). In dimensional regularization with minimal subtraction, on the other hand, the coupling C_0 is independent of μ (Kaplan, Savage, and Wise, 1996). In this scheme, the unitary limit cannot be reached for any finite value of the coupling.

b. Wilsonian renormalization group

The RG is generally useful for studying the behavior of the EFT. Extending previous work (Weinberg, 1990, 1991; Adhikari and Frederico, 1995; Adhikari and Ghosh, 1997; Beane, Cohen, and Phillips, 1998; Kaplan, Savage, and Wise, 1998a, 1998b, 1999; Phillips, Beane, and Cohen, 1998), Birse, McGovern, and Richardson (1999) studied the RG flow of an effective potential of the form

$$V_{2N}(\mathbf{p}', \mathbf{p}, k) = V_{2N}(\mathbf{p}', \mathbf{p}) + C_{02}k^2 + \cdots, \qquad (25)$$

where the additional energy-dependent terms compared to Eq. (16) come from a different choice of operators in the effective Lagrangian (11). It is possible to trade energy dependence for momentum dependence, and vice versa, by field redefinitions or, alternatively, by using the equation of motion. Within a Wilsonian formulation of the RG (Wilson, 1983), demanding that the off-shell amplitude stays invariant under a decrease in the momentum cutoff Λ in the Lippmann-Schwinger equation defines a running potential $V(p, p', k, \Lambda)$ that satisfies

$$\frac{\partial V}{\partial \Lambda} = \frac{m_N}{2\pi^2} V(p', \Lambda, k, \Lambda) \frac{\Lambda^2}{\Lambda^2 - k^2} V(\Lambda, p, k, \Lambda). \qquad (26)$$

Defining further a rescaled potential $\hat{V}$ by multiplying all quantities by appropriate powers of Λ, Birse, McGovern, and Richardson (1999) showed that in the limit where $\Lambda \to 0$ there exist two IR fixed points satisfying $\partial \hat{V}/\partial \Lambda = 0$. One of these, $\hat{V} = 0$, is trivial, whereas the second, nontrivial one corresponds to the unitary limit. Additional fixed points are accessible with further fine-tuning (Birse, Epelbaum, and Gegelia, 2016). An extensive study also including higher waves was carried out by Harada and Kubo (2006) and Harada, Kubo, and Ninomiya (2009). The RG analysis captures the results obtained from Feynman diagrams, which yield directly the solutions of the RG equations.[5] It unifies both the natural and fine-tuned cases discussed in Sec. II.B.2, and it is possible to derive the power counting for either case by studying perturbations of the potential around the fixed points.

5. Dibaryon fields

It is possible to efficiently capture the physics associated with the shallow *S*-wave two-body states by introducing in the effective Lagrangian *dimeron* (*molecular* or, here, *dibaryon*) fields with their quantum numbers, an idea first introduced in EFT by Kaplan (1997). For any single channel we can write, instead of Eq. (11),

$$\mathcal{L} = \psi^\dagger \left(i\partial_0 + \frac{\mathbf{\nabla}^2}{2m_N} \right) \psi + g[d^\dagger(\psi\psi) + \mathrm{H.c.}]$$
$$+ d^\dagger \left[\eta \left(i\partial_0 + \frac{\mathbf{\nabla}^2}{4m_N} \right) - \Delta \right] d + \cdots, \qquad (27)$$

where $\eta = \pm 1$ is a parameter that determines the sign of the effective range. It will be fixed to $\eta = -1$ in the remainder of this section to ensure that $r_0 > 0$. Instead of C_0 and C_2, we have the new parameters Δ (the *residual mass*) and g. With this choice, nucleons no longer couple directly, but only through the *s*-channel exchange of the dibaryon d. If one neglects the kinetic term for this field, it is possible to recover the leading terms in Eq. (11) by using the equation of motion for d,

---

[5]Weinberg (2005) gave a general discussion of the connection between the Wilsonian RG and the conventional renormalization program.

FIG. 6. Bubble sum for the dressed dibaryon propagator obtained from the bare propagator (double dashed line).

$$d = \frac{g}{\Delta} \psi\psi, \tag{28}$$

and identifying $C_0 = -g^2/\Delta$. Because of this redundancy, without loss of generality one may fix g at LO; a convenient choice is $g^2 \equiv 4\pi/m_N$ (Grießhammer, 2004) so that $\Delta = -1/a_0$ represents the low-energy scale M_{lo}. The d kinetic term leads to both energy- and momentum-dependent four-nucleon-field interactions, corresponding to a choice of operators that differs from Eq. (11) but can be shown to be equivalent up to higher orders and field redefinitions (Bedaque and Grießhammer, 2000).

The original bubble series with C_0 vertices turns into a self-energy correction for the dibaryon field. Whereas the tree-level bare propagator is just $iD(p_0, \mathbf{p}) = -i/\Delta$, summing up all bubble insertions as shown in Fig. 6 gives the full LO propagator as

$$iD^{(0)}(p_0, \mathbf{p}) = -i\left[\Delta + g^2 I_0\left(\sqrt{m_N p_0 - \mathbf{p}^2/4}\right)\right]^{-1}. \tag{29}$$

The center-of-mass NN scattering amplitude is recovered by attaching nucleon-dibaryon vertices on both ends: $T^{(0)} = -g^2 D^{(0)}(p_0 = k^2/m_N, \mathbf{p} = 0)$.

Not only is the dibaryon formalism useful to study processes with deuterons in the initial and/or final state (see the following), where it can conveniently be used as an interpolating field, but it also makes higher-order corrections particularly simple. For example, where before we had to insert C_2 vertices in different places (see Fig. 4), we now need only insert the dibaryon kinetic-energy operator into the LO propagator, giving

$$iD^{(1)}(p_0, \mathbf{p}) = i\left(p_0 - \frac{\mathbf{p}^2}{4m_N}\right)[D^{(0)}(p_0, \mathbf{p})]^2 \tag{30}$$

at NLO. As in the case without dibaryons, renormalization is carried out by relating $D^{(1)}$ to the NLO amplitude correction $T^{(1)}(k)$ and matching it to the effective-range term in Eq. (12b). A difference, however, is that now this is carried out with an energy-dependent operator—note the dependence of Eq. (30) on the Galilei-invariant energy $\tilde{p}_0 = p_0 - \mathbf{p}^2/4m_N$—whereas our choice of C_2 terms in Eq. (11) includes only momentum-dependent operators. The NLO component of g can be adjusted to reproduce r_0, and g and Δ are now independent. This means that these parameters have RG runnings that differ from those for C_0 and C_2 (Birse, McGovern, and Richardson, 1999).

With a dibaryon, range effects can be resummed using the propagator

$$iD^{\mathrm{resum}}(p_0, \mathbf{p}) = \frac{-i}{\Delta + g^2 I_0(\sqrt{m_N \tilde{p}_0}) - \tilde{p}_0}. \tag{31}$$

The Wigner bound is automatically avoided by allowing the dibaryon to be a ghost field. In fact, Beane and Savage (2001) proposed that the relatively large sizes of the NN effective ranges (about $2m_\pi^{-1}$) justify their resummation as an LO effect. This procedure leads to two S-matrix poles per channel and is thus more likely to be interpreted as a resummation of NLO interactions, which includes additional higher-order effects.

6. Spin-isospin projection and parametrizations

For a fixed NN channel it is convenient to use the effective Lagrangian (11), with ψ a nucleon field for which the combination $\psi^\dagger\psi$ has definite spin and isospin (S, I). The Pauli principle dictates that only the isospin triplet $t \equiv (0, 1)$ and the isospin singlet $s \equiv (1, 0)$ are allowed combinations. We use subscripts s and t here in reference to isospin, with a warning that the same subscripts are sometimes used in reference to spin. To go beyond the description of an isolated two-nucleon system, it is desirable to treat both combinations on the same footing. To this end, it is convenient to introduce a nucleon field N that is a doublet in both spin and isospin space, along with projection operators

$$(P_s)^i = \sigma^2\sigma^i\tau^2/\sqrt{8}, \qquad (P_t)^A = \sigma^2\tau^2\tau^A/\sqrt{8}, \tag{32}$$

where σ^i (τ^A) denotes the three Pauli matrices in spin (isospin) space, and we use lowercase (uppercase) indices to further distinguish between the two spaces. The Lagrangian for the NN system can then be written as

$$\mathcal{L} = N^\dagger\left(i\partial_0 + \frac{\mathbf{\nabla}^2}{2m_N}\right)N - \frac{C_{0s}}{2}(N^T P_s N)^\dagger(N^T P_s N)$$
$$- \frac{C_{0t}}{2}(N^T P_t N)^\dagger(N^T P_t N) + \cdots, \tag{33}$$

where the ellipsis represents analogous terms with $C_{2s/t}$ as well as higher-order operators. Fierz rearrangements can be used to generate equivalent interactions. Analogously, Eq. (27) is generalized to the nuclear case by introducing two dibaryon fields, one for each NN S-wave channel, using the same projection operators $P_{s,t}$ (Bedaque and van Kolck, 1998).

The two channels are somewhat different concerning both sign and magnitude of the scattering lengths. It has been customary to treat both a_s^{-1} and $|a_t|^{-1}$ as M_{lo}, although we return to this issue in Sec. II.B.7. The ERE Eq. (12b) has a certain radius of convergence, set by the nearest singularity to the expansion point $k^2 = 0$. The pion-exchange cut on the imaginary k axis starting at $m_\pi/2$ leaves the deuteron pole within the radius of convergence of the ERE, and indeed it is well known that the properties of this pole can be expressed in terms of the ERE parameters (Goldberger and Watson, 1967), cf. Sec. II.B.1. For example, the deuteron binding momentum is

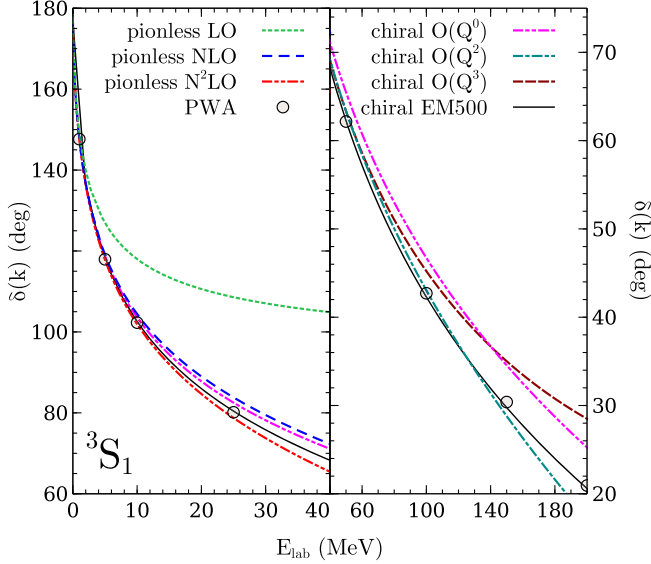$$\gamma_d = \frac{1}{a_s}\left(1 + \frac{r_s}{2a_s} + \cdots\right). \tag{34}$$

FIG. 7. The NN scattering phase shift δ as a function of the nucleon laboratory energy E_{lab} in the $^3S_1$ partial wave for pionless EFT and chiral EFT at various orders (Long and Yang, 2012a) (from C.-J. Yang), and the chiral potential "EM500" (Entem and Machleidt, 2003). For comparison, we show the partial-wave analysis (PWA) of Navarro Pérez, Amaro, and Ruiz Arriola (2013), with error bars smaller than the symbols.

Alternatively, and this is in fact what was done first historically (Bethe, 1949), one can perform the ERE directly about this pole (i.e., about the point $i\gamma_d$ in the complex momentum plane),

$$k \cot \delta_d(k) = -\gamma_d + \frac{\rho_d}{2}(k^2 + \gamma_d^2) + \cdots, \qquad (35)$$

where $\rho_d \simeq 1.765$ fm (de Swart, Terheggen, and Stoks, 1995) is the deuteron effective range. The motivation for using Eq. (35) instead of the ERE about zero momentum is that it captures the exact location of the pole already at LO. Grießhammer (2004) extended the procedure to the $^1S_0$ channel, where it is possible to define the ERE about the virtual-state pole.

The first detailed comparison of the $^3S_1$ phase shift obtained in pionless EFT with empirical values was carried out up to N²LO by Chen, Rupak, and Savage (1999a), with LECs fitted to Eq. (35). In Fig. 7 we show results fitted to Eq. (12b) instead, which are qualitatively similar: convergence is seen at low energies, and already at NLO a good description is achieved. The corresponding results for $^1S_0$ up to N²LO were presented by Beane, Bedaque, Haxton *et al.* (2001).

7. Coulomb effects and other isospin breaking

Since almost all nuclear systems involve more than one proton, the inclusion of electromagnetic effects is generally important. In the low-energy regime, the dominant effect is given by "Coulomb photons," i.e., the familiar, static potential $(\sim \alpha/r)$ between charged particles. It originates from the replacement of derivatives in the effective Lagrangian with covariant ones,

$$D_\mu = \partial_\mu + ieA_\mu \hat{Q}, \qquad (36)$$

where $\hat{Q}$ is an appropriate charge operator, e.g., $\hat{Q} = (1 + \tau_3)/2$ for nucleons. The Coulomb photon-nucleon coupling ie comes from the gauging of the nucleon time derivative in Eq. (33), while the Coulomb-photon propagator is $i/(\mathbf{q}^2 + \lambda^2)$, where λ is an IR-regulating photon mass that is eventually taken to zero. Finer electromagnetic effects enter through operators with more covariant derivatives and also directly through the field strength, or alternatively the electric $(E_i = \partial_0 A_i - \partial_i A_0)$ and magnetic $(B_i = \epsilon_{ijm}\partial^j A^m)$ fields.

Kong and Ravndal (1999b, 2000) were the first to study proton-proton (pp) scattering in pionless EFT. The challenge here lies in the fact that the Coulomb interaction is important at very low energies: we see from Eq. (8) for the Coulomb potential $V \sim e^2/Q^2$ that the Coulomb interaction is nonperturbative for $Q \lesssim \alpha m_N/2 \equiv k_C$, which is in the low-energy region of pionless EFT. Subtracting the pure-Coulomb amplitude T_C from the full amplitude T, one can write

$$T_{SC} = T - T_C = -\frac{4\pi}{m_N}\frac{e^{2i\sigma_C}}{k \cot \delta_{pp}(k) - ik} \qquad (37)$$

in terms of the "subtracted" pp phase shift $\delta_{pp}(k)$ and the pure-Coulomb phase shift $\sigma_C = \arg \Gamma(1 + i\eta)$. Renormalization can be carried out by matching to the "Coulomb-modified" ERE (Bethe, 1949)

$$C_\eta^2[k \cot \delta_{pp}(k) - ik] + \alpha m_N H(\eta)$$
$$= -\frac{1}{a_{pp}} + \frac{r_{pp}}{2}k^2 + \cdots, \qquad (38)$$

where $a_{pp} \simeq -7.8$ fm and $r_{pp} \simeq 2.8$ fm (Bergervoet *et al.*, 1988) are the ERE parameters, $C_\eta^2 = 2\pi\eta[\exp(2\pi\eta) - 1]^{-1}$ is the Sommerfeld factor in terms of $\eta = k_C/k$, and $H(\eta) = \Re[\psi(1 + i\eta)] - \ln\eta + iC_\eta^2/(2\eta)$ in terms of the digamma function ψ. It should be emphasized that the pp scattering amplitude, and thus also the effective-range parameters, are always defined in the presence of the Coulomb interaction and cannot be divided into strong and electromagnetic parts in a model-independent way (Kong and Ravndal, 1999b; Gegelia, 2004). For particles with nonunit charges, the definition of the Coulomb momentum k_C is generalized in Sec. III; see Eq. (69).

In pionless EFT, T_{SC} is obtained by replacing all empty bubbles in Fig. 3 with the dressed one shown in Fig. 8. The initial- and final-state Coulomb interactions are accounted for by the construction in Eq. (37). *Dressing* here refers to resumming the Coulomb interaction to all orders between each pair of C_0 vertices, which Kong and Ravndal (1999b, 2000) were able to do using a known analytic expression for the pure-Coulomb Green's function. With dimensional regularization,

$$\frac{4\pi}{m_N C_0^{pp}(\mu)} = \frac{1}{a_{pp}} - \mu + \alpha m_N \left(\frac{1}{\epsilon} + \ln \frac{\mu}{\alpha m_N} + \text{const} \right). \qquad (39)$$

The term linear in the renormalization scale μ comes from the PDS prescription, but Coulomb exchange now introduces an
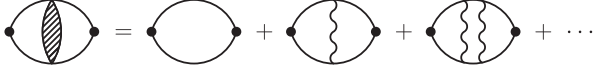
FIG. 8. Bubble diagram dressed with Coulomb exchange (wavy line).

additional logarithmic divergence, reflected in the pole in $\varepsilon = d - 3$, where d is the number of spatial dimensions. Range corrections were considered at NLO by Kong and Ravndal (2000) and at N²LO by Ando *et al.* (2007). An equivalent formulation in terms of a *pp* dibaryon exists (Ando and Birse, 2010). The RG analysis of Birse, McGovern, and Richardson (1999) discussed in Sec. II.B.4 has also been extended to the charged-particle sector (Barford and Birse, 2003; Ando and Birse, 2008).

The LEC $C_0^{pp} = C_{0t} + \Delta C_{0(+)}$ in Eq. (39) contains an isospin-dependent contribution $\Delta C_{0(+)}$, which is a short-range (or *indirect*) electromagnetic effect. The EFT includes also isospin breaking from the quark masses (van Kolck, 1993, 1995). While electromagnetic interactions break isospin more generally (*charge dependence*), effects that are linear in the quark masses break charge symmetry (a rotation of π around the second axis in isospin space) specifically. Introducing the projectors $P_{(\pm)} = (P_t^1 \mp iP_t^2)/\sqrt{2}$ to the *pp* and *nn* channel, the isospin-breaking Lagrangian takes the form

$$\mathcal{L}_{ib} = \delta m_N N^\dagger \tau_3 N - \frac{\Delta C_{0(+)}}{2}(N^T P_{(+)}N)^\dagger(N^T P_{(+)}N)$$
$$- \frac{\Delta C_{0(-)}}{2}(N^T P_{(-)}N)^\dagger(N^T P_{(-)}N) + \cdots. \qquad (40)$$

NDA [see Eq. (9)] indicates that the neutron-proton mass splitting $\delta m_N = \mathcal{O}(\varepsilon \bar{m}, \alpha m_N/(4\pi))$. It is well known that the two types of contributions are comparable in magnitude, $\varepsilon \bar{m} \sim \alpha m_N/4\pi$, valid up to a scale-dependent factor of a few, but have opposite signs, the quark masses tilting the balance in favor of the neutron. The mass-splitting term can be removed by a redefinition of the nucleon field (Friar *et al.*, 2004) and reappears as an $\mathcal{O}(\delta m_N/m_N)$ effect in the nucleon kinetic term. The most important quark-mass effects in the *NN* system lie in the short-range LECs $\Delta C_{0(\pm)}$. The reduced quark mass is $(\varepsilon \bar{m})_{\text{red}} = \varepsilon \bar{m}/M_{\text{hi}}$ and together with the *S*-to-*S*-wave enhancement discussed in Sec. II.B.2 leads to $(a_{nn} - a_t)/a_t \sim \Delta C_{0(-)}/C_{0t} = \mathcal{O}(\varepsilon \bar{m} a_t) \simeq 0.2$, cf. König *et al.* (2016). A similar contribution exists for $\Delta C_{0(+)}$, which is, however, dominated by the electromagnetic contribution $\Delta C_{0(+)}/C_{0t} = \mathcal{O}(\alpha m_N a_t)$, consistent with Eq. (39).

For most of the region of validity of pionless EFT, $Q \gtrsim \alpha m_N$ and *all* electromagnetic interactions are expected to be perturbative. In this region, $Q \gtrsim 1/a_t$ as well. König *et al.* (2016) developed an expansion in powers of $\alpha m_N/Q$ and $1/Qa_t$ in addition to the standard Q/M_{hi} expansion. For simplicity, they paired the expansions by taking $\alpha m_N \sim a_t^{-1} = \mathcal{O}(M_{\text{lo}}^2/M_{\text{hi}})$ and $\varepsilon \bar{m} = \mathcal{O}(M_{\text{lo}}^3/M_{\text{hi}}^2)$. In this case, LO in the $^1S_0$ channel consists of the isospin-symmetric unitary amplitude, that is, Eq. (12a) with $k \cot \delta_t = 0$. The first short-range and electromagnetic corrections break isospin symmetry at NLO, reproducing a_{pp} and leading to equal scattering lengths in the other two $^1S_0$ isospin channels. In addition, at NLO

there is the standard, isospin-symmetric C_{2t} interaction, while quark-mass effects (and the *nn* splitting from *np*) first enter at N²LO. This is consistent with the observed relation $r_{pp} \simeq r_t$.

8. External currents

One of the great advantages of the EFT approach is that it is straightforward to include external currents in addition to interactions between nucleons. Power counting leads to a systematic expansion of current operators, which had previously been classified only as one-body and many-body pieces (also known as meson-exchange currents).

Photons are introduced in the effective Lagrangian as described earlier. In addition, weak interactions are accounted for by current-current interactions, where the currents have the well-known vector-axial $(V - A)$ form. Power counting is similar to that described in Sec. II.B.2, with current operators subject to the same enhancement by powers of M_{lo}^{-1} when *S* waves are involved (Chen, Rupak, and Savage, 1999a). Electromagnetic couplings were analyzed with the Wilsonian RG by Kvinikhidze and Birse (2018).

The earliest example in the context of pionless EFT involved calculations of static deuteron properties by Chen, Rupak, and Savage (1999a), paralleling previous work by Kaplan, Savage, and Wise (1999) and Savage, Scaldeferri, and Wise (1999) in chiral EFT with perturbative pions. Chen, Rupak, and Savage (1999a) calculated several deuteron properties (charge, magnetic dipole, and electric quadrupole form factors, as well as electric polarizabilities) beyond LO, including relativistic corrections. Results were found to be in good agreement both with experimental data and, at low orders, with those obtained from effective-range theory (Lucas and Rustgi, 1968; Friar and Fallieros, 1984; Wong, 1994). At higher orders, the EFT goes beyond the effective-range approach (which is based on input from elastic *NN* scattering only) because new operators appear with undetermined coefficients. For example, there are magnetic four-nucleon-one-photon couplings at NLO,

$$\mathcal{L}_{\text{mag}}^{(1)} = eL_1(N^T P_s^i N)^\dagger(N^T P_t^3 N)B_i$$
$$- ieL_2\epsilon_{ijk}(N^T P_s^i N)^\dagger(N^T P_s^j N)B^k + \text{H.c.} \qquad (41)$$

This is the two-nucleon analog of the single-particle "Pauli term" that describes the direct $\vec{S} \cdot \vec{B}$ coupling of the nucleon spin to a magnetic field, which accounts for the nucleon anomalous magnetic moment. Here L_1 and L_2 are LECs that contribute to the deuteron dipole magnetic moment as well as to the capture process $np \rightarrow d\gamma$.

Motivated by the original work of Bethe (1949) and Bethe and Longmire (1950), Phillips, Rupak, and Savage (2000) proposed a new scheme to incorporate NLO and higher orders in processes involving the deuteron. Up to the higher-order corrections contained in the ellipsis, we can read off the residue of the deuteron pole from Eq. (35),

$$Z_d = (1 - \gamma_d \rho_d)^{-1} = 1 + \gamma_d \rho_d + (\gamma_d \rho_d)^2 + \cdots. \qquad (42)$$

This residue is directly related to the long-range tail of the deuteron wave function in configuration space. Phillips,

Rupak, and Savage (2000) argued that the convergence of deuteron observables (at least those sensitive to the long-range tail of the wave function) can be dramatically improved by fitting to Z_d exactly right at NLO—rather than building it up perturbatively as given in Eq. (42)—while not spoiling convergence for the $^3S_1$ phase shifts.

A deuteron dibaryon field (see Sec. II.B.5) is particularly convenient for processes with external deuterons. The dressed dibaryon can be used directly as an interpolating field to define the S matrix provided that its wave-function renormalization is properly taken into account. With a dibaryon, the effects of a resummation of the effective range can be assessed (Beane and Savage, 2001; Ando and Hyun, 2005).

A number of processes have been carefully addressed with these tools. A precise and controlled theoretical prediction of the $np \to d\gamma$ cross section is important because it enters as an input parameter into big-bang nucleosynthesis calculations. The low-energy values required are difficult to access experimentally but are ideally suited for an application of pionless EFT. The pionless analysis of this process started by Chen, Rupak, and Savage (1999a) was refined in subsequent papers (Chen and Savage, 1999; Chen, Rupak, and Savage, 1999b). Rupak (2000) carried the analysis out to N⁴LO, giving a prediction that is accurate to a theoretical uncertainty below 1%. This reaction was revisited with dibaryon fields at NLO and a resummation of effective-range effects by Ando et al. (2006).

The related processes of deuteron electrodisintegration and photodisintegration are experimentally accessible, and discrepancies between phenomenological potential models and data have been reported. Dibaryon fields implementing a resummation of range effects have been used to N²LO for $ed \to e'pn$ (Christlmeier and Grießhammer, 2008) and $d\gamma \to np$ (Ando et al., 2011; Song, Ando, and Hyun, 2017), with results generally supporting phenomenological models. For example, Christlmeier and Grießhammer (2008) concluded that no consistent theoretical calculation could describe the data because the EFT calculation, unlike the potential-model approach, comes with a rigorous uncertainty estimate. Subsequently, the resolution of a problem with the data analysis gave agreement between experiment and the EFT calculation (Ryezayeva et al., 2008); see Fig. 9.

The proton-proton fusion process $pp \to de^+\nu_e$ is of similar importance for an understanding of the Sun. Obviously, Coulomb effects play an important role for this reaction at extremely low energies. Kong and Ravndal (1999a, 1999c, 2001), building upon their previous work on pp scattering (see Sec. II.B.7), presented the first calculation in pionless EFT at NLO. This calculation was later extended to N⁴LO by Butler and Chen (2001). An NLO calculation using a dibaryon field to resum effective-range corrections was presented by Ando et al. (2008). Chen, Liu, and Yu (2013) extended the calculation of the astrophysical pp S factor to also include its energy derivatives.

The inverse process, neutrino-deuteron breakup scattering, was considered by Butler, Chen, and Kong (2001) to N²LO, along the lines of an earlier NLO perturbative-pion calculation (Butler and Chen, 2000). At NLO, the axial-vector counterparts of Eq. (41) appear, with two analogous LECs usually
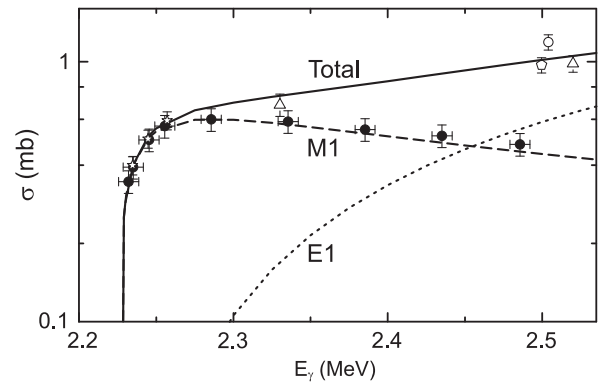

FIG. 9. Total cross section σ for deuteron electrodisintegration as function of the photon energy E_γ. Good agreement is seen between measured data points and theoretical calculation (lines), which was achieved after the pionless calculation of Christlmeier and Grießhammer (2008) helped resolve a problem with the experimental analysis. Adapted from Ryezayeva et al., 2008. Courtesy of H. W. Grießhammer.

denoted as $L_{1,A}$ and $L_{2,A}$. However, because of the quantum numbers of the initial and final states, only the isovector $L_{1,A}$, which contributes to $pp \to de^+\nu_e$ as well, is significant. Various constraints on $L_{1,A}$ have been discussed by Butler, Chen, and Vogel (2002), Balantekin and Yuksel (2003), Chen, Heeger, and Robertson (2003), and Chen et al. (2005), confirming SNO's conclusions about neutrino oscillations.

Additionally, single-nucleon properties can be inferred from nuclear data. Compton scattering is influenced by the nucleon polarizabilities, which are response functions that carry much information about hadron dynamics and thus QCD. While proton polarizabilities can be extracted directly, neutron polarizabilities can be probed only in nuclear Compton scattering. Compton scattering on the deuteron was studied to N²LO by Grießhammer and Rupak (2002), who resummed the effective ranges and fitted Z_d. Values for the isoscalar, scalar electric and magnetic polarizabilities were extracted by Grießhammer and Rupak (2002). Additional features of the cross section were considered by Chen, Ji, and Li (2005a, 2005b). Sum rules for vector and tensor polarizabilities were given by Ji and Li (2004), while a low-energy theorem for the spin-dependent Compton amplitude was obtained by Chen, Ji, and Li (2004).

All in all, these calculations support the convergence of pionless EFT for momenta below the pion mass, with the power counting discussed in Sec. II.B.2. They provide theoretically controlled cross sections that impact astrophysics and particle physics. Heavier probes, such as pions (Beane and Savage, 2003a), can be considered as well through a heavy-field treatment. Most interesting for nuclear physics are processes with additional nucleons, which we consider next.

C. Light nuclei: Bound and scattered

Pionless EFT extends effective-range theory into the nuclear realm, where it leads to a striking emergence of structure related to the Efimov phenomenon (Efimov, 1970, 1981), which we discuss in more detail in the context of halo/cluster EFT in Sec. III.C.
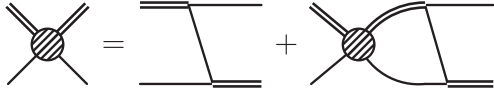
FIG. 10. Integral equation for nd scattering in the spin-quartet channel. A pair of similar but coupled equations describes the doublet channel.

1. Extension to three particles

The simplest three-body system that can be studied in pionless EFT is neutron-deuteron (nd) scattering in the quartet S-wave channel (total spin 3/2 and zero orbital angular momentum). The Pauli principle dictates that only the same configuration can appear in the intermediate state. Bedaque and van Kolck (1998) calculated the nd quartet scattering length in a framework using a deuteron dibaryon field; see Sec. II.B.5. The driving mechanism is the exchange of a nucleon (neutron) between ingoing and outgoing deuterons. The EFT power counting says that all diagrams with an arbitrary number of such exchanges are of the same order. Analogous to the two-body bubble chain, they can be conveniently resummed into an integral equation for the scattering amplitude, shown diagrammatically in Fig. 10. The loop integrals converge, but for a numerical treatment it is still convenient to introduce a momentum cutoff. Resumming effective-range corrections to all orders in the deuteron sector, Bedaque and van Kolck (1998) calculated the scattering length to be 6.33 fm, in excellent agreement with the experimental value 6.35(2) fm (Dilg, Koester, and Nistler, 1971). A perturbative treatment of effective-range corrections according to Eq. (35) gives $(5.09 + 0.98 + 0.21)$ fm $= 6.28$ fm to N²LO, with an estimated 3% uncertainty. The LO result of 5.09 fm agrees with the much older result of Skorniakov and Ter Martirosian (1957), who used a zero-range model that is equivalent to pionless EFT at LO. Bedaque, Hammer, and van Kolck (1998) and Bedaque and Grießhammer (2000) extended the EFT calculation to nd scattering at finite energy.

2. The triton as a near-Efimov state

Three nucleons can also couple to an S-wave state with total spin 1/2, which is the channel of the trinucleon bound states: triton (³H) and helion (³He). The formalism used to calculate quartet-channel scattering can be extended directly to the doublet channel, where now $^1S_0$ intermediate states are also allowed. The result can be written as an integral equation for the nd T matrix with the same structure as in Fig. 10, but for the two coupled channels $n + np(^3S_1)$ and $n + np(^1S_0)$ (Skorniakov and Ter Martirosian, 1957). The triton should show up as a pole in this amplitude at a negative energy $E = -B(^3\text{H}) = -8.4818$ MeV. Since its relevant momentum scale is given by $\gamma_T = \sqrt{2m_N B(^3\text{H})/3} \sim 80$ MeV, it is within the expected range of validity of the EFT.

However, it has been known for a long time that the three-nucleon system is unstable when described solely with nonderivative two-body, short-range interactions: as the range of such a potential is sent to zero, one encounters the "Thomas collapse," i.e., the binding energy diverges (Thomas, 1935). Bedaque, Hammer, and van Kolck (2000), generalizing their

previous work on the three-boson system (Bedaque, Hammer, and van Kolck, 1999a, 1999b), showed that the same happens in pionless EFT: as the cutoff $\Lambda \gg M_{\text{lo}}$ is increased, the ground-state energy grows as Λ^2/m_N, and excited states appear repeatedly. Since the NN scattering lengths are large, one encounters an approximate realization of the Efimov effect (Efimov, 1970, 1981), i.e., a tower of three-body states with the ratio of neighboring binding energies approaching a universal constant.

a. The three-body force

The scattering amplitude in the doublet channel, obtained from the integral equations analogous to Fig. 10, does not approach a stable limit as the cutoff is increased. This lack of renormalization is a genuine nonperturbative effect since every diagram generated by iterations is finite by itself. Bedaque, Hammer, and van Kolck (2000) showed that the system can be stabilized by adding a nonderivative three-body contact interaction. Fierz rearrangements show that there is only one such interaction, which can be written in any one of various equivalents forms, for example,

$$\mathcal{L}_{3b} = -4h_0 C_{0t}^2 (N^T P_t^k N)^\dagger (N^\dagger \sigma^k \sigma^l N)(N^T P_t^l N) \quad (43)$$

where h_0 is a new LEC to be determined. In the formalism with dibaryon fields, every nucleon-exchange diagram has to be accompanied by a dibaryon-nucleon interaction with strength h_0, as shown in Fig. 11. Attaching the two-nucleon-dibaryon vertex g from Eq. (27) on both dibaryon ends recovers the six-nucleon operator (43) in the theory without a dibaryon field.

The $3N$ force is symmetric (Bedaque, Hammer, and van Kolck, 2000) under the group of combined spin and isospin transformations, Wigner's SU(4) (Wigner, 1937a, 1937b). Because the two-body amplitude is also SU(4) symmetric for momenta $a_s^{-1} < Q < M_{\text{hi}}$ (Mehen, Stewart, and Wise, 1999), the coupled integral equation illustrated in Fig. 10 is symmetric in the limit where all momenta are large compared to the inverse scattering lengths. This allowed Bedaque, Hammer, and van Kolck (2000) to study the UV behavior of the amplitude based on decoupling the two integral equations, with one of the rotated amplitudes behaving exactly like the amplitude for the three-boson system with two-body scattering length a_2. This in turn leads to the analytical result (Bedaque, Hammer, and van Kolck, 1999a, 1999b)

$$\frac{\Lambda^2 h_0(\Lambda)}{m_N} \equiv H(\Lambda) \approx -\frac{\sin\left[s_0 \log(\Lambda/\Lambda_*) - \arctan(s_0^{-1})\right]}{\sin\left[s_0 \log(\Lambda/\Lambda_*) + \arctan(s_0^{-1})\right]}, \quad (44)$$

conveniently written as a dimensionless function. Here $s_0 \simeq 1.0064$ is a universal constant (Danilov, 1961) and Λ_* is a

FIG. 11. Modification of the driving mechanism in Fig. 10, with the LO three-body force (solid circled) in the nd doublet channel.
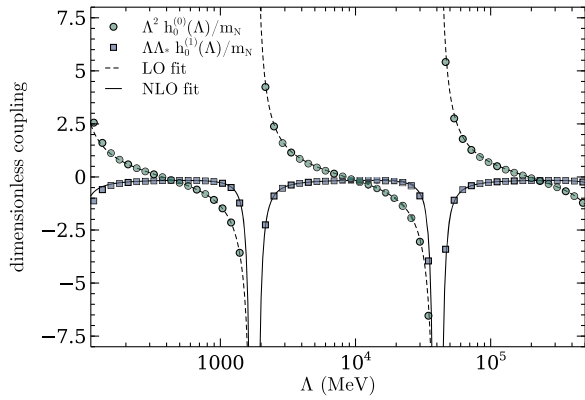
FIG. 12. RG running of the three-body coupling h_0 at LO and NLO. Numerical data points are fitted using Eq. (44) at LO and an analogous expression (Ji, Phillips, and Platter, 2012) at NLO.
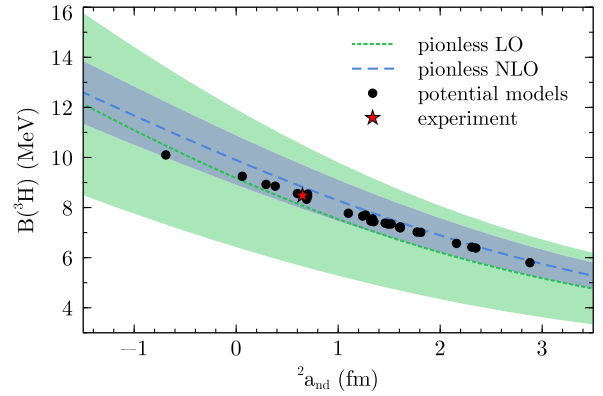

FIG. 13. Correlation between the triton binding energy $B(^3\text{H})$ and the doublet nd scattering length $^2a_{nd}$ (Phillips line) at LO and NLO, compared to results from various potential models and experiment. Bands indicate estimates of higher-order corrections: the larger band around the dotted line is LO, the smaller band around the dashed line is NLO.

parameter that has to be fixed to a three-body datum. The striking log-periodic dependence on the cutoff is shown in Fig. 12, where the overall prefactor in Eq. (44) depends on the details of the regularization scheme employed in a given calculation (Platter, Hammer, and Meißner, 2004; Braaten, Kang, and Platter, 2011). Hammer and Mehen (2001b) studied this "ultraviolet limit cycle" and derived the RG equation of which Eq. (44) is a solution. They realized that the explicit three-body force can be set to zero by working at a set of log-periodically spaced cutoffs $\Lambda_n = \Lambda_* \exp[s_0^{-1}(n\pi + \arctan s_0^{-1})]$, where n is an integer. Braaten and Hammer (2003) argued that the UV limit cycle observed in pionless EFT hints at an underlying *infrared* cycle in QCD.

Such a $3N$ force would be of higher order according to naive dimensional analysis. The fact that it has to be included already at LO to renormalize the three-body system is another consequence of the fine-tuning encountered in the two-body sector. After renormalization the Efimov tower of states is cutoff independent, its position determined by Λ_*. If the NN scattering lengths were in fact infinite, one would have a tower of shallow three-body states accumulating at zero energy. The large but finite physical scattering lengths cut off this spectrum in the IR, whereas the breakdown scale M_{hi} of the EFT sets a limit for the deepest state. In nuclear physics at physical quark masses, a_s and m_π are not large enough for the appearance of an excited $3N$ state. However, Rupak *et al.* (2019) showed in agreement with earlier model calculations (Adhikari and Tomio, 1982) that a shallow virtual state in nd scattering, known to exist for a long time (van Oers and Seagrave, 1967; Girard and Fuda, 1979), becomes the first excited bound state as a_s increases. Other situations were discussed by Braaten and Hammer (2003).

b. The Phillips line

Pionless EFT at LO offers a striking but simple explanation of the well-known "Phillips line," i.e., the fact that different model potentials for the nuclear interaction tuned to the same NN scattering data give different but highly correlated results for the triton binding energy and the doublet nd scattering length (Phillips, 1968). Pionless EFT allows one to understand this and other correlations among three-body observables as a

consequence of the RG, i.e., as a correlation originating in the variation of Λ_* (Bedaque, Hammer, and van Kolck, 2000). This is shown in Fig. 13. The proximity of the LO EFT line to the experimental point means that, whichever observable is used as input, the other comes out correct.

3. More neutron-deuteron scattering

a. Range corrections, partial resummation, and two-body parametrizations

At NLO one needs to account for the two-body ranges. In the dibaryon framework that means one insertion of each dibaryon kinetic-energy operator between LO amplitudes, as shown in Fig. 14. At N²LO the procedure of perturbative range insertions becomes tedious, and a direct calculation of the corrections requires fully off-shell LO amplitudes. To avoid this, range corrections can be resummed with Eq. (31). Bedaque and van Kolck (1998) already noted that this resummation introduces an artificial deep pole in the deuteron propagator. Located at a momentum scale of roughly 200 MeV, it is outside the range of validity of the EFT and thus, in principle, an irrelevant UV artifact, although it limits the range of cutoffs that can be used in the numerical solution of the scattering equations. This is especially true in the doublet S channel unless measures are taken to remove the pole. In the quartet channel, due to the Pauli principle, the solution is not sensitive to this deep pole and the cutoff can be made arbitrarily large. Considering effective ranges as LO as proposed by Beane and Savage (2001) effectively cuts off the integral of the three-body equation at $\sim r_0^{-1}$, eliminating the
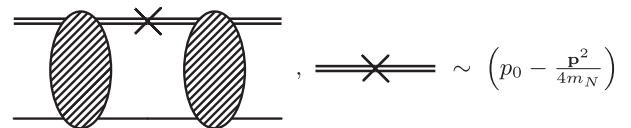

FIG. 14. Dibaryon kinetic-energy corrections for the nd quartet-channel scattering amplitude at NLO. In the doublet channel, there are analogous diagrams with $^1S_0$ dibaryons.

UV limit cycle and leaving only the IR limit cycle manifest in the Efimov effect. However, in general, there is no guarantee that the Efimov tower is at the correct location without a three-body force. Similar results are expected from any selective resummation of higher-order effects, such as relativistic corrections (Epelbaum *et al.*, 2017).

Bedaque *et al.* (2003) proposed a middle ground that partially reexpands the resummed propagators and uses terms up to order n for a calculation at N^{n}LO. Using these "partially resummed" propagators generates all desired terms at a given order, but still retains some higher-order corrections, which have to be assumed to be negligible. We note that for such an approach to be valid it is important to keep the cutoff at or below the breakdown scale of the theory. $^3S_1$-$^3D_1$ mixing as well as relativistic corrections formally enter at N^{2}LO but were not included by Bedaque *et al.* (2003). Grießhammer (2004) implemented the two-body parametrization (42) and found a substantially better description of data, particularly in the doublet S wave.

The first strictly perturbative NLO calculation of nd scattering in the doublet S channel was carried out by Hammer and Mehen (2001a), who implemented the procedure suggested by Bedaque, Hammer, and van Kolck (2000). Vanasse (2013) developed a scheme that avoids the numerically expensive determination of fully off-shell amplitudes made in earlier perturbative calculations (Ji, Phillips, and Platter, 2012; Ji and Phillips, 2013), requiring slightly less effort than the partial resummation of Bedaque *et al.* (2003). Beyond the practical benefit, the N^{2}LO calculation of Vanasse (2013) also showed that an anomalous unitarity-violating behavior of the quartet S-wave nd phase shift above the deuteron breakup threshold, known to practitioners as a consequence of the partial-resummation scheme, does not occur with a fully perturbative treatment of range corrections. The lesson is that even if terms are individually small, undesirable effects can be generated by their *infinite* resummation. Overall, Vanasse (2013) obtained nd phase shifts at N^{2}LO that were in good agreement with the empirical behavior up to laboratory energies of $\simeq 24$ MeV.

b. Higher partial waves

Even with only S-wave interactions in the two-body sector, the nucleon-exchange diagram driving the nd scattering equations (Fig. 10) generates contributions in all partial waves. Gabbiani, Bedaque, and Grießhammer (2000) calculated the scattering phase shifts up to G waves ($\ell = 4$) to N^{2}LO using the full resummation (31) but omitting $^3S_1$-$^3D_1$ mixing. They found good agreement with both potential-model calculations and available experimental data up to about 140 MeV center-of-mass momentum, indicating that the breakdown scale of pionless EFT is indeed close to being set by the pion mass, at least for these observables. Even better results are obtained with the two-body parametrization (42) (Grießhammer, 2004). The fully perturbative N^{2}LO calculation by Vanasse (2013) did include $^3S_1$-$^3D_1$ mixing and found reasonable agreement with potential-model results.

The vector analyzing power A_y has defied explanation with potential models even at energies as low as a few MeV, the A_y *puzzle*. Margaryan, Springer, and Vanasse (2016) employed the fully perturbative approach to calculate nd polarization observables at N^{3}LO. They found that varying the ^3P_J LECs (first entering at N^{3}LO) with the expected error (a 15% band around their central values) covers a range for A_y that is consistent with the experimental data.

c. Ordering of three-body forces

Bedaque, Hammer, and van Kolck (2000) argued that at NLO range corrections force a shift in the LEC of the $3N$ force (43), which was confirmed by Hammer and Mehen (2001a) in an explicit NLO calculation. Thus,

$$h(\Lambda) = h_0^{(0)}(\Lambda) + h_0^{(1)}(\Lambda) + \cdots, \qquad (45)$$

where $h_0^{(0)}(\Lambda)$ is given in Eq. (44) and $h_0^{(1)}(\Lambda)$, determined in a fully perturbative calculation with physical NN effective-range parameters, is shown in Fig. 12. At NLO, the numerical data are fit with the analytical result found by Ji, Phillips, and Platter (2012). The existence of the correction $h_0^{(1)}$ does not mean that there is a new three-body force at NLO, it is merely an adjustment of the LO coefficient carried out by demanding that the observable used to fixed $h_0^{(0)}(\Lambda)$ stays invariant after the inclusion of range corrections. Because there is no new three-body parameter at NLO, simple correlations through $\Lambda_\star$ survive with small shifts, as can be seen in the NLO line in Fig. 13. Since $h_0^{(1)}(\Lambda)$ depends on the two-body scattering lengths, if the latter are changed, further experimental input is needed to determine the NLO LEC (Ji, Phillips, and Platter, 2010).

The conclusion that despite having canonical dimension 9 the nonderivative three-body force appears at LO together with the nonderivative two-body force of dimension 6 raises the following questions: Do other three-body interactions have to be promoted? More generally, what is the ordering of three-body forces in the pionless power counting? Since according to Bedaque, Hammer, and van Kolck (2000) a new $3N$ force enters at N^{2}LO, Bedaque *et al.* (2003) used a Lepage-plot analysis (Lepage, 1997) to show that its inclusion reduces the errors in the calculation. A general and comprehensive analysis of pionless three-body forces using the asymptotic techniques of Bedaque, Hammer, and van Kolck (1999a, 1999b, 2000) was carried out by Grießhammer (2005), who identified a logarithmic divergence at N^{2}LO that mandates the inclusion of a new three-body force at this order. Grießhammer (2005) also cataloged the minimal orders at which $3N$ forces must first appear in various channels for proper renormalization. Using a subtractive renormalization scheme, Platter and Phillips (2006) argued that the LO three-body force is sufficient to achieve cutoff independence up to N^{2}LO, contradicting the findings of Bedaque *et al.* (2003). Ji, Phillips, and Platter (2012) and Ji and Phillips (2013), studying the three-boson system, later explained this discrepancy by noting that the conclusion of Platter and Phillips (2006) holds only in the limit where the three-body UV cutoff is taken to infinity, with the partial resummation of range corrections affecting the perturbative expansion at smaller cutoffs. Using a fully perturbative inclusion of range

corrections, Ji and Phillips (2013) concluded that a new three-body force indeed enters at N²LO. This term can be implemented using the same SU(4)-symmetric spin-isospin structure as the LO three-body force, with appropriate time derivatives included to give a linear dependence on the energy (Ji and Phillips, 2013; Vanasse, 2013).

Generalizing these results, the $3N$ potential takes the form of Eq. (7) with [cf. Grießhammer (2005)] $\mu = d + 2 - s_3$, where $s_3 = 0, 1, 2$ is the number of nucleon-deuteron (Nd) Wigner-symmetric S waves connected by the operator. The lowest-order forces are represented in Fig. 5. Amplitudes have the form of Eq. (3) with the normalization of Eq. (20) for $A = 3$.

4. Proton-deuteron scattering and helion

a. Nonperturbative Coulomb effects

As discussed in Sec. II.B.7, at the low energies potentially reached in scattering, Coulomb-photon exchange needs to be treated nonperturbatively, which poses additional technical challenges. The first attempt to study Coulomb effects was made in the simpler quartet S-wave pd scattering by Rupak and Kong (2003). They developed a power counting that with some approximations amounts to iterating a Coulomb potential between proton and deuteron to all orders, along with the one-nucleon-exchange diagram that also enters into nd scattering. Rupak and Kong (2003) calculated the Coulomb-subtracted S-wave phase shift in the quartet channel, but they could not reach convergence below a pd center-of-mass momenta of 20 MeV (the regime where Coulomb effects really are nonperturbative). Convergence down to 3 MeV was later achieved by König and Hammer (2011) owing to an improved numerical procedure. König and Hammer (2011) also extended the analysis to the doublet S-wave channel (including the helion) and applied the partial-resummation approach of Bedaque et al. (2003) to calculate higher orders.

Ando and Birse (2010) carried out a direct momentum-space calculation of helion based on a generalization of the nd integral equation discussed in Sec. II.C.2. Recasting methods developed by Kok, Struik, and van Haeringen (1979) and Kok et al. (1981) into EFT, Ando and Birse (2010) included Coulomb effects via a fully off-shell Coulomb T matrix and obtained at a single momentum cutoff $\Lambda_0 = 380.689$ MeV [the first cutoff value where the experimental triton binding energy is reproduced without a $3N$ force, $H(\Lambda_0) = 0$] a ³He binding energy $B(^3\text{He}) \simeq 7.66$ MeV, close to the experimental value of about 7.72 MeV. Ando and Birse (2010) treated all Coulomb effects nonperturbatively but considered the strong sector only at LO. Kirscher et al. (2010) obtained similar numerical results in a calculation that included NLO and selected higher-order interactions as part of an effective potential that was treated exactly.

The pionless calculation of pd scattering and helion was revisited and extended by König (2013) and König, Grießhammer, and Hammer (2015), who argued that the NLO pd system, within the partial-resummation approach, is not properly renormalized by the isospin-symmetric $3N$ force alone. The same conclusion was reached in a parallel analysis by Vanasse et al. (2014), who calculated pd scattering and ³He at NLO in strict perturbation theory. Using an asymptotic analysis, they showed that Coulomb effects at LO require a nonderivative $3N$ interaction at NLO (but not LO) to properly renormalize the pd system. At this level, one can no longer predict low-energy pd scattering from nd scattering without further input. Fixing the corresponding LEC to the ³He binding energy gives good agreement with an analytically derived expression, and it also provides cutoff-stable results for the phase shift. In contrast, Kirscher and Gazit (2016) argued that ³He is renormalized at NLO without an additional counterterm (pd scattering was not investigated). While both calculations use pionless EFT, they differ in the numerical implementation and regularization scheme.

A comparison of the different schemes for the counting of Coulomb effects in pd scattering up to NLO was provided by König and Hammer (2014). They argued that for the scattering of composite charged particles there is a certain arbitrariness in the definition of Coulomb-subtracted quantities (phase shifts and modified ERE parameters), namely, whether or not information about the deuteron substructure is included in the definition of the pure-Coulomb phase shift.

b. Perturbative Coulomb effects

Renewed interest and developments in the strict application of perturbation theory have also motivated a new look into the counting of Coulomb effects. The characteristic trinucleon momentum scale $\gamma_T \sim 80$ MeV $\gg \alpha m_N$ suggests that Coulomb effects should be a perturbative correction to the ³He binding energy (compared to the triton as its isospin mirror state). König, Grießhammer, and Hammer (2015) already showed that the calculation of Ando and Birse (2010) can be reproduced essentially unchanged when the fully off-shell Coulomb T matrix is replaced by one-photon-exchange diagrams. However, the calculation of König, Grießhammer, and Hammer (2015) is still nonperturbative because $B(^3\text{He})$ is extracted from the pole in the off-shell pd amplitude obtained from an integral equation that resums both one-nucleon exchange and $\mathcal{O}(\alpha)$ Coulomb diagrams. König et al. (2016) instead calculated the binding-energy difference $B(^3\text{H}) - B(^3\text{He})$ as a perturbation around an isospin-symmetric LO including a contribution missed in the earlier calculation of König, Grießhammer, and Hammer (2015). Once the logarithmic divergence generated by pp Coulomb effects is isolated and properly renormalized, the NLO ³He binding energy converges as the cutoff increases without an isospin-breaking $3N$ force. König et al. (2016) found $B(^3\text{He}) = (7.62 \pm 0.17)$ MeV, supporting the perturbative nature of Coulomb in this bound state. The same conclusion was reached independently by Kirscher and Gazit (2016). These results suggest that for nuclear ground states Coulomb is an NLO effect and isospin-breaking $3N$ forces do not enter up to this order. The same holds for pd scattering for center-of-mass momenta $k \gtrsim 20$ MeV, which König (2017) showed to be predicted from nd scattering up to NLO.

c. Dineutron constraints

Kirscher and Phillips (2011) used pionless EFT to constrain the neutron-neutron (nn) scattering length, for which there

exist conflicting experimental determinations of (-16.1 ± 0.4) fm (Huhn *et al.*, 2000a, 2000b) and (-18.7 ± 0.7) fm (Gonzalez Trotter *et al.*, 1999, 2006). Using a model-independent correlation between the difference of the *nn* and Coulomb-modified *pp* scattering lengths, on the one hand, and the ^{3}H-^{3}He binding-energy difference on the other hand, Kirscher and Phillips (2011) extracted $a_{nn} = (-22.9 \pm 4.1)$ fm from an LO calculation where isospin-breaking, nonderivative *NN* contact interactions were included.

Kirscher and Phillips (2011) considered only negative values for a_{nn}, thus excluding the possibility of a bound shallow state, the existence of which would correspond to a_{nn} large and positive. Motivated by renewed experimental interest in the existence of such a state, Hammer and König (2014) revisited the calculation and argued that the relevant parameter that enters the pionless calculation is not a_{nn} directly, but rather its inverse, such that going from large negative to large positive a_{nn} is only a small change. Extending the calculation of Kirscher and Phillips (2011) to NLO and taking into account the new *pd* counterterm identified by Vanasse *et al.* (2014), Hammer and König (2014) concluded that pionless EFT currently does not exclude a bound dineutron state.

5. Infrared regulators

Solving the EFT beyond the three-nucleon system poses significant technical challenges. All calculations so far have relied on the transition to the Hamiltonian and a solution of the Schrödinger equation or one of its many-body variants. One way to mitigate difficulties is to introduce an IR regulator in the form of a confining potential that produces discrete energy levels and, together with the UV regulator, reduces the solution of the Schrödinger equation to matrix inversion.

A simple choice is to confine the system to a periodic cubic box, first considered for EFT by Müller *et al.* (2000) and Abe, Seki, and Kocharian (2004). The case of *NN* in pionless EFT was dealt with by Beane *et al.* (2004), where a relation between phase shifts and energy levels within the box, originally obtained by Lüscher (1986, 1991), was rederived. The relations between *NN* LECs and ERE parameters for a large lattice were found by Seki and van Kolck (2006). Several papers have studied the limit cycle of the three-body system and the finite-volume corrections to three-body binding energies in periodic cubic boxes numerically (Kreuzer and Hammer, 2009, 2010, 2011; Kreuzer and Grießhammer, 2012). An analytical expression for the volume dependence of the three-body binding energy in the unitary limit was obtained by Meißner, Ríos, and Rusetsky (2015) and Hansen and Sharpe (2017). König and Lee (2018) studied the volume dependence of arbitrary *N*-body bound states, providing a more general perspective that reproduces the leading exponential dependence of the explicit three-body results just mentioned. The formulation of the three-particle quantization condition in a finite volume using the dibaryon formalism, which is required for the extraction of scattering phase shifts from lattice calculations, was considered by Briceno and Davoudi (2013) and Hammer, Pang, and Rusetsky (2017a, 2017b). Alternative approaches (Hansen and Sharpe, 2014; Mai *et al.*, 2017) were reviewed by Hansen and Sharpe (2019).

Nd scattering in the quartet *S*- and *P*-wave channels was calculated on a lattice by Elhatisari, Lee *et al.* (2016) and found to be in good agreement with the continuum results. Other reactions, such as $np \rightarrow d\gamma$ (Rupak and Lee, 2013) and *pp* fusion (Rupak and Ravi, 2015), are also accessible with this method.

Another widely employed confining potential is the harmonic oscillator, which can also be deployed to EFT (Stetcu *et al.*, 2010b). The analog of the Lüscher formula, due to Busch *et al.* (1998), also follows from pionless EFT (Luu *et al.*, 2010; Stetcu *et al.*, 2010a). Using this relation to determine the two- and three-nucleon LECs from, respectively, *NN* and *nd* phase shifts, Rotureau *et al.* (2012) generalized an earlier calculation for spin-1/2 fermions (Rotureau *et al.*, 2010) and reproduced previous NLO results for two and three nucleons in the limit of a wide harmonic oscillator. Tölle, Hammer, and Metsch (2011, 2013) investigated the related problem of up to six spinless bosons in a harmonic trap and provided explicit expressions for the running coupling constants. Using smeared contact interactions, they improved the convergence of the energy levels considerably. A recent refinement of the Busch formula was worked out by Zhang (2019).

6. Four nucleons

One of the virtues of encoding the Efimov effect in the three-body force is that its consequences for systems with more nucleons can be assessed in a model-independent way. A potential obstacle is the relatively strong binding of the $A = 4$ ground state, the alpha particle (^{4}He), whose binding energy $B(^4\text{He}) = 28.296$ MeV can be associated with a momentum scale $\gamma_\alpha = \sqrt{m_N B(^4\text{He})/2} \sim 110$ MeV that is not necessarily within the realm of pionless EFT.

The application of pionless EFT to the four-nucleon system was initiated by Platter, Hammer, and Meißner (2005), extending their previous work on the four-boson system with large two-body scattering length (Platter, Hammer, and Meißner, 2004). It was found that no 4*N* force is required for renormalization at LO, i.e., the alpha-particle binding energy converges as a function of increasing UV cutoff. Low-energy four-nucleon observables are then determined at LO only by two- and three-body input parameters. This means that, as for the Phillips line (Fig. 13), pionless EFT provides a natural explanation also for the phenomenological Tjon line (Tjon, 1975), an empirical correlation between $B(^4\text{He})$ and $B(^3\text{H})$. The surprising success of this LO calculation (Platter, Hammer, and Meißner, 2005) is apparent in Fig. 15. The renormalizability and good description of the alpha-particle binding at LO found by Platter, Hammer, and Meißner (2005) have been confirmed in other calculations, for example, those using the resonating-group (Kirscher *et al.*, 2010, 2015) and auxiliary-field diffusion Monte Carlo (Contessi *et al.*, 2017) methods.

Hammer and Platter (2007) later studied a four-body generalization of the Efimov effect in the four-boson system, demonstrating that the three-body ground state is associated with two four-body states, one very near the particle-trimer threshold, another deeper by a factor $\simeq 4$. The alpha-particle ground state is 3.7 times more bound than helion, and it has an excited, 0^+ state just below the neutron-helion threshold. The
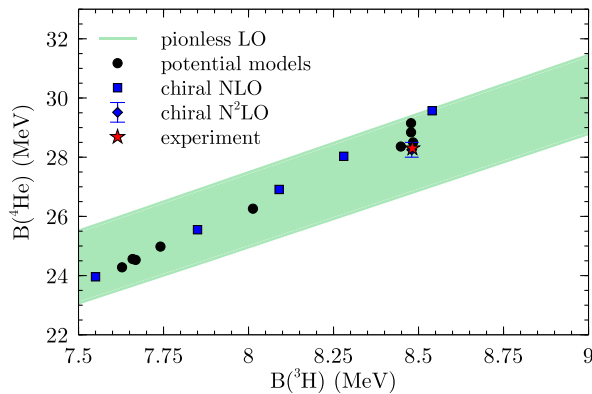
FIG. 15. Correlation between the alpha-particle binding energy $B(^4\text{He})$ and the triton binding energy $B(^3\text{H})$ (Tjon line) at LO in pionless EFT, compared to results from various chiral and phenomenological potentials, and experiment. The band indicates an estimate of higher-order corrections.

0^+ excited state was obtained at LO by Stetcu, Barrett, and van Kolck (2007), who solved the Schrödinger equation in a harmonic-oscillator basis, as done in the no-core shell-model approach. The three LECs were fitted to the deuteron, triton, and alpha ground-state energies, and the binding energy of the excited state, extrapolated in both UV and IR regulators, was found to be within 10% of the experimental value.

These calculations did not include the Coulomb interaction, which is consistent with the power counting developed later by König, Grießhammer, and Hammer (2015). Coulomb interactions have thus far been included only in calculations based on effective potentials solved nonperturbatively, as suggested originally by Weinberg (1991) in the context of chiral EFT. A variety of methods was used to solve the Schrödinger equation: resonating group (Kirscher et al., 2010), stochastic variational (Lensky, Birse, and Walet, 2016), and no-core shell model (Bansal et al., 2018). While results improve within a range of cutoff values, the resummation of subleading interactions (Sec. II.B.3) limits this range to small values and prevents conclusions about the RG beyond LO. In the first study of perturbative range corrections in $A \geq 4$ systems, Bazak et al. (2019) found that a four-body force is required to renormalize the universal four-boson system at NLO. This result directly carries over to pionless EFT and implies that an additional observable (most conveniently taken to be the ^4He binding energy) is required as input at NLO to set the scale of the four-body force.

Kirscher et al. (2010, 2013) pioneered the calculation of nucleon-trinucleon scattering in pionless EFT. New correlations between the neutron-helion and neutron-triton scattering lengths and the triton binding energy were identified. Proton-helion scattering was found in good agreement with an existing phase-shift analysis. These successes were tempered by an LO calculation (Deltuva, Lazauskas, and Platter, 2011) of the lowest, 0^- resonance in neutron-helion scattering, without Coulomb effects and an explicit $3N$ force, but with specific cutoff values for which the helion energy is correct. However, it is difficult to check the absence of regularization artifacts due to the absence of an explicit $3N$ interaction.

Except for this one calculation, all evidence thus far points to an unexpected triumph of the theory for $A = 4$.

7. Beyond four nucleons

Nuclear binding momenta generally increase with the number of nucleons, but it is not clear which scale (e.g., total binding energy or binding energy per nucleon) is most relevant for the EFT power counting. Consequently, it is an open question up to which number of nucleons pionless EFT should work. Successful applications to ^4He, which is already significantly more deeply bound than ^3He and ^3H, indicate that the binding energy per nucleon might be the relevant scale to estimate the binding momentum, but this remains to be firmly tested.

The first pionless EFT calculation beyond four nucleons was carried out by Stetcu, Barrett, and van Kolck (2007) with the no-core shell model. With the same parameters that led to an excellent postdiction of the ^4He excited state, the ground-state energy of ^6Li came out at 70% of the experimental value, which is consistent with the *a priori* LO uncertainty estimate from the pionless power counting. With the resonating-group method, Kirscher (2010) found that pionless EFT does not predict a bound five-nucleon state and carried out an exploratory study for the ^6He system. It was concluded that pionless EFT appears to support a shallow ^6He bound state, but a lack of numerical convergence prevented a strong assertion.

More recently, Contessi et al. (2017) used the auxiliary-field diffusion Monte Carlo method to study ^4He and ^{16}O at LO. No evidence was found for a ^{16}O that is stable with respect to breakup into four alpha particles. LO pionless EFT does not fail to provide sufficient saturation, but a small effect such as the ^{16}O energy relative to four alphas ($\sim$15% of the ^{16}O binding energy) requires a higher-order calculation. Bansal et al. (2018) used the coupled-cluster method to study the same systems and also ^{40}Ca, with qualitatively similar results at LO. With NLO interactions treated exactly, they found that ^{16}O and ^{40}Ca were stable, and in reasonable agreement with experiment.

Leading-order calculations all show convergence with increasing cutoff in the absence of $4N$ and higher-body forces, as is the case for bosons (Bazak, Eliyahu, and van Kolck, 2016). Bazak et al. (2019) showed that the five- and six-boson systems are renormalized by the four-body force at NLO and conjectured that yet-higher-body forces enter at subsequent orders. For nucleons, the Pauli principle is expected to suppress these forces relative to the bosonic case because at least two derivatives are required. Together, NLO results suggest that pionless EFT might work over a much wider range of A than originally anticipated.

There have been ambitious attempts to consider even larger systems. Kirscher (2017) investigated the possibility that a sufficiently large number of neutrons might bind. The properties of dilute, low-temperature neutron matter on a spacetime lattice (Lee and Schäfer, 2005, 2006a, 2006b; Abe and Seki, 2009a, 2009b) were found to be in qualitative agreement with potential-model calculations and expectations from other fermionic systems. While pionless EFT reproduces the long-standing results for the low-density expansion in a uniform Fermi system (Hammer and Furnstahl, 2000), various

resummations relevant for nuclear matter were discussed by Schäfer, Kao, and Cotanch (2005) and Kaiser (2011, 2012). Convergence of pionless EFT at saturation density is, however, not obvious.

8. External currents and reactions

The coupling to external currents works exactly as in the two-body sector (see Sec. II.B.8). Given the increased technical challenges, there are fewer calculations, and they mostly tackle triton and helion properties. Within this limited scope, they confirm the convergence of pionless EFT at low energies.

The simplest observable is the triton charge form factor—in particular, the charge radius—which determines the leading momentum dependence. Platter and Hammer (2006) used an effective quantum-mechanical framework to obtain the form factor in the impulse approximation, i.e., considering the electric charge operator between triton wave functions obtained by solving a Faddeev equation for the effective potential derived from the pionless Lagrangian at LO. Similar to the Phillips line (see Sec. II.C.2), the existence of a single LO three-body parameter in pionless EFT explains a correlation between the triton binding energy and charge radius that had previously been observed with different potential models (Friar *et al.*, 1985). An N^2LO calculation was reported by Sadeghi (2010), but few details were given. Recently, the fully perturbative treatment of higher-order corrections was extended to the triton and helion charge radii at N^2LO (Vanasse, 2017b, 2018), and magnetic moments and radii at NLO (Vanasse, 2018). Even though Coulomb interactions were neglected for ^{3}He, good agreement with experiment was found. Analogous results were obtained with a resummation of higher-order effects by Lensky, Birse, and Walet (2016), who also showed the correlation between the ^{4}He charge radius and other three- and four-nucleon observables.

Sadeghi and Bayegan (2005), Sadeghi, Bayegan, and Grießhammer (2006), and Sadeghi (2007) calculated the $nd \to {}^3$H γ capture cross section, finding good agreement with the available experimental data at N^2LO. Sadeghi and Bayegan (2010) calculated the inverse process of triton photodisintegration, which features the same amplitudes due to time-reversal symmetry. Several significant flaws in the calculation of Sadeghi, Bayegan, and Grießhammer (2006) were identified by Arani *et al.* (2014), who presented an updated calculation. At N^2LO, they still find reasonable agreement of the thermal nd capture cross section with experiment. The total cross section for the related reaction $pd \to {}^3$He γ was calculated to NLO in a range of energies amenable to perturbative Coulomb interactions by Nematollahi *et al.* (2016). The $3N$ force was fixed by the helion binding energy and data were reasonably described considering the uncertainty of the calculation. The even more challenging process of deuteron-deuteron radiative capture ($dd \to {}^4$He γ) was calculated at LO by Sadeghi and Khalili (2014), with the $3N$ force fitted to the alpha-particle energy. While the available data for the astrophysical S factor are apparently well described, a lack of technical details makes it difficult to assess the validity of the calculation.

New ground was broken with the extension to electroweak processes made by De-Leon, Platter, and Gazit (2016), who studied triton β decay to NLO. This work establishes a new way of fixing the LEC $L_{1,A}$ of the axial-vector counterpart of Eq. (41), which is relevant for other electroweak processes (pp fusion, in particular) as well. Calculations like this reveal the potential of pionless EFT to tackle interesting reactions involving more than two nucleons based, for example, on the general framework developed by De-Leon, Platter, and Gazit (2019).

D. Outstanding issues and current trends

Pionless EFT has fulfilled the long-standing goal of a renormalizable quantum field theory for nuclear physics. Although it has a narrow regime of strict validity, it seems to at least apply to $A \le 3$ bound states and possibly to extend to $A = 4$ and beyond. RG invariance, combined with the fine-tuning that places two-body bound states near zero energy, has led to a power counting that flies in the face of NDA, as summarized for the potential in Fig. 5. Yet, unresolved questions remain:

- How far in A can we describe nuclei within this framework? To date, all LO calculations ($A \le 40$) have given binding energies in agreement with experiment within the expected theoretical uncertainty, but finer details such as relative energies and thresholds have not been reproduced. Calculations for $A = 4$, 16, 40 where subleading interactions are resummed reinforce the surprising success of LO. However, at the moment no calculation exists for more than four nucleons where NLO and higher orders are treated perturbatively. There also remain issues about the power counting of Coulomb and other isospin-breaking interactions. Higher-order calculations for $A > 4$ are sorely needed.

- Wigner (1937a, 1937b) proposed an SU(4) spin-isospin symmetry to explain the strong binding of nuclei containing integer numbers of alpha particles. Since the $3N$ force in Eq. (43) is SU(4) symmetric (Bedaque, Hammer, and van Kolck, 2000), one cannot but wonder whether there are signs of SU(4) symmetry also in light nuclei. It was shown by Chen, Lee, and Schafer (2004) that binding energies of $A \le 4$ nuclei satisfy inequalities obtained from SU(4) symmetry. Accordingly, Vanasse and Phillips (2017) developed an expansion around an SU(4)-symmetric LO based on average $^1S_0$ and $^3S_1$ scattering lengths. They showed that this expansion is promising also for observables other than binding energies since it converges well for the triton charge radius up to NLO in the symmetry-breaking parameter (and including range corrections as well).

- In the same spirit, how far can we push the expansion around the nontrivial fixed point of the NN amplitude, i.e., the unitary limit where both the deuteron and the $^1S_0$ virtual state have zero energy? In this limit, the LO EFT has not only exact SU(4) symmetry but also discrete scale invariance. While the two-body amplitude is invariant under continuous scale transformations (Mehen, Stewart, and Wise, 2000), the three-body force in Eq. (44) is symmetric only under discrete scale

changes (Bedaque, Hammer, and van Kolck, 1999a, 1999b). This remaining symmetry leads to Efimov states in the three-body system and its descendants in the four- (Hammer and Platter, 2007) and higher-body systems. König (2017) and König *et al.* (2017), generalizing an earlier approach to the $^1S_0$ channel (König *et al.*, 2016), proposed an expansion around the unitary (or unitarity) limit also in the $^3S_1$ channel: expansions in both $1/Qa_t$ and $1/Qa_s$ are added to the standard pionless EFT expansion. A single LO parameter Λ_* provides the nonperturbative scaffolding, on top of which more quantitative results are built by perturbation theory. This radical expansion appears to converge remarkably well for three- and four-nucleon binding energies (König, 2017; König *et al.*, 2017). At LO, all binding energies are functions of Λ_*, and for bosons (Carlson *et al.*, 2017) they saturate according to the liquid-drop formula. The correlation between nuclear-matter saturation energy and density expressed in the Coester line (Coester *et al.*, 1970) would emerge from the variation of Λ_* (van Kolck, 2017) just as the Tjon line—if, that is, pionless EFT holds all the way to heavy nuclei. Related work that aims to simplify nuclear physics based on the closeness of the real world to the unitarity limit and/or Wigner SU(4) limit was carried out by Kievsky and Gattobigio (2016), Kievsky *et al.* (2018), Lu *et al.* (2018), and Gattobigio, Kievsky, and Viviani (2019).

III. HALO/CLUSTER EFT

A. Motivation

In this section we discuss efforts to go one step further in the application of low-energy universality by including tightly bound clusters of nucleons as explicit fields in the effective Lagrangian. This halo/cluster EFT framework is appropriate for halo nuclei and nuclei with a cluster structure. In both cases, the energy required to remove clusters or halo nucleons, characterized by a momentum scale M_{lo}, is much smaller than the energy required to break clusters apart associated with a momentum scale M_{hi}. The classic example is ^{6}He, where the energy to separate two neutrons from an alpha-particle core is $S_{2n} \simeq 0.975$ MeV $\ll B(^4\text{He})$. This class of systems can be thought of as nucleons orbiting one or more clusters, all separated by distances much larger than the cluster sizes. They typically lie at the limits of nuclear stability represented in the nuclear chart by the so-called driplines, and they are target of a vigorous experimental program at rare-isotope facilities worldwide. As we discuss later, they can display more than one low-momentum scale, e.g., when Coulomb interactions are present or when a cluster has an isolated low-energy excited state.

As in Eq. (3), observables are expanded in powers of M_{lo}/M_{hi} and Q/M_{hi}, where Q is a typical momentum. While halo/cluster EFT is mathematically similar to the pionless EFT for nucleons discussed in Sec. II—and in fact is a theory without explicit pions by itself, becoming pionless EFT for light nuclei when the cores are nucleons—there are a number of new aspects. First, higher partial waves between clusters, or between clusters and nucleons, are often enhanced, as for the

$n\alpha$ scattering relevant for ^{6}He. This causes a richer structure already in the two-body sector and requires modified power-counting schemes. Second, the antisymmetrization between nucleons in a cluster (which are not active degrees of freedom) and halo nucleons is not explicit.

One might ask what kind of error is introduced by using explicit fields for tightly bound clusters. The effect on observables of exchanging nucleons in the core with halo nucleons is governed by the overlap of the wave functions of the halo nucleons with the wave functions of the core nucleons. Since the range of the former is M_{lo}^{-1} while the range of the latter is M_{hi}^{-1}, this overlap is suppressed by M_{lo}/M_{hi} compared to the overlap of two halo nucleons. Therefore, these effects are controlled by the EFT expansion in M_{lo}/M_{hi} and are encoded in the LECs of halo/cluster EFT. The same argument applies for nucleons in different, widely separated clusters. For momenta Q of the order of the breakdown scale M_{hi} or above, when distances compared to the core size are probed, full antisymmetrization and other short-range physics have to be included explicitly.

Halo/cluster EFT exploits the scale separation between M_{lo} and M_{hi} independently of the mechanism creating it. Thus, it complements *ab initio* approaches to halo nuclei by zooming out to large distances and providing universal relations between different few-body observables. These relations can be combined with input from an underlying EFT or experiment to predict halo properties. Moreover, they allow us to test the consistency of different approaches and/or experiments. A particular strength lies in the possibility to describe the electroweak structure and reactions of halo nuclei in a model-independent way with controlled error estimates.

Halo/cluster EFT can be viewed as a generalization of nuclear cluster models and is usually referred to simply as halo EFT (Bertulani, Hammer, and van Kolck, 2002; Bedaque, Hammer, and van Kolck, 2003). We give a brief overview here, starting with S-wave neutron halos and Efimov states in Secs. III.B and III.C, respectively. The complementarity with *ab initio* methods, useful for exploring heavy halos, is discussed in Sec. III.D, and higher partial waves are tackled in Sec. III.E. We show how halo EFT connects with electromagnetic processes in Sec. III.F before sketching the changes needed for proton halos (Sec. III.G) and multicluster systems (Sec. III.H), and ending with an outlook (Sec. III.I). Our emphasis is complementary to Sec. II. A more in-depth discussion can be found in the review of halo EFT by Hammer, Ji, and Phillips (2017).

B. S-wave neutron halos

We start with the case of S-wave halo nuclei or cluster states without Coulomb interactions. For definitiveness, we consider one- and two-neutron halo nuclei using the formalism of Hagen, Hammer, and Platter (2013). The extension to other cases is straightforward. We also restrict our analysis to LO in M_{lo}/M_{hi}. Higher-order effects can be included as discussed in Sec. II for pionless EFT.

The effective Lagrangian for neutrons (n) and a spinless core (c) can be written as the sum of one-, two-, and three-body contributions $\mathcal{L} = \mathcal{L}_{1b} + \mathcal{L}_{2b} + \mathcal{L}_{3b} + \cdots$, where the the ellipsis denotes higher-order terms and

$$\mathcal{L}_{1b} = \psi_0^\dagger \left(i\partial_0 + \frac{\nabla^2}{2m_0} \right)\psi_0 + \psi_1^\dagger \left(i\partial_0 + \frac{\nabla^2}{2m_1} \right)\psi_1,$$

$$\mathcal{L}_{2b} = \Delta_1 d_1^\dagger d_1 - g_1 [d_1^\dagger (\psi_1\psi_0) + \text{H.c.}]$$

$$+ \Delta_0 d_0^\dagger d_0 - \frac{g_0}{2} [d_0^\dagger (\psi_1^T P \psi_1) + \text{H.c.}],$$

$$\mathcal{L}_{3b} = \Omega\, t^\dagger t - h[t^\dagger(\psi_0 d_0) + (\psi_0 d_0)^\dagger t]. \tag{46}$$

The notation is slightly changed compared to Sec. II [cf. Eq. (27)] to efficiently account for neutron and core fields, the Pauli spinor ψ_1, and the scalar ψ_0, respectively. The two-body part $\mathcal{L}_{2b}$ includes two dimerons, the scalar d_0 corresponding to an $^1S_0$ nn pair and the Pauli spinor d_1 for a cn pair. $P = i\sigma_2/\sqrt{2}$ projects the two neutrons on the spin singlet. Finally, $\mathcal{L}_{3b}$ represents the three-body interaction written in terms of a trimeron auxiliary field (Bedaque et al., 2003), which is particularly useful for form-factor calculations (Hagen, Hammer, and Platter, 2013; Vanasse, 2017b). It includes the bare trimeron residual mass Ω and the bare coupling h of the trimeron t to the d_0 dimeron (nn) and the c field ψ_0. Only the parameter combination h^2/Ω contributes to observables at LO. As in pionless EFT, there exists a whole class of equivalent theories with three-body forces acting in different channels. Integrating out the auxiliary fields, different choices of $\mathcal{L}_{2b}$ and $\mathcal{L}_{3b}$ can be transformed into the same theory without dimeron and trimeron fields up to four- and higher-body interactions.

In the following, we focus on the properties of the cn, nn, and cnn systems. For compact notation, we define the mass parameters

$$M_{\text{tot}} = m_0 + 2m_1, \qquad M_i = M_{\text{tot}} - m_i, \qquad m_{ij} = M_i - m_j,$$

$$\mu_i = \frac{m_0 m_1^2}{m_i M_i}, \qquad \tilde{\mu}_i = \frac{m_i M_i}{M_{\text{tot}}}. \tag{47}$$

The diagrams for the dressed dimeron propagator, Fig. 6, are completely analogous to that for the dibaryon field discussed in Sec. II.B.5. At LO, the full dimeron propagator for the dimeron d_i is

$$iD_i(p_0, \mathbf{p}) = \frac{2\pi i}{s_i g_i^2 \mu_i} \left[1/a_i - \sqrt{-2\mu_i \tilde{p}_0 - i\varepsilon} \right]^{-1}, \tag{48}$$

where $\tilde{p}_0 = p_0 - \mathbf{p}^2/(2M_i)$ and $s_i = \delta_{i0}/2 + \delta_{i1}$ is a symmetry factor. As before, a_i stands for the scattering length. For positive a_i, the propagator has a bound-state pole on the first Riemann sheet with residue $Z_i = 2\pi/s_i g_i^2 \mu_i^2 a_i$. For negative a_i, there is a pole on the second sheet corresponding to a virtual state.

The leading correction to the propagator in Eq. (48) is due to the effective range. It can be included by making the dimeron fields dynamical, as discussed in Sec. II.B.5. Here we stay at LO in the EFT expansion and neglect effective-range corrections. The pole momentum γ_i is then given by $\gamma_i = 1/a_i$.

Observables in the cnn system can be obtained from the T matrix for the scattering process of a dimeron and a particle. The universal properties and structure of two-neutron halos were also explored in an effective quantum-mechanical

framework (Canham and Hammer, 2008, 2010; Acharya, Ji, and Phillips, 2013) by solving the Faddeev equations for an effective potential reflecting the expansion in $M_{\text{lo}}/M_{\text{hi}}$ and for the renormalized zero-range model (Amorim, Frederico, and Tomio, 1997; Delfino et al., 2006). For a review of the latter work, see Frederico et al. (2012).

We consider the center-of-mass frame, in which the on-shell T matrix depends only on the total energy E and the relative momenta in the ingoing and outgoing channels $\mathbf{p}$ and $\mathbf{k}$, respectively. External dimeron legs are renormalized with the wave-function renormalization factors $\sqrt{|Z_i|}$. The absolute value is required only for $i = 0$ because $Z_0 < 0$, corresponding to the unbound nn pair. Here the factor provides a convenient redefinition of the amplitude but has no physical significance.

There are two possibilities for the initial or final state, depending on the identity of the particle and dimeron. Here we label the T-matrix element T_{ij} by the index i (j) of the dimeron and particle in the incoming (outgoing) channel. Keeping the matrix structure of T_{ij} implicit, the integral equation for the T matrix is given by Fig. 10 with the substitution in Fig. 11, where the contact three-body coupling is h^2/Ω. The T matrix can be decomposed into partial-wave contributions $T_{lm,l'm'} = \delta_{ll'}\delta_{mm'}T_l$. The resulting (2×2)-matrix integral equation for angular momentum l is a generalization of the Skorniakov–Ter Martirosian equation (Skorniakov and Ter Martirosian, 1957) and reads

$$T_l(E, p, k) = \int_0^\Lambda dq\, R_l(E, p, q)\bar{D}(E, q)T_l(E, q, k)$$

$$+ R_l(E, p, k) \tag{49}$$

when a sharp momentum-space cutoff Λ is imposed on the loop momentum in the three-body sector. For simplicity, we focus on the S wave, $l = 0$, and drop the subscript l on R and T. The components of the interaction matrix R are given by

$$R_{ij}(E, p, k) = \frac{2\pi\chi_{ij}m_{ij}}{|a_i a_j s_i s_j|^{1/2}\mu_i\mu_j}\frac{1}{pk}Q_0(c_{ij}) - \delta_{i0}\delta_{j0}H,$$

$$c_{ij} = \frac{m_{ij}}{pk}\left(\frac{p^2}{2\mu_j} + \frac{k^2}{2\mu_i} - E - i\varepsilon \right), \tag{50}$$

where $\chi_{ij} = 1 - \delta_{i0}\delta_{j0}$ and Q_0 is a Legendre function of the second kind. Moreover, $H = |Z_0|h^2/\Omega$ is the dimensionless three-body coupling defined in Eq. (44) that depends log-periodically on the cutoff Λ. It contributes only for angular momentum $l = 0$. The dimeron matrix is diagonal in the channel indices: $\bar{D} = \text{diag}(\bar{D}_0, \bar{D}_1)$ with

$$\bar{D}_i(E, q) = \frac{\mu_i|a_i|q^2}{2\pi^2}\left[-1/a_i + \sqrt{-2\mu_i\tilde{E} - i\varepsilon} \right]^{-1}, \tag{51}$$

and $\tilde{E} = E - q^2/(2\tilde{\mu}_i)$.

The transition amplitude near the energy of an S-wave three-body bound state can be decomposed into a regular and an irregular part. This yields the homogeneous bound-state equation

$$\mathcal{B}(p) = \int_0^\Lambda dq\, R(E, p, q)\bar{D}(E, q)\mathcal{B}(q), \qquad (52)$$

which has nontrivial solutions only at the bound-state energy $E = -B_{cnn}$.

For a given cutoff Λ, we can fix the unknown three-body parameter H such that Eq. (52) has a solution at the desired value $E = -B_{cnn}$. However, any other three-body observable can be used as well. In this way, the three-body coupling is renormalized and other three-body observables (including other three-body bound states) can be predicted. In particular, Eq. (49) can be solved numerically to determine the T matrix for three-body scattering observables. Since the two-neutron system is not bound, only the element T_{11} describes a particle-dimeron scattering process, namely, the scattering of a neutron from a cn bound state at energy $E = p^2/(2\tilde{\mu}_1) - 1/(2\mu_1 a_1^2)$:

$$T_{11}(E, p, p) = \frac{2\pi}{\tilde{\mu}_1}\frac{1}{p\cot\delta_{cn-n}(p) - ip}. \qquad (53)$$

The other elements contribute to three-body scattering and breakup.

A fully perturbative extension of this formalism to NLO was recently presented by Vanasse (2017a). NLO equations with resummed range corrections were previously given by Canham and Hammer (2010).

C. Excited Efimov states in halo nuclei

The bound-state solutions of Eq. (52) are a specific variant of Efimov states (Efimov, 1970, 1973). Thus, the Efimov effect provides a natural binding mechanism for two-neutron halos with dominantly S-wave interactions. However, the contributions of higher partial waves and partial-wave mixing complicate the situation. While halo EFT naturally accommodates resonant interactions in higher partial waves, as discussed in Sec. III.E, there is no Efimov effect in this case; see, e.g., Jona-Lasinio, Pricoupenko, and Castin (2008), Braaten et al. (2012), and Nishida (2012). A general overview of Efimov states in nuclear and particle physics was given by Hammer and Platter (2010). Here we review the possibility of identifying Efimov states in halo nuclei.

Since the strength of the interaction between the neutrons and the core is fixed, the identification of Efimov physics is more delicate than for ultracold atoms, where the effective scattering length can be dialed through an external magnetic field. In particular, the log-periodic dependence of observables on the scattering length cannot be used to identify Efimov physics. Instead, one may look for excited states that approximately satisfy the universal scaling relation for Efimov states (Efimov, 1970, 1973). Note that there are two relevant scattering lengths for a cnn system, $a_0 \equiv a_{nn}$ and $a_1 \equiv a_{cn}$. Since a_{nn} is the same for all halo nuclei and negative, we focus only on the dependence on a_{cn}. We define the three-body momentum as

$$K = \text{sgn}(E)\sqrt{2\tilde{\mu}_1|E|}, \qquad (54)$$

where the sign of the square root is taken as the sign of the energy E. The schematic dependence of the Efimov spectrum

on K and the inverse neutron-core scattering length a_{cn}^{-1} is illustrated in Fig. 16. The breakdown scale M_{hi} defines a region outside of which details of short-range physics matter and the bound states cease to be universal. Two typical situations are shown, with two universal states (at $a_{cn} > 0$) and one universal state (at $a_{cn} < 0$).

In the hypothetical unitary limit $a_{cn}^{-1} = a_{nn}^{-1} = 0$, the Efimov spectrum becomes geometric,

$$K^{(n)} = -\lambda_0^{-n}\kappa_*, \qquad (55)$$

where $\lambda_0 = e^{\pi/s_0}$ is the discrete scaling factor and κ_* is the binding momentum of the state with label $n = 0$. In general, s_0 and λ_0 depend on the number of interacting pairs and the masses and symmetry properties of the particles, and $\lambda_0 \approx 22.7$ for the equal-mass nucleons discussed in Sec. II. The value of κ_* is related by a regulator-dependent constant factor to the three-body parameter $\Lambda_\star$ that determines the three-body force H in Eq. (44). An explicit value for the case of identical bosons was given by Braaten and Hammer (2006). The spectrum shown in Fig. 16 is invariant under discrete scaling transformations with λ_0:

$$\kappa_* \to \kappa_*, \qquad a_{cn} \to \lambda_0^m a_{cn}, \qquad K \to \lambda_0^{-m}K, \qquad (56)$$

where m is any integer. This discrete scale invariance holds for all few-body observables and is a clear signature of an RG limit cycle in the three-body system (Bedaque, Hammer, and van Kolck, 1999a).

If more particles are added, no new parameters are needed for renormalization at LO (Platter, Hammer, and Meißner, 2004, 2005). As a consequence, all four-body observables in the universal regime are governed by the same limit cycle and can be characterized by a and κ_*. This leads to the universal correlations between three- and four-body observables already discussed in Secs. II.C.2 and II.C.6. Similar behavior is expected for higher-body observables.

Halo nuclei have been discussed as possible candidates for Efimov states for more than 30 years (Fedorov, Jensen, and
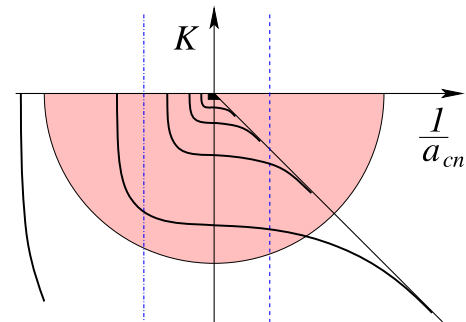
FIG. 16.   Illustration of the Efimov spectrum as a function of the three-body momentum K [cf. Eq. (54)] and the inverse neutron-core scattering length a_{cn}^{-1}. The diagonal line in the fourth quadrant represents the neutron-core threshold. The solid lines indicate the Efimov states. The window of universality for bound states is represented by the shaded half circle, while the dashed and dot-dashed lines indicate a typical system with $a_{cn} > 0$ and $a_{cn} < 0$, respectively.

FIG. 17. Boundary curves for the existence of excited Efimov states in two-neutron halo nuclei with different core masses A as a function of the square roots of the neutron-core energy E_{nc} and neutron-neutron energy E_{nn} in units of the three-body ground-state energy E_{gs}. The sign of the square root is taken as positive (negative) if the corresponding two-body system nc or nn has a bound state (virtual state). Established halo nuclei are shown by the data points, while the shaded area gives the parameter range for the predicted halo nucleus ^{62}Ca. From Hammer, 2018.

Riisager, 1994). As the full Efimov plot for cnn systems is three dimensional and depends on the two scattering lengths a_{nn} and a_{cn}, it is more instructive to plot candidate nuclei in a two-dimensional plane characterized by the neutron-core ener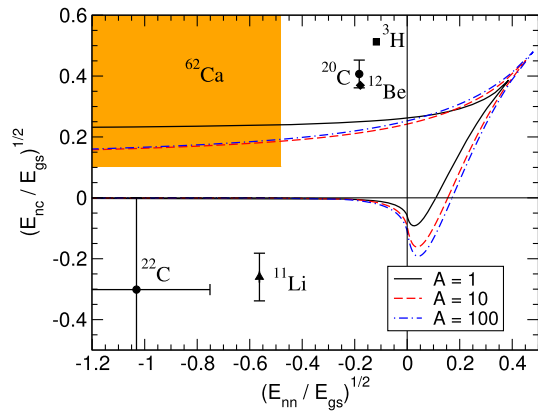gy E_{nc} and the neutron-neutron energy E_{nn}, in units of the three-body ground-state energy E_{gs}, as introduced by Amorim, Frederico, and Tomio (1997). If a given nucleus lies within a certain boundary curve that weakly depends on the mass number A of the core, it should display an excited Efimov state. The candidate nuclei ^{11}Li, ^{12}Be, ^{14}Be, ^{18}C, and ^{20}C were investigated in LO halo EFT assuming only resonant S-wave interactions by Canham and Hammer (2008). An update of this analysis with current halo candidates and established halo nuclei is shown in Fig. 17. The triton has also been added since it can be interpreted as a two-neutron halo with a proton core.

In 2010, ^{22}C was established as the then heaviest halo nucleus. In particular, ^{22}C was found to display a large matter radius (Tanaka et al., 2010) and a large S-wave component in its n-^{20}C subsystem (Horiuchi and Suzuki, 2006). Since the information on the neutron-core energy E_{nc} was ambiguous, Acharya, Ji, and Phillips (2013) used halo EFT to explore the correlation between the n-^{20}C energy and the two-neutron separation energy of ^{22}C. Combining this correlation with the matter-radius measurement, they demonstrated that an excited Efimov state in ^{22}C is unlikely. A recent update of this analysis by Hammer, Ji, and Phillips (2017), using the more precise matter radius from Togano et al. (2016) as input, reached the same conclusion.

Whether heavier neutron halos than ^{22}C exist is still an open question, although there is some experimental evidence that the ground states of ^{31}Ne and ^{37}Mg have a low one-neutron separation energy and can be considered deformed P-wave halo nuclei (Kobayashi et al., 2014; Nakamura et al., 2014).

This makes it worthwhile to investigate the possibility for Efimov states in heavier nuclei.

D. *Ab initio* methods and Efimov states in heavier nuclei

Halo EFT can be used in conjunction with *ab initio* calculations to extend the reach of the latter or to test the consistency of different approaches. Here we discuss an example of the former in the context of Efimov physics. Further examples regarding electromagnetic reactions are given later.

Coupled-cluster calculations by Hagen et al. (2012b) of neutron-rich calcium isotopes, which used a chiral potential with schematic $3N$ forces and included coupling to the scattering continuum, suggested that a large S-wave scattering length might occur in the ^{61}Ca system, with interesting implications for ^{62}Ca. Subsequently, Hagen et al. (2013) computed the elastic scattering of neutrons on ^{60}Ca while obtaining quantitative estimates for the scattering length and the effective range, and confirming that a large scattering length can be expected. These results were then used as input for halo EFT in the study of the ^{60}Ca-n-n system.

Specifically, the focus was on signals of Efimov physics that are a consequence of the large scattering lengths in the ^{60}Ca-n and n-n systems. This is illustrated in Fig. 18, where the universal correlation between the ^{61}Ca-n scattering length and the two-neutron separation energy of ^{62}Ca is shown. For ^{62}Ca with $m_0 = 60m_1$, the discrete scaling factor governing the energy spectrum is approximately $16^2 = 256$ (Braaten and Hammer, 2006), which is slightly more favorable than in the case of equal-mass particles. The asymptotic scaling ratio applies only for deep states or in the unitary limit of infinite scattering length. Away from the unitary limit, however, the ratio of energies near threshold can be significantly smaller; see Fig. 16 and the corresponding discussion by Braaten and Hammer (2006). In the case of ^{62}Ca, the whole energy region between $S_{2n} \approx$ 5–8 keV and the breakdown scale $S_{hi} \approx$ 500 keV is available for Efimov states. At $S_{2n} \approx 230$ keV, the ^{60}Ca-n scattering length jumps from $+\infty$ to $-\infty$ and an excited Efimov state appears. It is thus conceivable that ^{62}Ca
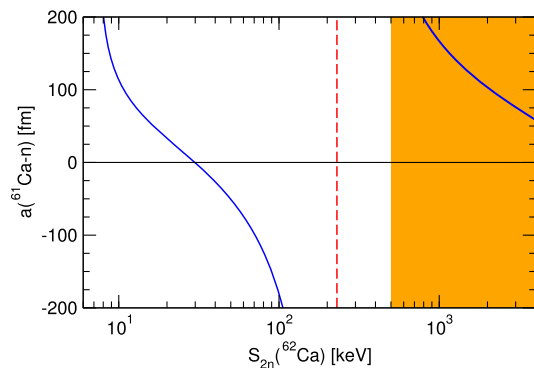

FIG. 18. Correlation between the ^{61}Ca-n scattering length and the two-neutron separation energy S_{2n} of ^{62}Ca. The emergence of an excited Efimov state around $S_{2n} = 230$ keV is indicated by the vertical dashed line. The shaded area indicates the region where halo EFT breaks down. From Hammer, 2016.

would display an excited Efimov state and unlikely that it would not display any Efimov states at all. The matter radius of ^{61}Ca relative to the ^{60}Ca core was found to be 4.9(4) fm, while the matter radius of ^{62}Ca could be even larger, depending on the precise value of S_{2n}.

One can summarize the situation on excited Efimov states in halo nuclei as follows. While the ground states of many S-wave halo nuclei are close to the Efimov limit, there is currently no observed halo nucleus that displays an excited Efimov state or is likely to display such a state. There is some theoretical evidence that the situation could be different for ^{62}Ca. The corresponding parameter range is indicated by the shaded square in Fig. 17. The results of Hagen *et al.* (2013) imply that ^{62}Ca is possibly the largest and heaviest halo nucleus in the chart of nuclei and demonstrated that a large number of observables would display characteristic features of Efimov physics. Measurement of these observables clearly poses a significant challenge for experiment. For example, ^{58}Ca is the heaviest calcium isotope that has been observed experimentally (Tarasov *et al.*, 2009). However, future radioactive-beam facilities might provide access to calcium isotopes as heavy as ^{68}Ca.

E. Higher partial waves and resonances

Next we discuss systems with resonant interactions in higher partial waves. Such interactions are ubiquitous in halo and cluster nuclei and lead to a richer power-counting structure.

Consider two-body scattering with reduced mass μ and energy $E = k^2/2\mu$ in the center-of-mass frame. Resonance behavior arises when the S matrix has a pair of poles in the two lower quadrants of the complex k plane. The projection of S into the resonant partial wave l can be written as

$$\frac{S_l}{s_l(k)} = \frac{k + k_+}{k - k_+} \frac{k + k_-}{k - k_-} = \frac{E - E_0 - i\Gamma(E)/2}{E - E_0 + i\Gamma(E)/2}. \quad (57)$$

Here $k_\pm = \pm k_R - ik_I$ with $k_{R,I} > 0$ are the pole positions, $s_l(k)$ is a smooth function in the energy region under consideration, $E_0 = (k_R^2 + k_I^2)/2\mu$ is the position of the resonance (where the corresponding phase shift crosses $\pi/2$), and $\Gamma(E)/2 = kk_I/\mu$ is referred to as the half-width of the resonance. A narrow resonance is one for which $\Gamma(E_0)/(2E_0) \ll 1$, that is, for which the poles are near the real axis, $k_I/k_R \ll 1$. We call the resonance shallow if $|k_\pm| \equiv M_{\text{lo}} \ll M_{\text{hi}}$. An example of a shallow, narrow resonance is given by the $^2P_{3/2}$ resonance in $n\alpha$ scattering (the ground state of ^{5}He), which has (Bertulani, Hammer, and van Kolck, 2002) $\Gamma(E_0)/2 \simeq 0.3$ MeV $\ll E_0 \simeq 0.8$ MeV $\ll E_\alpha \simeq$ 20 MeV or $k_I \simeq 6$ MeV $\ll k_R \simeq 34$ MeV $\ll \sqrt{m_N E_\alpha} \simeq 140$ MeV, where E_α is the excitation energy of the α core and m_N is the nucleon mass.

Shallow resonances can be described in halo EFT just as bound states. For notational simplicity, we take the two scattering particles to be identical, with mass $m = 2\mu$ and no spin. Generalization to other situations is straightforward. As with bound states, it is convenient to introduce a dimeron field with the quantum numbers of the resonance. Note that

the formulation with dimeron fields is equivalent to a formulation with particle contact interactions. [For details, see the discussion by Bertulani, Hammer, and van Kolck (2002) and, for S-wave states, Sec. II.] In the following, we focus on the case where the resonance is in the $l = 1$ state, in which case the dimeron field d has three components corresponding to spin 1. In a notation similar to Eq. (27),

$$\mathcal{L} = \psi^\dagger \left(i\partial_0 + \frac{\nabla^2}{2m} \right) \psi + d_l^\dagger \left[\eta_1 \left(i\partial_0 + \frac{\nabla^2}{4m} \right) - \Delta_1 \right] d_l$$
$$+ \frac{g_1}{4} [d_l^\dagger (\psi \overset{\leftrightarrow}{\nabla}_l \psi) + \text{H.c.}] + \cdots, \quad (58)$$

where the Galilean combination $\overset{\leftrightarrow}{\nabla} = \overset{\leftarrow}{\nabla} - \overset{\rightarrow}{\nabla}$ places the two particles in a P wave.

The full dimeron propagator, depicted in Fig. 6, is the bare propagator given by the inverse of the dimeron kinetic term and dressed by the bubbles generated by the $d\psi\psi$ interactions in Eq. (58). The two-particle T matrix is obtained by attaching external particle legs. The result reproduces the ERE for P waves, Eq. (12), with

$$\frac{1}{a_1} = \theta_3 \Lambda^3 - \frac{12\pi\Delta_1}{mg_1^2}, \qquad -\frac{r_1}{2} = \theta_1 \Lambda + \eta_1 \frac{12\pi}{m^2 g_1^2}, \quad (59)$$

where, as in Eq. (22), $\theta_{1,3}$ are numbers that depend on the chosen regularization. We see that both the scattering length and the effective range need to be included at LO to absorb all divergences (Bertulani, Hammer, and van Kolck, 2002). This requirement has to be reflected by the power counting for P waves. We note that the need to include additional interactions for renormalization at LO will become more severe in higher partial waves.

For the scaling of the parameters $a_1, r_1, \ldots$, different scenarios can be envisioned.

   (i) Naive dimensional analysis suggests that the typical size for the ERE parameters $a_1, r_1, \ldots$ is given by the appropriate power of the momentum scale M_{hi} where the EFT breaks down.

For instance, if the interaction between the particles is described by a potential of depth $\sim M_{\text{hi}}$ and range $\sim 1/M_{\text{hi}}$, one would expect $a_1 \sim 1/M_{\text{hi}}^3$ and $r_1 \sim M_{\text{hi}}$. In particular, a resonance or bound state, if present, generally occurs at the momentum scale M_{hi}.

Scenario (i) is clearly not appropriate for halo nuclei with shallow resonances or bound states. In such systems, the interactions are finely tuned in such a way as to produce a resonance or bound state close to threshold, at a scale M_{lo} much smaller than M_{hi}, violating the NDA estimate. This situation can occur when one or more of the ERE parameters have unnatural sizes related to M_{lo}.

  (ii) Bertulani, Hammer, and van Kolck (2002) proposed a different power counting assuming $a_1 \sim 1/M_{\text{lo}}^3$ and $r_1 \sim M_{\text{lo}}$, while all higher ERE parameters scale with M_{hi}.

With this scaling, all three terms of the ERE shown explicitly in Eqs. (12a) and (12b) are of the same order for momenta

$k \sim M_{\mathrm{lo}}$ and must be retained at LO. Higher ERE parameters are suppressed by powers of $M_{\mathrm{lo}}/M_{\mathrm{hi}}$ and thus are subleading.

Scenario (ii) requires that two combinations of constants, Δ_1/g_1^2 and $1/g_1^2$, be fine-tuned against the large values $\Lambda \gtrsim M_{\mathrm{hi}}$ in Eq. (59) to produce a result containing powers of the small scale M_{lo}. From a naturalness perspective, this makes it less likely to occur in nature than a scenario with one fine-tuning like the one for an S-wave bound state.

(iii) An alternative scaling was suggested by Bedaque, Hammer, and van Kolck (2003), where $a_1 \sim 1/M_{\mathrm{lo}}^2 M_{\mathrm{hi}}$, $r_1 \sim M_{\mathrm{hi}}$, and all other ERE parameters again scale with appropriate powers of M_{hi}.[6]

This scenario requires only *one* combination of constants, namely, Δ_1/g_1^2, to be fine-tuned.

With option (iii), the terms proportional to $1/a_1$ and $r_1 k^2$ in the dimeron propagator are of the same order for momenta $k \sim M_{\mathrm{lo}}$. The term stemming from the unitarity cut ik^3 is suppressed by one power of $M_{\mathrm{lo}}/M_{\mathrm{hi}}$ and is, therefore, subleading. The remaining terms in the ERE are even more suppressed. Thus, LO corresponds to taking the bare dimeron propagator while the effects of loops and higher-derivative interactions enter as higher-order corrections.

At LO the difference between the scalings (ii) and (iii) is the presence of the unitarity-cut term $\sim ik^3$. This difference disappears if instead of considering generic momenta k of order M_{lo} we focus onto a narrow region around the position of the resonance at $k = \sqrt{2/a_1 r_1}$. Owing to the near cancellation within a window of size $\Delta k = 2/a_1 r_1^2$ around the pole between the two terms that are leading in scenario (iii), the unitarity-cut term has to be resummed to all orders and provides a width to the resonance. In this kinematic range, there are two fine tunings: one implicit in the short-distance physics leading to the unnatural value of a_1, and another one explicitly caused by the choice of kinematics close to the pole. Power counting for resonances has been discussed further by Gelman (2009), Alhakami (2017), and Schmidt, Jansen, and Hammer (2018).

If the underlying theory cannot be solved, the appropriate scaling for a specific physical system can be inferred from the data, i.e., from the numerical values of the ERE parameters. However, such a determination is not always unique and/or different scalings might apply in different kinematic regions. In the first papers on halo EFT, Bertulani, Hammer, and van Kolck (2002) and Bedaque, Hammer, and van Kolck (2003) applied scalings (ii) and (iii), respectively, to the lowest resonance in $n\alpha$ scattering. The experimental ERE parameters can be accommodated in both scalings such that both appear viable. Although the unitarization implicitly carried out in (iii) is not necessary except near the resonance, it improves the description throughout the low-energy region. In either case, scattering data determine the $n\alpha$ interaction parameters.

The two-neutron halo nucleus ^{6}He offers a further testing ground for halo EFT with resonant P waves. The $n\alpha$ interaction in that nucleus is dominated by the $^2P_{3/2}$

resonance. The structure and renormalization of ^{6}He were investigated by Rotureau and van Kolck (2013) and Ji, Elster, and Phillips (2014). Rotureau and van Kolck (2013) calculated ^{6}He at LO in the Gamow shell model using scenario (ii) and found that a three-body force, the analog of $\mathcal{L}_{3b}$ in Eq. (46), is required to stabilize the system. Ji, Elster, and Phillips (2014) solved the Faddeev equations in scenario (iii) but demoted the $^2S_{1/2}$ $n\alpha$ interaction to NLO. They also found that a three-body force is required for renormalization at LO and determined its running over a wide range of cutoffs. The observed behavior is not log periodic, although some periodicity is observed. Alternative formulations at LO were investigated by Ryberg, Forssén, and Platter (2017) and shown to be equivalent, while momentum-space probability densities of ^{6}He were calculated by Göbel *et al.* (2019).

The power counting for resonant partial waves with $l \geq 2$ was also discussed by Bertulani, Hammer, and van Kolck (2002) and Bedaque, Hammer, and van Kolck (2003). Their analysis of the power divergences of the one-loop self-energy showed that the first $l + 1$ ERE parameters are required to absorb all divergences. This was confirmed by the Wilsonian RG analysis of Harada, Kubo, and Ninomiya (2009), which considered the cases $l = 1, 2$ explicitly. An alternative power counting for bound states with $l = 2$ was proposed by Braun *et al.* (2018) and applied to the description of D-wave states in ^{15}C and ^{17}C (Braun, Hammer, and Platter, 2018).

F. Electromagnetic properties and reactions

For one-neutron halo nuclei, halo EFT essentially reproduces the ERE, but their electromagnetic structure and reactions can be predicted. The formalism is similar to that of pionless EFT (Sec. II.C.8) and serves to illustrate it. Moreover, the accuracy limits of cluster models can be estimated from the order at which gauge-invariant couplings to currents appear.

In the following, we exemplify the power of halo EFT in the electromagnetic sector using the example of ^{11}Be (Hammer and Phillips, 2011) and give a brief overview of results in other systems. The first excitation of ^{10}Be is 3.4 MeV above the ground state, which has $J^P = 0^+$. Meanwhile, ^{11}Be has a $1/2^+$ state with neutron separation energy $B_0 = 500$ keV, and a $1/2^-$ state with $2n$ separation energy $B_1 = 180$ keV (Ajzenberg-Selove, 1990), which we denote as ^{11}Be*. The shallowness of these two states of ^{11}Be compared to the bound states of ^{10}Be suggests that they have significant components in which a loosely bound neutron orbits a ^{10}Be core. In halo EFT, the $1/2^+$ state is described as an S-wave bound state of the neutron and the core, while $1/2^-$ is a P-wave bound state governed by scenario (iii) in Sec. III.E.

The effective Lagrangian for the system can be obtained by combining Eq. (46) for the $1/2^+$ ground state and Eq. (58) (generalized to unequal masses) for the $1/2^-$ excited state. Photons are included via the minimal substitution, Eq. (36), and through the field strength; see Hammer and Phillips (2011) for explicit expressions.

Here our focus is on electric properties, and the dominant pieces of the electric response follow from the minimal substitution in Eq. (36). But at higher orders in the

---

[6]A similar scheme was applied to the $\Delta(1232)$ resonance in chiral EFT by Pascalutsa and Phillips (2003) and Long and van Kolck (2010).

computation of these properties, gauge-invariant operators (counterterms) appear involving the electric field $\mathbf{E}$ and the fields c for the ^{10}Be core, n for the halo neutron, d for the ^{11}Be ground-state dimeron, and d^* for the ^{11}Be* excited-state dimeron. Possible one- and two-derivative operators with one power of the photon field are

$$\mathcal{L}_{\text{EM}} = L_{C0} d^\dagger (\boldsymbol{\nabla} \cdot \mathbf{E}) d + L_{C0}^{(*)} d^{*\dagger} (\boldsymbol{\nabla} \cdot \mathbf{E}) d^*$$
$$+ iL_{E1}^{(1/2)} ([dd^{*\dagger}]_l \mathbf{E}_l + \text{H.c.}) + \cdots, \qquad (60)$$

where $[\cdots]_l$ indicates the projection on $l = 1$. If magnetic properties are to be considered, we have to include operators involving the magnetic field $\mathbf{B}$ as well.

The electric interactions in Eq. (60) are gauge invariant by themselves, and we must determine the order at which they occur. Rescaling the fields to absorb all powers of M_{lo} as done by Beane and Savage (2001), the scaling of the coupling constants with M_{lo} can be obtained from NDA (Hammer and Phillips, 2011). As a consequence, the leading effects in the charge radius squared of the $1/2^-$ state in ^{11}Be are $\sim (r_1 M_{\text{lo}})^{-1} \sim (M_{\text{lo}} M_{\text{hi}})^{-1}$. The operator proportional to $L_{C0}^{(*)}$ produces effects of the order of $(r_1 M_{\text{hi}})^{-1} \sim (M_{\text{hi}})^{-2}$ and thus affects the prediction for the charge radius at NLO. Similarly, the $E1(1/2^+ \to 1/2^-)$ matrix element has parametric dependence $M_{\text{lo}}^{-1}(M_{\text{lo}} M_{\text{hi}})^{-1/2}$. Including the proper wave-function renormalization factors, the operator with LEC $L_{E1}^{1/2}$ yields an effect $\sim M_{\text{hi}}^{-1}(M_{\text{lo}} M_{\text{hi}})^{-1/2}$ and thus already occurs at NLO. Thus, for electric quantities involving the shallow $1/2^-$ excited state of ^{11}Be, there are two parameters in the halo EFT description at NLO that cannot be fixed with ^{10}Be-n scattering information alone. There are none at LO and presumably more at N^{2}LO.

1. Form factors

The form factor of the ^{11}Be ground state is computed by calculating the contribution to the irreducible vertex for $A_0 dd$ interactions shown in Fig. 19. There is no diagram coupling the photon to the neutron at this order since $Q_n = 0$. In the Breit frame, where the four-momentum of the virtual photon is $q = (0, \mathbf{q})$, the irreducible vertex for the A_0 photon coupling to the d field is $-ieQ_c G_E(|\mathbf{q}|)$, where Q_c is the charge of the core. A straightforward calculation yields

$$G_E(|\mathbf{q}|) = \frac{2\gamma_0}{f|\mathbf{q}|} \arctan\left(\frac{f|\mathbf{q}|}{2\gamma_0}\right), \qquad (61)$$
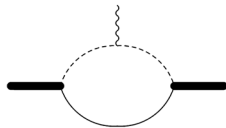

FIG. 19. The LO contribution to the irreducible vertex for an A_0 photon coupling to the ^{10}Be-neutron S-wave bound state. The thick solid line indicates the ^{11}Be ground state, while the solid, dashed, and curly lines represent the neutron, ^{10}Be core, and photon, respectively.

with $\gamma_0 = \sqrt{2\mu_1 B_0}$ and $f = (1 + m_0/m_1)^{-1}$, in the notation of Eq. (47). For the deuteron $m_0 = m_N$ and $f = 1/2$, Eq. (61) thus reduces to the LO pionless EFT result of Chen, Rupak, and Savage (1999a).

The form factor is a function of $\mathbf{q}^2$ only, and the charge radius is defined as $\langle r_E^2 \rangle = -6(d/d\mathbf{q}^2) G_E|_{\mathbf{q}^2=0}$. Applying this expression to Eq. (61) yields

$$\langle r_E^2 \rangle = \frac{f^2}{2\gamma_0^2}, \qquad (62)$$

which gives the charge radius of the ^{11}Be ground state relative to the charge radius of ^{10}Be. Thus, we have $\langle r_E^2 \rangle_{^{11}\text{Be}} - \langle r_E^2 \rangle_{^{10}\text{Be}} = f^2/2\gamma_0^2$. This relation can be understood by writing the charge distribution of ^{11}Be as a convolution of the charge distribution of ^{10}Be with that of the ^{10}Be-n halo system. Using the convolution theorem for the Fourier transform, one finds that the total mean-square radius is the sum of the squared radii for ^{10}Be and the ^{10}Be-n halo system.

The latter effect can be calculated in halo EFT. We note that the finite size of the core will also appear in halo EFT at higher orders (Chen, Rupak, and Savage, 1999a). An extended power-counting scheme that explicitly takes into account the scaling of the mass ratio f to move these contributions to lower orders was given by Ryberg et al. (2019).

Inserting $\gamma_0 = 0.15$ fm^{-1}, the relative radius becomes $\langle r_E^2 \rangle_{^{11}\text{Be}} - \langle r_E^2 \rangle_{^{10}\text{Be}} = 0.19$ fm^2. This is consistent with the experimental result $0.51(17)$ fm^2 (Nörtershauser et al., 2009) within the 40% uncertainty from NLO effects in this system. Using the experimental result for the ^{10}Be charge radius as further input, we find $\langle r_E^2 \rangle_{^{11}\text{Be}}^{1/2} = 2.40$ fm at LO. This is 2% to 3% smaller than the atomic-physics measurement, which yields $\langle r_E^2 \rangle_{^{11}\text{Be}}^{1/2} = 2.463(16)$ fm (Nörtershauser et al., 2009).

At NLO, a new operator associated with gauging the term $\sim d^\dagger \partial_0 d$ in the effective Lagrangian contributes. The calculation produces an increased charge radius as long as the S-wave n-^{10}Be effective range r_0 is positive [cf. Beane and Savage (2001)],

$$\langle r_E^2 \rangle_{^{11}\text{Be}} - \langle r_E^2 \rangle_{^{10}\text{Be}} = \frac{f^2}{2(1 - r_0\gamma_0)\gamma_0^2}. \qquad (63)$$

Using the value $r_0 = 2.7$ fm determined from Coulomb dissociation of ^{11}Be (discussed later), the relative radius becomes $\langle r_E^2 \rangle_{^{11}\text{Be}} - \langle r_E^2 \rangle_{^{10}\text{Be}} = 0.31(5)$ fm^2 at NLO, which improves the agreement with the atomic-physics measurement. The change is of the order of 40%, which is in agreement with the a priori expectation. As a consequence, the result for the full charge radius of the ^{11}Be ground state increases to $\langle r_E^2 \rangle_{^{11}\text{Be}}^{1/2} = 2.42$ fm. In contrast to observables involving the $1/2^-$ state, the radius of the ^{11}Be ground state does not receive any corrections from short-distance physics until N^{3}LO (Chen, Rupak, and Savage, 1999a). The remaining difference between the NLO and experimental values is

consistent with the presence of the short-distance operator $\sim L_{C0}$ from Eq. (60) at N^3LO in the expansion of the radius.

For the charge form factor of the $1/2^-$ excited state, NLO corrections might be expected to be smaller since its typical momentum is lower. However, a counterterm already enters at NLO for this observable. The form factor is given by the contribution to the irreducible vertex for $A_0 d^* d^*$ interactions. There are two diagrams at LO, the first of which is analogous to that for the $1/2^+$ state shown in Fig. 19, while the second represents a direct coupling of the photon from gauging the $d^{*\dagger}\partial_0 d^*$ term in the effective Lagrangian. The latter contributes at LO because the effective range r_1 corresponds to an LO operator for the $1/2^-$ state. The charge form factor of the $1/2^-$ state at LO is obtained as (Hammer and Phillips, 2011)

$$G_E^{(*)}(|\mathbf{q}|) = 1 - \frac{\gamma_1}{r_1} + \frac{f^2\mathbf{q}^2 + 2\gamma_1^2}{|\mathbf{q}|f r_1} \arctan\left(\frac{f|\mathbf{q}|}{2\gamma_1}\right), \quad (64)$$

where $\gamma_1 = \sqrt{2\mu_1 B_1}$ and r_1 is the P-wave effective range for n-^{10}Be scattering. Note that $G_E^{(*)}(0) = 1$, as required by charge conservation, while the charge radius of the $1/2^+$ state relative to the ^{10}Be ground state is

$$\langle r_E^2 \rangle^{(*)} = -\frac{5f^2}{2\gamma_1 r_1}. \quad (65)$$

This scales as $1/M_{\mathrm{lo}}M_{\mathrm{hi}}$ as expected. It seems counterintuitive that there is already a short-distance contribution to $\langle r_E^2 \rangle^{(*)}$ at NLO, especially when the corresponding effect does not occur in $\langle r_E^2 \rangle$ until N^3LO (Chen, Rupak, and Savage, 1999a). The reason for this enhanced sensitivity is that the probability distribution of P-wave states is drawn into shorter distances than the one of S-wave states, as it gets caught between the attractive potential that produces the P-wave state and the centrifugal barrier. Observables associated with a shallow P-wave bound state will, therefore, generically exhibit counterterms at lower order than those of their S-wave counterparts.

Numerical evaluation of the LO expression (65) leads to the prediction $\langle r_E^2 \rangle_{^{11}\mathrm{Be}^*} - \langle r_E^2 \rangle_{^{10}\mathrm{Be}} = 0.36$ fm^2, where we use the value $r_1 = -0.66$ fm from the $B(E1)$ value as input (discussed later). The NLO radius includes contributions from the counterterm $L_{C0}^{(*)}$ in Eq. (60), the coefficient of which is unknown. Hammer and Phillips (2011) estimated the NLO contributions to be of the order of 20%, assuming that the short-distance effects in $\langle r_E^2 \rangle_{^{11}\mathrm{Be}^*}^{1/2}$ scale with f. This assumption is in agreement with the expectation from the power counting. Again using the experimental result for the ^{10}Be charge radius (Nörtershauser et al., 2009), the prediction for the charge radius of ^{11}Be* at LO is $\langle r_E^2 \rangle_{^{11}\mathrm{Be}^*}^{1/2} = (2.43 \pm 0.1)$ fm. To date, there has been no experimental determination of this charge radius.

Halo EFT calculations for the charge and magnetic form factors of ^{11}Be and ^{19}C were performed to NLO by Fernando, Vaghani, and Rupak (2015). They considered ^{15}C as well and suggested the inclusion of the effective range as an LO effect in this case.
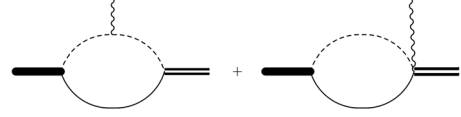

FIG. 20. The two diagrams contributing to the irreducible vertex for the S-to-P-state transition $\Gamma_{j\mu}$ at LO. The double line indicates the ^{11}Be excited state; the other lines are as in Fig. 19.

2. E1 transition and photodisintegration

Next we discuss the $E1$ transition from the $1/2^+$ state to the $1/2^-$ state. The irreducible vertex for this transition is depicted in Fig. 20. We compute the transition for a photon of arbitrary four-momentum $k = (\omega, \mathbf{k})$, and the sum of diagrams yields $-i\Gamma_{j\mu}$, where j is the angular momentum index of the d^* field and μ is the polarization index of the photon. The diagrams depicted in Fig. 20 are divergent, but their divergences cancel, providing a nontrivial check on the calculation. As long as both diagrams are considered, current conservation is also satisfied (Hammer and Phillips, 2011), $k^\mu \Gamma_{j\mu} = 0$. Note that if only the long-distance $E1$ mechanism on the left-hand side of Fig. 20 is considered, as was done, for example, by Typel and Baur (2008), then current conservation is not satisfied and it appears that some input from short-distance physics is needed to define the prediction for this observable.

Evaluating the diagrams in Fig. 20, we obtain the LO halo EFT result for $B(E1)$,

$$B(E1) = -\frac{Z_{\mathrm{eff}}^2 e^2}{3\pi} \frac{\gamma_0}{r_1} \left[\frac{2\gamma_1 + \gamma_0}{(\gamma_0 + \gamma_1)^2}\right]^2, \quad (66)$$

with $Z_{\mathrm{eff}} = fQ_c \approx 0.366$ the effective charge. No regularization is needed to get a finite result. We note that the resulting equation (66) is "universal" in the sense that it applies to any $E1$ S-to-P-wave transition in a one-neutron halo nucleus. Once r_1, γ_1, and γ_0 are known for a given one-neutron halo, the prediction embodied in Eq. (66) is accurate up to corrections of $\mathcal{O}(M_{\mathrm{lo}}/M_{\mathrm{hi}})$.

Since there is no experimental value for the P-wave effective range r_1, Hammer and Phillips (2011) extracted it from the experimental number $B(E1)(1/2^+ \rightarrow 1/2^-) = 0.105(12)e^2$ fm^2 (Summers et al., 2007), yielding $r_1^{\mathrm{LO}} = -0.66$ fm^{-1}. Short-distance effects enter $B(E1)$ through a counterterm in the NLO corrections. The $B(E1)$ $(1/2^+ \rightarrow 1/2^-)$ transition therefore cannot be predicted at NLO, which can be seen from the presence of the operator with LEC $L_{E1}^{(1/2)}$ in Eq. (60).

Comparing this calculation with a shell-model treatment of ^{11}Be, it is clear that one effect that is subsumed into the NLO counterterm $L_{E1}^{(1/2)}$ is the transition of a neutron from a $d_{5/2}$ to a $p_{3/2}$ orbital, with that neutron coupled to the 2^+ state of ^{10}Be. This 2^+ state is 3.4 MeV above the ^{10}Be ground state, so the dynamics associated with it takes place at distances $\sim M_{\mathrm{hi}}^{-1}$. Hence, in halo EFT it can only appear in short-distance operators such as that multiplying $L_{E1}^{(1/2)}$. The computation of Millener et al. (1983) suggests that such a contribution reduces the $E1$ matrix element by $\sim 30\%$, which is the
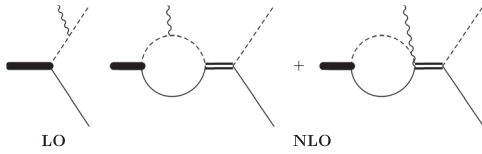
FIG. 21. Diagrams contributing to photodissociation of the ^{11}Be ground (S-wave) state. The notation is as in Fig. 20.

anticipated size of an NLO effect when the M_{lo}/M_{hi} expansion is employed in the ^{11}Be system. There are other effects of a similar size that will affect $B(E1)$ at NLO. Specifically, there are NLO corrections from the wave-function renormalization factors associated with the S- and P-wave fields. Both tend to increase $B(E1)$ over the LO prediction.

We move on to the photodisintegration of ^{11}Be into ^{10}Be plus a neutron. In practice, this process is measured using Coulomb excitation of the ^{11}Be nucleus, with the two reactions connected within the equivalent-photon approximation. There are three contributions to this process, as depicted in Fig. 21. The first diagram, denoted as "LO" in the figure, corresponds to the contribution from the plane-wave impulse approximation. The second and third diagrams, denoted as "NLO," include the final-state interactions between the neutron and the core in the $J = 1/2$ channel. As we show later, the first diagram is dominant over diagrams involving P-wave final-state interactions. From these diagrams, we obtain the differential $B(E1)$ strength distribution at NLO (Hammer and Phillips, 2011),

$$\frac{dB(E1)}{dE} = \frac{e^2 Z_{\mathrm{eff}}^2}{4\pi} \frac{12\mu_1\gamma_0|\mathbf{p}'|^3}{\pi^2(\mathbf{p}'^2 + \gamma_0^2)^4}$$
$$\times \left(1 + r_0\gamma_0 + \frac{2\gamma_0}{3r_1}\frac{3\mathbf{p}'^2 + \gamma_0^2}{\mathbf{p}'^2 + \gamma_1^2}\right), \quad (67)$$

where $\mathbf{p}'$ is the relative momentum of the outgoing ^{10}Be-n pair and $E = \mathbf{p}'^2/(2\mu_1)$ is the kinetic energy of the ^{10}Be-n pair in the center-of-mass frame.

The LO result corresponds to taking only the 1 in the parenthesis of Eq. (67). The NLO correction comes from two sources. The first is the shift of the wave-function renormalization to larger values due to $r_0 > 0$, which tends to increase the $B(E1)$ strength. Second, final-state interactions between the neutron and the core in the $J = 1/2$ channel enter at this order. Accurate measurements of the Coulomb dissociation spectrum therefore provide information on the S-wave n-^{10}Be effective range if the P-wave effective range is already fixed from another observable.

Up to LO accuracy for the bound-to-bound-state transition and NLO for the bound-to-continuum one, there are four LECs: γ_0 and γ_1 (which are known from separation energies) and the S- and P-wave effective ranges r_0 and r_1. At the next order, the counterterm $L_{E1}^{(1/2)}$ from Eq. (60) enters as well.

Folding the halo EFT result in Eq. (67) with the neutron detector resolution and the spectrum of $E1$ photons, the experimental data of Palit *et al.* (2003) are well described, as shown in Fig. 22. At NLO, if we take the value of r_1 fixed as mentioned, we have one free parameter, the value of the
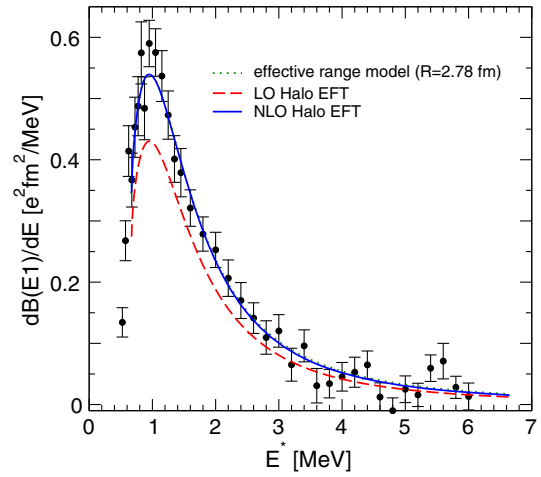

FIG. 22. Differential $B(E1)$ strength for Coulomb dissociation of ^{11}Be into ^{10}Be $+ n$ as a function of excess energy of the neutron E^*. The dashed (solid) lines show the halo EFT result of Hammer and Phillips (2011) at LO (NLO) folded with the detector resolution. The experimental data are from Palit *et al.* (2003), while the dotted line (almost on top of the solid line) gives the effective range model of Typel and Baur (2005). From Hammer and Phillips, 2011.

S-wave effective range r_0. A reasonable fit is found for $r_0 = 2.7$ fm, close to the effective-range result of Typel and Baur (2005) with all integrals cut off at $R = 2.78$ fm. This choice of cutoff corresponds to specific assumptions about the counterterms. Another experiment by Fukuda *et al.* (2004) can be described equally well but suggests a 3% to 4% larger value for r_0.

The Coulomb dissociation of the one-neutron halo nucleus ^{19}C was studied by Acharya and Phillips (2013) using the ^{18}C core and the neutron as effective degrees of freedom. In this case, there is no excited state present. Acharya and Phillips demonstrated the power of halo EFT by calculating various observables and extracted the ERE parameters and the separation energy of the halo neutron from the Coulomb dissociation data of Nakamura *et al.* (1999). In particular, they obtained the values $(575 \pm 55 \pm 20)$ keV for the one-neutron separation energy of ^{19}C, and $(7.75 \pm 0.35 \pm 0.3)$ fm for the ^{18}C-neutron scattering length, where the first error is statistical and the second error is an estimate of the EFT uncertainty. Their prediction for the longitudinal-momentum distribution is in good agreement with the data of Bazin *et al.* (1995) and confirms the S-wave dominance for ^{19}C.

The charge form factor and the Coulomb breakup of two-neutron halo nuclei were first calculated by Hagen, Hammer, and Platter (2013), Hagen (2014), and Acharya (2015) at LO. The calculation of the charge form factor was recently extended to NLO by Vanasse (2017a). [Vanasse also corrected an error in the prefactor of one term in the form-factor calculation of Hagen, Hammer, and Platter (2013).] Since the value of the neutron-core effective range is unknown and can merely be estimated, we quote in Table I only the LO charge radii for ^{11}Li, ^{12}Be, and ^{22}C from Vanasse (2017a), together with the input value for the two-neutron separation energy. The charge radius for ^{11}Li has been measured by

TABLE I. Two-neutron separation energies and LO charge radii squared for four different two-neutron halos. Adapted from Vanasse, 2017a.

Nucleus	S_{2n} (MeV)	$\langle r_E^2 \rangle$ (fm^2)
^{11}Li	0.3693(6)	0.744
^{14}Be	1.27(13)	0.126
^{22}C	0.11(6)	$0.519^{+\infty}_{-0.274}$

Puchalski, Moro, and Pachucki (2006) and Sanchez et al. (2006). The result $\langle r_E^2 \rangle = 1.104(85)$ fm^2 is consistent with the LO result within the estimated 40% uncertainty due to range effects. The charge radii of ^{14}Be and ^{22}C have not yet been measured.

Halo EFT has also been used to calculate the matter radii of the two-neutron halo nuclei listed in Table I up to NLO (i) using dimeron propagators with resummed range effects (Canham and Hammer, 2008, 2010) and (ii) with a fully perturbative treatment of range corrections (Vanasse, 2017a). Both methods lead to consistent results.

3. Correlations

EFTs in general, and halo EFT in particular, provide model-independent correlations between different observables. In pionless EFT, the most prominent universal correlations were discussed in Secs. II.C.2 and II.C.6. Such correlations have also proven useful in the analysis of universal properties of ultracold atoms (Braaten and Hammer, 2006).

Previously, we expressed the electromagnetic properties of the ^{11}Be system through the ERE parameters for n-^{10}Be scattering: γ_0, γ_1, r_0, and r_1. These expressions can be interpreted as correlations between scattering observables and electromagnetic properties. Analogously, there are correlations between different electromagnetic observables.

As a specific example, we consider the correlation between the $B(E1)$ strength and the radius of the $1/2^+$ state in ^{11}Be at LO. Using Eqs. (65) and (66), we obtain

$$B(E1) = \frac{2e^2 Q_c^2}{15\pi}(\langle r_E^2 \rangle_{^{11}\text{Be}^*} - \langle r_E^2 \rangle_{^{10}\text{Be}})x\left[\frac{1+2x}{(1+x)^2}\right]^2, \quad (68)$$

where Q_c is the charge of the core and $x = \sqrt{B_1/B_0}$ is the square root of the ratio of the neutron separation energies for the $1/2^-$ and $1/2^+$ states. The $B(E1)$ strength is thus proportional to the mean-square radius of the $1/2^-$ state. In the limit of vanishing neutron separation energy for the $1/2^-$ state, the $B(E1)$ strength vanishes linearly with x. Equation (68) can also be used to obtain the charge radius of the $1/2^-$ state $\langle r_E^2 \rangle_{^{11}\text{Be}^*}$ directly from the measured value of $B(E1)$ and the neutron separation energies B_1 and B_0. This gives $\langle r_E^2 \rangle_{^{11}\text{Be}^*} - \langle r_E^2 \rangle_{^{10}\text{Be}} = 0.35$–$0.39$ fm^2, depending on which experimental value of $B(E1)$ is used. Similar correlations can be derived for other observables.

These correlations make halo EFT a powerful tool for testing the consistency of experimental data and/or ab initio calculations based on general assumptions about the scaling of observables with M_{lo} and M_{hi}. They can be combined with ab initio results to obtain predictions for low-energy

observables as discussed in Sec. III.D and afterward. In this spirit, Braun et al. (2018) used a correlation between the $B(E2)$ value for the transition $5/2^+ \rightarrow 1/2^+$ and the quadrupole moment of the $5/2^+$ state in ^{15}C to predict the quadrupole moment from ab initio calculations of the $B(E2)$ value. Lei et al. (2018) used a correlation between the $d\alpha$ S-wave scattering length and the amount by which ^{6}Li is bound with respect to the $np\alpha$ threshold to argue that ^{6}Li is a two-nucleon halo nucleus.

4. Neutron capture

The inverse reaction of the photodissociation of one-neutron halo nuclei is radiative neutron capture on the core nucleus, which can be relevant for a variety of astrophysical processes. The corresponding efforts in halo EFT have been reviewed by Higa (2015) and Rupak (2016).

One example is the radiative neutron capture on ^{7}Li. This reaction was investigated in halo EFT by Rupak and Higa (2011). They expressed the cross section in terms of n-^{7}Li scattering parameters and showed that the LO uncertainty comes from the poorly known P-wave effective range r_1. The low-energy data for this reaction can be described well by a one-parameter fit yielding $r_1 = -1.47$ fm^{-1}. In subsequent work, Fernando, Higa, and Rupak (2012) extended this calculation to higher energies, where the 3^+ resonance becomes important. Their results suggest a resonance width about 3 times larger than the experimental value. They also presented power-counting arguments that establish a hierarchy for electromagnetic one- and two-body currents.

The radiative neutron capture on ^{7}Li was refined by Zhang, Nollett, and Phillips (2014b) in an approach combining halo EFT and ab initio calculations. They presented a halo EFT calculation that describes neutron capture to both the ground and first excited states of ^{8}Li. Each of the possible final states were treated as halo bound-state configurations of ^{7}Li plus a neutron, including low-lying excited states of the ^{7}Li core. The asymptotic normalization coefficients of these bound states were taken from an ab initio calculation using a phenomenological potential. In contrast to Rupak and Higa (2011), they found good agreement with the ratio of partial cross sections for different initial spin states. Moreover, they obtained excellent agreement with the measured branching ratios between the two final states.

Rupak, Fernando, and Vaghani (2012) applied halo EFT to the dominant $E1$ contribution to radiative neutron capture on ^{14}C, including contributions from both resonant and nonresonant interactions. They found that significant interference between these two mechanisms leads to a capture contribution that deviates from simple Breit-Wigner resonance form.

G. Proton halos

Proton halos are less common due to the delicate interplay between attraction from the strong interaction and the Coulomb repulsion. The presence of the Coulomb barrier introduces the Coulomb momentum

$$k_C = Z_1 Z_2 \alpha \mu_{12}, \quad (69)$$

with $Z_{1,2}$ the particle charges and μ_{12} their reduced mass, as a new scale corresponding to the inverse of the Bohr radius of the system. This scale is independent of the hadronic scales and complicates the power counting (cf. the discussion for protons in Sec. II). In general, the correct scaling of the Coulomb momentum with respect to strong-interaction scales strongly depends on the system considered. One focus of recent studies in halo EFT has been, therefore, on the underlying scaling relations in systems and reactions with Coulomb forces.

An EFT for S-wave proton-halo nuclei was developed by Ryberg *et al.* (2014b). They analyzed the universal features of proton halos bound due to a large S-wave scattering length and derived LO expressions for the charge form factor and the radiative proton-capture cross section. In subsequent work Ryberg *et al.* (2016) extended the calculation to higher orders and analyzed the effect of finite-range corrections. They calculated the charge radius to NLO and the astrophysical S factor for low-energy proton capture to fifth order in the low-energy expansion. Higher-order ERE parameters cannot contribute to the $E1$ capture reaction, and thus the accuracy is only limited by gauge-invariant counterterms. As an application, Ryberg *et al.* (2016) considered the S factor for proton capture on ^{16}O into the excited $1/2^+$ state of ^{17}F and quantified an energy-dependent model error to be utilized in data fitting. They also provided a general discussion of the suppression of proton halos compared to neutron halos by the need for two fine-tunings in the underlying theory. Schmickler, Hammer, and Hiyama (2019) and Schmickler, Hammer, and Volosniev (2019) investigated universal binding in few-body systems of up to four charged particles. They showed that range corrections are generically enhanced in the strong Coulomb case relevant for most nuclei.

The inclusion of Coulomb effects in P-wave halo nuclei was pioneered by Higa (2010), who looked at low-energy $p\alpha$ scattering. More extensive calculations were carried out later by Zhang, Nollett, and Phillips (2014a), extending their previous work for neutron capture to the proton halo in ^{7}Be$(p,\gamma)^8$B. This reaction is important for analyzing solar neutrino experiments (Adelberger *et al.*, 2011; Haxton, Hamish Robertson, and Serenelli, 2013). However, owing to the Coulomb barrier, it cannot be measured at the extremely low energies required for this purpose, and the data must be extrapolated. Zhang, Nollett, and Phillips (2014a) demonstrated that halo EFT together with input from *ab initio* calculations constitutes a powerful tool to carry out this extrapolation. They treated ^{8}B as a shallow P-wave bound state of a proton and a ^{7}Be core and included the first core excitation explicitly. The couplings were fixed using measured binding energies and p-^{7}Be S-wave scattering lengths, together with ^{8}B asymptotic normalization coefficients from *ab initio* calculations. They emphasized the important role of p-^{7}Be scattering parameters in determining the energy dependence of $S(E)$ and demonstrated that their present uncertainties significantly limit attempts to extrapolate the data to stellar energies. Zhang, Nollett, and Phillips (2015) extended this calculation to NLO and used Bayesian methods to determine the EFT parameters and the low-energy S factor, using measured cross sections and scattering lengths as inputs.
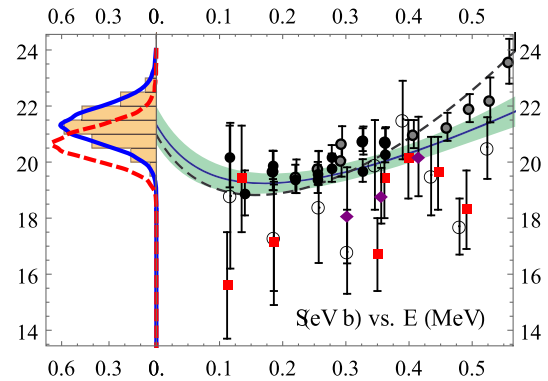

FIG. 23. (Right panel) NLO S factor as function of energy (solid blue curve). Shading indicates a 68% interval. The dashed line gives the LO result. (Left panel) One-dimensional probability distribution functions for $S(0)$ (blue line and histogram) and $S(20\text{ keV})$ (red dashed line). From Zhang, Nollett, and Phillips, 2015.

The results of their analysis, which reduced the uncertainty of $S(0)$ by a factor of 2, are shown in Fig. 23. Further details were given by Zhang, Nollett, and Phillips (2018a).

In related work, Ryberg *et al.* (2014a) pointed out that the charge radius of ^{8}B and the S factor for ^{7}Be$(p,\gamma)^8$B are correlated at LO in halo EFT. This correlation thus provides indirect access to the S factor at low energies and serves as a consistency check.

H. Cluster systems

Many nuclear states are close to a threshold for breakup into smaller clusters and are therefore amenable to an EFT approach where these smaller clusters are the relevant degrees of freedom. For example, several states of nuclei with $A = 4(n+1)$, $n \geq 1$ an integer, and equal numbers of proton and neutrons are thought to be made of alpha-particle clusters (Ikeda, Takigawa, and Horiuchi, 1968). The most famous example is the Hoyle state, the first 0^+ excited state of ^{12}C, which owing to its position near the 3α threshold plays an important role in the creation of ^{12}C and ^{16}O, and thus our type of life, in the Universe. Traditionally, these states have been investigated with a variety of phenomenological approaches (Freer *et al.*, 2018).

The first step to study these systems in halo EFT is $\alpha\alpha$ scattering. Higa, Hammer, and van Kolck (2008) developed a power counting for this system, which is highly fine-tuned. Because of the subtle interplay of strong and electromagnetic forces, there is a narrow resonance at an energy of about 0.1 MeV, the ^{8}Be ground state. The scenario explored by Higa, Hammer, and van Kolck (2008) can be viewed as an expansion around the limit where, when electromagnetic interactions are turned off, the ^{8}Be ground state is at threshold and exhibits conformal invariance. This implies treating the Coulomb momentum $k_C = 2\alpha m_\alpha \simeq 60$ MeV, where m_α is the alpha-particle mass, as a high-momentum scale and expanding observables in powers of $Q/(3k_C)$, where Q is a typical external momentum, in addition to the standard expansion in the strong interactions. The Coulomb-modified scattering
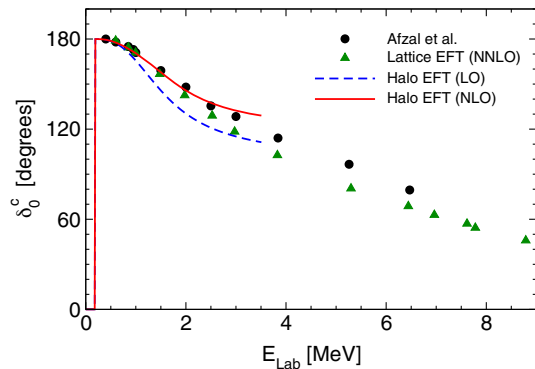
FIG. 24. Halo EFT results for the $\alpha\alpha$ S-wave phase shift by Higa, Hammer, and van Kolck (2008) as a function of the laboratory energy E_{lab}. LO and NLO phase shifts are given by the blue dashed and red solid lines, respectively. The experimental data are from Afzal, Ahmad, and Ali (1969), while the lattice EFT results are from Elhatisari *et al.* (2015).

length is very large, and the corresponding effective range almost saturates the Wigner bound for charged systems (König, Lee, and Hammer, 2013). The corresponding phase shifts are shown in Fig. 24 together with the experimental data from Afzal, Ahmad, and Ali (1969) and an *ab initio* lattice EFT calculation from Elhatisari *et al.* (2015). Agreement with the data seems to extend somewhat beyond the laboratory energy $E_{\text{lab}} = 2$ MeV corresponding to k_C. The sharp rise in the phase shift at low energies is a fine-tuned effect that is difficult to describe in the *ab initio* calculation, which displays a bound state instead. In contrast, the *ab initio* calculation extends to much higher energies than halo EFT.

An RG analysis of the coupled channels $p + {}^7\text{Li}$ and $n + {}^7\text{Be}$, which couple to a 2^- state of ${}^8\text{Be}$ close to the $n + {}^7\text{Be}$ threshold, was carried out by Lensky and Birse (2011). A more recent study involving ${}^8\text{Be}$ concerned a reported anomaly in the e^+e^- production from the decay of one of the 1^+ resonances to the ground state. A careful analysis inspired by halo EFT was carried by Zhang and Miller (2017), who concluded that nuclear physics is unlikely to explain the experimental result.

C and O production in stars also depends on the radiative capture of alpha particles by ${}^{12}\text{C}$, ${}^{12}\text{C}(\alpha, \gamma){}^{16}\text{O}$, at low energies. As in Sec. III.F, parameters from elastic α-${}^{12}\text{C}$ scattering enter in a halo EFT approach to the capture process. Ando (2016, 2018) developed a description of the elastic reaction taking the ${}^{12}\text{C}$ ground state as pointlike, and they obtained asymptotic normalization coefficients for some of the ${}^{16}\text{O}$ states from a fit to phase shifts.

Little has been done using halo EFT for other cluster systems. An early application of halo EFT for $l = 2$ to the reaction $d + t \to n + \alpha$ was carried out by Brown and Hale (2014). However, they used dimensional regularization with minimal subtraction and thus missed relevant parameters. Higa, Rupak, and Vaghani (2018) recently investigated another important process in the Sun, namely, the radiative capture of an α particle on ${}^3\text{He}$. They extracted an S factor slightly above the average in the literature, but consistent within error bars. Zhang, Nollett, and Phillips (2018b) recently performed a

Bayesian analysis of this reaction without relying on existing phase-shift analyses as a constraint.

I. Outlook

In this section, we reviewed the progress in halo/cluster EFT, a short-range EFT with explicit fields for nucleon and cluster degrees of freedom, designed for the description of halos and cluster nuclei. Such systems have a rich structure due to the emergence of new scales from the Coulomb interaction between the clusters. The Efimov effect plays an important role for neutron-halo nuclei and their application in the presence of Coulomb interactions presents an exciting opportunity for the discovery of new phenomena.

Halo EFT is conceptually similar to the pionless EFT discussed in Sec. II. As a description of nuclei not limited to the few-nucleon sector, it complements *ab initio* approaches by parametrizing universal relations between low-energy observables in systems dominated by shallow bound states and low-lying resonances, and it quantifies the corrections to these relations. While such *ab initio* calculations can be based on interactions from chiral EFT (which is reviewed in Sec. IV), for systems within its reach of applicability halo EFT sets up a more effective and efficient expansion. Halo EFT promises a quantitative description on the same footing of both nuclear structure and reactions of clusterized systems and exotic isotopes, which is a major challenge of contemporary nuclear theory. Nuclear reactions have been investigated both in strict halo EFT (Schmidt, Platter, and Hammer, 2019) and in accurate phenomenological models of reactions with a halo EFT motivated description of the projectile (Capel, Phillips, and Hammer, 2018; Yang and Capel, 2018). Many of these reactions have an impact on astrophysical processes and even on the quantification of nuclear uncertainties in experimental anomalies.

Future challenges include a better integration of *ab initio* methods and halo EFT to maximally benefit from the strengths of both approaches. The use of Bayesian statistics for the estimation of higher-order corrections provides a method to account for the different sources of theory errors beyond simple scaling arguments. Finally, hypernuclei are a new and almost unexplored arena for halo EFT and universality. As we discuss in Sec. V.C, experimental data are not abundant and a combination of halo EFT and *ab initio* methods therefore appears to be especially promising.

IV. CHIRAL EFT

A. Motivation

As the typical momentum in a nuclear process increases beyond the pion mass, pion effects can no longer be approximated by an expansion around the zero-range limit. As a response to the failure of early attempts to achieve RG invariance in pion theories, an approach gradually emerged in the 1950s where the nuclear potential and currents took purely phenomenological forms or, at best, came from the single (and, occasionally, double) exchange of an arbitrary selection of mesons. The potential was almost always constructed so as to be regular [i.e., not a singular potential (Frank, Land, and Spector, 1971)], which in the case of meson exchange was

ensured by including physical form factors. The relative ease of solving the two-nucleon Schrödinger equation numerically made it possible to produce exquisite fits to a large amount of two-nucleon data, frequently of the same quality even with different physical input into the potential. In contrast, a comparable description of $A > 2$ systems seems to require three-nucleon forces and two-nucleon currents, but the large variety of possible structures posed a significant obstacle to this purely phenomenological approach. Moreover, the connection to QCD and the assignment of systematic errors are not addressed.

Chiral EFT attempts to overcome these shortcomings by solving the RG problems of earlier pion theories. In hindsight, the latter were both too restrictive, in the sense of not including all interactions consistent with symmetries, and not restrictive enough, in the sense of not incorporating the constraints of chiral symmetry. Early forms of mesonic ChPT date back to the 1960s and were extremely important in the development of the EFT paradigm. The mature version of mesonic ChPT took shape in the 1980s (Weinberg, 1979; Gasser and Leutwyler, 1984, 1985), and processes for $A = 1$ (Gasser, Sainio, and Svarc, 1988; Bernard *et al.*, 1991; Bernard, Kaiser, and Meißner, 1991; Jenkins and Manohar, 1991a, 1991b) and $A \geq 2$ (Weinberg, 1990, 1991, 1992; Rho, 1991; Ordóñez and van Kolck, 1992; van Kolck, 1993) started receiving significant attention in the late 1980s and early 1990s. As this section reviews, substantial progress has been made in understanding the structure of the nuclear potential and currents, but chiral EFT has not yet produced a complete solution to the RG problems that plagued earlier pion theories.

Extensive reviews exist of chiral EFT applications to nuclear phenomenology by, for example, van Kolck (1999a), Beane, Bedaque, Haxton *et al.* (2001), Bedaque and van Kolck (2002), Epelbaum, Hammer, and Meißner (2009), Machleidt and Entem (2011), and Epelbaum and Meißner (2012). We focus here on some of the conceptual issues, which parallel those of pionless EFT (Sec. II) and halo/cluster EFT (Sec. III). Chiral EFT extends pionless EFT to processes with characteristic momentum $Q \sim M_{\mathrm{lo}}$, where $M_{\mathrm{lo}} \sim m_\pi \ll M_{\mathrm{QCD}}$. As discussed in Sec. IV.B, the breakdown scale $M_{\mathrm{hi}} \lesssim M_{\mathrm{QCD}}$ depends in part on the degrees of freedom being kept explicit. Section IV.B also discusses the pertinent symmetries and Lagrangian. The nuclear potential and currents, defined in Sec. I.C, are free of the IR enhancement that leads to nuclear bound states and resonances. As a consequence, contributions to the potential can be treated similarly to contributions to amplitudes in ChPT, as discussed in Sec. IV.C. The relation to experiment via amplitudes and the more complex issue of their renormalization are reviewed in Sec. IV.D. Analogous considerations afflict reactions with external light probes such as photons and pions, which are sketched in Sec. IV.E. Section IV.F lists some of the outstanding issues facing chiral EFT.

B. Basic elements

1. Degrees of freedom and symmetries

By extending the pionless EFT of Sec. II to include an isovector field $\vec{\pi}$ that collects the three charged pion states, one

develops a representation of QCD for $Q \sim m_\pi$, with m_π now among the low-energy scales collectively denoted by M_{lo}. In this EFT, pion exchange among nucleons generates amplitudes that are no longer given by the ERE or a simple generalization thereof. Instead, there appear nonanalytic functions of Q/m_π in all amplitudes.

The lightness of the pions relative to other hadrons can be explained naturally if they are identified with the pseudo Goldstone bosons of the spontaneous breaking of approximate chiral symmetry, $\mathrm{SU}(2)_L \times \mathrm{SU}(2)_R$ for two flavors. In the chiral limit ($\bar{m} = 0$, $\varepsilon = 0$, $e = 0$), the QCD Lagrangian (1) has an exact chiral symmetry. In contrast, the spectrum shows only an approximate isospin symmetry $\mathrm{SU}(2)_V$. Close to the chiral limit, $\mathrm{SU}(2)_L \times \mathrm{SU}(2)_R$ is an approximate symmetry of Eq. (1). Pions, which have vanishing mass in the chiral limit, acquire a relatively small but nonzero common squared mass $m_\pi^2 = \mathcal{O}(M_{\mathrm{QCD}} \bar{m})$ and a square-mass splitting $\delta m_\pi^2 = \mathcal{O}(\alpha M_{\mathrm{QCD}}^2/4\pi, \varepsilon^2 m_\pi^4/M_{\mathrm{QCD}}^2)$ between charged and neutral states.

Pions should play a special role as long as $\bar{m} \ll M_{\mathrm{QCD}}$. In this section we consider this regime, where we integrate out all other mesons because they are expected to have masses $\mathcal{O}(M_{\mathrm{QCD}})$. The lightest of these is the σ with spin $S = 0$ and isospin $I = 0$, and a mass (half-width) $m_\sigma = 441$ MeV ($\Gamma_\sigma/2 = 271$ MeV) (Caprini, Colangelo, and Leutwyler, 2006). This suggests that the EFT radius of convergence is no larger than $M_{\mathrm{hi}} \sim \sqrt{m_\sigma^2 + \Gamma_\sigma^2/4} \simeq 500$ MeV. The hadronic EFT of QCD beyond this scale is not known. The problem is power counting: by NDA, interactions with derivatives will produce powers of Q/M_{QCD} in amplitudes; thus, as Q approaches M_{QCD}, all interactions are equally important. To incorporate mesons in an EFT we need an argument that, at least at a formal level, justifies treating their masses and interactions as small with respect to M_{QCD}. Typically this is accomplished by assuming QCD to have further approximate symmetries. For example, scale symmetry has been invoked in the context of three flavors to justify the inclusion of a scalar-isoscalar meson (Crewther and Tunstall, 2015) and a dynamical "vector" symmetry (Georgi, 1989) postulated for the ρ meson. Although interesting, such schemes have thus far met with limited success, if any, away from the mesonic sector.

One must, however, consider the effects of nucleon excitations. As mentioned in Sec. I, for $Q \ll m_N \sim M_{\mathrm{QCD}}$ the nucleon mass is inert. For baryon-number-conserving processes, the relevant mass scale for other baryons is their mass splitting from the nucleon. The Delta isobar with $S = 3/2$ and $I = 3/2$ lies at $m_\Delta - m_N - i\Gamma_\Delta/2 \simeq (270 - 50i)$ MeV (Arndt *et al.*, 2006). Although the mass difference $m_\Delta - m_N$ does not vanish in the chiral limit, it is relatively small, in line with arguments based on a large number of colors N_c: when QCD is generalized to an $\mathrm{SU}(N_c)$ gauge theory $m_\Delta - m_N = \mathcal{O}(M_{\mathrm{QCD}}/N_c)$. A Deltaless version of chiral EFT exists where the Delta isobar is integrated out, but it fails before one reaches the Delta region in $A = 1$ processes, which leads to relatively large errors in $A \geq 2$ systems (Pandharipande, Phillips, and van Kolck, 2005). To increase the radius of convergence beyond $\sim \sqrt{(m_\Delta - m_N)^2 + \Gamma_\Delta^2/4} \simeq 275$ MeV, one introduces

(Jenkins and Manohar, 1991b; Hemmert, Holstein, and Kambor, 1998) a heavy field Δ, a four-component object in spin and isospin space with the nucleon mass m_N removed from its rest energy. As a consequence, the Delta kinetic energy and interactions are also expanded around the nonrelativistic limit. Apart from the spin/isospin structure, the main difference with respect to the nucleon is that a term linear in the mass difference $m_\Delta - m_N$ (included in M_{lo}) remains in the Lagrangian. Explicit Delta propagation improves the description of data beyond threshold (Fettes and Meißner, 2001) and enlarges the realm of chiral EFT beyond the Delta region once the power counting is properly reformulated (Pascalutsa and Phillips, 2003; Long and van Kolck, 2010).

Whether other nucleon excitations should be introduced in chiral EFT is less clear. The Roper resonance (Roper, 1964) is special for several reasons (Long and van Kolck, 2011). First, its pole appears at an energy not much above the Delta, $m_R - m_N - i\Gamma_R/2 \simeq (420 - 80i)$ MeV (Arndt *et al.*, 2006). Other resonances lie at least $M_{\text{hi}} \simeq 500$ MeV above threshold [the next resonance S_{11} has a mass $m_{S_{11}} - m_N \simeq 500$ MeV (Arndt *et al.*, 2006)], and it is difficult to see why they should be incorporated into the EFT without the concomitant inclusion of meson resonances. Second, the Roper width is, numerically, $\Gamma_R \sim \Gamma_\Delta (m_R - m_N)^3/[2(m_\Delta - m_N)^3]$, as expected from ChPT widths scaling as Q^3/M_{QCD}^2. This is not true for higher resonances, which typically have relatively smaller widths. As a consequence, the Delta and the Roper nearly saturate the Adler-Weisberger sum rule, a result that suggests that, together with the nucleon, they fall into a simple reducible representation of the chiral group (Weinberg, 1969; Beane and van Kolck, 2005). Inclusion of an explicit Roper field (Banerjee and Milana, 1996; Gegelia, Meißner, and Yao, 2016) improves the convergence of chiral EFT around the Delta resonance (Long and van Kolck, 2011), but this has not been systematically investigated. In the following, we consider chiral EFT with nucleon and Delta fields only.

2. Chiral Lagrangian

The construction of the most general chiral Lagrangian is based on the theory of the nonlinear realization of a symmetry (Weinberg, 1968; Callan, *et al.*, 1969; Coleman, Wess, and Zumino, 1969). Different parametrizations of the three-dimensional sphere $\text{SU}(2)_L \times \text{SU}(2)_R/\text{SU}(2)_V \sim \text{SO}(4)/\text{SO}(3) \sim S^3$ correspond to different choices of pion fields. Observables are, of course, independent of this choice. Pions appear in the chiral Lagrangian always as $\vec{\pi}/f_\pi$, where the pion decay constant $f_\pi \simeq 92$ MeV is determined by the radius of S^3. Because the three pions cannot provide a linear realization of $\text{SO}(4)$, they transform nonlinearly under chiral symmetry, so each term in the chiral Lagrangian is associated with an infinite tower of interactions in powers of $(\vec{\pi}/f_\pi)^2$. Nucleon $N = (p\, n)^T$ and Delta $\Delta = (\Delta^{++} \Delta^+ \Delta^0 \Delta^-)^T$ fields can be chosen to transform under chiral symmetry just as under an isospin rotation, but with an angle linear in the pion field. Covariant derivatives of the pion and baryon fields can be defined so that they transform in the same way. They are $D_\mu = (1 - \vec{\pi}^2/4f_\pi^2 + \cdots)\partial_\mu$ and $\mathcal{D}_\mu = \partial_\mu + i\vec{\tau} \cdot (\vec{\pi} \times \partial_\mu \vec{\pi})/4f_\pi^2 + \cdots$ for the pion and nucleon,

respectively, where $\vec{\tau}$ are the Pauli matrices in isospin space. For the Delta, the form is the same as for the nucleon, with $\vec{\tau}$ replaced by the $I = 3/2$ representation of SO(3). Delta-nucleon transition operators involve a set of 2×4 isospin matrices $\vec{T}$. Details were given by Ordóñez, Ray, and van Kolck (1996).

The chiral Lagrangian is automatically chiral invariant if it is built from isospin-symmetric operators involving the baryon fields, their covariant derivatives, and the pion covariant derivative. Chiral-symmetric interactions of the pions are thus proportional to the momentum. Away from the chiral limit, quark masses and electromagnetic interactions break chiral symmetry and even the isospin subgroup. The symmetry-breaking pattern is known from Eq. (1), and interactions in the EFT are constructed to behave the same way. Thus, although chiral symmetry is not exact, information about QCD is contained also in the chiral-symmetry-breaking interactions. These interactions do not necessarily involve derivatives but must be proportional to powers of the small parameters $\bar{m}/M_{\text{QCD}}$, ε, and e, as well as the coefficients of higher-dimensional operators (including violations of parity, time-reversal, and possibly baryon-number and Lorentz invariance). The parameter $\bar{m}/M_{\text{QCD}}$ can be traded for m_π^2/M_{QCD}^2, while ε and e govern isospin-breaking quantities. Electromagnetic interactions are constrained by $U(1)_{\text{em}}$ gauge invariance and appear in two ways: (i) between low-energy photons and other fields via chiral-covariant derivatives enlarged to be gauge covariant as well, and via the electromagnetic field strength, and (ii) among hadronic fields that originate in integrating out energetic photons.

Overall, chiral symmetry and its known breaking pattern lead to a low-energy expansion because all interactions of pions among themselves or with nucleons involve derivatives (which bring powers of $Q \sim M_{\text{lo}}$ to amplitudes), powers of $m_\pi^2 \sim M_{\text{lo}}^2$, or powers of smaller parameters. Choices of fields with different chiral-transformation properties do not change this feature but do, in general, require delicate cancellations among different interactions.

As in pionless EFT, it is most convenient to choose a heavy nucleon for which the Dirac matrices reduce to the Pauli spin matrices $\boldsymbol{\sigma}$. Analogously, one can employ a heavy Delta field using the corresponding $S = 3/2$ matrices. Nucleon-Delta bilinears can be constructed with 2×4 spin transition matrices $\boldsymbol{S}$ analogous to the isospin transition matrices $\vec{T}$. Incorporating Lorentz invariance in an expansion in Q/m_N is thus no more difficult in chiral EFT than in pionless EFT. In recent years it has become popular to use "covariant" baryon fields from which the nucleon mass is not subtracted. As any field redefinition, such choices cannot affect observables in an essential way: amplitudes obtained from different fields but the same power counting can only differ by higher-order terms. Although these differences are sometimes interpreted as an indication of the "best" field choice, they merely reflect the error of the truncation.

The baryon-number-conserving chiral Lagrangian can be split into pieces with even numbers of fermion fields, $\mathcal{L} = \mathcal{L}_{f=0} + \mathcal{L}_{f=2} + \mathcal{L}_{f\geq 4}$, where

$$\mathcal{L}_{f=0} = \frac{1}{2}\left[(D_0\vec{\pi})^2 - (\boldsymbol{D}\vec{\pi})^2 - m_\pi^2\vec{\pi}^2\left(1 - \frac{\vec{\pi}^2}{4f_\pi^2} + \cdots\right)\right] + \cdots, \tag{70a}$$

$$\mathcal{L}_{f=2} = N^\dagger\left(i\mathcal{D}_0 + \frac{\boldsymbol{\mathcal{D}}^2}{2m_N}\right)N + \frac{g_A}{2f_\pi}N^\dagger\vec{\tau}\boldsymbol{\sigma}N\cdot\boldsymbol{D}\vec{\pi} + \Delta^\dagger(i\mathcal{D}_0 + m_N - m_\Delta)\Delta + \frac{h_A}{2f_\pi}(N^\dagger\vec{T}\boldsymbol{S}\Delta + \mathrm{H.c.})\cdot\boldsymbol{D}\vec{\pi} + \cdots, \tag{70b}$$

$$\mathcal{L}_{f\geq4} = -\frac{C_{0t}}{2}(N^TP_tN)^\dagger(N^TP_tN) - \frac{1}{2}\left[C_{0s} + D_{2s}m_\pi^2\left(1 - \frac{\vec{\pi}^2}{2f_\pi^2} + \cdots\right)\right](N^TP_sN)^\dagger(N^TP_sN)$$
$$- \frac{C_{2s}}{8}\{(N^TP_sN)^\dagger[N^TP_s\boldsymbol{\mathcal{D}}^2N + (\boldsymbol{\mathcal{D}}^2N)^TP_sN] + \mathrm{H.c.}\} - \frac{C'_{2t}}{4}[(N^TP_t\boldsymbol{\mathcal{D}}N)^\dagger\cdot(N^TP_t\boldsymbol{\mathcal{D}}N) + ((\boldsymbol{\mathcal{D}}N)^TP_tN)^\dagger\cdot((\boldsymbol{\mathcal{D}}N)^TP_tN)]$$
$$+ \frac{G_A}{2f_\pi}N^\dagger NN^\dagger\boldsymbol{\sigma}\vec{\tau}N\cdot\boldsymbol{D}\vec{\pi} - H_0N^\dagger NN^\dagger NN^\dagger N + \cdots, \tag{70c}$$

with LECs g_A, h_A, $C_{0s,t}$, D_{2s}, C_{2s}, C'_{2t}, G_A, and H_0, and where we used a notation similar to Eq. (33). Only a few representative interactions are shown explicitly here, with others (more fields, derivatives, powers of m_π^2, isospin breaking, etc.) being relegated to the ellipsis. Note that many terms can be written in different forms with Fierz reordering and/or field redefinitions. One can also introduce dibaryon fields as described in Sec. II.B.5 and as done, for example, by Soto and Tarrus (2012) and Long (2013).

Particularly convenient for nuclear processes, where nucleon energies and momenta are of significantly different magnitudes, is to use field redefinitions to eliminate time derivatives of the nucleon field in favor of spatial derivatives. When interaction terms that depend on time derivatives appear in the classical Lagrangian, the effective Lagrangian obtained via the path integral of the Hamiltonian contains additional terms (Charap, 1970, 1971; Salam and Strathdee, 1970; Gerstein et al., 1971; Honerkamp and Meetz, 1971). These do not vanish, in general, if a momentum cutoff is used. Generally, the easiest way to respect symmetries is to implement regulators as operators in the chiral Lagrangian constructed from chiral-covariant objects (Slavnov, 1971; Djukanovic et al., 2005; Long and Mei, 2016).

If $m_\Delta - m_N$ is considered a large scale, the Delta is integrated out and appears only through LECs starting at 1 order higher than in the Deltaful EFT. If m_π is also considered a large scale, pions are integrated out as well. Although the chiral Lagrangian formally reduces to the pionless form in Eq. (33) when terms with pions and Deltas are omitted from Eq. (70), one should keep in mind that the remaining LECs depend on which degrees of freedom appear in the EFT.

C. Chiral perturbation theory and the nuclear potential

A great advantage of EFT over earlier attempts to describe nuclear physics from field theory is its explicit focus on the regime of momenta well below the nucleon mass, where the theory splits into sectors of fixed nucleon number A. As pointed out in Sec. I, there are significant differences between $A \leq 1$ and $A \geq 2$ processes.

1. Power counting

To express amplitudes in an expansion in powers of Q/M_{QCD}, as in Eq. (3), one needs to count powers of both $Q \sim M_{lo}$ and M_{QCD}. For Q, one first relates nucleon energies and momenta, and this relation, in general, depends on the sector of the theory. For $A \leq 1$, typically (but not always) $E = \mathcal{O}(Q)$, while $A \geq 2$ processes with only nucleons in external legs involve energies $E = \mathcal{O}(Q^2/m_N)$. For pions, since we count m_π as M_{lo}, $E = \mathcal{O}(Q)$. The crucial assumption in counting powers of M_{QCD} is naturalness, namely, that an LEC needed to eliminate cutoff dependence of a loop at a certain order has finite pieces of the same order.

For an $A \leq 1$ Feynman diagram, the various elements scale after renormalization as

$$\text{derivative} \sim Q, \tag{71a}$$

$$\text{baryon, pion propagator} \sim Q^{-1}, Q^{-2}, \tag{71b}$$

$$\text{pion loop integral} \sim (4\pi)^{-2}Q^4, \tag{71c}$$

where the factor of $(4\pi)^{-2}$ is typical of relativistic loops. The sizes of LECs can be estimated via NDA; see Eq. (9). Chiral-symmetric operators depend on arbitrary powers of the reduced strong-coupling constant $g_{red} = g/(4\pi)$, which for consistency should be taken as 1. NDA applied to Eq. (70a) gives $f_\pi = \mathcal{O}(M_{QCD}/4\pi)$, and for a generic LEC (Manohar and Georgi, 1984; Georgi and Randall, 1986)

$$c_i = \mathcal{O}\left(\frac{c_{i,red}}{f_\pi^{f_i+p_i-2}M_{QCD}^{\Delta_i}}\right), \qquad \Delta_i \equiv d_i + f_i/2 - 2, \tag{72}$$

where d_i, f_i, and p_i, respectively, represent the number of derivatives, baryon fields, and pion fields of the corresponding operator. The reduced LEC $c_{i,red} = \mathcal{O}(1)$ for a chiral-symmetric operator. NDA is consistent with the nonrelativistic expansion since applied to Eq. (70b) it gives $m_N = \mathcal{O}(M_{QCD})$. Keeping explicit Deltas means, however, that we are taking $(m_\Delta - m_N)_{red} = \mathcal{O}(M_{lo}/M_{QCD}) \ll 1$, as suggested by large-$N_c$ arguments. A chiral-symmetry-breaking operator stemming from the quark masses will have a reduced LEC proportional to powers of $\bar{m}_{red} = \bar{m}/M_{QCD} = \mathcal{O}(m_\pi^2/M_{QCD}^2) = \mathcal{O}(M_{lo}^2/M_{QCD}^2)$ and $\varepsilon \lesssim \mathcal{O}(1)$, using that $m_\pi^2 = \mathcal{O}(M_{QCD}\bar{m})$ when NDA is again applied to Eq. (70a). The effect of integrating out hard photons is given by powers of $e_{red}^2 = [e/(4\pi)]^2 \lesssim \mathcal{O}(M_{lo}^3/M_{QCD}^3)$ (van Kolck, 1993, 1995)

in the corresponding reduced LEC.[7] If we take $\varepsilon = \mathcal{O}(1)$, then $c_{i,\mathrm{red}} = \mathcal{O}(M_{\mathrm{lo}}^{n_i}/M_{\mathrm{hi}}^{n_i})$ where n_i counts the powers of the low-energy scales m_π, $m_\Delta - m_N$, and $[e/(4\pi)]^{2/3} m_N$. It is convenient to enlarge the definition of d_i to include n_i. The interactions displayed in Eqs. (70a) and (70b) then have $\Delta_i = 0$, except for the nucleon recoil term $\mathcal{D}^2/2m_N$ with $\Delta_i = 1$. Chiral symmetry guarantees that $\Delta_i \geq 0$ for all interactions stemming from the terms shown explicitly in Eq. (1).[8]

Using standard identities for connected graphs, a diagram with L loops and V_i vertices with chiral index Δ_i contributes to the amplitude in Eq. (3) a term with (Weinberg, 1979)[9]

$$\nu = 2L + \sum_i V_i \Delta_i, \qquad \mathcal{N} = f_\pi^{4-3A-E_b}, \qquad (73)$$

where E_b is the number of external bosons. The factor $2L$ implies that ChPT amplitudes are, in general, perturbative; i.e., the nonanalytic functions $F^{(\nu)}$ in Eq. (3) can be obtained from a finite number of Feynman diagrams. Because of the way NDA was inferred, these loop diagrams are accompanied by higher-index interactions that provide the necessary counterterms for RG invariance in the sense of Eq. (5). Because of chiral symmetry, $\nu \geq 0$.[10] LO [$\mathcal{O}(\mathcal{N})$] and NLO [relative $\mathcal{O}(Q/M_{\mathrm{QCD}})$] consist of tree-level ($L = 0$) diagrams made out of interactions with chiral index $\Delta = 0$ and, respectively, no or one interaction with $\Delta = 1$. They are equivalent to ancient current algebra. Baryons are not only nonrelativistic but also approximately static. Quantum-mechanical corrections ($L \geq 1$) start at N²LO [relative $\mathcal{O}(Q^2/M_{\mathrm{QCD}}^2)$]. As ν increases, progressively more short-range physics is included, which accounts for details of hadron structure. Many good reviews of ChPT exist; see, for example, Bernard, Kaiser, and Meißner (1995) and Bernard (2008).

That is not to say that within certain regions of phase space perturbation theory does not break down. The power counting in Eq. (73) is meant as a general rule only and is bound to fail in specific situations. For example, within a momentum window of size $\mathcal{O}(Q^3/M_{\mathrm{QCD}}^2)$ around the Delta pole, where $E \simeq m_\Delta - m_N$, the one-loop diagrams that make for most of the Delta width become important and a resummation is necessary at LO (Pascalutsa and Phillips, 2003; Long and van Kolck, 2010). Similarly, around certain points below threshold where energies are $\mathcal{O}(Q^2/M_{\mathrm{QCD}})$, nucleon recoil needs to be resummed and elevated to LO (Lv and Long, 2016). The latter resummation is naturally incorporated by the use of nonheavy baryon fields (Becher and Leutwyler, 1999; Fuchs et al., 2003), but in the literature it is often wrongly implied that such a choice is necessary. In general, the choice of fields is unimportant, but one should always ensure that the power counting in Eq. (73) applies to the kinematic region of interest. Any resummation needs to be done carefully so as not to break RG invariance.

Nucleon-only $A \geq 2$ processes have $E = \mathcal{O}(Q^2/m_N)$ and require a resummation as well (Weinberg, 1991). We return to this in Sec. IV.D, focusing for now on the sum of "irreducible" diagrams involving $A \geq 2$ nucleons (and $E_b = 0$), which is defined (see Sec. I.C) as the full nuclear potential.[11] The analogous currents are briefly discussed in Sec. IV.E.

By construction, the potential is free of IR enhancement, and we expect a power counting similar to ChPT's to apply as long as interactions with $f \geq 4$ also obey NDA. A complication is that the full potential introduced in Sec. I.C includes disconnected diagrams. Each disconnected piece scales as $(4\pi)^n Q^{-4}$, where n is an integer, coming from the fact that the extra four-dimensional delta function, which enforces momentum conservation, also eliminates a loop integral. Weinberg (1991, 1992), Ordóñez and van Kolck (1992), and van Kolck (1993) assumed $n = 2$ on the basis of Eq. (71c), while Friar (1997) took $n = 1$, which is consistent with the nonrelativistic nature of reducible loops discussed in Sec. IV.D.3. As a consequence, a diagram with $1 \leq C \leq A - 1$ separately connected pieces contributes to the potential in Eq. (7) with (Weinberg, 1991; Friar, 1997)

$$\mu = n(A - 1 - C) + 2L + \sum_i V_i \Delta_i,$$
$$\tilde{N} = (4\pi)^{(2-n)A} f_\pi^{4-3A}. \qquad (74)$$

This power counting (with $n = 2$) has been used in most studies of chiral potentials to date.

2. Nuclear potential

In chiral EFT, Fig. 2 is undone: pion exchange appears explicitly in the potential, with the remaining contact interactions accounting for higher-momentum physics. In contrast to pionless EFT, the potential itself involves (irreducible) loops, where energies are comparable to momenta and nucleons are approximately static. The long-range pion-exchange contributions appear in all partial waves and yield many-body forces consistent with $2N$ forces and the hadronic physics described by ChPT. They are not known to violate the estimate in Eq. (74).

---

[7]How one accounts for e_{red} relative to other parameters is somewhat ambiguous, and to some extent a matter of convenience. Sometimes the choice $e_{\mathrm{red}}^2 = \mathcal{O}(M_{\mathrm{lo}}^2/M_{\mathrm{QCD}}^2)$ is made in the literature. This choice leads a pion mass splitting $\delta m_\pi^2 = \mathcal{O}(\alpha M_{\mathrm{QCD}}^2/4\pi) = \mathcal{O}(m_\pi^2)$ and to a Coulomb potential comparable to OPE for momenta $Q \sim m_\pi$. That means electromagnetic effects at LO, an overestimate. A similar ambiguity affects $\varepsilon \simeq 1/3$, which can be counted as $\mathcal{O}(1)$ or as $\mathcal{O}(M_{\mathrm{lo}}/M_{\mathrm{QCD}})$.

[8]The choice of heavy baryon fields makes this evident by removing positive powers of the large nucleon mass from the Lagrangian.

[9]Note that ν can be written in various ways that differ by an additive factor and by the overall normalization. In writing Eq. (73), as well as Eq. (74), we choose a form where LO corresponds to $\nu = 0$.

[10]If interactions in the ellipsis in Eq. (1) are considered, Δ and ν can be negative. However, these interactions are small due to strengths that are much smaller than our expansion parameter Q/M_{QCD}. Such interactions can still be included perturbatively.

[11]For a recent attempt to treat pions dynamically instead through quantum Monte Carlo methods, see Madeira et al. (2018).

Pion loops also generate short-range contributions that cannot be separated from contact interactions in the potential. The piece of an LEC that removes the cutoff dependence in irreducible loops, or more generally the piece that obeys NDA, is sometimes referred to as a primordial counterterm (Long and Yang, 2012a, 2012b). This is to distinguish it from another piece that renormalizes the reducible loops of the full amplitude. This additional piece may violate NDA and be present at a lower order than the primordial piece, as discussed in Sec. IV.D. As in pionless EFT, the potential is *not* cutoff independent.

a. Leading order

The full LO potential has maximum C ($C_{\max} = A - 1$, from $A - 2$ disconnected lines): it consists of the sum over pairs of the $2N$ potential at tree level ($L = 0$) constructed entirely from $\Delta = 0$ interactions. The long-range $2N$ potential consists of static one-pion exchange (OPE) and the primordial counterterms are the two LECs of the nonderivative chiral-symmetric contact interactions in Eq. (70c):

$$V^{(0)} = -\frac{4\pi}{m_N M_{NN}} \frac{\vec{\tau}_1 \cdot \vec{\tau}_2}{\boldsymbol{q}^2 + m_\pi^2} \left(S_{12}(\boldsymbol{q}) - \frac{m_\pi^2}{3} \boldsymbol{\sigma}_1 \cdot \boldsymbol{\sigma}_2 \right)$$
$$+ C_{0s} P_s + C_{0t} P_t, \tag{75}$$

where the indices 1 and 2 label the two nucleons, $\boldsymbol{q}$ is the transferred momentum, and $S_{12}(\boldsymbol{q}) = (\boldsymbol{\sigma}_1 \cdot \boldsymbol{q})(\boldsymbol{\sigma}_2 \cdot \boldsymbol{q}) - q^2(\boldsymbol{\sigma}_1 \cdot \boldsymbol{\sigma}_2)/3$ is the tensor operator. OPE is static because the transferred energy, related to nucleon recoil, is small [relative $\mathcal{O}(Q/M_{\text{QCD}})$] compared to $|\boldsymbol{q}|$. The scale that controls the OPE strength, in a form we can compare with short-range interactions in pionless EFT, was introduced by Kaplan, Savage, and Wise (1998a, 1998b) as

$$M_{NN} = \frac{16\pi f_\pi^2}{g_A^2 m_N} = \mathcal{O}(f_\pi), \tag{76}$$

using NDA. OPE gives rise in coordinate space to (i) a tensor potential that is as singular $\sim 1/r^3$ as $r \to 0$, and (ii) the regular Yukawa potential. The tensor potential is nonvanishing only for total spin $s = 1$ and can mix waves with $l = j \pm 1$. It is attractive in some uncoupled waves like $^3P_0$ and $^3D_2$, and in one of the eigenchannels of each coupled wave. The Yukawa potential is attractive in isovector (isoscalar) channels for $s = 0$ ($s = 1$). The other two terms in Eq. (75) are contact interactions, which for large cutoffs contribute only to the $^3S_1$ and $^1S_0$ channels. A contact interaction from OPE has been eliminated through the redefinition

$$C_{0s} + \frac{4\pi}{m_N M_{NN}} \to C_{0s} = \mathcal{O}\left(\frac{4\pi}{m_N M_{NN}}\right). \tag{77}$$

b. Subleading orders

The order increases as the chiral index Δ, the number of loops L, and the number of nucleons in connected pieces increase. In much of the literature the potential at relative $\mathcal{O}(Q^\mu/M_{\text{QCD}}^{\mu})$ is referred to as N$^{\mu-1}$LO, but this notation is not

flexible enough to accommodate changes in the power counting described in Sec. IV.D, which suggest $n = 1$ in Eq. (74) and also departures from NDA. For clarity, we denote the order of contributions using their explicit scaling throughout the rest of this section. The structure of the long-range nuclear potential is shown schematically in Fig. 25.

The first few-body forces arise (van Kolck, 1993, 1994) at $\mathcal{O}(Q^n/M_{\text{QCD}}^{n})$ compared to LO, from $\Delta = 0$ and $L = 0$ with $C = A - 2$:

- A $3N$ two-pion exchange (TPE) force via an intermediate Delta, the Fujita-Miyazawa force (Fujita and Miyazawa, 1957) shown in Fig. 25.
- Nucleon-only $3N$ and "double-pair" forces (for $A \geq 4$) when, in a time-ordered diagram, a $2N$ interaction occurs while a pion is flying between two nucleons.

Forces of the second type exactly cancel against nucleon recoil in the $2N$ OPE once the latter is inserted into the Lippmann-Schwinger equation (Weinberg, 1991; Ordóñez and van Kolck, 1992; van Kolck, 1993, 1994). But recoil is an $\mathcal{O}(Q/m_N)$ effect compared to LO: the cancellation implies that $(4\pi)^{2-n} Q^2/M_{\text{QCD}}^2 \sim Q/m_N$. For $n = 2$, one obtains $Q/m_N \sim Q^2/M_{\text{QCD}}^2$ at variance with the NDA that underlies the power counting. In contrast, if one takes NDA seriously, $m_N = \mathcal{O}(M_{\text{QCD}}) = \mathcal{O}(4\pi f_\pi)$, then $n = 1$ and $Q \sim f_\pi = \mathcal{O}(M_{NN})$. As we discuss in Sec. IV.D, this is consistent with the counting of factors of 4π suggested by pionless EFT. Not all practitioners count m_N, and thus implicitly choose n, in the same way. However, regardless of how m_N is counted, chiral EFT, just as pionless EFT, implements the constraints of Lorentz invariance in a Q/m_N expansion.
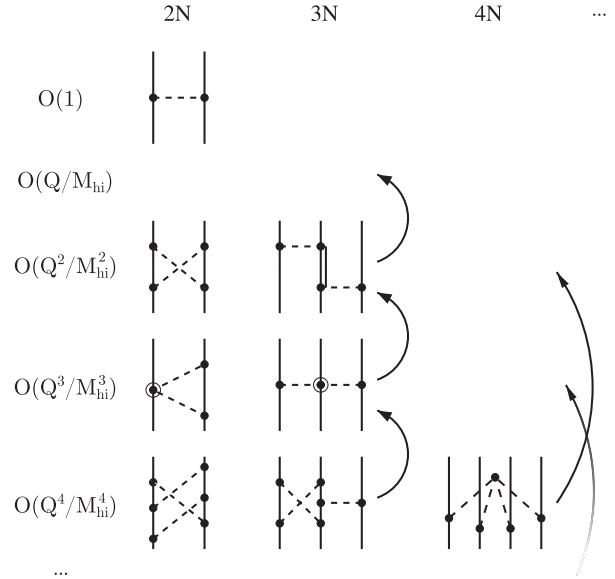
FIG. 25. Sample of diagrams representing the pion-range components of the AN nuclear potential in chiral EFT according to Eq. (74) with $n = 2$. The order of the contributions is indicated as $\mathcal{O}(Q^\mu/M_{\text{hi}}^{\mu})$, $\mu \geq 0$, where $Q \sim m_\pi$ and $M_{\text{hi}} \sim M_{\text{QCD}}$. Arrows in the $3N$ and $4N$ columns indicate the changes for $n = 1$. A solid (double) line stands for a nucleon (nucleon excitation), while a dashed line stands for a pion. A circle around the central solid circle denotes an inverse power of M_{hi}.

After this cancellation, the 2N potential vanishes at relative $\mathcal{O}(Q/M_{\text{QCD}})$ if we neglect parity violation (Weinberg, 1991; Ordóñez and van Kolck, 1992; van Kolck, 1993, 1994). For $n = 1$, the Fujita-Miyazawa 3N force survives at this order. It is demoted to relative $\mathcal{O}(Q^2/M_{\text{QCD}}^2)$ if $n = 2$, in which case the full potential vanishes at $\mathcal{O}(Q/M_{\text{QCD}})$. More generally, the first aN force ($L = 0$, all interactions with $\Delta = 0$) is expected to appear at relative $\mathcal{O}(Q^{n(a-2)}/M_{\text{QCD}}^{n(a-2)})$. The relative suppression of few-body forces (Weinberg, 1991; Ordóñez and van Kolck, 1992; van Kolck, 1993, 1994) is in agreement with the experience drawn from phenomenological potentials containing explicit pion exchange, for which 3N forces are usually found to be necessary at the 10% level, for example, to provide ~1 MeV to the triton binding energy $\simeq 8.5$ MeV. The explanation for the smallness, but non-negligibility, of phenomenological few-body forces was an early success of chiral EFT.

c. 2N potential

At relative $\mathcal{O}(Q^2/M_{\text{QCD}}^2)$, corrections to OPE merely shift existing couplings: for example, g_A in Eq. (76) receives a contribution proportional to m_π^2, the so-called Goldberger-Treiman discrepancy. The long-range 2N potential consists of TPE, the so-called box, crossed-box (shown in Fig. 25), triangle, and football diagrams built out of $\pi N^\dagger N$ and $2\pi N^\dagger N$ interactions with chiral index $\Delta = 0$. For the last three types, all combinations of nucleons and Deltas need to be considered in intermediate states. For the box diagram with nucleons only, once-iterated OPE needs to be subtracted. The primordial counterterms consist of all possible two-derivative chiral-symmetric contact interactions (Ordóñez and van Kolck, 1992; van Kolck, 1993; Ordóñez, Ray, and van Kolck, 1996), including the C_{2s} and C'_{2t} terms in Eq. (70c), and no-derivative chiral-symmetry-breaking terms that are linear in the quark masses, such as D_{2s}. The constraints imposed by relativity on these primordial counterterms were discussed by Girlanda *et al.* (2010).

At relative $\mathcal{O}(Q^3/M_{\text{QCD}}^3)$, apart from further contributions to OPE parameters, the 2N potential is made up of TPE with one $\Delta = 1$ vertex, such as the triangle diagram shown in Fig. 25. For $n = 1$, Galilean corrections ($\propto m_N^{-1}$) should be kept, while for $n = 2$ they contribute only at next order. There are no new contact interactions at this order.

The isospin-symmetric 2N potential up to $\mathcal{O}(Q^3/M_{\text{QCD}}^3)$ was derived early on (Ordóñez and van Kolck, 1992; van Kolck, 1993; Ordóñez, Ray, and van Kolck, 1996; Kaiser, Brockmann, and Weise, 1997; Kaiser, Gerstendorfer, and Weise, 1998) and has been rederived many times since. Epelbaum, Glöckle, and Meißner (1998) introduced the unitary transformation method, which allows for the separation of the iterated OPE with a consistent set of $1/m_N$ corrections. Friar (1999) discussed the various forms, including pre-EFT results, and the issues involved in the separation of iterated OPE. The potential at this order resembles phenomenological potentials where pion exchange is supplemented by a short-range structure. The TPE part, which carries information about the chiral symmetry of QCD, involves LECs that can be determined from pion-nucleon scattering.

[For recent work in this direction, see Hoferichter *et al.* (2015) and Siemens *et al.* (2017).] It is a chiral analog of the van der Waals potential and behaves at short distances as $1/r^5$, $1/r^6$, or $1/r^7$ depending on the order and the number of intermediate Deltas, and has the qualitative features of heavier-meson-exchange potentials (Kaiser, Brockmann, and Weise, 1997; Kaiser, Gerstendorfer, and Weise, 1998). The TPE from chiral EFT without explicit Deltas successfully replaces heavier-meson exchange in the Nijmegen partial-wave analysis of 2N data (Rentmeester *et al.*, 1999; Rentmeester, Timmermans, and de Swart, 2003); for a modern version, see Navarro Pérez, Amaro, and Ruiz Arriola (2014, 2015).

The 2N potential has now been extended to higher orders. One- and two-loop TPE and two-loop three-pion exchange (see Fig. 25) diagrams at $\mathcal{O}(Q^4/M_{\text{QCD}}^4)$ were calculated by Kaiser (1999, 2000, 2001b, 2001c, 2015). More recently, the long-range Deltaless potential was constructed at $\mathcal{O}(Q^5/M_{\text{QCD}}^5)$ (Kaiser, 2001a; Entem *et al.*, 2015a; Epelbaum, Krebs, and Meißner, 2015b), and even $\mathcal{O}(Q^6/M_{\text{QCD}}^6)$ (Entem *et al.*, 2015a). By parity conservation, primordial counterterms appear only at even orders.

d. 3N potential

Beyond the Fujita-Miyazawa term, 3N forces have a similar hierarchy. At $\mathcal{O}(Q^{n+1}/M_{\text{QCD}}^{n+1})$, the 3N potential contains TPE diagrams where one interaction has $\Delta = 1$; see Fig. 25. Again, the form of TPE is constrained by chiral symmetry and provides a chiral-corrected version of the earlier Tucson-Melbourne (TM) potential (Coon *et al.*, 1979), sometimes called the TM' potential (Friar, Huber, and van Kolck, 1999; Coon and Han, 2001; Huber *et al.*, 2001), and close in form to the Brazil potential (Coelho, Das, and Robilotta, 1983). There are no additional isospin-symmetric contributions from Deltas (Epelbaum, Krebs, and Meißner, 2008a), but there are mixed one-pion–short-range and purely short-range components originating in the interactions with LECs G_A and H_0, respectively, in Eq. (70c) (van Kolck, 1994; Epelbaum *et al.*, 2002). Again, parity conservation implies primordial counterterms only at every second order.

The primordial counterterms at $\mathcal{O}(Q^{n+3}/M_{\text{QCD}}^{n+3})$ were listed by Girlanda, Kievsky, and Viviani (2011). Relativistic corrections, which appear at this order for $n = 1$, were calculated by Bernard *et al.* (2011). At $\mathcal{O}(Q^{n+2}/M_{\text{QCD}}^{n+2})$ the first loops in the 3N force appear as indicated in Fig. 25, and they were derived without Deltas by Ishikawa and Robilotta (2007) and Bernard *et al.* (2008, 2011). The long-range Deltaless and Deltaful potentials at 1 order higher [$\mathcal{O}(Q^{n+3}/M_{\text{QCD}}^{n+3})$] have been given by Krebs, Gasparyan, and Epelbaum (2012, 2013, 2018).

One must also look into higher-order double-pair or other disconnected diagrams where more than two clusters of nucleons interact at the same time. Epelbaum (2006b, 2007) found that double-pair diagrams with a recoil correction [$\mathcal{O}(Q^{2n}/M_{\text{QCD}}^{2n})$], with one insertion of a $\Delta = 2$ interaction [$\mathcal{O}(Q^{n+2}/M_{\text{QCD}}^{n+2})$], or with $L = 1$ [$\mathcal{O}(Q^{n+2}/M_{\text{QCD}}^{n+2})$] all add up to nothing without Deltas.

e. 4N potential

Four-body forces first appear at relative $\mathcal{O}(Q^{2n}/M_{\text{QCD}}^{2n})$, among them the one from the four-pion interaction displayed in Fig. 25. They are all of long range and contain no free parameters. The components without Deltas were given by Epelbaum (2006b, 2007). A first estimate (Rozpedzik *et al.*, 2006) of the effect of these components in ^{4}He gives an additional binding of a few hundred keV. The first contact $4N$ force is of $\mathcal{O}(Q^{2(n+1)}/M_{\text{QCD}}^{2(n+1)})$; since it has no derivatives, the exclusion principle allows only one such interaction, as was verified explicitly by Girlanda, Kievsky, and Viviani (2011).

f. Isospin violation

As discussed in Sec. II, Coulomb exchange is nonperturbative only at small energies; in the region that chiral EFT power counting is designed for, the Coulomb potential can be treated in perturbation theory. The way e_{red} was counted earlier ensures that the Coulomb potential appears at $\mathcal{O}(M_{\text{lo}}/M_{\text{QCD}})$, not LO. Other purely electromagnetic components are even smaller and can be incorporated as in ChPT. More interesting is the isospin breaking coming from the interactions in Eq. (70), where hard photons are integrated out and/or the quark-mass difference $\bar{m}\varepsilon$ [see Eq. (1)] appears. These interactions lead to the charge-neutral pion mass splitting $\delta m_\pi^2 = \mathcal{O}(M_{\text{lo}}^3/M_{\text{QCD}}) > 0$ and the neutron-proton mass difference $\delta m_N = \mathcal{O}(M_{\text{lo}}^2/M_{\text{QCD}}) > 0$. Likewise, other isospin-violating effects are suppressed by at least 1 power of M_{QCD}^{-1} (van Kolck, 1993, 1995), which means that isospin is an accidental symmetry: although broken in QCD, it is a symmetry of the LO EFT.

In contrast to many models, chiral EFT produces relatively simple isospin-violating forces that are invariant under both gauge transformations and pion-field redefinitions. The isospin-violating $2N$ potential was calculated up to relative $\mathcal{O}(Q^3/M_{\text{QCD}}^3)$ by van Kolck (1993, 1995), van Kolck, Friar, and Goldman (1996), van Kolck *et al.* (1998), Friar and van Kolck (1999), Niskanen (2002), Friar *et al.* (2003, 2004), Epelbaum and Meißner (2005), and Epelbaum, Krebs, and Meißner (2008a, 2008b), including the pion mass splitting in OPE and TPE, the most important isospin-breaking pion-nucleon coupling in OPE, simultaneous photon-pion exchange, the nucleon mass difference in TPE, and primordial counterterms. In standard terminology (Miller, Nefkens, and Slaus, 1990), class I forces refer to isospin symmetry, class II refers to forces that break charge independence but not charge symmetry, defined as a rotation of π around the 2-axis in isospin space, class III refers to forces that break charge symmetry but vanish in the np system, and class IV refers to those that break charge symmetry but cause isospin mixing in the np system. Class M forces are first found at $\mathcal{O}(Q^{M-1}/M_{\text{QCD}}^{M-1})$, which provides a justification for the pre-EFT phenomenology, where this hierarchy was observed (Miller, Nefkens, and Slaus, 1990).

Isospin violation first appears in the $3N$ potential at relative $\mathcal{O}(Q^{n+1}/M_{\text{QCD}}^{n+1})$, where it breaks charge symmetry through the nucleon mass difference in TPE (Friar *et al.*, 2004; Epelbaum, Meißner, and Palomar, 2005; Friar, Payne, and van Kolck, 2005). However, since δm_N is the result of a partial cancellation between quark-mass and electromagnetic effects, isospin breaking in the $3N$ potential is relatively small.

g. Summary

The nuclear potential—its long-range form and its primordial counterterms—has been derived in chiral EFT to a considerably high order. Although some of its elements had been anticipated using phenomenological methods, new forces have also been found, particularly those carrying the hallmark of QCD via chiral symmetry. Small differences of implementation remain regarding the related assignments of order to few-body forces and to the inverse nucleon mass. A more detailed exposition of the chiral potential was given by Epelbaum (2006a) and Machleidt and Entem (2011). We turn now to some of the important issues that arise when connecting these forces to data.

D. Nuclear amplitudes and observables

Observables are determined by the T matrix, which in turn is obtained by using the potential with the appropriate dynamical framework: the Lippmann-Schwinger or Schrödinger equation or one of its many-body variants. This process involves reducible diagrams for which the power counting of Sec. IV.C.1 does not apply. The original prescription of Weinberg (1990, 1991) was to truncate the potential and solve the corresponding equation exactly. The hope, based on experience with regular potentials, was that if corrections are small in the potential, they generate only small corrections at the amplitude level even if they are treated nonperturbatively. However, chiral potentials are regular only due to the regularization procedure, which means that reducible diagrams generate further regulator dependence. As in pionless EFT (Sec. II), non-negative powers of Λ are generated this way that, if not compensated for by the LECs, lead not only to potentially large corrections from subleading orders but also to model dependence through the regulator choice. The relevant question is, to what extent does Eq. (5) affect the ordering of the short-range interactions in the potential?

1. Weinberg's prescription

The first numerical study of chiral potentials with Weinberg's prescription by Ordóñez, Ray, and van Kolck (1994, 1996) yielded a reasonable description of $2N$ data at $\mathcal{O}(Q^3/M_{\text{QCD}}^3)$ with explicit Deltas for a Gaussian regulator on the transferred momentum with cutoff values $\Lambda = 500$, 800, 1000 MeV, but it used an overcomplete set of interactions. A drawback of such a local but nonseparable regulator is that it allows a contact interaction to contribute to all partial waves in a manner consistent with the exclusion principle. In the large-Λ limit the contribution of a contact interaction to all but one wave disappears, but at any finite cutoff data fitting is highly coupled and complicated. Epelbaum, Glöckle, and Meißner (2000) carried out the first fit with the minimum number of seven LECs at $\mathcal{O}(Q^2/M_{\text{QCD}}^2)$. That work as well as subsequent fits employed different regulators for the potential and the dynamical equation, with a separable, nonlocal regulator for the latter. Fits of higher quality were achieved, and it eventually emerged that they do depend on the choice of

regulator; only for a limited range of cutoff values $\Lambda \lesssim M_{QCD}$ have good fits been obtained (Epelbaum and Meißner, 2013; Marji *et al.*, 2013). A milestone was a fit (Entem and Machleidt, 2003) to $2N$ data at $\mathcal{O}(Q^4/M_{QCD}^4)$ without explicit Deltas for a nonlocal, super-Gaussian exponential regulator with $\Lambda = 500$ MeV. This achieved accuracy comparable to that of phenomenological potentials (for the $^3S_1$ phase shifts, see the curve labeled "EM500" in Fig. 7). Since then other high-quality fits have been achieved at this or even lower or incomplete orders (Epelbaum, Glöckle, and Meißner, 2004b, 2005; Ekström *et al.*, 2013, 2014; Epelbaum, Krebs, and Meißner, 2015a; Piarulli *et al.*, 2015). State of the art are the $\mathcal{O}(Q^5/M_{QCD}^5)$ fits of Entem, Machleidt, and Nosyk (2017) and Reinert, Krebs, and Epelbaum (2018).[12] We might expect increasingly accurate results as newly developed fitting-optimization procedures are applied to higher-order potentials.

To the orders where good fits to $2N$ data have been achieved, the chiral potential is expected, as discussed in Sec. IV.C.2, to include $3N$ forces, whichever value one takes for n. In most calculations, where $n = 2$ is assumed and the Delta is integrated out, the leading $3N$ forces appear at $\mathcal{O}(Q^3/M_{QCD}^3)$, and its two parameters G_A and H_0 [Eq. (70c)] are fitted to few-nucleon data. An obvious observable to fit with H_0 is the triton binding energy, as is frequently done in pionless EFT. Possible ways to determine G_A include a $2N$ process such as $NN \to NN\pi$ (Hanhart, van Kolck, and Miller, 2000; Baru *et al.*, 2009), another $3N$ quantity, such as the doublet neutron-deuteron (nd) scattering length (Epelbaum *et al.*, 2002) or the triton half-life (Gardestig and Phillips, 2006; Nakamura, 2008; Gazit, Quaglioni, and Navratil, 2009; Ekström *et al.*, 2014; Baroni *et al.*, 2016), and a $4N$ quantity, such as the ^{4}He binding energy (Nogga *et al.*, 2006; Ekström *et al.*, 2013). Kalantar-Nayestanaki *et al.* (2012) reviewed chiral $3N$ forces in light nuclei. Recently, a simultaneous fit to $A \leq 4$ properties (Carlsson *et al.*, 2016) was performed up to $\mathcal{O}(Q^3/M_{QCD}^3)$ without explicit Deltas. Overall, a good description of $A \leq 4$ systems, including scattering, can be achieved at this order and higher, as long as a "good" regulator with a cutoff parameter $\Lambda \lesssim M_{QCD}$ is employed.

Owing to their symmetry connection with QCD, chiral potentials have become increasingly popular within the nuclear-structure/reaction community, particularly after the milestone fit of Entem and Machleidt (2003). Remarkable progress has been achieved in the development of *ab initio* many-body methods for the solution of the Schrödinger equation starting from a given potential. Typically, additional UV and IR regulators (see Sec. II.C.5) are introduced, and EFT suggests extrapolations for mitigating their effects (Coon *et al.*, 2012; Furnstahl, Hagen, and Papenbrock, 2012; Kruse *et al.*, 2013; More *et al.*, 2013; Tölle, Hammer, and Metsch, 2013; Furnstahl, Papenbrock, and More, 2014; König *et al.*, 2014; Furnstahl, Hagen *et al.*, 2015; Wendt *et al.*, 2015; Coon and

Kruse, 2016). Extensive benchmarking—for examples, see Kamada *et al.* (2001), Hagen *et al.* (2007), and Abe *et al.* (2012)—has ensured that, while not entirely controlled, results are found to be in satisfactory agreement with each other. *Ab initio* methods are now at a stage where they can contribute substantially to the understanding of the input interactions by relating parameters of these interactions to $A > 4$ data. The majority of today's *ab initio* calculations use chiral potentials as input, for many of the new methods are flexible enough to accommodate the nonlocalities of both the interactions themselves and the chosen regulators.

Weinberg's prescription is simple to implement because it is the same as that used for a phenomenological potential: the various components are treated equally in the solution of the Schrödinger equation. The availability of many-body calculations has led to an increased use of $A > 4$ data to constrain the potential parameters, particularly those of the $3N$ force, which proves important in describing some nuclear quantities such as the ground-state spin of ^{10}Be (Navratil *et al.*, 2007), the dripline in oxygen isotopes (Otsuka *et al.*, 2010; Hagen *et al.*, 2012a), and the evolution of shell structure in calcium isopes (Hagen *et al.*, 2012b; Holt *et al.*, 2012). These achievements were reviewed by Hammer, Nogga, and Schwenk (2013), and more recently in a compilation of articles (Dudek, 2016) celebrating the 40-year anniversary of the 1975 Nobel Prize. While much of the nuclear data has been well described—for example, a reproduction of $A \leq 12$ spectra (Piarulli *et al.*, 2018)—there are also challenges in reproducing bulk properties of both nuclei (Somà *et al.*, 2014; Binder *et al.*, 2018) and nuclear matter (Hagen *et al.*, 2014; Drischler, Hebeler, and Schwenk, 2019), as well as some $A = 3$ scattering observables, including the recalcitrant A_y puzzle (Binder *et al.*, 2018; Piarulli *et al.*, 2018).

The issue of the optimal set of data to fit has come to the fore. In a controlled EFT, a change in input data at a given order is not ordinarily a systematic improvement because it represents a change that can be compensated at higher orders. However, this is not necessarily true when correlated data are employed (Lupu, Barnea, and Gazit, 2015). If only data at $Q \sim M_{lo}$ are used as input, we expect no particular correlations. Guaranteeing that this is the case is made difficult by the relative closeness between M_{lo} and M_{hi} in chiral EFT, aggravated by the use of cutoff parameters $\Lambda \lesssim M_{hi}$. If one employs data characterized by $Q < M_{lo}$, which are better described by a lower-energy EFT, correlations might appear. Examples of correlations among few-nucleon observables were given in Secs. II and III. If one attempts to use, say, the triton binding energy and the doublet nd scattering length to fix two parameters of the $3N$ force, one might expect one parameter combination to be relatively poorly determined. These are low-energy data within the realm of pionless EFT, which reorganizes interactions into the appropriate low-energy combinations. Since one expects larger systems to be increasingly within the regime of chiral EFT, it is possible that using properties of heavier nuclei provides real improvement. A concrete example is the so-called NNLO$_{sat}$ potential (Ekström *et al.*, 2015), a Deltaless chiral potential at $\mathcal{O}(Q^3/M_{QCD}^3)$ where the LECs are simultaneously adjusted not only for $A \leq 4$ but also to binding energies and radii of carbon and oxygen

---

[12]The relatively large size of TPE for the cutoff values employed by Reinert, Krebs, and Epelbaum (2018) might call into question the expansion of the potential shown in Fig. 25. However, the potential is not directly observable and its expansion must be judged according to its effects on renormalized amplitudes.
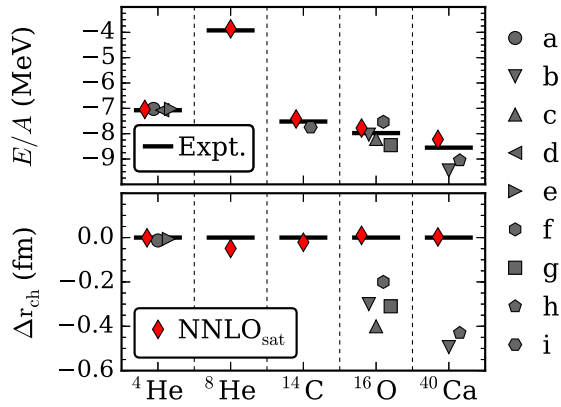
FIG. 26. (Top panel) Ground-state energy (negative of the binding energy) per nucleon, and (bottom panel) residuals (differences between computed and experimental values) of charge radii for selected nuclei computed with a variety of chiral potentials (labeled a–i and NNLO$_{sat}$). From Ekström *et al.*, 2015.

isotopes. Examples of the corresponding predictions for other nuclei are shown in Fig. 26. In a similar spirit, Elhatisari *et al.* (2015, 2016), implementing chiral EFT in a lattice framework, showed that the alpha-alpha interaction can be used as a sensitive handle to determine internucleon interactions.

The role of the regulator has also been under increasing scrutiny in *ab initio* calculations. A powerful tool for many-body calculations is the quantum Monte Carlo method, which pioneered the modern solution of many-nucleon systems but is best suited for local potentials. In chiral EFT, it favors local interactions and regulators. Antisymmetrization among nucleons can be used to eliminate some nonlocal contact interactions (Gezerlis *et al.*, 2013, 2014; Lynn *et al.*, 2014; Logoteta, Bombaci, and Kievsky, 2016; Piarulli *et al.*, 2016), enabling various new calculations. For example, the effects of the $\mathcal{O}(Q^2/M_{\mathrm{QCD}}^2)$ potential in neutron matter have been studied (Gezerlis *et al.*, 2013, 2014; Lynn *et al.*, 2016; Tews *et al.*, 2016). Because of antisymmetrization, different spin-isospin forms of the $3N$ contact interaction can be written; they are all equivalent and consistent with zero within the EFT truncation error for $\Lambda \gtrsim M_{\mathrm{QCD}}$. In contrast, the limitation to $\Lambda \lesssim M_{\mathrm{QCD}}$ leads to relatively large regulator artifacts above saturation density (Lynn *et al.*, 2016). This indicates that a lack of RG invariance, besides destroying model independence, also has undesirable phenomenological consequences.

2. Renormalization of singular potentials

The regulator dependence of Weinberg's prescription has been understood for a long time. Historically, the first observation was that the potential (75) can be solved semi-analytically in the $^1S_0$ channel: if $\boldsymbol{p}$ ($\boldsymbol{p}'$) denotes the relative incoming (outgoing) momentum in the center-of-mass frame and k^2/m_N denotes the energy, the LO amplitude can be written as (Kaplan, Savage, and Wise, 1996; Gegelia, 1999b; Eiras and Soto, 2003; Long and Yang, 2012b)

$$T^{(0)}(\boldsymbol{p}',\boldsymbol{p};k) = T_Y(\boldsymbol{p}',\boldsymbol{p};k) + \frac{\chi(\boldsymbol{p}';k)\chi(\boldsymbol{p};k)}{C_{0s}^{-1}(\Lambda) - I(\Lambda;k)}, \quad (78)$$

where T_Y is the amplitude for a pure Yukawa potential and

$$\chi(\boldsymbol{p};k) = 1 + m_N \int \frac{d^3l}{(2\pi)^3} \frac{T_Y(\boldsymbol{l},\boldsymbol{p};k)}{k^2 - l^2 + i\epsilon}, \quad (79)$$

$$I(\Lambda;k) = m_N \int \frac{d^3l}{(2\pi)^3} \frac{\chi^2(\boldsymbol{l};k)}{k^2 - l^2 + i\epsilon}, \quad (80)$$

where we keep the regularization implicit. When $T_Y = 0$, $I(\Lambda;k)$ reduces to the $I_0(\Lambda;k)$ of Eq. (22), and Eq. (78) reduces to Eq. (13). While T_Y and χ have no non-negative power dependence on Λ, $I(\Lambda;k)$ has two types of inadmissible cutoff dependence: $\propto \Lambda$ and $\propto (m_\pi^2/M_{NN}) \ln(\Lambda/M_{NN})$. The former is the same cutoff dependence that one sees in pionless EFT (Sec. II), and it can be absorbed in C_{0s}. The latter cutoff dependence, which appears despite the fact that the Yukawa interaction is regular by itself and is formally the same as the logarithmic divergence generated by the Coulomb interaction (see Sec. II.B.7), comes from the interference between contact interaction and OPE. It does not appear in other singlet channels (Eiras and Soto, 2003; Nogga, Timmermans, and van Kolck, 2005), but it cannot be absorbed in C_{0s}, which is the LEC of a chiral-invariant interaction and thus is not linear in m_π^2. Instead, one has to modify the LO potential in Eq. (75) to (Kaplan, Savage, and Wise, 1996)

$$C_{0s} \to C_{0s} + m_\pi^2 D_{2s} = \mathcal{O}\left(\frac{4\pi}{m_N M_{NN}}\right). \quad (81)$$

Even though NDA estimates that $D_{2s} = \mathcal{O}(C_{0s}/M_{\mathrm{QCD}}^2)$, renormalization requires $D_{2s} = \mathcal{O}(C_{0s}/M_{\mathrm{lo}}^2)$. Because of the different transformation properties under chiral symmetry, the two operators with LECs C_{0s} and D_{2s} differ in their pion interactions; see Eq. (70c). Of course, one cannot see this problem numerically in the $2N$ system unless one varies m_π, which is not done in most nuclear work, and even then the divergence is only logarithmic. The additional pion interactions from D_{2s} should have effects on other processes, such as pion-nucleus scattering, but only when there is a significant contribution from the $^1S_0$ $2N$ partial wave. Regardless of its phenomenological relevance, this is the simplest example where the renormalization of observables in chiral EFT is not guaranteed by NDA. This result has been confirmed in many other studies (Beane *et al.*, 2002; Pavón Valderrama and Ruiz Arriola, 2004, 2006a).

A similar but more dramatic renormalization effect concerns the momentum dependence of OPE. The tensor potential is singular, behaving at short distances as $-\alpha/r^n$ with $n = 3$ and, in some channels, $\alpha > 0$. It is well known (Frank, Land, and Spector, 1971) that such potentials need to be treated carefully because both solutions of the radial Schrödinger equation are irregular at $r = 0$. For two particles of reduced mass μ, the zero-energy S-wave radial wave function behaves at short distances as[13]

---

[13]Particularly interesting is $n = 2$, which is equivalent (Efimov, 1971) to the three-boson system at unitarity; see Sec. II. In this case, $\sqrt{2\mu\alpha}r^{1-n/2}/(n/2-1) \to \sqrt{2\mu\alpha - 1/4}\ln(r/r_0)$, with r_0 an arbitrary dimensionful parameter, and $\phi_2 = \phi_2(r_0)$. This is an example of an anomaly (Camblong and Ordóñez, 2003, 2005) where the scale invariance of the classical system is broken by renormalization to discrete scale invariance.

$$\psi(r) = r^{n/4-1} \cos\left(\frac{\sqrt{2\mu\alpha}r^{1-n/2}}{n/2-1} + \phi_n\right) + \cdots, \quad (82)$$

where ϕ_n is a phase related to the scattering length and, more generally, the phase shifts. In EFT, the phase is determined by a contact interaction, the LEC of which displays an oscillatory dependence on the cutoff (Beane, Bedaque, Childress *et al.*, 2001; Bawin and Coon, 2003; Braaten and Phillips, 2004; Alberg, Bawin, and Brau, 2005; Hammer and Swingle, 2006; Bouaziz and Bawin, 2014; Odell *et al.*, 2019), characteristic of a limit cycle or more complicated attractor. For RG analyses and reviews of limit cycles, see Barford and Birse (2003, 2005) and Pavón Valderrama and Ruiz Arriola (2008), and Hammer and Platter (2011) and Bulycheva and Gorsky (2014), respectively. Without the contact interaction, the increasing attraction of the singular potential leads to the repeated appearance of low-energy bound states as the momentum cutoff increases. With the contact interaction, not only the two-body system but also the three-body system is renormalized properly (Odell *et al.*, 2019), at least for $n = 3$.

The argument can be generalized to the tensor force (Beane *et al.*, 2002; Birse, 2006), which is attractive in some uncoupled channels and has one attractive eigenvalue in coupled channels. In ${}^3S_1$-${}^3D_1$ mixing, the C_{0t} interaction in Eq. (75) is sufficient to absorb the cutoff dependence and fix the low-energy phase shifts (Frederico, Timoteo, and Tomio, 1999; Beane *et al.*, 2002; Pavón Valderrama and Ruiz Arriola, 2005, 2006a; Yang, Elster, and Phillips, 2008), as suggested by NDA. However, in higher partial waves the effects of C_{0t} are cutoff artifacts that disappear at large cutoffs. As the cutoff increases, bound states accrue in the higher partial waves where the tensor OPE is attractive (${}^3P_0, {}^3P_2$-${}^3F_2, {}^3D_2, {}^3D_3$-${}^3G_3$, etc.), leading to wild variation in the corresponding low-energy phase shifts (Nogga, Timmermans, and van Kolck, 2005; Pavón Valderrama and Ruiz Arriola, 2006b). This problem can be cured (Nogga, Timmermans, and van Kolck, 2005) by a short-range interaction in each such wave, e.g., including a term $C'_{2t}(\mathbf{p'} \cdot \mathbf{p})P_t$ in Eq. (75). As primordial counterterm, $C'_{2t} = \mathcal{O}(C_{0s}/M_{\mathrm{QCD}}^2)$ appears only at $\mathcal{O}(Q^2/M_{\mathrm{QCD}}^2)$, and similarly for the counterterms in other attractive, singular waves. The absence in Weinberg's prescription of the appropriate counterterms explains the need for a "physical cutoff" $\Lambda_{\mathrm{phys}} \lesssim 1$ GeV, where ${}^3P_0$ would develop a bound state (Nogga, Timmermans, and van Kolck, 2005). In other waves, bound states cross threshold at higher cutoffs. In triplet waves where OPE is repulsive, there is no need for such counterterms at LO (Eiras and Soto, 2003; Nogga, Timmermans, and van Kolck, 2005).

Renormalization problems have been reported (Pavón Valderrama and Ruiz Arriola, 2006a, 2006b; Entem *et al.*, 2008; Yang, Elster, and Phillips, 2009a, 2009b; Zeoli, Machleidt, and Entem, 2013) within Weinberg's prescription also for higher-order potentials, which are increasingly singular and attractive in other waves as well. In contrast, a perturbative treatment of more-singular corrections to singular potentials can be properly renormalized (Long and van Kolck, 2008) with counterterms containing more derivatives, as expected from NDA. Renormalization of chiral potentials

seems to demand that at least some parts of the potential be treated in perturbation theory, just as in pionless EFT.[14]

3. Connection with pionless EFT

Experience with pionless EFT (van Kolck, 1997, 1999b; Bedaque, Hammer, and van Kolck, 1998; Bedaque and van Kolck, 1998; Kaplan, Savage, and Wise, 1998a, 1998b) shows that the factors associated with reducible loops are

$$\text{potential} \sim 4\pi m_N^{-1} M_{\mathrm{lo}}^{-1}(Q M_{\mathrm{QCD}}^{-1})^\mu, \quad (83a)$$

$$\text{nucleon propagator} \sim m_N Q^{-2}, \quad (83b)$$

$$\text{reducible loop integral} \sim (4\pi m_N)^{-1} Q^5, \quad (83c)$$

where the factor of $(4\pi)^{-1}$ is typical of integrals involving Schrödinger propagators. One iteration of the order-μ potential adds a reducible loop and two nucleon propagators, or $(Q/M_{\mathrm{lo}})(Q/M_{\mathrm{QCD}})^\mu$. This is an IR enhancement of $m_N/(4\pi Q)$ over the factor that arises from Eqs. (71b) and (71c). As a consequence, the perturbative series in the LO potential ($\mu = 0$) fails to converge for $Q \sim M_{\mathrm{lo}}$, while subleading potentials ($\mu \geq 1$) should be amenable to perturbation theory.

The LO chiral potential (75) has the form of Eq. (83a) if $M_{NN} = \mathcal{O}(M_{\mathrm{lo}})$. Since bound states indicate a breakdown of perturbation theory, one expects binding energies per nucleon

$$\frac{B_A}{A} \sim \frac{M_{NN}^2}{M_{\mathrm{QCD}}} \sim \frac{f_\pi}{4\pi} \sim 10 \text{ MeV}, \quad (84)$$

which is in the right ballpark for heavy nuclei. Thus, chiral symmetry together with this IR enhancement provides a natural explanation (Bedaque and van Kolck, 2002) for the shallowness of nuclei compared to M_{QCD}, $B_A/A \ll M_{\mathrm{QCD}}$, long considered a mystery.

The factor of 4π in the IR enhancement was not recognized before pionless EFT was developed, but it has implications for the natural size of few-body forces. Connecting an aN potential to another nucleon to make it an $(a+1)N$ potential without changing L or Δ involves an additional factor $4\pi m_N^{-1} M_{\mathrm{lo}}^{-2}$ from the extra $2N$ interaction and the extra nucleon propagator inside the aN potential. At the same time, it adds a reducible loop and one nucleon propagator at the amplitude level, resulting in an overall suppression by Q/m_N. For $m_N = \mathcal{O}(M_{\mathrm{QCD}})$, as dictated by NDA for $A = 1$, where it works well, this is the $n = 1$ suppression of Friar (1997). In contrast, missing the 4π in the IR enhancement would require $Q/m_N \sim Q^2/M_{\mathrm{QCD}}^2$, as found in Sec. IV.C.2 for $n = 2$ (Weinberg, 1991, 1992; Ordóñez and van Kolck, 1992; van Kolck, 1993). Thus, counting factors of 4π in reducible

---

[14]The simple toy model of a regular long-range potential plus a short-range interaction that yields a natural two-body scattering length illustrates how treating the subleading EFT contact interaction nonperturbatively, similar to the "peratization" of Fermi theory (Feinberg and Pais, 1963, 1964), prevents a large cutoff (Epelbaum and Gegelia, 2009).

loops leads to Friar's power counting, which, however, has not been widely tested so far.

4. Perturbative pions

A radical solution to the renormalization problems of Weinberg's prescription was proposed by Kaplan, Savage, and Wise (1998a, 1998b): assume that the contact interactions carry a low-energy scale characteristic of the binding momenta of light nuclei, $M_{lo} \ll M_{NN}$, and treat M_{NN} as a high-energy scale. Pion exchange in nuclear amplitudes appears in two expansions:

(1) The expansion in $Q/(4\pi f_\pi)$ of the nuclear potential, which, as discussed in Sec. IV.C.2, is similar to the ChPT expansion for $A \leq 1$.

(2) An expansion in Q/M_{NN} in the solution of the dynamical equation, which is similar to the pionless EFT expansion for $A \geq 2$.

Thus, if $Q \sim m_\pi \ll M_{NN} \lesssim M_{QCD}$, one can treat all pion exchanges in perturbation theory. Numerically, M_{NN} could be larger than the NDA estimate $M_{NN} \sim f_\pi$.

This version of chiral EFT closely resembles pionless EFT (Sec. II), with similar M_{lo} scaling of the LECs but different values, and additional pion exchanges. The range of validity of the EFT is enlarged, at least near the chiral limit where integrating out pions becomes a restrictive condition. At LO the two EFTs are formally the same, so the corresponding results from pionless EFT carry over (there are two nonderivative $2N$ contact interactions and one nonderivative three-nucleon force), but m_π is now counted as M_{lo} together with the $2N$ binding momenta.

At relative $\mathcal{O}(Q/M_{NN})$, however, there are not only two-derivative two-nucleon contact terms ($\propto Q^2$) but also OPE, which provides a shape function that goes beyond the first two terms in the effective-range expansion. In perturbation theory, the $m_\pi^2 \ln \Lambda$ cutoff dependence in the $^1S_0$ channel (Sec. IV.D.2) comes from a diagram where OPE appears between two LO interactions. The corresponding chiral-symmetry-breaking counterterm ($\propto m_\pi^2$) must be NLO as well. Both Q^2 and m_π^2 corrections appear at the same order, as in ChPT, but they are suppressed by only 1 power of Q/M_{NN}. The two-nucleon amplitude is well reproduced (Kaplan, Savage, and Wise, 1998a, 1998b; Soto and Tarrus, 2008). [For the renormalization issues associated with a resummation of effective-range effects with and without dibaryon fields, see Ando and Hyun (2012) and Nieves (2003), respectively.] There is only one calculation of the effects of perturbative OPE in the three-nucleon system, quartet nd scattering below and above breakup (Bedaque and Grießhammer, 2000), and it gives similar results to those from pionless EFT (Sec. II.C.3).

N²LO (Cohen and Hansen, 1999b; Fleming, Mehen, and Stewart, 2000a, 2000b; Soto and Tarrus, 2010), i.e., relative $\mathcal{O}(Q^2/M_{NN}^2)$, is a crucial test of this expansion since it is the first manifestation of iterated OPE. It was demonstrated (Cohen and Hansen, 1999b; Fleming, Mehen, and Stewart, 2000b) that, while the expansion works well at small momenta, in the low, spin-triplet partial waves where the OPE tensor force is attractive, it fails for momenta $Q \sim 100$ MeV. Fleming, Mehen, and Stewart (2000b) employed dimensional regularization with a subtraction

(PDS) (Kaplan, Savage, and Wise, 1998a, 1998b) designed to facilitate power counting, but of course other regularization and subtraction schemes give equivalent results (Cohen and Hansen, 1998; Mehen and Stewart, 1999a, 1999b). [For an RG discussion, see Harada, Kubo, and Yamamoto (2011).] A calculation employing a procedure similar to Pauli-Villars regularization gave better results (Beane, Kaplan, and Vuorinen, 2009) in channels with LECs, but not in the spin-triplet channels lacking LECs at that order. These signs of the breakdown of perturbative pions are consistent with an expansion in Q/M_{NN} where $M_{NN} \sim f_\pi$, as indicated by NDA.

There has also been criticism of the perturbative-pion expansion based on the poor convergence of threshold observables (Cohen and Hansen, 1999a, 1999c). This suggests that the expansion in m_π/M_{NN} is not great for the real world, again pointing to the low value of M_{NN}. However, it is the reorganization of interactions in pionless EFT that is optimized for momenta $Q \ll m_\pi$, where the ERE holds. The effectiveness of a power counting in chiral EFT should be judged from the convergence of observables at $Q \sim m_\pi$. At such momenta, for example, the scattering length contribution is small, and one might start from the unitary limit instead (Soto and Tarrus, 2008, 2010), as discussed in Sec. II.D. In the $^1S_0$ channel, the perturbative-pion expansion does converge (Beane *et al.*, 2002), despite claims to the contrary based on an NLO calculation (Gegelia, 1998a). The slow convergence can be attributed to the short-range interactions. For analyses of perturbative pions in the better-controlled context of toy models, see Kaplan and Steele (1999), Rupak and Shoresh (1999), and Steele and Furnstahl (1999).

In the real world, this version of chiral EFT does not seem to work much beyond the regime of validity of pionless EFT. Because the latter is simpler and holds for larger pion masses, it has been preferred in most low-energy applications. However, chiral EFT retains the constraints of chiral symmetry that are lost in pionless EFT; when such constraints are useful, chiral EFT with perturbative pions can be deployed. Moreover, at smaller pion masses chiral EFT with perturbative pions is expected to have a considerably larger range of applicability than pionless EFT.

5. Partly perturbative pions

For a couple of years the choice facing the field was between a power counting that lacks counterterms in the sense discussed in Sec. IV.D.2 (which ensure that all divergences at a given order can be absorbed) but works well phenomenologically (Sec. IV.D.1), and another one that has all of the counterterms but fails to converge even at relatively small energies (Sec. IV.D.4). A way out was suggested by Nogga, Timmermans, and van Kolck (2005) and carried out by Long and Yang (2011, 2012a, 2012b) and Pavón Valderrama (2011a, 2011b). Perhaps not surprisingly in hindsight this solution is a middle ground between Weinberg's prescription and fully perturbative pions. It is based on two observations:

(1) Pions are perturbative in sufficiently high two-nucleon partial waves. For an orbital angular momentum $l > l_{cr}$, where $l_{cr}(l_{cr} + 1) \sim M_{hi}/M_{NN}$, the centrifugal barrier dominates over OPE at all distances $r \gtrsim 1/M_{hi}$

that are relevant when $Q \lesssim M_{\mathrm{hi}}$. In these waves, OPE should be perturbative for the external momenta where chiral EFT holds (Nogga, Timmermans, and van Kolck, 2005). In other words, OPE in the radial Schrödinger equation is an expansion in $Q/M_{NN}^{(l)}$, where $M_{NN}^{(0)} = M_{NN}$ but $M_{NN}^{(l)}$ increases with l. For $l \leq l_{\mathrm{cr}}$, OPE is nonperturbative. In these waves, and these waves only, OPE needs to be iterated at LO, as observed by Fleming, Mehen, and Stewart (2000b). The LECs needed for renormalization (Sec. IV.D.2) should, of course, be iterated as well. All subleading interactions are to be treated in distorted-wave perturbation theory for $l \leq l_{\mathrm{cr}}$, and in ordinary perturbation theory for $l > l_{\mathrm{cr}}$.

(2) Multiple-pion exchange, being suppressed by powers of $Q/(4\pi f_\pi)$, should be small after renormalization and thus amenable to perturbation theory in all waves. It is more singular than OPE but can be renormalized perturbatively with a finite number of LECs (Long and van Kolck, 2008).

Since the OPE tensor force survives in the chiral limit, for $m_\pi \lesssim M_{NN}$ one can perform an additional expansion around the chiral limit (Beane *et al.*, 2002), but, as discussed in Sec. IV.D.4, this expansion is not likely to be useful much beyond the physical pion mass.

For $M_{\mathrm{hi}} > M_{NN}$, i.e., M_{NN} counted as a low-energy scale, one expects $l_{\mathrm{cr}} \geq 1$. Of course, other dimensionless factors stemming from spin and isospin make the transition from nonperturbative to perturbative OPE somewhat fuzzy, which, however, does not mean that such a transition does not exist. Early studies of perturbative pions with and without Deltas (Kaiser, Brockmann, and Weise, 1997; Ballot, Robilotta, and da Rocha, 1998; Kaiser, Gerstendorfer, and Weise, 1998), which did not discriminate between iterated pion exchange and multiple-pion exchange in the potential, indicated that pion exchange might be perturbative for $l \gtrsim 3$. This interpretation is also consistent with subsequent investigations of peripheral waves with chiral potentials up to $\mathcal{O}(Q^6/M_{\mathrm{QCD}}^6)$ (Entem and Machleidt, 2002; Epelbaum, Glöckle, and Meißner, 2004a; Krebs, Epelbaum, and Meißner, 2007; Entem *et al.*, 2015a, 2015b). Qualitatively, this result has been confirmed for OPE (Nogga, Timmermans, and van Kolck, 2005). A semianalytical estimate (Birse, 2006) of the momenta where the tensor part of OPE needs to be treated nonperturbatively in the lower triplet waves is given in Table II. Some evidence thus points to $l_{\mathrm{cr}} \approx 3$. More detailed, recent analyses suggest, however, that pions are perturbative up to a relatively high scale in all waves other than $^3S_1$-$^3D_1$ and $^3P_0$ (Kaplan, 2019; Wu and Long, 2019).

In the low 2N waves where $l \leq l_{\mathrm{cr}}$ and $M_{NN}^{(l)} \approx M_{NN}$, the situation at LO is similar to Weinberg's prescription, except that more short-range interactions are needed for renormalization (Nogga, Timmermans, and van Kolck, 2005) than implied by NDA. For example, in the $^1S_0$ channel OPE at LO solves the problem of the slow convergence of perturbative pions (Beane *et al.*, 2002) at the cost of the additional D_{2s} LEC in Eq. (81). The residual $1/\Lambda$ dependence then means (Long and Yang, 2012b) that a correction appears at

TABLE II. Estimate of the critical values p_{cr} of the relative momentum in the lowest two-nucleon triplet channels above which the OPE tensor force cannot be treated perturbatively (Birse, 2006).

Channel	p_{cr} (MeV)	Channel	p_{cr} (MeV)	Channel	p_{cr} (MeV)
$^3S_1$-$^3D_1$	66	$^3P_0$	182	$^3P_1$	365
$^3P_2$-$^3F_2$	470	$^3D_2$	403	$^3D_3$-$^3G_3$	382
$^3F_3$	2860	$^3F_4$-$^3H_4$	2330	$^3G_4$	1870

$\mathcal{O}(Q/M_{\mathrm{QCD}})$ from the two-derivative contact interaction responsible for the short-range contribution to the effective range, similar to pionless EFT (Sec. II.B.3). At higher orders in the lower partial waves, multiple-pion exchanges appear and require at $\mathcal{O}(Q^\mu/M_{\mathrm{QCD}}^\mu)$ LECs with up to μ derivatives more than the LECs appearing at LO (Long and van Kolck, 2008).

This approach was confronted with empirical phase shifts for the lower 2N partial waves by Nogga, Timmermans, and van Kolck (2005), Long and Yang (2011, 2012a, 2012b), Pavón Valderrama (2011a, 2011b), Epelbaum and Meißner (2013), and Yang (2016). The results of Long and Yang (2012a) are included in Fig. 7, whereas Fig. 27 shows the $^3P_0$ results of Pavón Valderrama (2011b) as a further example. While in both cases $\mathcal{O}(Q^2/M_{\mathrm{QCD}}^2)$ improves on $\mathcal{O}(1)$, $\mathcal{O}(Q^3/M_{\mathrm{QCD}}^3)$ goes in the wrong direction, perhaps an indication that a better description of the pion-nucleon subamplitude with an explicit Delta isobar is needed.

Little is known quantitatively about partly perturbative pions beyond the two-nucleon system. The three-nucleon system is renormalized properly without a three-nucleon force at LO (Nogga, Timmermans, and van Kolck, 2005; Song, Lazauskas, and van Kolck, 2017) and, without explicit Deltas,
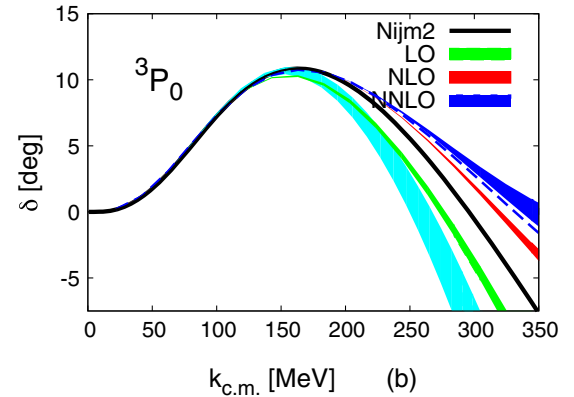

FIG. 27. The NN $^3P_0$ phase shift δ as a function of the center-of-mass momentum $k_{\mathrm{c.m.}}$ at different chiral orders: $\mathcal{O}(1)$ (green), $\mathcal{O}(Q^2/M_{\mathrm{QCD}}^2)$ (red), and $\mathcal{O}(Q^3/M_{\mathrm{QCD}}^3)$ (blue). Bands represent the variation of a coordinate-space cutoff in the range 0.6–0.9 fm, with the dashed line showing the $\mathcal{O}(Q^3/M_{\mathrm{QCD}}^3)$ results with a 0.3 fm cutoff. The cyan band shows the $\mathcal{O}(Q^3/M_{\mathrm{QCD}}^3)$ potential in Weinberg's prescription with the regularization procedure of Epelbaum, Glöckle, and Meißner (2004b), where the momentum-space cutoff in pion loops (the Lippmann-Schwinger equation) is varied between 500 and 700 (450 and 650) MeV. The solid black line is the Nijmegen phase-shift analysis (Stoks *et al.*, 1993). From Pavón Valderrama, 2011b.

also at NLO (Song, Lazauskas, and van Kolck, 2017). The truncation in l needed at LO is reminiscent of the truncation in total two-nucleon angular momentum typically invoked in solutions of the Faddeev and Faddeev-Yakubovsky equations for three- and four-nucleon systems with phenomenological potentials. However, to go to higher orders the l dependence of $M_{NN}^{(l)}$ must be quantified. Thus far, this has been done only in singlet waves (Pavón Valderrama *et al.*, 2017).

At LO symmetric nuclear matter was found to saturate, but with significant underbinding, in a cutoff-converged Brueckner pair approximation (Machleidt *et al.*, 2010). This is in contrast to Weinberg's prescription, where Deltaless (Sammarruca *et al.*, 2018) or Deltafull (Ekström *et al.*, 2018) potentials of $\mathcal{O}(1)$ and $\mathcal{O}(Q^2/M_{\text{QCD}}^2)$ do not saturate within the EFT domain. The fact that higher-order potentials with this prescription do saturate (Ekström *et al.*, 2018; Sammarruca *et al.*, 2018; Drischler, Hebeler, and Schwenk, 2019) suggests that, if nuclear matter is within the regime of chiral EFT, the LO potential requires more interactions than prescribed by NDA.

Although they differ in detail from the field-theoretical renormalization outlined previously, RG analyses of the Schrödinger equation (Birse, 2006, 2011; Pavón Valderrama, 2016) support the conclusion that counterterms in two-nucleon attractive singular waves appear at lower order than expected on the basis of NDA. The case is further strengthened by removing the effect of OPE and (perturbative) TPE from empirical two-nucleon phase shifts (Birse, 2007; Ipson, Helmke, and Birse, 2011). The Schrödinger RG analysis also predicts the enhancement of some three-body forces (Birse, 2011).

6. Other approaches

The renormalization of chiral EFT described in Secs. IV.D.2–IV.D.5 was criticized by Epelbaum *et al.* (2018), who provided examples where the nonperturbatively renormalized amplitude exhibits positive powers of the cutoff Λ when expanded in Planck's constant $\hbar$. Since no observable considered in that work is affected, however, the significance of this claim for an EFT is unclear. Moreover, Pavón Valderrama (2019a) argued that these powers of Λ can be eliminated by changing the Λ^{-1} running of the LECs (Pavón Valderrama, 2016); see also Epelbaum *et al.* (2019).

An alternative approach to the renormalization woes of Weinberg's prescription was articulated by Epelbaum *et al.* (2018), building on earlier work (Gegelia, 1998a, 1998b, 1999a, 1999b; Gegelia and Japaridze, 2001; Gegelia and Scherer, 2006; Epelbaum and Gegelia, 2009). It consists of renormalizing the perturbative series and subsequently resumming the renormalized contributions; that is, it includes at each order the infinite number of LECs needed to eliminate the cutoff dependence of all diagrams to be resummed. These LECs exist because an EFT contains all interactions allowed by symmetry, but even without pions they are difficult or impossible to write down explicitly. In a stark departure from naturalness, only the LECs prescribed by NDA are assumed to contribute finite parameters, which amounts to an infinite number of fine-tunings. The resummation of an infinite number of derivative interactions introduces an intrinsic

nonlocality in all channels at every order, not only LO in, say, the NN $^1S_0$ (Beane and Savage, 2001; Sánchez, Sánchez *et al.*, 2018) or the $N\alpha$ $^2P_{3/2}$ (Bertulani, Hammer, and van Kolck, 2002) channels, where there are shallow poles.

In this approach, there are no constraints on the EFT from renormalization, for example, there is no Wigner bound on the effective range [(Wigner, 1955); see Sec. II.B.3] when C_2 or higher-order interactions are resummed (Gegelia, 1998b) and no explanation (Epelbaum *et al.*, 2017, 2019) for the emergence of a single, independent three-body scale in the three-body system at LO, which determines the position of the Efimov tower of states [(Efimov, 1970); see Sec. II.C.2]. Thus, the justification for power counting from the combination of renormalization and naturalness, which in the perturbative context gives NDA (Manohar and Georgi, 1984; Georgi and Randall, 1986), is absent. NDA becomes an *ad hoc* rule. It does not, for example, reproduce the established scaling of range corrections in amplitudes resulting from short-range potentials, which is represented in pionless EFT through Eq. (18).

To date, this approach has been implemented only in the $^1S_0$ channel, where significant dependence on the choice of (low-energy) subtraction points is seen (Gegelia, 1998a, 1999a, 1999b; Gegelia and Japaridze, 2001). On the basis of a toy model, Epelbaum, Gegelia, and Meißner (2017) concluded that Weinberg's prescription is satisfactory as long as the renormalization scale $\mu = \mathcal{O}(M_{\text{hi}})$. Chiral EFT's overlapping integrals in other channels prevent the explicit resummation of "renormalized diagrams," and it is not known whether this procedure, if it can be carried out at all, reproduces the nonperturbative solution of the Lippmann-Schwinger equation. Further discussion of renormalization from the perspective of subtraction schemes was given by Timoteo *et al.* (2011), Szpigel and Timoteo (2012), Batista, Szpigel, and Timóteo (2017).

Gegelia and Japaridze (2001) offer the solution that the cutoff should not be varied significantly around the breakdown scale in chiral EFT. In the absence of renormalization, non-negative powers of the cutoff should appear in the truncated amplitude given by Eq. (4) as corrections of $\mathcal{O}(Q^{\mathcal{V}+1-i}\Lambda^i/M_{\text{hi}}^{\mathcal{V}+1-j}M_{\text{lo}}^j)$ with non-negative integers i and j. If $j = 0$, the corrections should be small for $\Lambda \ll M_{\text{hi}}$ (Gegelia and Scherer, 2006), but $j > 0$ arises when the LO potential, which does not involve M_{hi}, is singular.

An attempt to mitigate cutoff artifacts was made by Djukanovic *et al.* (2007), Epelbaum and Gegelia (2012), Epelbaum *et al.* (2014) and Epelbaum, Gasparyan, Gegelia, and Krebs (2015), with the most recent formulations developed by Behrendt *et al.* (2016) and Baru, Epelbaum, Gegelia, and Ren (2019). A nucleon propagator with faster large-momentum falloff is constructed by demanding that states satisfy a relativistic, Lorentz-invariant normalization condition, while the treatment is still nonrelativistic overall. This softer UV behavior helps to obtain LO amplitudes with well-defined large-cutoff limits. While Behrendt *et al.* (2016) state that higher orders should be treated in perturbation theory if this feature is to be maintained beyond LO, from a practical point of view they still advocate a nonperturbative treatment (where the cutoff is then limited again to a finite range, argued

to be larger than what is typically used with standard Weinberg counting). Moreover, Behrendt *et al.* (2016) found that with their approach a $^3P_0$ LEC has to be promoted compared to NDA, as in the purely nonrelativistic context (Nogga, Timmermans, and van Kolck, 2005). There is, nevertheless, growing interest in the development of a covariant version of chiral EFT, which could perhaps be used as input to relativistic formulations of nuclear physics (Petschauer and Kaiser, 2013; Ren *et al.*, 2017, 2018).

E. Pion and electroweak reactions

One of the advantages of a quantum-field-theoretical foundation of nuclear physics is not only that many-body forces can be constructed consistently with two-body forces but also that many-body currents can be derived consistently with internucleon interactions. This virtue was realized early on (Rho, 1991; Weinberg, 1991), and some of the pioneering papers on reactions have been dedicated to electroweak currents (Park, Min, and Rho, 1993, 1996; Phillips and Cohen, 2000), neutron radiative capture on the proton (Park, Min, and Rho, 1995; Park *et al.*, 1998a), proton-proton fusion (Park *et al.*, 1998b), Compton scattering on the deuteron (Beane *et al.*, 1999), pion photoproduction (Beane, Lee, and van Kolck, 1995; Beane *et al.*, 1997) and electroproduction (Bernard, Krebs, and Meißner, 2000) off the deuteron, pion photoproduction off the trinucleon (Lenkewitz *et al.*, 2011, 2013), and pion scattering on the deuteron (Beane *et al.*, 1998) and helion (Liebig *et al.*, 2011), as well as pion production in $2N$ collisions (Cohen *et al.*, 1996; Park *et al.*, 1996; van Kolck, Miller, and Riska, 1996; Sato *et al.*, 1997). The goal is not only to supply information to other areas of physics where these reactions play a role, but also to extract nucleon properties (especially for the neutron, for which good targets do not exist) to infer properties of the QCD dynamics.

The early work, reviewed by van Kolck (1999a) and Bedaque and van Kolck (2002), was based on Weinberg's prescription, where, in addition to the potential, also the kernel of the reaction process is expanded according to NDA. For probes with energies $E \sim Q \sim m_\pi$, the kernel is defined as the subdiagrams to which the external probes are attached, energies are comparable to momenta, and nucleons are approximately static. Like the potential, kernels can be multiply connected, and power counting is similar to Eqs. (73) and (74). For any kernel, a figure like Fig. 25 can be drawn. However, some subtleties need to be taken into account when probes have other typical energy or momentum:

- $E \sim M_{NN}^2/M_{QCD}$ (e.g., Compton scattering): a resummation is needed between kernels because infrared enhancements appear in intermediate states, where nucleons are not static (Beane *et al.*, 1999).
- $Q \sim \sqrt{m_\pi m_N}$ (e.g., pion production):[15] intermediate states containing only nucleons can be part of the kernel, but these nucleons are not static (Cohen *et al.*, 1996).

---

[15]Although parametrically $\sqrt{m_\pi m_N} = \mathcal{O}(\sqrt{m_\pi M_{QCD}}) < M_{QCD}$, one should keep in mind that the breakdown scale M_{QCD} of chiral EFT is not known precisely.

The full amplitude is given by the matrix element of the kernel with wave functions obtained from the potential. In Weinberg's prescription, these wave functions are exact solutions of a truncated potential. Much of the work predating phenomenologically successful chiral potentials employed a "hybrid" approach where the kernel was calculated in chiral EFT but wave functions from "realistic" phenomenological potentials were used. Emphasis has since been shifting toward increased consistency between wave functions and kernels. Reactions are an area of renewed interest in chiral EFT, in consonance with the revival of development in the broader area of nuclear reactions, including *ab initio* approaches. Of particular recent interest have been electroweak currents, where earlier work was revisited and significantly improved upon; see the reviews by Phillips (2016) and Riska and Schiavilla (2017). There has also been substantial work on reactions involving pions, particularly pion production in two-nucleon collisions, which has now been calculated up to 3 orders in the chiral expansion (Baru, Hanhart, and Myhrer, 2014).

The process that has been most thoroughly examined in chiral EFT is Compton scattering (CS). It gives access to nucleon polarizabilities, response functions that carry much information about hadron dynamics. While proton polarizabilities can be extracted directly, neutron polarizabilities can be probed only in nuclear CS. Chiral EFT allows for a consistent treatment of both of these cases and, at the same time, enables a connection with lattice QCD through variation in the pion mass. Recent work has capitalized on all advances in EFT and provides an analysis of CS that is a model for future work on nuclear reactions. At the one-nucleon level, CS was calculated in ChPT with an explicit Delta isobar (McGovern, Phillips, and Grießhammer, 2013), including the resummation (Pascalutsa and Phillips, 2003) needed to go through the Delta peak. At the nuclear level, the kernel was calculated according to Weinberg's prescription (Grießhammer *et al.*, 2012). Proton (McGovern, Phillips, and Grießhammer, 2013) and deuteron (Myers *et al.*, 2014, 2015) data were fitted and polarizabilities were extracted; see Fig. 28. The average quark mass was then varied to produce predictions, with uncertainties determined via Bayesian techniques (Furnstahl, Klco *et al.*, 2015; Furnstahl, Phillips, and Wesolowski, 2015; Wesolowski *et al.*, 2016), for the polarizabilities at unphysical pion masses (Grießhammer, McGovern, and Phillips, 2016b), to which lattice QCD results can be compared. Analyses of this type for other processes should increasingly become standard in this field, allowing one to bridge from QCD to nuclear reactions just as to nuclear structure.

The renormalization problems of Weinberg's prescription demand scrutiny in the treatment of reactions as well. The emergence of a perturbative-pion formulation of chiral EFT has led to a reexamination of many of the reactions that had been studied earlier with Weinberg's prescription. With perturbative pions, not only the kernel but also the wave function is expanded in perturbation theory. For the deuteron, the target of most, if not all, perturbative-pion studies, the analytical nature of the calculations makes it easier to establish proper renormalization. In most cases, the LO calculation is the same as in pionless EFT (Secs. II.B.8 and II.C.8), and pion
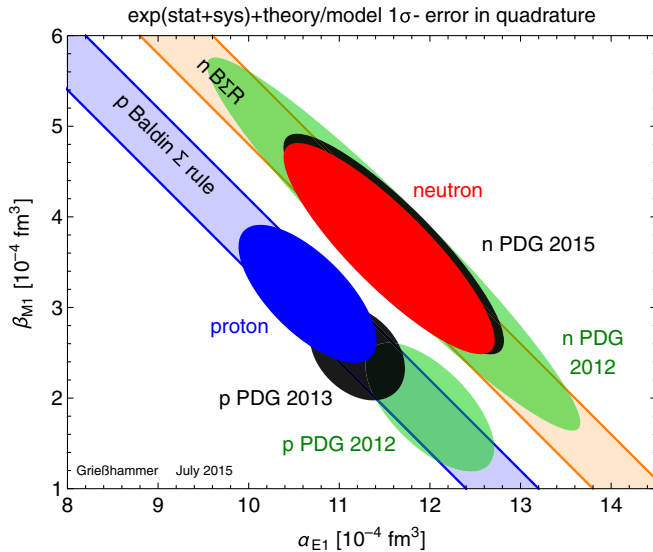
FIG. 28. Nucleon electric (α_{E1}) and magnetic (β_{M1}) polarizabilities extracted with chiral EFT. Ellipses show the 1σ-error fits of McGovern, Phillips, and Grießhammer (2013) for proton (blue, on lower band) and neutron (red, on upper band), where statistic, systematic, and theory errors are added in quadrature. For comparison, Particle Data Group averages before (large green ellipses) and after (small black ellipses) these fits are also given. The bands are the constraints from the Baldin sum rule. From Grießhammer, McGovern, and Phillips, 2016a.

effects enter explicitly at subleading orders. For example, the charge, magnetic dipole, and electric quadrupole form factors of the deuteron were calculated to NLO by Kaplan, Savage, and Wise (1999). Other reactions include neutron radiative capture on the proton (Savage, Scaldeferri, and Wise, 1999), deuteron Compton scattering and polarizability (Chen *et al.*, 1998a, 1998b; Chen, 1999), and neutrino-deuteron scattering (Butler and Chen, 2000). Generally, this approach has been successful for the low-energy properties of the deuteron, in comparison both with data and with nonperturbative-pion calculations.

F. Outstanding issues and current trends

Within Weinberg's prescription, work continues in pushing potential and kernels to higher orders, as well as developing better fitting strategies. Meanwhile, an RG-invariant formulation of chiral EFT has not yet achieved the level of phenomenological impact of Weinberg's prescription. Some of the outstanding questions are as follows:

- What is the role of fine-tuning in chiral EFT? The scattering length is particularly large in the $^1S_0$ two-nucleon channel, where short-range interactions show strong energy dependence (Birse, 2010). In particular, short-range contributions to the effective range are anomalously large, which has led to the suggestion that the two-derivative contact interaction [C_{2s} in Eq. (70c)] should be treated as LO (Beane *et al.*, 2002; Long, 2013), following a similar proposal in pionless EFT (Beane and Savage, 2001) (Sec. II.B.5) and chiral EFT with perturbative pions (Ando and Hyun, 2012)

(Sec. IV.D.4). Although an improved description is achieved, convergence deteriorates quickly with momentum, at least in a calculation without Deltas (Long, 2013). The role of the relatively low-energy zero of the amplitude remains to be fully investigated (Lutz, 2000; Sánchez, Sánchez *et al.*, 2018).

- What is the pion-mass variation of nuclear amplitudes? To determine this variation, we need lattice data within the region of validity of chiral EFT. While lattice QCD data exist at relatively large m_π, not all competing collaborations are in agreement. Moreover, differences exist within chiral EFT depending on the approach used. Among the issues for extrapolations is the role of "radiation" pions, which are present only at relatively high order. Real pions can be produced in $2N$ collisions for momenta $Q \gtrsim \sqrt{m_\pi m_N}$; at lower Q the effects of the corresponding virtual pions are indistinguishable from the LECs (Ordóñez, Ray, and van Kolck, 1996; Epelbaum, Glöckle, and Meißner, 1998). These contributions have been investigated in the perturbative-pion context (Mehen and Stewart, 2000; Mondejar and Soto, 2007; Soto and Tarrus, 2012) where they give rise to powers of $m_\pi^{1/2}$.

- The NDA-based organization of pion-exchange contributions to the potential is not affected by the renormalization issues that plague Weinberg's prescription, except for the possible enhancement factors of 4π in few-nucleon forces (Sec. IV.C.2). Once the $2N$ system has been properly renormalized, one must ask whether short-range many-body forces are immune to the enhancements seen in pionless EFT (Sec. II.C.2). Most work on many-body forces in chiral EFT takes Weinberg's power counting for granted. Nogga, Timmermans, and van Kolck (2005) and Song, Lazauskas, and van Kolck (2017) found no renormalization evidence for a $3N$ force in LO or $\mathcal{O}(Q/M_{QCD})$, but they obtained a triton binding energy that is only about half of the experimental value, perhaps because this is a very low-energy observable in the sense of being within the regime of pionless EFT. Kievsky *et al.* (2017) argued from continuity with pionless EFT that the H_0 three-body force in Eq. (70c) should be included at LO.

- The most important problem facing reaction theory in chiral EFT echoes the renormalization woes of Weinberg's prescription for nuclear structure. To maintain model independence, one must ensure that the average of the reaction kernel has a well-defined limit as the cutoff is increased. Only for electroweak reactions on the deuteron has this been investigated (Pavón Valderrama and Phillips, 2015; Phillips, 2016), with the conclusion that enhancements over NDA appear there as well. The impact of this observation on previously studied reactions and future reaction theory remains to be investigated.

- To which extent can an RG-invariant formulation of chiral EFT be incorporated in calculations of larger nuclei? Distorted-wave perturbation theory usually becomes demanding in second order where the fully off-shell A-body propagation is needed in intermediate states.

In pionless EFT, this problem has been sidestepped by a reformulation in terms of the solution of further integral equations (Vanasse, 2013, 2017b). It is an open issue whether this or another method can be applied to the A-nucleon problem in chiral EFT.

- Although not RG invariant, Weinberg's prescription has several practical advantages because it is most closely related to previous phenomenological approaches. For example, it provides fits to data of comparable quality to "realistic" phenomenological potentials (Sec. IV.D.1), it explains some of the qualitative features of these potentials (Sec. IV.C.2), and it can be employed in already existing *ab initio* codes. Its successes beg the question, is it possible that a particular choice of regulator allows for a small-cutoff formulation of chiral EFT that is equivalent to its RG-invariant form? It is conceivable that one can iterate subleading terms of the latter, as is done in the former, within a limited range of cutoffs, just as iterating momentum-dependent contact interactions in pionless EFT requires cutoff values $\Lambda \lesssim 1/r_0$ (Wigner bound); see Sec. II.B.3. If achieved, such an understanding of Weinberg's prescription might justify current uses of chiral EFT without requiring further development of *ab initio* methods. Furthermore, it will likely make it desirable to choose a regulator that optimizes convergence for the problem at hand, for example, neutron matter (Lynn *et al.*, 2016). First steps in this direction were made recently by Tews, Huth, and Schwenk (2018) and Pavón Valderrama (2019b).

- Irrespective of other issues discussed earlier and throughout this section, it is a highly nontrivial task to determine the LECs of chiral EFT, which are quite substantial in number at higher orders, from fitting calculated observables to data. One wants to do this in such a way that the EFT can fulfill its promises of providing systematic model independence and fully quantified uncertainties. For that, one should account for the truncation error of the EFT expansion directly as part of the fitting procedure and propagate forward all this information to the final result of a calculation. Following the initial suggestion of Schindler and Phillips (2009), Bayesian methods have emerged in recent years (Furnstahl, Klco *et al.*, 2015; Furnstahl, Phillips, and Wesolowski, 2015; Wesolowski *et al.*, 2016, 2019; Melendez, Wesolowski, and Furnstahl, 2017) as an important tool to address the issue in a robust and comprehensive way.

V. BROADER APPLICATIONS

Many of the ideas originating in nuclear EFTs have found applications to other systems. Pionless EFT, while clearly being connected to QCD as a low-energy limit, is driven largely by the universal features that arise from the large *NN* scattering lengths and the associated large sizes of light nuclei. As a consequence, the EFT for nuclear halo states discussed in Sec. III can be constructed as a generalization of pionless EFT. But universality goes beyond nuclear physics: it is relevant to any system dominated by short-range interactions, when one

is interested in distance scales much larger than the range of the interactions.

As one probes distances comparable to the interaction range, issues similar to the ones discussed in chiral EFT emerge. For example, can the long-range part of the interaction be treated in perturbation theory? In other hadronic systems, the long-range interaction might still be one-pion exchange, and chiral EFT then applies except that other heavy particles are substituted for nucleons.

In this section, we briefly describe some of the systems where versions of pionless and chiral EFTs have found applications. We start by discussing how these EFTs arise from QCD.

A. Connection with QCD

The inclusion of all possible interactions consistent with QCD symmetries ensures that nuclear EFTs capture the low-energy limit of QCD. This means that in principle one can follow a top-down approach and determine low-energy constants that appear in an EFT from a direct solution of the more general theory. While such solutions of QCD (in the highly nonperturbative low-energy regime) are elusive analytically, lattice calculations have made significant progress toward nuclear systems. Matching EFT to LQCD serves to extend the predictions of QCD in essentially two directions.

(1) Larger distances: a solution by *ab initio* methods of an EFT with parameters fixed by LQCD allows for predictions of properties of larger nuclei and their reactions, which are difficult to simulate directly from QCD.

(2) Smaller pion masses: with the relative importance of chiral-symmetry-breaking interactions understood, chiral EFT can be used as an extrapolation tool from larger quark, and thus pion, masses to the physical point.

Moreover, remnants of QCD's color gauge symmetry can be traced down to nuclear EFTs. In particular, it is possible to consider the inverse number of colors $1/N_c$ as an expansion parameter to constrain nuclear forces. This has been studied, for example, by Kaplan and Manohar (1997), Phillips and Schat (2013), Phillips, Samart, and Schat (2015), Samart *et al.* (2016), and Schindler, Singh, and Springer (2018).

1. Nuclear physics at large quark masses

The pion mass is a tunable parameter in LQCD. With calculations getting more expensive for lower pion masses, results are typically extracted for values of m_π well above the physical point. Observables like hadron spectra can by now be described with amazing accuracy (Kronfeld, 2012), and results for hadronic properties have become available even at or below the physical pion masses. Direct QCD calculations of few-nucleon systems, however, still use relatively large pion masses [Beane *et al.* (2011) reviewed the framework], and even then significant discrepancies exist among the outcomes from various groups. EFT calculations have used a subset of these results and tested their consistency with increasing nucleon number A.

Barnea *et al.* (2015) showed how LQCD input for few-nucleon systems at a fixed pion mass can be used in conjunction with *ab initio* solutions of EFT to predict the properties of larger nuclei. Using the LQCD results of Beane *et al.* (2013) at $m_\pi = 805$ MeV for $A = 2, 3$ to fix the pionless LECs at LO, Barnea *et al.* (2015) predicted binding energies for $A = 4, 5, 6$. The $A = 4$ result was consistent with the direct LQCD prediction, lending credibility to both approaches. Within the large uncertainties of the LQCD input and of LO pionless EFT, the pattern of binding energies resembles that of the physical world, but with larger binding momenta that nevertheless remain below the pion mass. These results were extended to $A = 16$ and to lattice input from Yamazaki *et al.* (2012) at $m_\pi = 510$ MeV by Contessi *et al.* (2017), and further to resummed NLO and $A = 40$ by Bansal *et al.* (2018).

Simple reactions can be calculated directly in LQCD. Beane *et al.* (2015) extracted the pionless LEC L_1 that appears in Eq. (41), thus allowing for a parameter-free calculation of the $np \to d\gamma$ capture process (as well as the inverse photodisintegration process) that is in good agreement with the experimental capture cross section. The nuclear matrix element determining the $pp \to de^+\nu_e$ fusion cross section and the Gamow-Teller matrix element contributing to tritium β decay were calculated in LQCD by Savage *et al.* (2017), allowing for a direct extraction of the leading two-nucleon axial counterterm $L_{1,A} = 3.9(0.1)(1.0)(0.3)(0.9)$ fm^3 in pionless EFT. For larger nuclei, one can use pionless EFT to turn LQCD bound-state input into predictions for reactions, as shown by Kirscher *et al.* (2015). They calculated nd scattering observables at LO and obtained the Phillips and Tjon line correlations at unphysical pion masses. Other observables such as magnetic moments and polarizabilities of light nuclei (Chang *et al.*, 2015; Kirscher *et al.*, 2017) have been studied as well. Mapping the patterns of nuclear properties at unphysical pion masses could shed light into the nature of the fine-tuning that pervades nuclear physics.

2. Fine-tuning in chiral EFT and infrared limit cycle

Chiral EFT, constituting the many-nucleon generalization of ChPT, yields the pion-mass dependence of nuclear observables. If LQCD data are within the limit of validity of the theory, the latter can be used to extrapolate toward smaller values of the quark (and thus pion) masses.

If M_{NN} is considered a low-energy scale, the pion-mass dependence arises at LO from the explicit pion mass in OPE and from the chiral-symmetry-breaking D_{2s} interaction in the $^1S_0$ channel, Eq. (81). At subleading orders, it enters not only through the explicit pion mass in multiple-pion exchange but also through the quark-mass dependence of other LECs. There have been various calculations of the pion-mass dependence of two-nucleon (Beane *et al.*, 2002; Epelbaum, Meißner, and Glöckle, 2002, 2003; Beane and Savage, 2003b, 2003c; Chen *et al.*, 2012; Soto and Tarrus, 2012; Berengut *et al.*, 2013) and three-nucleon (Hammer, Phillips, and Platter, 2007) observables, which differ in the power counting used and related issues (order, range of cutoffs, etc.), and assumptions about presently unknown LECs. Qualitatively, the observation of Beane *et al.* (2002) has been confirmed: the deuteron

($^1S_0$ virtual state) becomes unbound (bound) at a pion mass close (very close) to physical.

Although we do not know why these critical values of m_π are close to physical, the pion-mass dependence offers a plausible mechanism for the fine-tuning observed in the real world, where the NN binding energies are small compared to the scale set by Eq. (84), and scattering lengths large with respect to M_{NN}^{-1}. Except in the vicinity of an m_π critical value, these quantities attain values more in line with expectation. To produce shallow poles, short-range physics does not need to be particularly strong but must be fine-tuned to negatively interfere with OPE, or vice versa. [For example, in the $^1S_0$ channel with nonperturbative OPE the finite, energy-independent terms of $I(\Lambda; k)$ in Eq. (78) must partially cancel the short-range term.]

A variation of the pion mass has an effect similar to the variation of an external magnetic field near a Feshbach resonance. Braaten and Hammer (2003), using the pion-mass dependence of the NN S-wave scattering lengths calculated within chiral EFT by Epelbaum, Meißner, and Glöckle (2003), studied the consequences for the three-body spectrum as a function of the pion mass. They found that an excited state of the triton appears at $m_\pi \approx 175$ MeV, indicating that slightly changing the parameters to increase the pion mass brings QCD closer yet to an infrared limit cycle. Based on this, it is conjectured that it should be possible to tune QCD exactly to the limit cycle by changing the up and down quark masses separately. In this case, the triton would have infinitely many excited states. Epelbaum *et al.* (2006) showed that parameters sets exist that make both NN S waves diverge for critical pion masses between 179 and about 200 MeV. Hammer, Phillips, and Platter (2007) extended this analysis to higher orders and also calculated three-nucleon scattering observables as a function of the pion mass. The triton spectrum in the vicinity of a limit cycle found in that work is shown in Fig. 29. Some of the implications to primordial nucleosynthesis were pointed out by Bedaque, Luu, and Platter (2011) and Berengut *et al.* (2013).
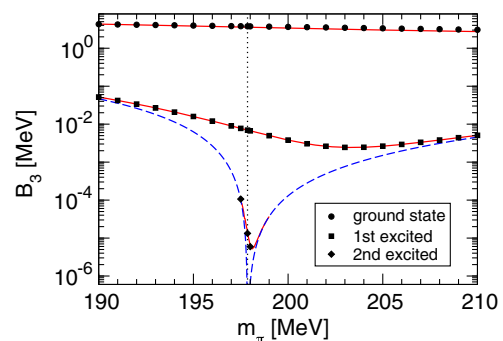

FIG. 29. Triton spectrum in the vicinity of a limit cycle as function of the pion mass. The circles, squares, and diamonds give the chiral-potential result of Epelbaum *et al.* (2006), while the solid lines are N^{2}LO calculations in pionless EFT (Hammer, Phillips, and Platter, 2007). The vertical dotted line indicates the critical pion mass. The thresholds for stable three-nucleon states are given by the dashed lines. From Hammer, Phillips, and Platter, 2007.

B. Antinucleon systems

While nucleon-antinucleon pairs can be integrated out at low energies, nuclear EFTs apply as well to systems where antinucleons, a consequence of the Lorentz invariance of QCD, appear in initial states. The simplest such system is antinucleon-nucleon ($\bar{N}N$) scattering. While the details of annihilation involve short distances, low-energy antinucleon-nucleus scattering can be described in ways similar to nucleon-nucleus scattering provided that the loss of flux to annihilation is accounted for with complex LECs. Other ingredients are similar and are related by charge conjugation C to the nuclear potential summarized in Fig. 25.

The use of chiral EFT for $\bar{p}p$ was pioneered by Chen, Dong, and Ma (2010) and Chen and Ma (2011), along the lines of Kaplan, Savage, and Wise (1996) for the spin-singlet NN channel. The $\bar{N}N$ potential was derived to $\mathcal{O}(Q^4/M_{\mathrm{QCD}}^4)$ by Kang, Haidenbauer, and Meißner (2014) and Dai, Haidenbauer, and Meißner (2017), who also obtained a successful description of $\bar{p}p$ observables using Weinberg's prescription together with the promotion of some interactions and the demotion of others. The final-state interactions generated by these potentials (Chen, Dong, and Ma, 2010; Kang, Haidenbauer, and Meißner, 2015) explain the near-threshold enhancement in the $\bar{p}p$ invariant-mass spectrum seen in charmonium decays and e^+e^- annihilation. Chiral two-pion exchange had already been incorporated in the partial-wave analysis of elastic and charge-exchange scattering $\bar{p}p$ data by Zhou and Timmermans (2012), following the earlier Nijmegen approach to NN (Rentmeester et al., 1999; Rentmeester, Timmermans, and de Swart, 2003).

C. Hypernuclei

In the ellipsis in Eq. (1) we find the kinetic, mass, and strong and electromagnetic interaction terms of the strange quarks. Chiral EFT can be extended to $\mathrm{SU}(3)_L \times \mathrm{SU}(3)_R$ in an attempt to incorporate kaon and eta exchange to describe hypernuclei. The difficulty is the intermediate value of the strange quark mass: it prevents one from integrating the strange quark out at a perturbative scale, as is done for heavier quarks, but leads to poor convergence of the ChPT expansion (Donoghue, Holstein, and Borasoy, 1999) because of the relatively large kaon and eta masses m_K and m_η.

Nevertheless, by counting m_K and m_η as low-energy scales, one can formally apply the power counting of Sec. IV.C.1 to organize the interbaryon potential along the lines of Sec. IV.C.2. The two-baryon potential was derived up to $\mathcal{O}(Q^2/M_{\mathrm{QCD}}^2)$ by Polinder, Haidenbauer, and Meißner (2006), Haidenbauer and Meißner (2010), Haidenbauer et al. (2013), and Haidenbauer, Meißner, and Petschauer (2016). With Weinberg's prescription, a description of hyperon-nucleon data is obtained of quality comparable to the most advanced phenomenological models. The leading three-baryon forces, which appear at $\mathcal{O}(Q^{n+1}/M_{\mathrm{QCD}}^{n+1})$, have also been written down (Petschauer et al., 2016). A large-N_c analysis of hyperon-nucleon interactions was carried out by Liu et al. (2019), while a covariant formulation was presented by Li et al. (2016, 2018). If m_K or m_η are considered large scales,

the onset of η-nuclear binding can be considered in a pionless EFT approach to derive constraints on the ηN scattering length (Barnea et al., 2017; Barnea, Friedman, and Gal, 2017).

Certain hypernuclei are also amenable to pionless and halo EFT. The process of Λd scattering and the properties of the hypertriton $^3_\Lambda\mathrm{H}$ in the SU(3) limit were first studied in pionless EFT by Hammer (2002). Since the hypertriton is extremely shallow, the low-energy observables in this channel are insensitive to the exact values of the ΛN low-energy parameters, as any shift can be absorbed by changing the three-body force. By constructing a system of coupled integral equations in the spin-isospin basis, Ando, Raha, and Oh (2015) investigated the viability of the $nn\Lambda$ bound state suggested by the recent experiment of the HypHI Collaboration at GSI (Rappold et al., 2013). The three-body force present at LO prevented any definitive conclusions about the existence of the $nn\Lambda$ bound state. More recently, Hildenbrand and Hammer (2019) calculated the structure of $nn\Lambda$ and $^3_\Lambda\mathrm{H}$ and clarified the value of the corresponding scaling factors. For physical hyperon and nucleon masses, they obtained the Λd scattering length $a_{\Lambda d} = 13.8^{+3.8}_{-2.0}$ fm, where the error is dominated by the uncertainty in the hypertriton binding energy. Implications of three-body universality to systems with two neutrons and a flavored meson (such as K^- and D^0) were considered by Raha et al. (2018).

Pionless EFT for states with strangeness -1 was extended up to $^5_\Lambda\mathrm{He}$ by Contessi, Barnea, and Gal (2018), presenting a solution to the "overbinding problem" observed with previous approaches based on nucleon-hyperon model interactions. Light nuclear states with strangeness -2 were also examined by Contessi et al. (2019). With the $\Lambda\Lambda$ contact interaction estimated from correlations observed in relativistic heavy ion collisions and the $\Lambda\Lambda N$ three-body force constrained by the binding energy of $^6_{\Lambda\Lambda}\mathrm{He}$, the conditions for $^{3,4}_{\Lambda\Lambda}n$, $^{4,5}_{\Lambda\Lambda}\mathrm{He}$, and $^5_{\Lambda\Lambda}\mathrm{H}$ binding were discussed.

In parallel, $^4_{\Lambda\Lambda}\mathrm{H}$ and $^6_{\Lambda\Lambda}\mathrm{He}$ have been described in halo EFT as three-body systems where the two hyperons orbit around, respectively, deuteron (Ando, Yang, and Oh, 2014) and alpha-particle (Ando and Oh, 2014) cores. In the spin-singlet channel of S-wave $^3_\Lambda\mathrm{H}$-Λ scattering, there is no bound state and no three-body force at LO. In this case, the $^3_\Lambda\mathrm{H}$-Λ scattering length was found to be $a_0 = (16.0 \pm 3.0)$ fm. In the spin-triplet channel, a $\Lambda\Lambda d$ contact interaction is required at LO to obtain a cutoff-independent $^4_{\Lambda\Lambda}\mathrm{H}$ binding energy. Similarly, a $\Lambda\Lambda\alpha$ three-body force is needed for $^6_{\Lambda\Lambda}\mathrm{He}$ renormalization already at LO, but the correlation between the double-Λ separation energy of $^6_{\Lambda\Lambda}\mathrm{He}$ and the S-wave $\Lambda\Lambda$ scattering length could be investigated.

The paucity of experimental information on hypernuclei represents an important opportunity for lattice QCD to impact nuclear physics through EFT; see Sec. V.A.1.

D. Hadronic molecules

Universality also bridges the gap between the seemingly unrelated domains of atomic and hadronic physics. In recent years, a large number of new "quarkonium" states in the charmonium and bottomonium region have been identified in

various experiments (Patrignani *et al.*, 2016). Many of these states are close to the thresholds for decays into charm and bottom mesons, which strongly influences their properties; see the reviews by Swanson (2006) and Brambilla *et al.* (2011). A new "flavored nuclear physics" has emerged in which nucleons are replaced by hadrons containing heavy quarks, which is amenable to EFTs that parallel those deployed in conventional nuclear physics.

A prominent member of this family of so-called *XYZ* states is the $X(3872)$, where the number in parentheses refers to the center-of-mass energy (in MeV) at which the state was first observed. The closeness of the $X(3872)$ to the $\bar{D}^0 D^{*0}$ threshold as well as its quantum numbers $J^{PC} = 1^{++}$ (Aaij *et al.*, 2013) quickly led to the conjecture that it can be interpreted, at least in part, as a shallow bound or virtual state of these two mesons. Braaten and Kusunoki (2004a) first used an EFT assuming a large $\bar{D}^0 D^{*0}$ scattering length to describe the $X(3872)$, with a number of further papers building upon this, for example, Braaten, Kusunoki, and Nussinov (2004), Braaten and Kusunoki (2004b, 2005a, 2005b), and Braaten and Lu (2007, 2008). An extension of this EFT to the three-body sector was given by Canham, Hammer, and Springer (2009), who studied D and D^* scattering off the $X(3872)$. The consequences of this pionless EFT for other states, including the effects of heavy quark symmetry, were discussed by AlFiky, Gabbiani, and Petrov (2006), Mehen and Powell (2011), Nieves and Pavón Valderrama (2012), Guo *et al.* (2013a, 2013b), Wilbring, Hammer, and Meißner (2013), Albaladejo *et al.* (2015), Liu *et al.* (2018), and Pavón Valderrama (2018).

The corrections to universality can be calculated systematically using an EFT for the X with explicit pions, called XEFT, which was developed by Fleming *et al.* (2007). The analog of the scale in Eq. (76) is

$$M_{DD^*} = \frac{8\pi f_\pi^2}{g^2 \mu_{D^0 D^{*0}}}, \tag{85}$$

where $\mu_{D^0 D^{*0}} \simeq 967$ MeV is the reduced mass and $g \simeq 0.5$–0.7 is the transition coupling of the pion to $\bar{D}^0 - D^{*0}$. M_{DD^*} is larger than M_{NN}, while the mass associated with OPE is smaller, $[(m_{D^{*0}} - m_{D^0})^2 - m_\pi^2]^{-1/2} \simeq 45$ MeV instead of m_π. As a consequence, one expects pions to be perturbative (Fleming *et al.*, 2007; Baru *et al.*, 2011; Pavón Valderrama, 2012; Alhakami and Birse, 2015; Braaten, 2015) in the region of energies where the bound state might lie. XEFT is analogous to the version of chiral EFT discussed in Sec. IV.D.4.

A number of aspects of exotic mesons were investigated in this approach, such as light-quark-mass (Jansen, Hammer, and Jia, 2014) and finite-volume (Jansen, Hammer, and Jia, 2015) effects on the $X(3872)$ binding energy, various decays of the $X(3872)$ (Fleming *et al.*, 2007; Fleming and Mehen, 2008; Baru *et al.*, 2011; Mehen and Springer, 2011; Fleming and Mehen, 2012; Mehen, 2015), the decay $\psi(4160) \to X(3872)\gamma$ as a probe the $X(3872)$'s molecular content (Margaryan and Springer, 2013), the triangle singularity in $e^+ e^- \to X(3872)\gamma$ (Braaten, He, and Ingles, 2019b), scattering of low-energy pions on the $X(3872)$ (Braaten, Hammer, and Mehen, 2010), the role of exact Galilei invariance for the $X(3872)$ and its line

shape (Braaten, 2015; Schmidt, Jansen, and Hammer, 2018), $X(3872)$ production in colliders (Braaten, He, and Ingles, 2018, 2019a), and heavy- and light-quark symmetries (Hidalgo-Duque, Nieves, and Valderrama, 2013).

The role of pion exchange has been further discussed for the $X(3872)$ at physical (Nieves and Pavón Valderrama, 2011; Kalashnikova and Nefediev, 2013; Wang and Wang, 2013; Baru, Epelbaum, Filin, Guo *et al.*, 2015) and unphysical (Baru *et al.*, 2013; Baru, Epelbaum, Filin, Gegelia, and Nefediev, 2015) quark masses, as well as in the context of other states and the implications of heavy quark symmetry (Baru *et al.*, 2017, 2016; Liu, Li, and Zhu, 2014; Cleven *et al.*, 2015; Geng, Lu, and Valderrama, 2018; Geng *et al.*, 2018; Wang *et al.*, 2018; Baru, Epelbaum, Filin *et al.*, 2019; Lu, Geng, and Pavón Valderrama, 2019; Wang, Liu, and Liu, 2019; Xu *et al.*, 2019).

E. Fundamental symmetries

According to QCD, nuclei ultimately emerge from the interaction between quarks and gluons. The quarks and gluons, however, are subject not only to the strong and electromagnetic interactions displayed explicitly in Eq. (1) but also to weak and possibly other interactions found in the ellipsis. Allowing for violation of symmetries such as parity P and time reversal T from higher-dimensional interactions in Eq. (1) introduces other components to the nuclear potential and currents. Nuclear EFT enables us to incorporate the effects of weak and beyond-the-standard-model interactions in the description of low-energy hadronic and nuclear processes. Input from lattice QCD is particularly desirable in this context (Cirigliano *et al.*, 2019).

1. Parity violation

Besides being responsible for beta decay, weak interactions also imply that there should be small P-violating operators in the nuclear force and currents. Since they stem mostly from four-quark interactions proportional to the Fermi constant $G_F \simeq 1.17 \times 10^{-5}$ GeV^{-2}, NDA [Eq. (9)] suggests that for T-conserving P violation the suppression factor is $G_F f_\pi^2 \sim 10^{-7}$. The framework for the incorporation of P-violating effects in nuclear EFTs was developed by Zhu *et al.* (2005). A major motivation for this program is to understand the tension that exists among different experiments (Holstein, 2010) when they are analyzed with quark and meson-exchange models (Desplanques, Donoghue, and Holstein, 1980).

In the pionless theory, P violation in the nuclear force is manifest as S-to-P-wave contact interactions, five of which are independent at LO (Zhu *et al.*, 2005; Girlanda, 2008). Phillips, Schindler, and Springer (2009) pointed out that pionless EFT is well suited to describing a number of existing and planned NN scattering experiments and calculated the relevant relationships between observables (typically spin-polarization asymmetries) at LO in the P-violating sector. Schindler, Springer, and Vanasse (2016) argued that large-N_c arguments can be used to reduce the number of LO P-violating operators from five to two. Grießhammer and Schindler (2010) showed that no P-violating 3N force occurs up to and including NLO,

enabling predictions for *P*-violating elastic neutron-deuteron scattering (Grießhammer, Schindler, and Springer, 2012; Vanasse, 2012) based on the two-nucleon LECs. However, Vanasse (2019) concluded that a *P*-violating 3*N* force is required at NLO after all.

The first pionless calculations of the deuteron anapole (or toroidal dipole) moment and *P*-violating effects in the $np \rightarrow d\gamma$ capture process were presented by Savage (2001), building upon previous work in the theory with explicit, perturbative pions (Savage and Springer, 1998, 2001; Kaplan *et al.*, 1999). Schindler and Springer (2010), Vanasse and Schindler (2014), and Shin, Ando, and Hyun (2010) looked at *P*-violating asymmetries in the $np \rightarrow d\gamma$ process. Spin polarization in the inverse process was studied by Ando *et al.* (2011). Moeini Arani and Bayegan (2013) and Arani and Bayegan (2014) studied *P* violation in the $nd \rightarrow {}^3\text{H}\gamma$ radiative-capture reaction, and Mahboubi *et al.* (2016) included electromagnetic effects to calculate polarized *pd* scattering.

Some of these processes have also been considered in chiral EFT. As far as strong interactions are concerned, the power μ of a contribution to the potential[see Eq. (74)] can now be negative, but of course the corresponding terms are suppressed by small factors. The lowest orders of the *T*-conserving, *P*-violating potential and electromagnetic currents were obtained by Zhu *et al.* (2005), Kaiser (2007), Liu and Zhu (2008), Girlanda (2008), Viviani *et al.* (2014), and de Vries *et al.* (2014). They display new elements, such as TPE, compared to the one-meson-exchange potentials usually employed to study *P* violation (Desplanques, Donoghue, and Holstein, 1980). Calculations of *P* violation in few-nucleon systems have thus far been based on Weinberg's prescription, as reviewed by de Vries and Meißner (2016).

2. Time-reversal violation

In the case of *T*, there is potential violation from the QCD vacuum angle $\bar{\theta}$ and from higher-dimensional operators, all contained in the ellipsis in Eq. (1). While the former is anomalously small [$\bar{\theta} \lesssim 10^{-10}$ (Tanabashi *et al.*, 2018)], the latter are suppressed by at least 2 powers of a large scale. All violation from operators of dimension up to six is accompanied by *P* violation. These interactions induce *T*-violating nuclear form factors, such as electric dipole and magnetic quadrupole, which could be probed in the proposed storage-ring experiments (Pretz, 2013). In nuclear EFT, they are calculated within the same framework used for nucleon electric dipole moments.

The lowest-order *P*- and *T*-violating potential calculated in chiral EFT by Maekawa *et al.* (2011) and de Vries *et al.* (2013) showed, as its *P*-conserving counterpart, new ingredients compared to one-meson-exchange potentials (Liu and Timmermans, 2004). The implications of an additional large-N_c expansion were discussed by Samart *et al.* (2016). Together with *P*- and *T*-violating currents, form factors were calculated for the deuteron in chiral EFT with perturbative pions by de Vries, Mereghetti *et al.* (2011) and with Weinberg's prescription by de Vries, Higa *et al.* (2011), Liu *et al.* (2012), and Bsaisou *et al.* (2013, 2015); good accord was found among these calculations. de Vries, Higa *et al.* (2011) and Bsaisou *et al.* (2015) also calculated the electric dipole

moments of triton and helion with Weinberg's prescription. The deuteron also possesses a *P*-conserving, *T*-violating form factor, the toroidal quadrupole. The contribution to this moment from the same *P*- and *T*-violating operators in conjunction with weak interactions was obtained with perturbative pions by Mereghetti *et al.* (2013). *T* violation in few-nucleon systems was reviewed by Mereghetti and van Kolck (2015), where it was shown how measurements of the electric dipole moments of nuclei, together with further theoretical advances, could at least partially disentangle the various possible sources of *T* violation.

3. Other symmetries

Higher-dimensional operators in the standard model break also other symmetries like lepton (*L*) and baryon (*B*) number, but less work exists in the context of nuclear EFTs. Of particular contemporary interest is *L* violation, especially through the only dimension-5 operator, which leads to Majorana neutrino masses. The most sensitive laboratory probe of *L* violation (by two units) is neutrinoless double-beta decay ($0\nu\beta\beta$), which is, however, afflicted by severe nuclear-physics uncertainties. Traditionally, $0\nu\beta\beta$ has been calculated from the exchange of an explicit Majorana neutrino together with phenomenological nuclear models, but more recently nuclear EFTs have been deployed (Cirigliano *et al.*, 2018a). It has been uncovered that a short-range LEC must enter at LO for proper renormalization in both pionless (Cirigliano, Dekens, Mereghetti, and Walker-Loud, 2018) and chiral (Cirigliano *et al.*, 2018b) EFTs. The first *ab initio* calculations of these contributions in light nuclei are becoming available (Cirigliano *et al.*, 2018b; Pastore *et al.*, 2018). Operators of higher dimensions have been considered as well (Prezeau, Ramsey-Musolf, and Vogel, 2003; Cirigliano *et al.*, 2017). Implementation of these operators in the shell model are starting to appear (Horoi and Neacsu, 2017, 2018).

Analogous to *L* violation is *B* violation by two units. The process of neutron-antineutron oscillation in a nucleus leads to decay after the antineutron annihilates with a nucleon. An NLO calculation of this process in the deuteron (Oosterhof *et al.*, 2019) gives a lifetime in pionless EFT that is comparable to earlier zero-range models, while in chiral EFT (with perturbative pions) it is a factor of $\simeq 2.5$ smaller than existing potential-model calculations.

Extensions of the standard model can be constructed that account for possible violation of Lorentz and (then unprotected) *CPT* symmetries at high energies, allowing for operators with low dimensions. Most tests of these symmetries take place at low energies where QCD is nonperturbative, impeding direct bounds on operators involving strongly interacting particles. Among the lowest-dimensional operators of this type is a Lorentz-violating but *CPT*-conserving purely gluonic operator. The nuclear potential induced by this operator and its possible effects on atomic-clock comparisons and on the spin precession of the deuteron and other light nuclei in storage-ring experiments were discussed by Noordmans (2017). Dimension-5 operators were similarly discussed by Noordmans, de Vries, and Timmermans (2016). A more detailed analysis of the nuclear implications of these interactions is needed.

F. Dark-matter detection

Nuclear EFTs have also been used to describe dark-matter scattering off heavy nuclei in direct-detection experiments. The dark-matter particles must be nonrelativistic to be bound in the dark-matter halo by gravitation, with typical velocities of order 0.001 times the speed of light. Since the recoil momentum is comparable to the typical momentum of a nucleon in the nucleus, it is crucial for the interpretation of current experimental limits [cf. Liu, Chen, and Ji (2017)] that nuclear-structure factors be properly addressed.

The calculation of nuclear-structure factors in nuclear EFT has been organized in two different ways. First, a pionless EFT for nucleon and dark-matter fields (Fan, Reece, and Wang, 2010; Fitzpatrick *et al.*, 2012, 2013; Anand, Fitzpatrick, and Haxton, 2014) allows for a study of nuclear response functions in terms of effective couplings, and the extraction of limits on the coefficients of the operators. This approach reaches its limit at the largest momentum transfers for scattering off heavy nuclei, where the details of pion exchange are resolved. Second, chiral EFT has been used to predict the nuclear-structure factors for spin-independent and spin-dependent scattering. The analysis within chiral EFT establishes relations between different operators in the pionless framework, and it provides a counting scheme that indicates at which order two-nucleon operators contribute. Recent work in this direction includes chiral EFT-based structure factors for the spin-dependent response (Menéndez, Gazit, and Schwenk, 2012; Klos *et al.*, 2013), aspects of spin-independent scattering (Cirigliano, Graesser, and Ovanesyan, 2012; Cirigliano *et al.*, 2014; Vietze *et al.*, 2015), scattering off light nuclei (Körber, Nogga, and de Vries, 2017), inelastic scattering (Baudis *et al.*, 2013), and a general chiral EFT analysis of one- and two-body currents (Hoferichter, Klos, and Schwenk, 2015; Hoferichter *et al.*, 2016, 2019) and improved limits for dark-matter models from experimental searches (Hoferichter *et al.*, 2017; Aprile *et al.*, 2019).

G. Bosons with large scattering length

Up to technical details that arise from spin and isospin degrees of freedom, pionless EFT is virtually identical to a theory that describes a system of bosons with a large two-body scattering length. Throughout the history of pionless EFT, this fact has been used repeatedly, the few-boson system serving to guide analogous analyses in the few-nucleon sector.

But such bosonic systems are relevant far beyond serving as a toy problem. Experimentally, they are realized in cold atomic gases, where the two-body interaction can in fact be tuned arbitrarily by varying an external magnetic field, the Feshbach-resonance mechanism. In particular, the Efimov effect has been established experimentally by exploiting the fact that the occurrence of three-body states close to points where the two-body scattering length is tuned to infinity (Kraemer *et al.*, 2006), with many more experiments since the first observation. A comprehensive discussion of the theoretical treatment of universal few-body systems was given by Braaten and Hammer (2006). The current status of the field was recently reviewed by Naidon and Endo (2017).

VI. CONCLUSION

As shown in Fig. 1, a significant portion of low-energy nuclear physics is amenable to an EFT description, with different theories tailored specifically to different regions. With increasing energy, a tower of EFTs starts from the simple pionless case, an expansion around the unitary limit of large *NN* scattering lengths. Its range of applicability can be extended by the inclusion of pions—first perturbatively and then nonperturbatively—in chiral EFT, constructed as an expansion around the eponymous chiral limit of vanishing quark masses. Although there is a fundamental difference regarding how pions are treated (a heavy degree of freedom in pionless EFT, but a light one in chiral EFT), these theories are low-energy limits of QCD. They are both formulated as theories of pointlike nucleons with interactions that give rise to low-energy poles of the S matrix.

The fact that nucleons, being composite hadrons, in reality have substructure is encoded in the EFT expansion, namely, in local operators with an increasing number of derivatives. Establishing the ordering of such interactions is the crucial element that enables a systematic description of observables.

The usefulness of EFT does not stop at this point because new scale separations arise in nuclei. A particular case, halo/cluster EFT, has been discussed in this review as a promising way to describe clusterlike nuclei. On yet another level, efforts are under way to construct EFTs for rotational and vibrational modes in heavy nuclei (Papenbrock, 2011). Moreover, applications to other composite systems, from dark matter to cold atoms, show how nonperturbative EFTs are a driving force behind many important developments in modern theoretical physics.

EFTs are ideally suited to root nuclear physics in the standard model EFT, elegantly exploiting its emergence from QCD as the underlying theory of the strong interaction, particularly through lattice simulations. EFTs have become the *initio* of *ab initio* methods for the solution of few- and many-nucleon dynamics and have engendered such an explosion of activity that it is difficult to draw a line to conclude this review. We have already reached the point where calculated nuclear properties are being used to identify deficiencies in the nuclear interactions used as input.

Ab initio calculations now almost unanimously follow (mostly in chiral EFT, but increasingly in pionless EFT) Weinberg's original prescription; i.e., they do not expand on the subleading components of the potential. Our emphasis in this review was on approaches that pursue the long-standing goal of RG invariance through the perturbative expansion of the S matrix on the subleading interactions. This approach has led to a new and unified description of few-body "Efimov physics" under the umbrella of pionless EFT. It remains to establish, however, to which extent this framework can share the efficiency of Weinberg's approach without dependence on the form of the regulator, or perhaps to explain its phenomenological success for larger nuclei within narrow cutoff windows.

It is thus our hope that this review will not only provide a unified overview of what has been done but will also inspire future research toward a comprehensive and solid

understanding of nuclear structure and reactions from an EFT, and ultimately a QCD, perspective.

ACKNOWLEDGMENTS

REFERENCES

Aaij, R., *et al.* (LHCb Collaboration), 2013, Phys. Rev. Lett. **110**, 222001.

Abe, T., P. Maris, T. Otsuka, N. Shimizu, Y. Utsuno, and J. P. Vary, 2012, Phys. Rev. C **86**, 054301.

Abe, T., and R. Seki, 2009a, Phys. Rev. C **79**, 054003.

Abe, T., and R. Seki, 2009b, Phys. Rev. C **79**, 054002.

Abe, T., R. Seki, and A. N. Kocharian, 2004, Phys. Rev. C **70**, 014315; **71**, 059902(E) (2005).

Acharya, B., 2015, Ph.D. thesis (Ohio University).

Acharya, B., C. Ji, and D. R. Phillips, 2013, Phys. Lett. B **723**, 196.

Acharya, B., and D. R. Phillips, 2013, Nucl. Phys. **A913**, 103.

Adelberger, E. G., *et al.*, 2011, Rev. Mod. Phys. **83**, 195.

Adhikari, S. K., and T. Frederico, 1995, Phys. Rev. Lett. **74**, 4572.

Adhikari, S. K., and A. Ghosh, 1997, J. Phys. A **30**, 6553.

Adhikari, S. K., and L. Tomio, 1982, Phys. Rev. C **26**, 83.

Afzal, S. A., A. A. Z. Ahmad, and S. Ali, 1969, Rev. Mod. Phys. **41**, 247.

Ajzenberg-Selove, F., 1990, Nucl. Phys. **A506**, 1.

Albaladejo, M., F. K. Guo, C. Hidalgo-Duque, J. Nieves, and M. P. Valderrama, 2015, Eur. Phys. J. C **75**, 547.

Alberg, M., M. Bawin, and F. Brau, 2005, Phys. Rev. A **71**, 022108.

AlFiky, M. T., F. Gabbiani, and A. A. Petrov, 2006, Phys. Lett. B **640**, 238.

Alhakami, M. H., 2017, Phys. Rev. D **96**, 056019.

Alhakami, M. H., and M. C. Birse, 2015, Phys. Rev. D **91**, 054019.

Amorim, A. E. A., T. Frederico, and L. Tomio, 1997, arXiv:nucl-th/9708023.

Anand, N., A. L. Fitzpatrick, and W. C. Haxton, 2014, Phys. Rev. C **89**, 065501.

Ando, S., R. H. Cyburt, S. W. Hong, and C. H. Hyun, 2006, Phys. Rev. C **74**, 025809.

Ando, S.-i., and M. C. Birse, 2008, Phys. Rev. C **78**, 024004.

Ando, S.-i., and M. C. Birse, 2010, J. Phys. G **37**, 105108.

Ando, S.-i., and C. H. Hyun, 2005, Phys. Rev. C **72**, 014008.

Ando, S.-I., 2016, Eur. Phys. J. A **52**, 130.

Ando, S.-I., 2018, Phys. Rev. C **97**, 014604.

Ando, S.-I., and C. H. Hyun, 2012, Phys. Rev. C **86**, 024002.

Ando, S.-I., and Y. Oh, 2014, Phys. Rev. C **90**, 037301.

Ando, S.-I., U. Raha, and Y. Oh, 2015, Phys. Rev. C **92**, 024325.

Ando, S.-I., J. W. Shin, C. H. Hyun, and S. W. Hong, 2007, Phys. Rev. C **76**, 064001.

Ando, S.-I., J. W. Shin, C. H. Hyun, S. W. Hong, and K. Kubodera, 2008, Phys. Lett. B **668**, 187.

Ando, S.-I., Y. H. Song, C. H. Hyun, and K. Kubodera, 2011, Phys. Rev. C **83**, 064002.

Ando, S.-I., G.-S. Yang, and Y. Oh, 2014, Phys. Rev. C **89**, 014318.

Aprile, E., *et al.* (XENON Collaboration), 2019, Phys. Rev. Lett. **122**, 071301.

Arani, M. M., and S. Bayegan, 2014, Few-Body Syst. **55**, 1099.

Arani, M. M., H. Nematollahi, N. Mahboubi, and S. Bayegan, 2014, Phys. Rev. C **89**, 064005.

Arndt, R. A., W. J. Briscoe, I. I. Strakovsky, and R. L. Workman, 2006, Phys. Rev. C **74**, 045205.

Balantekin, A. B., and H. Yuksel, 2003, Phys. Rev. C **68**, 055801.

Ballot, J. L., M. R. Robilotta, and C. A. da Rocha, 1998, Phys. Rev. C **57**, 1574.

Banerjee, M. K., and J. Milana, 1996, Phys. Rev. D **54**, 5804.

Bansal, A., S. Binder, A. Ekström, G. Hagen, G. R. Jansen, and T. Papenbrock, 2018, Phys. Rev. C **98**, 054301.

Barford, T., and M. C. Birse, 2003, Phys. Rev. C **67**, 064006.

Barford, T., and M. C. Birse, 2005, J. Phys. A **38**, 697.

Barnea, N., B. Bazak, E. Friedman, and A. Gal, 2017, Phys. Lett. B **771**, 297; **775**, 364(E) (2017).

Barnea, N., L. Contessi, D. Gazit, F. Pederiva, and U. van Kolck, 2015, Phys. Rev. Lett. **114**, 052501.

Barnea, N., E. Friedman, and A. Gal, 2017, Nucl. Phys. **A968**, 35.

Baroni, A., L. Girlanda, A. Kievsky, L. E. Marcucci, R. Schiavilla, and M. Viviani, 2016, Phys. Rev. C **94**, 024003.

Baru, V., E. Epelbaum, A. Filin, C. Hanhart, A. Nefediev, and Q. Wang, 2019, Phys. Rev. D **99**, 094013.

Baru, V., E. Epelbaum, A. A. Filin, J. Gegelia, and A. V. Nefediev, 2015, Phys. Rev. D **92**, 114016.

Baru, V., E. Epelbaum, A. A. Filin, F. K. Guo, H.-W. Hammer, C. Hanhart, U.-G. Meißner, and A. V. Nefediev, 2015, Phys. Rev. D **91**, 034002.

Baru, V., E. Epelbaum, A. A. Filin, C. Hanhart, U.-G. Meißner, and A. V. Nefediev, 2013, Phys. Lett. B **726**, 537.

Baru, V., E. Epelbaum, A. A. Filin, C. Hanhart, U.-G. Meißner, and A. V. Nefediev, 2016, Phys. Lett. B **763**, 20.

Baru, V., E. Epelbaum, A. A. Filin, C. Hanhart, and A. V. Nefediev, 2017, J. High Energy Phys. 06, 158.

Baru, V., E. Epelbaum, J. Gegelia, and X. L. Ren, 2019, arXiv:1905.02116.

Baru, V., E. Epelbaum, J. Haidenbauer, C. Hanhart, A. E. Kudryavtsev, V. Lensky, and U.-G. Meißner, 2009, Phys. Rev. C **80**, 044003.

Baru, V., A. A. Filin, C. Hanhart, Yu. S. Kalashnikova, A. E. Kudryavtsev, and A. V. Nefediev, 2011, Phys. Rev. D **84**, 074029.

Baru, V., C. Hanhart, and F. Myhrer, 2014, Int. J. Mod. Phys. E **23**, 1430004.

Batista, E. F., S. Szpigel, and V. S. Timóteo, 2017, Adv. High Energy Phys. **2017**, 2316247.

Baudis, L., G. Kessler, P. Klos, R. F. Lang, J. Menéndez, S. Reichard, and A. Schwenk, 2013, Phys. Rev. D **88**, 115014.

Bawin, M., and S. A. Coon, 2003, Phys. Rev. A **67**, 042712.

Bazak, B., M. Eliyahu, and U. van Kolck, 2016, Phys. Rev. A **94**, 052502.

Bazak, B., J. Kirscher, S. König, M. Pavón Valderrama, N. Barnea, and U. van Kolck, 2019, Phys. Rev. Lett. **122**, 143001.

Bazin, D., *et al.*, 1995, Phys. Rev. Lett. **74**, 3569.

Beane, S. R., P. F. Bedaque, L. Childress, A. Kryjevski, J. McGuire, and U. van Kolck, 2001, Phys. Rev. A **64**, 042103.

Beane, S. R., P. F. Bedaque, W. C. Haxton, D. R. Phillips, and M. J. Savage, 2001, in *At the Frontier of Particle Physics*, edited by M. Shifman (World Scientific, Singapore), pp. 133–269.

Beane, S. R., P. F. Bedaque, K. Orginos, and M. J. Savage, 2006, Phys. Rev. Lett. **97**, 012001.

Beane, S. R., P. F. Bedaque, A. Parreno, and M. J. Savage, 2004, Phys. Lett. B **585**, 106.

Beane, S. R., P. F. Bedaque, M. J. Savage, and U. van Kolck, 2002, Nucl. Phys. **A700**, 377.

Beane, S. R., V. Bernard, T. S. H. Lee, and U. G. Meißner, 1998, Phys. Rev. C **57**, 424.

Beane, S. R., V. Bernard, T. S. H. Lee, U.-G. Meißner, and U. van Kolck, 1997, Nucl. Phys. **A618**, 381.

Beane, S. R., E. Chang, S. D. Cohen, W. Detmold, H. W. Lin, T. C. Luu, K. Orginos, A. Parreno, M. J. Savage, and A. Walker-Loud (NPLQCD Collaboration), 2013, Phys. Rev. D **87**, 034506.

Beane, S. R., E. Chang, W. Detmold, K. Orginos, A. Parreño, M. Savage, and B. C. Tiburzi (NPLQCD Collaboration), 2015, Phys. Rev. Lett. **115**, 132001.

Beane, S. R., T. D. Cohen, and D. R. Phillips, 1998, Nucl. Phys. **A632**, 445.

Beane, S. R., W. Detmold, K. Orginos, and M. J. Savage, 2011, Prog. Part. Nucl. Phys. **66**, 1.

Beane, S. R., D. B. Kaplan, and A. Vuorinen, 2009, Phys. Rev. C **80**, 011001.

Beane, S. R., C. Y. Lee, and U. van Kolck, 1995, Phys. Rev. C **52**, 2914.

Beane, S. R., M. Malheiro, D. R. Phillips, and U. van Kolck, 1999, Nucl. Phys. **A656**, 367.

Beane, S. R., and M. J. Savage, 2001, Nucl. Phys. **A694**, 511.

Beane, S. R., and M. J. Savage, 2003a, Nucl. Phys. **A717**, 104.

Beane, S. R., and M. J. Savage, 2003b, Nucl. Phys. **A717**, 91.

Beane, S. R., and M. J. Savage, 2003c, Nucl. Phys. **A713**, 148.

Beane, S. R., and U. van Kolck, 2005, J. Phys. G **31**, 921.

Becher, T., and H. Leutwyler, 1999, Eur. Phys. J. C **9**, 643.

Bedaque, P. F., and H. W. Grießhammer, 2000, Nucl. Phys. **A671**, 357.

Bedaque, P. F., H.-W. Hammer, and U. van Kolck, 1998, Phys. Rev. C **58**, R641.

Bedaque, P. F., H.-W. Hammer, and U. van Kolck, 1999a, Phys. Rev. Lett. **82**, 463.

Bedaque, P. F., H.-W. Hammer, and U. van Kolck, 1999b, Nucl. Phys. **A646**, 444.

Bedaque, P. F., H.-W. Hammer, and U. van Kolck, 2000, Nucl. Phys. **A676**, 357.

Bedaque, P. F., H.-W. Hammer, and U. van Kolck, 2003, Phys. Lett. B **569**, 159.

Bedaque, P. F., T. Luu, and L. Platter, 2011, Phys. Rev. C **83**, 045803.

Bedaque, P. F., G. Rupak, H. W. Grießhammer, and H.-W. Hammer, 2003, Nucl. Phys. **A714**, 589.

Bedaque, P. F., and U. van Kolck, 1998, Phys. Lett. B **428**, 221.

Bedaque, P. F., and U. van Kolck, 2002, Annu. Rev. Nucl. Part. Sci. **52**, 339.

Behrendt, J., E. Epelbaum, J. Gegelia, U.-G. Meißner, and A. Nogga, 2016, Eur. Phys. J. A **52**, 296.

Berengut, J. C., E. Epelbaum, V. V. Flambaum, C. Hanhart, U.-G. Meißner, J. Nebreda, and J. R. Pelaez, 2013, Phys. Rev. D **87**, 085018.

Bergervoet, J. R., P. C. van Campen, W. A. van der Sanden, and J. J. de Swart, 1988, Phys. Rev. C **38**, 15.

Bernard, V., 2008, Prog. Part. Nucl. Phys. **60**, 82.

Bernard, V., E. Epelbaum, H. Krebs, and U.-G. Meißner, 2008, Phys. Rev. C **77**, 064004.

Bernard, V., E. Epelbaum, H. Krebs, and U.-G. Meißner, 2011, Phys. Rev. C **84**, 054001.

Bernard, V., N. Kaiser, J. Gasser, and U.-G. Meißner, 1991, Phys. Lett. B **268**, 291.

Bernard, V., N. Kaiser, and U.-G. Meißner, 1991, Phys. Rev. Lett. **67**, 1515.

Bernard, V., N. Kaiser, and U.-G. Meißner, 1995, Int. J. Mod. Phys. E **04**, 193.

Bernard, V., H. Krebs, and U.-G. Meißner, 2000, Phys. Rev. C **61**, 058201.

Bertulani, C. A., H.-W. Hammer, and U. van Kolck, 2002, Nucl. Phys. **A712**, 37.

Bethe, H., and R. Peierls, 1935a, Proc. R. Soc. A **148**, 146.

Bethe, H. A., and R. Peierls, 1935b, Proc. R. Soc. A **149**, 176.

Bethe, H. A., 1949, Phys. Rev. **76**, 38.

Bethe, H. A., and C. Longmire, 1950, Phys. Rev. **77**, 647.

Binder, S., *et al.* (LENPIC Collaboration), 2018, Phys. Rev. C **98**, 014002.

Birse, M. C., 2006, Phys. Rev. C **74**, 014003.

Birse, M. C., 2007, Phys. Rev. C **76**, 034002.

Birse, M. C., 2010, Eur. Phys. J. A **46**, 231.

Birse, M. C., 2011, Phil. Trans. R. Soc. A **369**, 2662.

Birse, M. C., E. Epelbaum, and J. Gegelia, 2016, Eur. Phys. J. A **52**, 26.

Birse, M. C., J. A. McGovern, and K. G. Richardson, 1999, Phys. Lett. B **464**, 169.

Bouaziz, D., and M. Bawin, 2014, Phys. Rev. A **89**, 022113.

Braaten, E., 2015, Phys. Rev. D **91**, 114007.

Braaten, E., P. Hagen, H.-W. Hammer, and L. Platter, 2012, Phys. Rev. A **86**, 012711.

Braaten, E., and H.-W. Hammer, 2003, Phys. Rev. Lett. **91**, 102002.

Braaten, E., and H.-W. Hammer, 2006, Phys. Rep. **428**, 259.

Braaten, E., H.-W. Hammer, and T. Mehen, 2010, Phys. Rev. D **82**, 034018.

Braaten, E., L.-P. He, and K. Ingles, 2018, arXiv:1811.08876.

Braaten, E., L.-P. He, and K. Ingles, 2019a, arXiv:1902.03259.

Braaten, E., L.-P. He, and K. Ingles, 2019b, arXiv:1904.12915.

Braaten, E., D. Kang, and L. Platter, 2011, Phys. Rev. Lett. **106**, 153005.

Braaten, E., and M. Kusunoki, 2004a, Phys. Rev. D **69**, 074005.

Braaten, E., and M. Kusunoki, 2004b, Phys. Rev. D **69**, 114012.

Braaten, E., and M. Kusunoki, 2005a, Phys. Rev. D **72**, 054022.

Braaten, E., and M. Kusunoki, 2005b, Phys. Rev. D **71**, 074005.

Braaten, E., M. Kusunoki, and S. Nussinov, 2004, Phys. Rev. Lett. **93**, 162001.

Braaten, E., and M. Lu, 2007, Phys. Rev. D **76**, 094028.

Braaten, E., and M. Lu, 2008, Phys. Rev. D **77**, 014029.

Braaten, E., and D. Phillips, 2004, Phys. Rev. A **70**, 052111.

Brambilla, N., *et al.*, 2011, Eur. Phys. J. C **71**, 1534.

Braun, J., W. Elkamhawy, R. Roth, and H.-W. Hammer, 2018, arXiv:1803.02169.

Braun, J., H.-W. Hammer, and L. Platter, 2018, Eur. Phys. J. A **54**, 196.

Briceno, R. A., and Z. Davoudi, 2013, Phys. Rev. D **87**, 094507.

Brown, L. S., and G. M. Hale, 2014, Phys. Rev. C **89**, 014622.

Bsaisou, J., J. de Vries, C. Hanhart, S. Liebig, U.-G. Meißner, D. Minossi, A. Nogga, and A. Wirzba, 2015, J. High Energy Phys. 03, 104; 2015 05, 83(E).

Bsaisou, J., C. Hanhart, S. Liebig, U.-G. Meißner, A. Nogga, and A. Wirzba, 2013, Eur. Phys. J. A **49**, 31.

Bulycheva, K. M., and A. S. Gorsky, 2014, Usp. Fiz. Nauk **184**, 182 [Phys. Usp. **57**, 171 (2014)].

Burgess, C. P., 2015, in *Post-Planck Cosmology, Proceedings of the 100th Les Houches Summer School*, edited by C. Deffayet, P. Peter, B. Wandelt, M. Zaldarriaga, L. F. Cugliandolo (Oxford University, Oxford), pp. 149–197.

Busch, T., B.-G. Englert, K. Rzążewski, and M. Wilkens, 1998, Found. Phys. **28**, 549.

Butler, M., and J.-W. Chen, 2000, Nucl. Phys. **A675**, 575.

Butler, M., and J.-W. Chen, 2001, Phys. Lett. B **520**, 87.

Butler, M., J.-W. Chen, and X. Kong, 2001, Phys. Rev. C **63**, 035501.

Butler, M., J.-W. Chen, and P. Vogel, 2002, Phys. Lett. B **549**, 26.

Callan, Jr., C. G., S. R. Coleman, J. Wess, and B. Zumino, 1969, Phys. Rev. **177**, 2247.

Camblong, H. E., and C. R. Ordóñez, 2003, Phys. Rev. D **68**, 125013.

Camblong, H. E., and C. R. Ordóñez, 2005, Phys. Lett. A **345**, 22.

Canham, D. L., and H.-W. Hammer, 2008, Eur. Phys. J. A **37**, 367.

Canham, D. L., and H.-W. Hammer, 2010, Nucl. Phys. **A836**, 275.

Canham, D. L., H.-W. Hammer, and R. P. Springer, 2009, Phys. Rev. D **80**, 014009.

Capel, P., D. R. Phillips, and H.-W. Hammer, 2018, Phys. Rev. C **98**, 034610.

Caprini, I., G. Colangelo, and H. Leutwyler, 2006, Phys. Rev. Lett. **96**, 132001.

Carlson, J., S. Gandolfi, U. van Kolck, and S. A. Vitiello, 2017, Phys. Rev. Lett. **119**, 223002.

Carlsson, B. D., A. Ekström, C. Forssén, D. F. Strömberg, G. R. Jansen, O. Lilja, M. Lindby, B. A. Mattsson, and K. A. Wendt, 2016, Phys. Rev. X **6**, 011019.

Chang, E., W. Detmold, K. Orginos, A. Parreno, M. J. Savage, B. C. Tiburzi, and S. R. Beane (NPLQCD Collaboration), 2015, Phys. Rev. D **92**, 114502.

Charap, J. M., 1970, Phys. Rev. D **2**, 1554.

Charap, J. M., 1971, Phys. Rev. D **3**, 1998.

Chen, G. Y., H. R. Dong, and J. P. Ma, 2010, Phys. Lett. B **692**, 136.

Chen, G. Y., and J. P. Ma, 2011, Phys. Rev. D **83**, 094029.

Chen, J.-W., 1999, Nucl. Phys. **A653**, 375.

Chen, J.-W., H. W. Grießhammer, M. J. Savage, and R. P. Springer, 1998a, Nucl. Phys. **A644**, 245.

Chen, J.-W., H. W. Grießhammer, M. J. Savage, and R. P. Springer, 1998b, Nucl. Phys. **A644**, 221.

Chen, J.-W., K. M. Heeger, and R. G. H. Robertson, 2003, Phys. Rev. C **67**, 025801.

Chen, J.-W., T. Inoue, X.-d. Ji, and Y.-c. Li, 2005, Phys. Rev. C **72**, 061001.

Chen, J.-W., X.-d. Ji, and Y.-c. Li, 2004, Phys. Lett. B **603**, 6.

Chen, J.-W., X.-d. Ji, and Y.-c. Li, 2005a, Phys. Lett. B **620**, 33.

Chen, J.-W., X.-d. Ji, and Y.-c. Li, 2005b, Phys. Rev. C **71**, 044321.

Chen, J.-W., D. Lee, and T. Schäfer, 2004, Phys. Rev. Lett. **93**, 242302.

Chen, J.-W., T.-K. Lee, C. P. Liu, and Y.-S. Liu, 2012, Phys. Rev. C **86**, 054001.

Chen, J.-W., C.-P. Liu, and S.-H. Yu, 2013, Phys. Lett. B **720**, 385.

Chen, J.-W., G. Rupak, and M. J. Savage, 1999a, Nucl. Phys. **A653**, 386.

Chen, J.-W., G. Rupak, and M. J. Savage, 1999b, Phys. Lett. B **464**, 1.

Chen, J.-W., and M. J. Savage, 1999, Phys. Rev. C **60**, 065205.

Chen, Q. B., N. Kaiser, U.-G. Meißner, and J. Meng, 2018, Phys. Rev. C **97**, 064320.

Chen, Q. B., N. Kaiser, U.-G. Meißner, and J. Meng, 2019, Phys. Rev. C **99**, 064326.

Chisholm, J. S. R., 1961, Nucl. Phys. **26**, 469.

Christlmeier, S., and H. W. Grießhammer, 2008, Phys. Rev. C **77**, 064001.

Cirigliano, V., Z. Davoudi, T. Bhattacharya, T. Izubuchi, P. E. Shanahan, S. Syritsyn, and M. L. Wagman (USQCD Collaboration), 2019, arXiv:1904.09704.

Cirigliano, V., W. Dekens, J. de Vries, M. L. Graesser, and E. Mereghetti, 2017, J. High Energy Phys. 12, 082.

Cirigliano, V., W. Dekens, J. de Vries, M. L. Graesser, and E. Mereghetti, 2018a, J. High Energy Phys. 12, 097.

Cirigliano, V., W. Dekens, J. de Vries, M. L. Graesser, E. Mereghetti, S. Pastore, and U. van Kolck, 2018b, Phys. Rev. Lett. **120**, 202001.

Cirigliano, V., W. Dekens, E. Mereghetti, and A. Walker-Loud, 2018, Phys. Rev. C **97**, 065501.

Cirigliano, V., M. L. Graesser, and G. Ovanesyan, 2012, J. High Energy Phys. 10, 025.

Cirigliano, V., M. L. Graesser, G. Ovanesyan, and I. M. Shoemaker, 2014, Phys. Lett. B **739**, 293.

Cleven, M., F.-K. Guo, C. Hanhart, Q. Wang, and Q. Zhao, 2015, Phys. Rev. D **92**, 014005.

Coelho, H. T., T. K. Das, and M. R. Robilotta, 1983, Phys. Rev. C **28**, 1812.

Coello Pérez, E. A., J. Menéndez, and A. Schwenk, 2018a, Phys. Rev. C **98**, 045501.

Coello Pérez, E. A., J. Menéndez, and A. Schwenk, 2018b, arXiv:1809.04443.

Coello Pérez, E. A., and T. Papenbrock, 2015, Phys. Rev. C **92**, 064309.

Coello Pérez, E. A., and T. Papenbrock, 2016, Phys. Rev. C **94**, 054316.

Coester, F., S. Cohen, B. Day, and C. M. Vincent, 1970, Phys. Rev. C **1**, 769.

Cohen, T. D., 1997, Phys. Rev. C **55**, 67.

Cohen, T. D., J. L. Friar, G. A. Miller, and U. van Kolck, 1996, Phys. Rev. C **53**, 2661.

Cohen, T. D., and J. M. Hansen, 1998, Phys. Lett. B **440**, 233.

Cohen, T. D., and J. M. Hansen, 1999a, Phys. Rev. C **59**, 13.

Cohen, T. D., and J. M. Hansen, 1999b, arXiv:nuclth/9908049.

Cohen, T. D., and J. M. Hansen, 1999c, Phys. Rev. C **59**, 3047.

Coleman, S. R., J. Wess, and B. Zumino, 1969, Phys. Rev. **177**, 2239.

Contessi, L., N. Barnea, and A. Gal, 2018, Phys. Rev. Lett. **121**, 102502.

Contessi, L., A. Lovato, F. Pederiva, A. Roggero, J. Kirscher, and U. van Kolck, 2017, Phys. Lett. B **772**, 839.

Contessi, L., M. Schäfer, N. Barnea, A. Gal, and J. Mareš, 2019, arXiv:1905.06775.

Coon, S. A., M. I. Avetian, M. K. G. Kruse, U. van Kolck, P. Maris, and J. P. Vary, 2012, Phys. Rev. C **86**, 054002.

Coon, S. A., and H. K. Han, 2001, Few-Body Syst. **30**, 131.

Coon, S. A., and M. K. G. Kruse, 2016, Int. J. Mod. Phys. E **25**, 1641011.

Coon, S. A., M. D. Scadron, P. C. McNamee, B. R. Barrett, D. W. E. Blatt, and B. H. J. McKellar, 1979, Nucl. Phys. **A317**, 242.

Crewther, R. J., and L. C. Tunstall, 2015, Phys. Rev. D **91**, 034016.

Dai, L.-Y., J. Haidenbauer, and U.-G. Meißner, 2017, J. High Energy Phys. 07, 078.

Danilov, G., 1961, Sov. Phys. JETP **13**, 349.

De-Leon, H., L. Platter, and D. Gazit, 2016, arXiv:1611.10004.

De-Leon, H., L. Platter, and D. Gazit, 2019, arXiv:1902.07677.

Delfino, A., T. Frederico, V. S. Timoteo, and L. Tomio, 2006, Phys. Lett. B **634**, 185.

Deltuva, A., R. Lazauskas, and L. Platter, 2011, Few-Body Syst. **51**, 235.

Desplanques, B., J. F. Donoghue, and B. R. Holstein, 1980, Ann. Phys. (N.Y.) **124**, 449.

de Swart, J. J., C. P. F. Terheggen, and V. G. J. Stoks, 1995, arXiv: nucl-th/9509032.

de Vries, J., R. Higa, C. P. Liu, E. Mereghetti, I. Stetcu, R. G. E. Timmermans, and U. van Kolck, 2011, Phys. Rev. C **84**, 065501.

de Vries, J., N. Li, U.-G. Meißner, N. Kaiser, X. H. Liu, and S. L. Zhu, 2014, Eur. Phys. J. A **50**, 108.

de Vries, J., and U.-G. Meißner, 2016, Int. J. Mod. Phys. E **25**, 1641008.

de Vries, J., E. Mereghetti, R. G. E. Timmermans, and U. van Kolck, 2011, Phys. Rev. Lett. **107**, 091804.

de Vries, J., E. Mereghetti, R. G. E. Timmermans, and U. van Kolck, 2013, Ann. Phys. (Amsterdam) **338**, 50.

Dilg, W., L. Koester, and W. Nistler, 1971, Phys. Lett. **36B**, 208.

Djukanovic, D., J. Gegelia, S. Scherer, and M. R. Schindler, 2007, Few-Body Syst. **41**, 141.

Djukanovic, D., M. R. Schindler, J. Gegelia, and S. Scherer, 2005, Phys. Rev. D **72**, 045002.

Donoghue, J. F., B. R. Holstein, and B. Borasoy, 1999, Phys. Rev. D **59**, 036002.

Drischler, C., K. Hebeler, and A. Schwenk, 2019, Phys. Rev. Lett. **122**, 042501.

Dudek, J. E., 2016, Phys. Scr. **91**, 030301.

Dürr, S., 2015, *Proc. Sci.* LATTICE2014, 006 [arXiv:1412.6434].

Efimov, V., 1970, Phys. Lett. **33B**, 563.

Efimov, V., 1971, Sov. J. Nucl. Phys. **12**, 589.

Efimov, V., 1973, Nucl. Phys. **A210**, 157.

Efimov, V., 1981, Nucl. Phys. **A362**, 45.

Eiras, D., and J. Soto, 2003, Eur. Phys. J. A **17**, 89.

Ekström, A., G. Hagen, T. D. Morris, T. Papenbrock, and P. D. Schwartz, 2018, Phys. Rev. C **97**, 024332.

Ekström, A., G. R. Jansen, K. A. Wendt, G. Hagen, T. Papenbrock, S. Bacca, B. Carlsson, and D. Gazit, 2014, Phys. Rev. Lett. **113**, 262504.

Ekström, A., G. R. Jansen, K. A. Wendt, G. Hagen, T. Papenbrock, B. D. Carlsson, C. Forssén, M. Hjorth-Jensen, P. Navrátil, and W. Nazarewicz, 2015, Phys. Rev. C **91**, 051301.

Ekström, A., *et al.*, 2013, Phys. Rev. Lett. **110**, 192502.

Elhatisari, S., D. Lee, U.-G. Meißner, and G. Rupak, 2016, Eur. Phys. J. A **52**, 174.

Elhatisari, S., D. Lee, G. Rupak, E. Epelbaum, H. Krebs, T. A. Lähde, T. Luu, and U.-G. Meißner, 2015, Nature (London) **528**, 111.

Elhatisari, S., *et al.*, 2016, Phys. Rev. Lett. **117**, 132501.

Entem, D. R., N. Kaiser, R. Machleidt, and Y. Nosyk, 2015a, Phys. Rev. C **92**, 064001.

Entem, D. R., N. Kaiser, R. Machleidt, and Y. Nosyk, 2015b, Phys. Rev. C **91**, 014002.

Entem, D. R., and R. Machleidt, 2002, Phys. Rev. C **66**, 014002.

Entem, D. R., and R. Machleidt, 2003, Phys. Rev. C **68**, 041001.

Entem, D. R., R. Machleidt, and Y. Nosyk, 2017, Phys. Rev. C **96**, 024004.

Entem, D. R., E. Ruiz Arriola, M. Pavón Valderrama, and R. Machleidt, 2008, Phys. Rev. C **77**, 044006.

Epelbaum, E., 2006a, Prog. Part. Nucl. Phys. **57**, 654.

Epelbaum, E., 2006b, Phys. Lett. B **639**, 456.

Epelbaum, E., 2007, Eur. Phys. J. A **34**, 197.

Epelbaum, E., A. M. Gasparyan, J. Gegelia, and H. Krebs, 2015, Eur. Phys. J. A **51**, 71.

Epelbaum, E., A. M. Gasparyan, J. Gegelia, and U.-G. Meißner, 2018, Eur. Phys. J. A **54**, 186.

Epelbaum, E., A. M. Gasparyan, J. Gegelia, and U.-G. Meißner, 2019, arXiv:1903.01273.

Epelbaum, E., A. M. Gasparyan, J. Gegelia, and M. R. Schindler, 2014, Eur. Phys. J. A **50**, 51.

Epelbaum, E., and J. Gegelia, 2009, Eur. Phys. J. A **41**, 341.

Epelbaum, E., and J. Gegelia, 2012, Phys. Lett. B **716**, 338.

Epelbaum, E., J. Gegelia, and U.-G. Meißner, 2017, Nucl. Phys. **B925**, 161.

Epelbaum, E., J. Gegelia, U.-G. Meißner, and D.-L. Yao, 2017, Eur. Phys. J. A **53**, 98.

Epelbaum, E., W. Glöckle, and U.-G. Meißner, 1998, Nucl. Phys. **A637**, 107.

Epelbaum, E., W. Glöckle, and U.-G. Meißner, 2000, Nucl. Phys. **A671**, 295.

Epelbaum, E., W. Glöckle, and U.-G. Meißner, 2004a, Eur. Phys. J. A **19**, 125.

Epelbaum, E., W. Glöckle, and U.-G. Meißner, 2004b, Eur. Phys. J. A **19**, 401.

Epelbaum, E., W. Glöckle, and U.-G. Meißner, 2005, Nucl. Phys. **A747**, 362.

Epelbaum, E., H.-W. Hammer, and U.-G. Meißner, 2009, Rev. Mod. Phys. **81**, 1773.

Epelbaum, E., H.-W. Hammer, U.-G. Meißner, and A. Nogga, 2006, Eur. Phys. J. C **48**, 169.

Epelbaum, E., H. Krebs, and U.-G. Meißner, 2008a, Nucl. Phys. **A806**, 65.

Epelbaum, E., H. Krebs, and U.-G. Meißner, 2008b, Phys. Rev. C **77**, 034006.

Epelbaum, E., H. Krebs, and U.-G. Meißner, 2015a, Eur. Phys. J. A **51**, 53.

Epelbaum, E., H. Krebs, and U.-G. Meißner, 2015b, Phys. Rev. Lett. **115**, 122301.

Epelbaum, E., and U.-G. Meißner, 2005, Phys. Rev. C **72**, 044001.

Epelbaum, E., and U.-G. Meißner, 2012, Annu. Rev. Nucl. Part. Sci. **62**, 159.

Epelbaum, E., and U.-G. Meißner, 2013, Few-Body Syst. **54**, 2175.

Epelbaum, E., U.-G. Meißner, and W. Glöckle, 2002, arXiv:nucl-th/0208040.

Epelbaum, E., U.-G. Meißner, and W. Glöckle, 2003, Nucl. Phys. **A714**, 535.

Epelbaum, E., U.-G. Meißner, and J. E. Palomar, 2005, Phys. Rev. C **71**, 024001.

Epelbaum, E., A. Nogga, W. Glöckle, H. Kamada, U. G. Meißner, and H. Witała, 2002, Phys. Rev. C **66**, 064001.

Fan, J., M. Reece, and L.-T. Wang, 2010, J. Cosmol. Astropart. Phys. 11, 042.

Fedorov, D. V., A. S. Jensen, and K. Riisager, 1994, Phys. Rev. C **49**, 201.

Feinberg, G., and A. Pais, 1963, Phys. Rev. **131**, 2724.

Feinberg, G., and A. Pais, 1964, Phys. Rev. **133**, B477.

Fermi, E., 1936, Ric. Sci. **7**, 13.

Fernando, L., R. Higa, and G. Rupak, 2012, Eur. Phys. J. A **48**, 24.

Fernando, L., A. Vaghani, and G. Rupak, 2015, arXiv:1511.04054.

Fettes, N., and U.-G. Meißner, 2001, Nucl. Phys. **A679**, 629.

Fitzpatrick, A. L., W. Haxton, E. Katz, N. Lubbers, and Y. Xu, 2012, arXiv:1211.2818.

Fitzpatrick, A. L., W. Haxton, E. Katz, N. Lubbers, and Y. Xu, 2013, J. Cosmol. Astropart. Phys. 02, 004.

Fleming, S., M. Kusunoki, T. Mehen, and U. van Kolck, 2007, Phys. Rev. D **76**, 034006.

Fleming, S., and T. Mehen, 2008, Phys. Rev. D **78**, 094019.

Fleming, S., and T. Mehen, 2012, Phys. Rev. D **85**, 014016.

Fleming, S., T. Mehen, and I. W. Stewart, 2000a, Phys. Rev. C **61**, 044005.

Fleming, S., T. Mehen, and I. W. Stewart, 2000b, Nucl. Phys. **A677**, 313.

Frank, W., D. J. Land, and R. M. Spector, 1971, Rev. Mod. Phys. **43**, 36.

Frederico, T., A. Delfino, L. Tomio, and M. T. Yamashita, 2012, Prog. Part. Nucl. Phys. **67**, 939.

Frederico, T., V. S. Timoteo, and L. Tomio, 1999, Nucl. Phys. **A653**, 209.

Freer, M., H. Horiuchi, Y. Kanada-En'yo, D. Lee, and U.-G. Meißner, 2018, Rev. Mod. Phys. **90**, 035004.

Friar, J. L., 1997, Few-Body Syst. **22**, 161.

Friar, J. L., 1999, Phys. Rev. C **60**, 034002.

Friar, J. L., and S. Fallieros, 1984, Phys. Rev. C **29**, 232.

Friar, J. L., B. F. Gibson, C. R. Chen, and G. L. Payne, 1985, Phys. Lett. **161B**, 241.

Friar, J. L., D. Huber, and U. van Kolck, 1999, Phys. Rev. C **59**, 53.

Friar, J. L., G. L. Payne, and U. van Kolck, 2005, Phys. Rev. C **71**, 024003.

Friar, J. L., and U. van Kolck, 1999, Phys. Rev. C **60**, 034006.

Friar, J. L., U. van Kolck, G. L. Payne, and S. A. Coon, 2003, Phys. Rev. C **68**, 024003.

Friar, J. L., U. van Kolck, M. C. M. Rentmeester, and R. G. E. Timmermans, 2004, Phys. Rev. C **70**, 044001.

Fuchs, T., J. Gegelia, G. Japaridze, and S. Scherer, 2003, Phys. Rev. D **68**, 056005.

Fujita, J., and H. Miyazawa, 1957, Prog. Theor. Phys. **17**, 360.

Fukuda, N., et al., 2004, Phys. Rev. C **70**, 054606.

Furnstahl, R. J., G. Hagen, and T. Papenbrock, 2012, Phys. Rev. C **86**, 031301.

Furnstahl, R. J., G. Hagen, T. Papenbrock, and K. A. Wendt, 2015, J. Phys. G **42**, 034032.

Furnstahl, R. J., N. Klco, D. R. Phillips, and S. Wesolowski, 2015, Phys. Rev. C **92**, 024005.

Furnstahl, R. J., T. Papenbrock, and S. N. More, 2014, Phys. Rev. C **89**, 044301.

Furnstahl, R. J., D. R. Phillips, and S. Wesolowski, 2015, J. Phys. G **42**, 034028.

Gabbiani, F., P. F. Bedaque, and H. W. Grießhammer, 2000, Nucl. Phys. **A675**, 601.

Gardestig, A., and D. R. Phillips, 2006, Phys. Rev. Lett. **96**, 232301.

Gartenhaus, S., 1955, Phys. Rev. **100**, 900.

Gasser, J., and H. Leutwyler, 1984, Ann. Phys. (N.Y.) **158**, 142.

Gasser, J., and H. Leutwyler, 1985, Nucl. Phys. **B250**, 465.

Gasser, J., M. E. Sainio, and A. Svarc, 1988, Nucl. Phys. **B307**, 779.

Gattobigio, M., A. Kievsky, and M. Viviani, 2019, arXiv:1903.08900.

Gazit, D., S. Quaglioni, and P. Navratil, 2009, Phys. Rev. Lett. **103**, 102502.

Gegelia, J., 1998a, arXiv:nucl-th/9806028.

Gegelia, J., 1998b, Phys. Lett. B **429**, 227.

Gegelia, J., 1999a, J. Phys. G **25**, 1681.

Gegelia, J., 1999b, Phys. Lett. B **463**, 133.

Gegelia, J., 2004, Eur. Phys. J. A **19**, 355.

Gegelia, J., and G. Japaridze, 2001, Phys. Lett. B **517**, 476.

Gegelia, J., U.-G. Meißner, and D.-L. Yao, 2016, Phys. Lett. B **760**, 736.

Gegelia, J., and S. Scherer, 2006, Int. J. Mod. Phys. A **21**, 1079.

Gelman, B. A., 2009, Phys. Rev. C **80**, 034005.

Geng, L.-S., J.-X Lu, and M. P. Valderrama, 2018, Phys. Rev. D **97**, 094036.

Geng, L.-S., J.-X. Lu, M. P. Valderrama, and X.-L. Ren, 2018, Phys. Rev. D **97**, 091501.

Georgi, H., 1989, Phys. Rev. Lett. **63**, 1917.

Georgi, H., and L. Randall, 1986, Nucl. Phys. **B276**, 241.

Gerstein, I. S., R. Jackiw, S. Weinberg, and B. W. Lee, 1971, Phys. Rev. D **3**, 2486.

Gezerlis, A., I. Tews, E. Epelbaum, M. Freunek, S. Gandolfi, K. Hebeler, A. Nogga, and A. Schwenk, 2014, Phys. Rev. C **90**, 054323.

Gezerlis, A., I. Tews, E. Epelbaum, S. Gandolfi, K. Hebeler, A. Nogga, and A. Schwenk, 2013, Phys. Rev. Lett. **111**, 032501.

Girard, B. A., and M. G. Fuda, 1979, Phys. Rev. C **19**, 579.

Girlanda, L., 2008, Phys. Rev. C **77**, 067001.

Girlanda, L., A. Kievsky, and M. Viviani, 2011, Phys. Rev. C **84**, 014001.

Girlanda, L., S. Pastore, R. Schiavilla, and M. Viviani, 2010, Phys. Rev. C **81**, 034005.

Göbel, M., H. W. Hammer, C. Ji, and D. R. Phillips, 2019, arXiv:1904.07182.

Goldberger, M. L., and K. M. Watson, 1967, Collision Theory (John Wiley & Sons, New York).

Gonzalez Trotter, D. E., et al., 1999, Phys. Rev. Lett. **83**, 3788.

Gonzalez Trotter, D. E., et al., 2006, Phys. Rev. C **73**, 034001.

Grießhammer, H. W., 2004, Nucl. Phys. **A744**, 192.

Grießhammer, H. W., 2005, Nucl. Phys. **A760**, 110.

Grießhammer, H. W., 2016, Proc. Sci. CD15, 104 [arXiv:1511.00490].

Grießhammer, H. W., J. A. McGovern, and D. R. Phillips, 2016a, AIP Conf. Proc. **1735**, 040010.

Grießhammer, H. W., J. A. McGovern, and D. R. Phillips, 2016b, Eur. Phys. J. A **52**, 139.

Grießhammer, H. W., J. A. McGovern, D. R. Phillips, and G. Feldman, 2012, Prog. Part. Nucl. Phys. **67**, 841.

Grießhammer, H. W., and G. Rupak, 2002, Phys. Lett. B **529**, 57.

Grießhammer, H. W., and M. R. Schindler, 2010, Eur. Phys. J. A **46**, 73.

Grießhammer, H. W., M. R. Schindler, and R. P. Springer, 2012, Eur. Phys. J. A **48**, 7.

Guo, F.-K., C. Hidalgo-Duque, J. Nieves, and M. P. Valderrama, 2013a, Phys. Rev. D **88**, 054007.

Guo, F.-K., C. Hidalgo-Duque, J. Nieves, and M. P. Valderrama, 2013b, Phys. Rev. D **88**, 054014.

Hagen, G., D. J. Dean, M. Hjorth-Jensen, T. Papenbrock, and A. Schwenk, 2007, Phys. Rev. C **76**, 044305.

Hagen, G., P. Hagen, H.-W. Hammer, and L. Platter, 2013, Phys. Rev. Lett. **111**, 132501.

Hagen, G., M. Hjorth-Jensen, G. R. Jansen, R. Machleidt, and T. Papenbrock, 2012a, Phys. Rev. Lett. **108**, 242501.

Hagen, G., M. Hjorth-Jensen, G. R. Jansen, R. Machleidt, and T. Papenbrock, 2012b, Phys. Rev. Lett. **109**, 032502.

Hagen, G., T. Papenbrock, A. Ekström, K. A. Wendt, G. Baardsen, S. Gandolfi, M. Hjorth-Jensen, and C. J. Horowitz, 2014, Phys. Rev. C **89**, 014319.

Hagen, P., 2014, Ph.D. thesis (University of Bonn), http://hss.ulb.uni-bonn.de/2014/3526/3526.htm.

Hagen, P., H.-W. Hammer, and L. Platter, 2013, Eur. Phys. J. A **49**, 118.

Haidenbauer, J., and U.-G. Meißner, 2010, Phys. Lett. B **684**, 275.

Haidenbauer, J., U.-G. Meißner, and S. Petschauer, 2016, Nucl. Phys. **A954**, 273.

Haidenbauer, J., S. Petschauer, N. Kaiser, U.-G. Meißner, A. Nogga, and W. Weise, 2013, Nucl. Phys. **A915**, 24.

Hammer, H.-W., 2002, Nucl. Phys. **A705**, 173.

Hammer, H.-W., 2016, in Eur. Phys. J. Web Conf., **113**, 01004.

Hammer, H.-W., 2018, Few-Body Syst. **59**, 58.

Hammer, H.-W., and R. J. Furnstahl, 2000, Nucl. Phys. **A678**, 277.

Hammer, H.-W., C. Ji, and D. R. Phillips, 2017, J. Phys. G **44**, 103002.

Hammer, H.-W., and S. König, 2014, Phys. Lett. B **736**, 208.

Hammer, H.-W., and T. Mehen, 2001a, Phys. Lett. B **516**, 353.

Hammer, H.-W., and T. Mehen, 2001b, Nucl. Phys. **A690**, 535.

Hammer, H.-W., A. Nogga, and A. Schwenk, 2013, Rev. Mod. Phys. **85**, 197.

Hammer, H.-W., J.-Y. Pang, and A. Rusetsky, 2017a, J. High Energy Phys. 09, 109.

Hammer, H.-W., J.-Y. Pang, and A. Rusetsky, 2017b, J. High Energy Phys. 10, 115.

Hammer, H.-W., and D. R. Phillips, 2011, Nucl. Phys. **A865**, 17.

Hammer, H.-W., D. R. Phillips, and L. Platter, 2007, Eur. Phys. J. A **32**, 335.

Hammer, H.-W., and L. Platter, 2007, Eur. Phys. J. A **32**, 113.

Hammer, H.-W., and L. Platter, 2010, Annu. Rev. Nucl. Part. Sci. **60**, 207.

Hammer, H.-W., and L. Platter, 2011, Phil. Trans. R. Soc. A **369**, 2679.

Hammer, H.-W., and B. G. Swingle, 2006, Ann. Phys. (Amsterdam) **321**, 306.

Hanhart, C., U. van Kolck, and G. A. Miller, 2000, Phys. Rev. Lett. **85**, 2905.

Hansen, M. T., and S. R. Sharpe, 2014, Phys. Rev. D **90**, 116003.

Hansen, M. T., and S. R. Sharpe, 2017, Phys. Rev. D **95**, 034501.

Hansen, M. T., and S. R. Sharpe, 2019, arXiv:1901.00483.

Harada, K., and H. Kubo, 2006, Nucl. Phys. **B758**, 304.

Harada, K., H. Kubo, and A. Ninomiya, 2009, Int. J. Mod. Phys. A **24**, 3191.

Harada, K., H. Kubo, and Y. Yamamoto, 2011, Phys. Rev. C **83**, 034002.

Haxton, W. C., R. G. Hamish Robertson, and A. M. Serenelli, 2013, Annu. Rev. Astron. Astrophys. **51**, 21.

Hemmert, T. R., B. R. Holstein, and J. Kambor, 1998, J. Phys. G **24**, 1831.

Hidalgo-Duque, C., J. Nieves, and M. P. Valderrama, 2013, Phys. Rev. D **87**, 076006.

Higa, R., 2010, EPJ Web Conf. **3**, 06001.

Higa, R., 2015, Few-Body Syst. **56**, 761.

Higa, R., H.-W. Hammer, and U. van Kolck, 2008, Nucl. Phys. **A809**, 171.

Higa, R., G. Rupak, and A. Vaghani, 2018, Eur. Phys. J. A **54**, 89.

Hildenbrand, F., and H.-W. Hammer, 2019, arXiv:1904.05818.

Hoferichter, M., P. Klos, J. Menéndez, and A. Schwenk, 2016, Phys. Rev. D **94**, 063505.

Hoferichter, M., P. Klos, J. Menéndez, and A. Schwenk, 2017, Phys. Rev. Lett. **119**, 181803.

Hoferichter, M., P. Klos, J. Menéndez, and A. Schwenk, 2019, Phys. Rev. D **99**, 055031.

Hoferichter, M., P. Klos, and A. Schwenk, 2015, Phys. Lett. B **746**, 410.

Hoferichter, M., J. Ruiz de Elvira, B. Kubis, and U.-G. Meißner, 2015, Phys. Rev. Lett. **115**, 192301.

Holstein, B. R., 2010, Nucl. Phys. **A844**, 160C.

Holt, J. D., T. Otsuka, A. Schwenk, and T. Suzuki, 2012, J. Phys. G **39**, 085111.

Honerkamp, J., and K. Meetz, 1971, Phys. Rev. D **3**, 1996.

't Hooft, G., 1980, NATO ASI Ser., Ser. B **59**, 135.

Horiuchi, W., and Y. Suzuki, 2006, Phys. Rev. C **74**, 034311.

Horoi, M., and A. Neacsu, 2017, arXiv:1706.05391.

Horoi, M., and A. Neacsu, 2018, Phys. Rev. C **98**, 035502.

Huber, D., J. L. Friar, A. Nogga, H. Witała, and U. van Kolck, 2001, Few-Body Syst. **30**, 95.

Huhn, V., L. Wätzold, C. Weber, A. Siepe, W. von Witsch, H. Witała, and W. Glöckle, 2000a, Phys. Rev. C **63**, 014003.

Huhn, V., L. Wätzold, C. Weber, A. Siepe, W. von Witsch, H. Witała, and W. Glöckle, 2000b, Phys. Rev. Lett. **85**, 1190.

Ikeda, K., N. Takigawa, and H. Horiuchi, 1968, Prog. Theor. Phys. Suppl. **E68**, 464.

Ipson, K. L., K. Helmke, and M. C. Birse, 2011, Phys. Rev. C **83**, 017001.

Ishikawa, S., and M. R. Robilotta, 2007, Phys. Rev. C **76**, 014006.

Jackson, J. D., and J. M. Blatt, 1950, Rev. Mod. Phys. **22**, 77.

Jansen, M., H.-W. Hammer, and Y. Jia, 2014, Phys. Rev. D **89**, 014033.

Jansen, M., H.-W. Hammer, and Y. Jia, 2015, Phys. Rev. D **92**, 114031.

Jenkins, E., and A. V. Manohar, 1991a, Phys. Lett. B **255**, 558.

Jenkins, E. E., and A. V. Manohar, 1991b, Phys. Lett. B **259**, 353.

Ji, C., C. Elster, and D. R. Phillips, 2014, Phys. Rev. C **90**, 044004.

Ji, C., and D. R. Phillips, 2013, Few-Body Syst. **54**, 2317.

Ji, C., D. R. Phillips, and L. Platter, 2010, Europhys. Lett. **92**, 13003.

Ji, C., D. R. Phillips, and L. Platter, 2012, Ann. Phys. (Amsterdam) **327**, 1803.

Ji, X.-d., and Y.-c. Li, 2004, Phys. Lett. B **591**, 76.

Jona-Lasinio, M., L. Pricoupenko, and Y. Castin, 2008, Phys. Rev. A **77**, 043611.

Kaiser, N., 1999, Phys. Rev. C **61**, 014003.

Kaiser, N., 2000, Phys. Rev. C **62**, 024001.

Kaiser, N., 2001a, Phys. Rev. C **63**, 044010.

Kaiser, N., 2001b, Phys. Rev. C **64**, 057001.

Kaiser, N., 2001c, Phys. Rev. C **65**, 017001.

Kaiser, N., 2007, Phys. Rev. C **76**, 047001.

Kaiser, N., 2011, Nucl. Phys. **A860**, 41.

Kaiser, N., 2012, Eur. Phys. J. A **48**, 148.

Kaiser, N., 2015, Phys. Rev. C **92**, 024002.

Kaiser, N., R. Brockmann, and W. Weise, 1997, Nucl. Phys. **A625**, 758.

Kaiser, N., S. Gerstendorfer, and W. Weise, 1998, Nucl. Phys. **A637**, 395.

Kalantar-Nayestanaki, N., E. Epelbaum, J. G. Messchendorp, and A. Nogga, 2012, Rep. Prog. Phys. **75**, 016301.

Kalashnikova, Yu. S., and A. V. Nefediev, 2013, Pis'ma Zh. Eksp. Teor. Fiz. **97** 76 [JETP Lett. **97**, 70 (2013)].

Kamada, H., et al., 2001, Phys. Rev. C **64**, 044001.

Kamefuchi, S., L. O'Raifeartaigh, and A. Salam, 1961, Nucl. Phys. **28**, 529.

Kang, X.-W., J. Haidenbauer, and U.-G. Meißner, 2014, J. High Energy Phys. 02, 113.

Kang, X.-W., J. Haidenbauer, and U.-G. Meißner, 2015, Phys. Rev. D **91**, 074003.

Kaplan, D. B., 1997, Nucl. Phys. **B494**, 471.

Kaplan, D. B., 2019, arXiv:1905.07485.

Kaplan, D. B., and A. V. Manohar, 1997, Phys. Rev. C **56**, 76.

Kaplan, D. B., M. J. Savage, R. P. Springer, and M. B. Wise, 1999, Phys. Lett. B **449**, 1.

Kaplan, D. B., M. J. Savage, and M. B. Wise, 1996, Nucl. Phys. **B478**, 629.

Kaplan, D. B., M. J. Savage, and M. B. Wise, 1998a, Phys. Lett. B **424**, 390.

Kaplan, D. B., M. J. Savage, and M. B. Wise, 1998b, Nucl. Phys. **B534**, 329.

Kaplan, D. B., M. J. Savage, and M. B. Wise, 1999, Phys. Rev. C **59**, 617.

Kaplan, D. B., and J. V. Steele, 1999, Phys. Rev. C **60**, 064002.

Kievsky, A., and M. Gattobigio, 2016, Few-Body Syst. **57**, 217.

Kievsky, A., M. Viviani, M. Gattobigio, and L. Girlanda, 2017, Phys. Rev. C **95**, 024001.

Kievsky, A., M. Viviani, D. Logoteta, I. Bombaci, and L. Girlanda, 2018, Phys. Rev. Lett. **121**, 072701.

Kirscher, J., 2010, Ph.D. thesis (George Washington University), arXiv:1506.00347.

Kirscher, J., 2013, Phys. Lett. B **721**, 335.

Kirscher, J., 2017, arXiv:1709.02821.

Kirscher, J., N. Barnea, D. Gazit, F. Pederiva, and U. van Kolck, 2015, Phys. Rev. C **92**, 054002.

Kirscher, J., and D. Gazit, 2016, Phys. Lett. B **755**, 253.

Kirscher, J., H. W. Grießhammer, D. Shukla, and H. M. Hofmann, 2010, Eur. Phys. J. A **44**, 239.

Kirscher, J., E. Pazy, J. Drachman, and N. Barnea, 2017, Phys. Rev. C **96**, 024001.

Kirscher, J., and D. R. Phillips, 2011, Phys. Rev. C **84**, 054004.

Klos, P., J. Menéndez, D. Gazit, and A. Schwenk, 2013, Phys. Rev. D **88**, 083516; **89**, 029901(E) (2014).

Kobayashi, N., *et al.*, 2014, Phys. Rev. Lett. **112**, 242501.

Kok, L. P., D. J. Struik, J. E. Holwerda, and H. van Haeringen, 1981, University of Groningen Report No. 170.

Kok, L. P., D. J. Struik, and H. van Haeringen, 1979, University of Groningen Report No. 151.

Kong, X., and F. Ravndal, 1999a, Nucl. Phys. **A656**, 421.

Kong, X., and F. Ravndal, 1999b, Phys. Lett. B **450**, 320.

Kong, X., and F. Ravndal, 1999c, Phys. Lett. B **470**, 1.

Kong, X., and F. Ravndal, 2000, Nucl. Phys. **A665**, 137.

Kong, X., and F. Ravndal, 2001, Phys. Rev. C **64**, 044002.

König, S., 2013, Ph.D. thesis (University of Bonn).

König, S., 2017, J. Phys. G **44**, 064007.

König, S., S. K. Bogner, R. J. Furnstahl, S. N. More, and T. Papenbrock, 2014, Phys. Rev. C **90**, 064007.

König, S., H. W. Grießhammer, and H.-W. Hammer, 2015, J. Phys. G **42**, 045101.

König, S., H. W. Grießhammer, H.-W. Hammer, and U. van Kolck, 2016, J. Phys. G **43**, 055106.

König, S., H. W. Grießhammer, H.-W. Hammer, and U. van Kolck, 2017, Phys. Rev. Lett. **118**, 202501.

König, S., and H.-W. Hammer, 2011, Phys. Rev. C **83**, 064001.

König, S., and H.-W. Hammer, 2014, Phys. Rev. C **90**, 034005.

König, S., and D. Lee, 2018, Phys. Lett. B **779**, 9.

König, S., D. Lee, and H.-W. Hammer, 2013, J. Phys. G **40**, 045106.

Körber, C., A. Nogga, and J. de Vries, 2017, Phys. Rev. C **96**, 035805.

Kraemer, T., *et al.*, 2006, Nature (London) **440**, 315.

Krebs, H., E. Epelbaum, and U.-G. Meißner, 2007, Eur. Phys. J. A **32**, 127.

Krebs, H., A. Gasparyan, and E. Epelbaum, 2012, Phys. Rev. C **85**, 054006.

Krebs, H., A. Gasparyan, and E. Epelbaum, 2013, Phys. Rev. C **87**, 054007.

Krebs, H., A. M. Gasparyan, and E. Epelbaum, 2018, Phys. Rev. C **98**, 014003.

Kreuzer, S., and H. W. Grießhammer, 2012, Eur. Phys. J. A **48**, 93.

Kreuzer, S., and H.-W. Hammer, 2009, Phys. Lett. B **673**, 260.

Kreuzer, S., and H.-W. Hammer, 2010, Eur. Phys. J. A **43**, 229.

Kreuzer, S., and H.-W. Hammer, 2011, Phys. Lett. B **694**, 424.

Kronfeld, A. S., 2012, Annu. Rev. Nucl. Part. Sci. **62**, 265.

Kruse, M. K. G., E. D. Jurgenson, P. Navrátil, B. R. Barrett, and W. E. Ormand, 2013, Phys. Rev. C **87**, 044301.

Kvinikhidze, A. N., and M. C. Birse, 2018, Eur. Phys. J. A **54**, 216.

Lee, D., and T. Schäfer, 2005, Phys. Rev. C **72**, 024006.

Lee, D., and T. Schäfer, 2006a, Phys. Rev. C **73**, 015201.

Lee, D., and T. Schäfer, 2006b, Phys. Rev. C **73**, 015202.

Lei, J., L. Hlophe, C. Elster, A. Nogga, F. M. Nunes, and D. R. Phillips, 2018, Phys. Rev. C **98**, 051001.

Lenkewitz, M., E. Epelbaum, H.-W. Hammer, and U.-G. Meißner, 2011, Phys. Lett. B **700**, 365.

Lenkewitz, M., E. Epelbaum, H.-W. Hammer, and U.-G. Meißner, 2013, Eur. Phys. J. A **49**, 20.

Lensky, V., and M. C. Birse, 2011, Eur. Phys. J. A **47**, 142.

Lensky, V., M. C. Birse, and N. R. Walet, 2016, Phys. Rev. C **94**, 034003.

Lepage, G. P., 1989a, in *From Actions to Answers: Proceedings of the 1989 Theoretical Advanced Study Institute in Elementary Particle Physics*, edited by T. A. DeGrand and D. Touissaint (World Scientific, Singapore), pp. 97–120.

Lepage, G. P., 1989b, in *From Actions to Answers: Proceedings of the 1989 Theoretical Advanced Study Institute in Elementary Particle Physics*, edited by T. A. DeGrand and D. Touissaint (World Scientific, Singapore), pp. 483–508.

Lepage, G. P., 1997, arXiv:nucl-th/9706029.

Li, K.-W., X.-L. Ren, L.-S. Geng, and B. Long, 2016, Phys. Rev. D **94**, 014029.

Li, K.-W., X.-L. Ren, L.-S. Geng, and B.-W. Long, 2018, Chin. Phys. C **42**, 014105.

Liebig, S., V. Baru, F. Ballout, C. Hanhart, and A. Nogga, 2011, Eur. Phys. J. A **47**, 69.

Liu, C. P., J. de Vries, E. Mereghetti, R. G. E. Timmermans, and U. van Kolck, 2012, Phys. Lett. B **713**, 447.

Liu, C. P., and R. G. E. Timmermans, 2004, Phys. Rev. C **70**, 055501.

Liu, J., X. Chen, and X. Ji, 2017, Nat. Phys. **13**, 212.

Liu, M.-Z., F.-Z. Peng, M. Sánchez Sánchez, and M. Pavón Valderrama, 2018, Phys. Rev. D **98**, 114030.

Liu, X., V. Limkaisang, D. Samart, and Y. Yan, 2019, Phys. Lett. B **789**, 530.

Liu, Y.-R., and S.-L. Zhu, 2008, Chin. Phys. C **32**, 700.

Liu, Z.-W., N. Li, and S.-L. Zhu, 2014, Phys. Rev. D **89**, 074015.

Logoteta, D., I. Bombaci, and A. Kievsky, 2016, Phys. Rev. C **94**, 064001.

Long, B., 2013, Phys. Rev. C **88**, 014002.

Long, B., and Y. Mei, 2016, Phys. Rev. C **93**, 044003.

Long, B., and U. van Kolck, 2008, Ann. Phys. (Amsterdam) **323**, 1304.

Long, B., and U. van Kolck, 2010, Nucl. Phys. **A840**, 39.

Long, B., and U. van Kolck, 2011, Nucl. Phys. **A870-871**, 72.

Long, B., and C. J. Yang, 2011, Phys. Rev. C **84**, 057001.

Long, B., and C. J. Yang, 2012a, Phys. Rev. C **85**, 034002.

Long, B., and C. J. Yang, 2012b, Phys. Rev. C **86**, 024001.

Lu, B.-N., N. Li, S. Elhatisari, D. Lee, E. Epelbaum, and U.-G. Meißner, 2018, arXiv:1812.10928.

Lu, J.-X., L.-S. Geng, and M. Pavón Valderrama, 2019, Phys. Rev. D **99**, 074026.

Lucas, J., and M. Rustgi, 1968, Nucl. Phys. **A112**, 503.

Luke, M. E., and A. V. Manohar, 1992, Phys. Lett. B **286**, 348.

Luke, M. E., and A. V. Manohar, 1997, Phys. Rev. D **55**, 4129.

Lupu, S., N. Barnea, and D. Gazit, 2015, arXiv:1508.05654.

Lüscher, M., 1986, Commun. Math. Phys. **105**, 153.

Lüscher, M., 1991, Nucl. Phys. **B354**, 531.

Lutz, M., 2000, Nucl. Phys. **A677**, 241.

Luu, T., M. J. Savage, A. Schwenk, and J. P. Vary, 2010, Phys. Rev. C **82**, 034003.

Lv, S., and B. Long, 2016, arXiv:1605.06712.

Lynn, J. E., J. Carlson, E. Epelbaum, S. Gandolfi, A. Gezerlis, and A. Schwenk, 2014, Phys. Rev. Lett. **113**, 192501.

Lynn, J. E., I. Tews, J. Carlson, S. Gandolfi, A. Gezerlis, K. E. Schmidt, and A. Schwenk, 2016, Phys. Rev. Lett. **116**, 062501.

Machleidt, R., 2017, Int. J. Mod. Phys. E **26**, 1730005.

Machleidt, R., and D. R. Entem, 2011, Phys. Rep. **503**, 1.

Machleidt, R., P. Liu, D. R. Entem, and E. Ruiz Arriola, 2010, Phys. Rev. C **81**, 024001.

Madeira, L., A. Lovato, F. Pederiva, and K. E. Schmidt, 2018, Phys. Rev. C **98**, 034005.

Maekawa, C. M., E. Mereghetti, J. de Vries, and U. van Kolck, 2011, Nucl. Phys. **A872**, 117.

Mahboubi, N., S. Bayegan, H. Nematollahi, and M. M. Arani, 2016, Phys. Rev. C **94**, 054003.

Mai, M., B. Hu, M. Doring, A. Pilloni, and A. Szczepaniak, 2017, Eur. Phys. J. A **53**, 177.

Manohar, A., and H. Georgi, 1984, Nucl. Phys. **B234**, 189.

Margaryan, A., and R. P. Springer, 2013, Phys. Rev. D **88**, 014017.

Margaryan, A., R. P. Springer, and J. Vanasse, 2016, Phys. Rev. C **93**, 054001.

Marji, E., A. Canul, Q. MacPherson, R. Winzer, C. Zeoli, D. R. Entem, and R. Machleidt, 2013, Phys. Rev. C **88**, 054002.

Marshak, R. E., 1952, *Meson Physics* (Dover Publications, New York).

Matthews, P. T., and A. Salam, 1951, Rev. Mod. Phys. **23**, 311.

McGovern, J. A., D. R. Phillips, and H. W. Grießhammer, 2013, Eur. Phys. J. A **49**, 12.

Mehen, T., 2015, Phys. Rev. D **92**, 034019.

Mehen, T., and J. W. Powell, 2011, Phys. Rev. D **84**, 114013.

Mehen, T., and R. Springer, 2011, Phys. Rev. D **83**, 094009.

Mehen, T., and I. W. Stewart, 1999a, Phys. Lett. B **445**, 378.

Mehen, T., and I. W. Stewart, 1999b, Phys. Rev. C **59**, 2365.

Mehen, T., and I. W. Stewart, 2000, Nucl. Phys. **A665**, 164.

Mehen, T., I. W. Stewart, and M. B. Wise, 1999, Phys. Rev. Lett. **83**, 931.

Mehen, T., I. W. Stewart, and M. B. Wise, 2000, Phys. Lett. B **474**, 145.

Meißner, U.-G., G. Ríos, and A. Rusetsky, 2015, Phys. Rev. Lett. **114**, 091602; **117**, 069902(E) (2016).

Melendez, J. A., S. Wesolowski, and R. J. Furnstahl, 2017, Phys. Rev. C **96**, 024003.

Menéndez, J., D. Gazit, and A. Schwenk, 2012, Phys. Rev. D **86**, 103511.

Mereghetti, E., J. de Vries, R. G. E. Timmermans, and U. van Kolck, 2013, Phys. Rev. C **88**, 034001.

Mereghetti, E., and U. van Kolck, 2015, Annu. Rev. Nucl. Part. Sci. **65**, 215.

Millener, D. J., J. W. Olness, E. K. Warburton, and S. S. Hanna, 1983, Phys. Rev. C **28**, 497.

Miller, G. A., B. M. K. Nefkens, and I. Slaus, 1990, Phys. Rep. **194**, 1.

Moeini Arani, M., and S. Bayegan, 2013, Eur. Phys. J. A **49**, 117.

Mondejar, J., and J. Soto, 2007, Eur. Phys. J. A **32**, 77.

More, S. N., A. Ekström, R. J. Furnstahl, G. Hagen, and T. Papenbrock, 2013, Phys. Rev. C **87**, 044326.

Müller, H. M., S. E. Koonin, R. Seki, and U. van Kolck, 2000, Phys. Rev. C **61**, 044320.

Myers, L. S., *et al.* (COMPTON@MAX-lab Collaboration), 2014, Phys. Rev. Lett. **113**, 262506.

Myers, L. S., *et al.*, 2015, Phys. Rev. C **92**, 025203.

Naidon, P., and S. Endo, 2017, Rep. Prog. Phys. **80**, 056001.

Nakamura, S. X., 2008, Phys. Rev. C **77**, 054001.

Nakamura, T., *et al.*, 1999, Phys. Rev. Lett. **83**, 1112.

Nakamura, T., *et al.*, 2014, Phys. Rev. Lett. **112**, 142501.

Navarro Pérez, R., J. E. Amaro, and E. Ruiz Arriola, 2013, Phys. Rev. C **88**, 064002; **91**, 029901(E) (2015).

Navarro Pérez, R., J. E. Amaro, and E. Ruiz Arriola, 2014, Phys. Rev. C **89**, 024004.

Navarro Pérez, R., J. E. Amaro, and E. Ruiz Arriola, 2015, Phys. Rev. C **91**, 054002.

Navratil, P., V. G. Gueorguiev, J. P. Vary, W. E. Ormand, and A. Nogga, 2007, Phys. Rev. Lett. **99**, 042501.

Nematollahi, H., S. Bayegan, N. Mahboubi, and M. M. Arani, 2016, Phys. Rev. C **94**, 054004.

Nieves, J., 2003, Phys. Lett. B **568**, 109.

Nieves, J., and M. Pavón Valderrama, 2011, Phys. Rev. D **84**, 056015.

Nieves, J., and M. Pavón Valderrama, 2012, Phys. Rev. D **86**, 056004.

Nishida, Y., 2012, Phys. Rev. A **86**, 012710.

Niskanen, J. A., 2002, Phys. Rev. C **65**, 037001.

Nogga, A., P. Navratil, B. R. Barrett, and J. P. Vary, 2006, Phys. Rev. C **73**, 064002.

Nogga, A., R. G. E. Timmermans, and U. van Kolck, 2005, Phys. Rev. C **72**, 054006.

Noordmans, J. P., 2017, Phys. Rev. D **95**, 075030.

Noordmans, J. P., J. de Vries, and R. G. E. Timmermans, 2016, Phys. Rev. C **94**, 025502.

Nörtershauser, W., *et al.*, 2009, Phys. Rev. Lett. **102**, 062503.

Odell, D., A. Deltuva, J. Bonilla, and L. Platter, 2019, arXiv:1903.00034.

Oosterhof, F., B. Long, J. de Vries, R. G. E. Timmermans, and U. van Kolck, 2019, Phys. Rev. Lett. **122**, 172501.

Ordóñez, C., L. Ray, and U. van Kolck, 1994, Phys. Rev. Lett. **72**, 1982.

Ordóñez, C., L. Ray, and U. van Kolck, 1996, Phys. Rev. C **53**, 2086.

Ordóñez, C., and U. van Kolck, 1992, Phys. Lett. B **291**, 459.

Otsuka, T., T. Suzuki, J. D. Holt, A. Schwenk, and Y. Akaishi, 2010, Phys. Rev. Lett. **105**, 032501.

Palit, R., *et al.* (FRS/LAND Collaboration), 2003, Phys. Rev. C **68**, 034318.

Pandharipande, V. R., D. R. Phillips, and U. van Kolck, 2005, Phys. Rev. C **71**, 064002.

Papenbrock, T., 2011, Nucl. Phys. **A852**, 36.

Papenbrock, T., and H. A. Weidenmueller, 2014, Phys. Rev. C **89**, 014334.

Park, B. Y., F. Myhrer, J. R. Morones, T. Meissner, and K. Kubodera, 1996, Phys. Rev. C **53**, 1519.

Park, T.-S., K. Kubodera, D.-P. Min, and M. Rho, 1998a, Phys. Rev. C **58**, R637.

Park, T.-S., K. Kubodera, D.-P. Min, and M. Rho, 1998b, Astrophys. J. **507**, 443.

Park, T.-S., D.-P. Min, and M. Rho, 1993, Phys. Rep. **233**, 341.

Park, T.-S., D.-P. Min, and M. Rho, 1995, Phys. Rev. Lett. **74**, 4153.

Park, T.-S., D.-P. Min, and M. Rho, 1996, Nucl. Phys. **A596**, 515.

Pascalutsa, V., and D. R. Phillips, 2003, Phys. Rev. C **67**, 055202.

Pastore, S., J. Carlson, V. Cirigliano, W. Dekens, E. Mereghetti, and R. B. Wiringa, 2018, Phys. Rev. C **97**, 014606.

Patrignani, C., *et al.* (Particle Data Group), 2016, Chin. Phys. C **40**, 100001.

Pavón Valderrama, M., 2011a, Phys. Rev. C **83**, 024003.

Pavón Valderrama, M., 2011b, Phys. Rev. C **84**, 064002.

Pavón Valderrama, M., 2012, Phys. Rev. D **85**, 114037.

Pavón Valderrama, M., 2016, Int. J. Mod. Phys. E **25**, 1641007.

Pavón Valderrama, M., 2018, Phys. Rev. D **98**, 034017.

Pavón Valderrama, M., 2019a, arXiv:1901.10398.

Pavón Valderrama, M., 2019b, arXiv:1902.08172.

Pavón Valderrama, M., and D. R. Phillips, 2015, Phys. Rev. Lett. **114**, 082502.

Pavón Valderrama, M., and E. Ruiz Arriola, 2004, Phys. Lett. B **580**, 149.

Pavón Valderrama, M., and E. Ruiz Arriola, 2005, Phys. Rev. C **72**, 054002.

Pavón Valderrama, M., and E. Ruiz Arriola, 2006a, Phys. Rev. C **74**, 054001.

Pavón Valderrama, M., and E. Ruiz Arriola, 2006b, Phys. Rev. C **74**, 064004; **75**, 059905(E) (2007).

Pavón Valderrama, M., and E. Ruiz Arriola, 2008, Ann. Phys. (Amsterdam) **323**, 1037.

Pavón Valderrama, M., M. Sánchez Sánchez, C. J. Yang, B. Long, J. Carbonell, and U. van Kolck, 2017, Phys. Rev. C **95**, 054001.

Petschauer, S., and N. Kaiser, 2013, Nucl. Phys. **A916**, 1.

Petschauer, S., N. Kaiser, J. Haidenbauer, U.-G. Meißner, and W. Weise, 2016, Phys. Rev. C **93**, 014001.

Phillips, A. C., 1968, Nucl. Phys. **A107**, 209.

Phillips, D. R., 2016, Annu. Rev. Nucl. Part. Sci. **66**, 421.

Phillips, D. R., S. R. Beane, and M. C. Birse, 1999, J. Phys. A **32**, 3397.

Phillips, D. R., S. R. Beane, and T. D. Cohen, 1998, Ann. Phys. (N.Y.) **263**, 255.

Phillips, D. R., and T. D. Cohen, 1997, Phys. Lett. B **390**, 7.

Phillips, D. R., and T. D. Cohen, 2000, Nucl. Phys. **A668**, 45.

Phillips, D. R., G. Rupak, and M. J. Savage, 2000, Phys. Lett. B **473**, 209.

Phillips, D. R., D. Samart, and C. Schat, 2015, Phys. Rev. Lett. **114**, 062301.

Phillips, D. R., and C. Schat, 2013, Phys. Rev. C **88**, 034002.

Phillips, D. R., M. R. Schindler, and R. P. Springer, 2009, Nucl. Phys. **A822**, 1.

Piarulli, M., L. Girlanda, R. Schiavilla, A. Kievsky, A. Lovato, L. E. Marcucci, S. C. Pieper, M. Viviani, and R. B. Wiringa, 2016, Phys. Rev. C **94**, 054007.

Piarulli, M., L. Girlanda, R. Schiavilla, R. Navarro Pérez, J. E. Amaro, and E. Ruiz Arriola, 2015, Phys. Rev. C **91**, 024003.

Piarulli, M., *et al.*, 2018, Phys. Rev. Lett. **120**, 052503.

Platter, L., and H.-W. Hammer, 2006, Nucl. Phys. **A766**, 132.

Platter, L., H.-W. Hammer, and U.-G. Meißner, 2004, Phys. Rev. A **70**, 052101.

Platter, L., H.-W. Hammer, and U.-G. Meißner, 2005, Phys. Lett. B **607**, 254.

Platter, L., and D. R. Phillips, 2006, Few-Body Syst. **40**, 35.

Polinder, H., J. Haidenbauer, and U.-G. Meißner, 2006, Nucl. Phys. **A779**, 244.

Pretz, J. (JEDI Collaboration), 2013, Hyperfine Interact. **214**, 111.

Prezeau, G., M. Ramsey-Musolf, and P. Vogel, 2003, Phys. Rev. D **68**, 034016.

Puchalski, M., A. M. Moro, and K. Pachucki, 2006, Phys. Rev. Lett. **97**, 133001.

Raha, U., Y. Kamiya, S.-I. Ando, and T. Hyodo, 2018, Phys. Rev. C **98**, 034002.

Rappold, C., *et al.* (HypHI Collaboration), 2013, Phys. Rev. C **88**, 041001.

Reinert, P., H. Krebs, and E. Epelbaum, 2018, Eur. Phys. J. A **54**, 86.

Ren, X.-L., K.-W. Li, L.-S. Geng, B.-W. Long, P. Ring, and J. Meng, 2018, Chin. Phys. C **42**, 014103.

Ren, X.-L., K.-W. Li, L.-S. Geng, and J. Meng, 2017, arXiv: 1712.10083.

Rentmeester, M. C. M., R. G. E. Timmermans, and J. J. de Swart, 2003, Phys. Rev. C **67**, 044001.

Rentmeester, M. C. M., R. G. E. Timmermans, J. L. Friar, and J. J. de Swart, 1999, Phys. Rev. Lett. **82**, 4992.

Rho, M., 1991, Phys. Rev. Lett. **66**, 1275.

Riska, D. O., and R. Schiavilla, 2017, Int. J. Mod. Phys. E **26**, 1740022.

Roper, L. D., 1964, Phys. Rev. Lett. **12**, 340.

Rotureau, J., I. Stetcu, B. R. Barrett, M. C. Birse, and U. van Kolck, 2010, Phys. Rev. A **82**, 032711.

Rotureau, J., I. Stetcu, B. R. Barrett, and U. van Kolck, 2012, Phys. Rev. C **85**, 034003.

Rotureau, J., and U. van Kolck, 2013, Few-Body Syst. **54**, 725.

Rozpedzik, D., *et al.*, 2006, Acta Phys. Pol. B **37**, 2889.

Rupak, G., 2000, Nucl. Phys. **A678**, 405.

Rupak, G., 2016, Int. J. Mod. Phys. E **25**, 1641004.

Rupak, G., L. Fernando, and A. Vaghani, 2012, Phys. Rev. C **86**, 044608.

Rupak, G., and R. Higa, 2011, Phys. Rev. Lett. **106**, 222501.

Rupak, G., and X.-W. Kong, 2003, Nucl. Phys. **A717**, 73.

Rupak, G., and D. Lee, 2013, Phys. Rev. Lett. **111**, 032502.

Rupak, G., and P. Ravi, 2015, Phys. Lett. B **741**, 301.

Rupak, G., and N. Shoresh, 1999, Phys. Rev. C **60**, 054004.

Rupak, G., A. Vaghani, R. Higa, and U. van Kolck, 2019, Phys. Lett. B **791**, 414.

Ryberg, E., C. Forssén, H.-W. Hammer, and L. Platter, 2014a, Eur. Phys. J. A **50**, 170.

Ryberg, E., C. Forssén, H.-W. Hammer, and L. Platter, 2014b, Phys. Rev. C **89**, 014325.

Ryberg, E., C. Forssén, H.-W. Hammer, and L. Platter, 2016, Ann. Phys. (Amsterdam) **367**, 13.

Ryberg, E., C. Forssén, D. R. Phillips, and U. van Kolck, 2019, arXiv:1905.01107.

Ryberg, E., C. Forssén, and L. Platter, 2017, Few-Body Syst. **58**, 143.

Ryezayeva, N., *et al.*, 2008, Phys. Rev. Lett. **100**, 172501.

Sadeghi, H., 2007, Phys. Rev. C **75**, 044002.

Sadeghi, H., 2010, Prog. Theor. Phys. **124**, 1037.

Sadeghi, H., and S. Bayegan, 2005, Nucl. Phys. **A753**, 291.

Sadeghi, H., and S. Bayegan, 2010, Few-Body Syst. **47**, 167.

Sadeghi, H., S. Bayegan, and H. W. Grießhammer, 2006, Phys. Lett. B **643**, 263.

Sadeghi, H., and H. Khalili, 2014, Astrophys. Space Sci. **352**, 637.

Salam, A., and J. A. Strathdee, 1970, Phys. Rev. D **2**, 2869.

Samart, D., C. Schat, M. R. Schindler, and D. R. Phillips, 2016, Phys. Rev. C **94**, 024001.

Sammarruca, F., L. E. Marcucci, L. Coraggio, J. W. Holt, N. Itaco, and R. Machleidt, 2018, arXiv:1807.06640.

Sanchez, R., *et al.*, 2006, Phys. Rev. Lett. **96**, 033002.

Sánchez Sánchez, M., C. J. Yang, B. Long, and U. van Kolck, 2018, Phys. Rev. C **97**, 024001.

Sato, T., T. S. H. Lee, F. Myhrer, and K. Kubodera, 1997, Phys. Rev. C **56**, 1246.

Savage, M. J., 2001, Nucl. Phys. **A695**, 365.

Savage, M. J., K. A. Scaldeferri, and M. B. Wise, 1999, Nucl. Phys. **A652**, 273.

Savage, M. J., P. E. Shanahan, B. C. Tiburzi, M. L. Wagman, F. Winter, S. R. Beane, E. Chang, Z. Davoudi, W. Detmold, and K. Orginos, 2017, Phys. Rev. Lett. **119**, 062002.

Savage, M. J., and R. P. Springer, 1998, Nucl. Phys. **A644**, 235; **A657**, 457(E) (1999).

Savage, M. J., and R. P. Springer, 2001, Nucl. Phys. **A686**, 413.

Scaldeferri, K. A., D. R. Phillips, C. W. Kao, and T. D. Cohen, 1997, Phys. Rev. C **56**, 679.

Schäfer, T., C.-W. Kao, and S. R. Cotanch, 2005, Nucl. Phys. **A762**, 82.

Schindler, M. R., and D. R. Phillips, 2009, Ann. Phys. (Amsterdam) **324**, 682; **324**, 2051(E) (2009).

Schindler, M. R., H. Singh, and R. P. Springer, 2018, Phys. Rev. C **98**, 044001.

Schindler, M. R., and R. P. Springer, 2010, Nucl. Phys. **A846**, 51.

Schindler, M. R., R. P. Springer, and J. Vanasse, 2016, Phys. Rev. C **93**, 025502.

Schmickler, C. H., H. W. Hammer, and E. Hiyama, 2019, arXiv:1901.03643.

Schmickler, C. H., H. W. Hammer, and A. G. Volosniev, 2019, arXiv:1904.00913.

Schmidt, M., M. Jansen, and H. W. Hammer, 2018, Phys. Rev. D **98**, 014032.

Schmidt, M., L. Platter, and H.-W. Hammer, 2019, Phys. Rev. C **99**, 054611.

Schwinger, J., 1947, Phys. Rev. **72**, 742.

Seki, R., and U. van Kolck, 2006, Phys. Rev. C **73**, 044006.

Shin, J. W., S. Ando, and C. H. Hyun, 2010, Phys. Rev. C **81**, 055501.

Siemens, D., J. Ruiz de Elvira, E. Epelbaum, M. Hoferichter, H. Krebs, B. Kubis, and U.-G. Meißner, 2017, Phys. Lett. B **770**, 27.

Skorniakov, G. V., and K. A. Ter Martirosian, 1957, Sov. Phys. JETP **4**, 648.

Slavnov, A. A., 1971, Nucl. Phys. **B31**, 301.

Somà, V., A. Cipollone, C. Barbieri, P. Navrátil, and T. Duguet, 2014, Phys. Rev. C **89**, 061301.

Sommer, R., 2010, in *Modern Perspectives in Lattice QCD: Quantum Field Theory and High Performance Computing*, *Proceedings of the Les Houches Summer School, Session 93*, edited by L. Lellouch, R. Sommer, B. Svetitsky, A. Vladikas, and L. F. Cugliandolo (Oxford University, Oxford), pp. 517–590.

Song, Y.-H., S.-I. Ando, and C. H. Hyun, 2017, Phys. Rev. C **96**, 014001.

Song, Y.-H., R. Lazauskas, and U. van Kolck, 2017, Phys. Rev. C **96**, 024002.

Soto, J., and J. Tarrus, 2008, Phys. Rev. C **78**, 024003.

Soto, J., and J. Tarrus, 2010, Phys. Rev. C **81**, 014005.

Soto, J., and J. Tarrus, 2012, Phys. Rev. C **85**, 044001.

Steele, J. V., and R. J. Furnstahl, 1999, Nucl. Phys. **A645**, 439.

Stetcu, I., B. R. Barrett, and U. van Kolck, 2007, Phys. Lett. B **653**, 358.

Stetcu, I., J. Rotureau, B. R. Barrett, and U. van Kolck, 2010a, Ann. Phys. (Amsterdam) **325**, 1644.

Stetcu, I., J. Rotureau, B. R. Barrett, and U. van Kolck, 2010b, J. Phys. G **37**, 064033.

Stoks, V. G. J., R. A. M. Klomp, M. C. M. Rentmeester, and J. J. de Swart, 1993, Phys. Rev. C **48**, 792.

Summers, N. C., *et al.*, 2007, Phys. Lett. B **650**, 124.

Swanson, E. S., 2006, Phys. Rep. **429**, 243.

Szpigel, S., and V. S. Timoteo, 2012, J. Phys. G **39**, 105102.

Tanabashi, M., *et al.* (Particle Data Group), 2018, Phys. Rev. D **98**, 030001.

Tanaka, K., *et al.*, 2010, Phys. Rev. Lett. **104**, 062701.

Tarasov, O. B., *et al.*, 2009, Phys. Rev. Lett. **102**, 142501.

Tews, I., S. Gandolfi, A. Gezerlis, and A. Schwenk, 2016, Phys. Rev. C **93**, 024305.

Tews, I., L. Huth, and A. Schwenk, 2018, Phys. Rev. C **98**, 024001.

Thacker, B. A., and G. P. Lepage, 1991, Phys. Rev. D **43**, 196.

Thomas, L. H., 1935, Phys. Rev. **47**, 903.

Timoteo, V. S., T. Frederico, A. Delfino, and L. Tomio, 2011, Phys. Rev. C **83**, 064005.

Tjon, J. A., 1975, Phys. Lett. **56B**, 217.

Togano, Y., *et al.*, 2016, Phys. Lett. B **761**, 412.

Tölle, S., H.-W. Hammer, and B. C. Metsch, 2011, C.R. Phys. **12**, 59.

Tölle, S., H.-W. Hammer, and B. C. Metsch, 2013, J. Phys. G **40**, 055004.

Typel, S., and G. Baur, 2005, Nucl. Phys. **A759**, 247.

Typel, S., and G. Baur, 2008, Eur. Phys. J. A **38**, 355.

Vanasse, J., 2012, Phys. Rev. C **86**, 014001.

Vanasse, J., 2013, Phys. Rev. C **88**, 044001.

Vanasse, J., 2017a, Phys. Rev. C **95**, 024318.

Vanasse, J., 2017b, Phys. Rev. C **95**, 024002.

Vanasse, J., 2018, Phys. Rev. C **98**, 034003.

Vanasse, J., 2019, Phys. Rev. C **99**, 054001.

Vanasse, J., D. A. Egolf, J. Kerin, S. König, and R. P. Springer, 2014, Phys. Rev. C **89**, 064003.

Vanasse, J., and D. R. Phillips, 2017, Few-Body Syst. **58**, 26.

Vanasse, J., and M. R. Schindler, 2014, Phys. Rev. C **90**, 044001.

van Kolck, U., 1994, Phys. Rev. C **49**, 2932.

van Kolck, U., 1995, in *Proceedings of the 6th International Conference on Mesons and Light Nuclei, Straz pod Ralskem, Czech Republic, 1995*, Vol. 9, edited by J. Adam, J. Dobes, R. Mach, M. Sotona, and J. Dolejsi (Springer, New York), pp. 444–448.

van Kolck, U., 1997, Lect. Notes Phys. **513**, 62.

van Kolck, U., 1999a, Prog. Part. Nucl. Phys. **43**, 337.

van Kolck, U., 1999b, Nucl. Phys. **A645**, 273.

van Kolck, U., 2017, Few-Body Syst. **58**, 112.

van Kolck, U., J. L. Friar, and T. Goldman, 1996, Phys. Lett. B **371**, 169.

van Kolck, U., G. A. Miller, and D. O. Riska, 1996, Phys. Lett. B **388**, 679.

van Kolck, U., M. C. M. Rentmeester, J. L. Friar, T. Goldman, and J. J. de Swart, 1998, Phys. Rev. Lett. **80**, 4386.

van Kolck, U. L., 1993, Ph.D. thesis (University of Texas).

van Oers, W. T. H., and J. D. Seagrave, 1967, Phys. Lett. **24B**, 562.

Veltman, M. J. G., 1981, Acta Phys. Pol. B **12**, 437.

Vietze, L., P. Klos, J. Menéndez, W. C. Haxton, and A. Schwenk, 2015, Phys. Rev. D **91**, 043520.

Viviani, M., A. Baroni, L. Girlanda, A. Kievsky, L. E. Marcucci, and R. Schiavilla, 2014, Phys. Rev. C **89**, 064004.

Wang, B., Z.-W. Liu, and X. Liu, 2019, Phys. Rev. D **99**, 036007.

Wang, P., and X. G. Wang, 2013, Phys. Rev. Lett. **111**, 042002.

Wang, Q., V. Baru, A. A. Filin, C. Hanhart, A. V. Nefediev, and J. L. Wynen, 2018, Phys. Rev. D **98**, 074023.

Weinberg, S., 1968, Phys. Rev. **166**, 1568.

Weinberg, S., 1969, Phys. Rev. **177**, 2604.

Weinberg, S., 1979, Physica (Amsterdam) **96A**, 327.

Weinberg, S., 1990, Phys. Lett. B **251**, 288.

Weinberg, S., 1991, Nucl. Phys. **B363**, 3.

Weinberg, S., 1992, Phys. Lett. B **295**, 114.

Weinberg, S., 2005, *The Quantum Theory of Fields. Vol. 1: Foundations* (Cambridge University Press, Cambridge, England).

Wendt, K. A., C. Forssén, T. Papenbrock, and D. Sääf, 2015, Phys. Rev. C **91**, 061301.

Wesolowski, S., R. J. Furnstahl, J. A. Melendez, and D. R. Phillips, 2019, J. Phys. G **46**, 045102.

Wesolowski, S., N. Klco, R. J. Furnstahl, D. R. Phillips, and A. Thapaliya, 2016, J. Phys. G **43**, 074001.

Wigner, E., 1937a, Phys. Rev. **51**, 106.

Wigner, E., 1937b, Phys. Rev. **51**, 947.

Wigner, E. P., 1955, Phys. Rev. **98**, 145.

Wilbring, E., H. W. Hammer, and U. G. Meißner, 2013, Phys. Lett. B **726**, 326.

Wilson, K. G., 1983, Rev. Mod. Phys. **55**, 583.

Wong, C. W., 1994, Int. J. Mod. Phys. E **03**, 821.

Wu, S., and B. Long, 2019, Phys. Rev. C **99**, 024003.

Xu, H., B. Wang, Z.-W. Liu, and X. Liu, 2019, Phys. Rev. D **99**, 014027.

Yamazaki, T., K.-i. Ishikawa, Y. Kuramashi, and A. Ukawa, 2012, Phys. Rev. D **86**, 074514.

Yang, C.-J., 2016, Phys. Rev. C **94**, 064004.

Yang, C.-J., C. Elster, and D. R. Phillips, 2008, Phys. Rev. C **77**, 014002.

Yang, C.-J., C. Elster, and D. R. Phillips, 2009a, Phys. Rev. C **80**, 034002.

Yang, C.-J., C. Elster, and D. R. Phillips, 2009b, Phys. Rev. C **80**, 044002.

Yang, J., and P. Capel, 2018, Phys. Rev. C **98**, 054602.

Zeoli, C., R. Machleidt, and D. R. Entem, 2013, Few-Body Syst. **54**, 2191.

Zhang, X., 2019, arXiv:1905.05275.

Zhang, X., and G. A. Miller, 2017, Phys. Lett. B **773**, 159.

Zhang, X., K. M. Nollett, and D. R. Phillips, 2014a, Phys. Rev. C **89**, 051602.

Zhang, X., K. M. Nollett, and D. R. Phillips, 2014b, Phys. Rev. C **89**, 024613.

Zhang, X., K. M. Nollett, and D. R. Phillips, 2015, Phys. Lett. B **751**, 535.

Zhang, X., K. M. Nollett, and D. R. Phillips, 2018a, Phys. Rev. C **98**, 034616.

Zhang, X., K. M. Nollett, and D. R. Phillips, 2018b, arXiv: 1811.07611.

Zhou, D., and R. G. E. Timmermans, 2012, Phys. Rev. C **86**, 044003.

Zhu, S.-L., C. M. Maekawa, B. R. Holstein, M. J. Ramsey-Musolf, and U. van Kolck, 2005, Nucl. Phys. **A748**, 435.